Développement d'une plateforme de laboratoire sur puce intégrant microcapteurs électrochimiques pour la détection des contaminants de l'eau basée sur le suivi de la physiologie des algues

Aliki Tsopela

THÈSE

En vue de l'obtention du

DOCTORAT DE L'UNIVERSITÉ DE TOULOUSE

Délivré par *l'Université Toulouse III - Paul Sabatier*
Discipline ou spécialité : *Micro et nano systèmes*

Présentée et soutenue par
Aliki Theodora TSOPELA

Le *10 février 2015*

Titre : *Development of a lab-on-chip platform integrating electrochemical microsensors for the detection of water contaminants based on algal physiology monitoring*

JURY
Stéphane ARBAULT (DR)
Thierry CAMPS (PR)
Rosaria FERRIGNO (PR)
Ricardo IZQUIERDO (PR)
Philippe JUNEAU (PR)
Wojtek WROBLEWSKI (PR)

Ecole doctorale : *Génie électrique, électronique et Télécommunications (GEET)*
Unité de recherche : *LAAS-CNRS*
Directeur(s) de Thèse : *Jérôme LAUNAY*
Rapporteurs : *Stéphane ARBAULT & Wojtek WROBLEWSKI*

Σα βγεις στον πηγαιμό για την Ιθάκη,
να εύχεσαι νάναι μακρύς ο δρόμος,
γεμάτος περιπέτειες, γεμάτος γνώσεις.

Η Ιθάκη σ' έδωσε τ' ωραίο ταξίδι.
Χωρίς αυτήν δεν θάβγαινες στον δρόμο.
Άλλα δεν έχει να σε δώσει πια.

Κι αν πτωχική την βρεις, η Ιθάκη δεν σε γέλασε.
Έτσι σοφός που έγινες, με τόση πείρα,
ήδη θα το κατάλαβες η Ιθάκες τι σημαίνουν.

Quand tu partiras pour Ithaque,
souhaite que le chemin soit long,
riche en péripéties et en expériences.

Ithaque t'a donné le beau voyage:
sans elle, tu ne te serais pas mis
en route.
Elle n'a plus rien d'autre à te donner.

Si tu la trouves pauvre, Ithaque ne t'a pas trompé.
Sage comme tu l'es devenue à la suite de tant d'experiences, tu as enfin compris ce que signifient les Ithaques.

Constantin Cavafis, *Ithaque*

Traduit par Marguerite Yourcenar et Constantin Dimaras.

Acknowledgements

Même si les 170 pages de présentation scientifique qui suivent dans ce manuscrit de thèse, je n'ai pas eu le courage de les rédiger en français, malgré les solicitations de mon entourage, je tenais à faire un clin d'œil à ma terre d'accueil de ces quatre dernières années en écrivant ces remerciements en français.

Je voudrais remercier plusieurs personnes qui ont fait ce voyage avec moi et qui m'ont aidé à "garder sans cesse Ithaque présente à mon esprit".

Les travaux de thèse présentés ici, se sont déroulés entre le LAAS-CNRS de Toulouse et l'UQAM à Montréal. Je voudrais alors remercier les deux laboratoires qui m'ont accueillie et intégrée dans leurs équipes.

Mes remerciements les plus chaleureux vont à mon directeur de thèse **Jérôme LAUNAY**. Jérôme merci de m'avoir montré le chemin dans le monde des capteurs, de m'avoir montré tous les « secrets » de la techno et les méthodologies scientifiques. Merci pour toutes nos discussions. Tu étais toujours une source d'optimisme, d'enthousiasme et d'idées pour moi. Merci de m'avoir aidé à surmonter toutes les difficultés et d'avoir été si patient et encourageant pendant tous mes moments de stress, déprime, « perfectionnisme ».

Je souhaite également remercier tous mes encadrants de thèse au LAAS, **Isabelle SEGUY** et **Pierre TEMPLE-BOYER** ainsi que mes encadrants à l'UQAM, **Philippe JUNEAU** et **Ricardo IZQUIERDO** pour leur immense apport, leurs conseils, la confiance qu'ils m'ont portée et parce qu'ils étaient toujours disponibles pour m'aider et me guider. Pierre merci de m'avoir transmis toutes ces connaissances sur la partie capteurs, de m'avoir conseillé et aidé sur différents sujets et de m'avoir initié à la version aveyronnaise de la moussaka ! Isabelle et Ricardo merci pour tous vos conseils sur tous les différents aspects de ce projet et surtout pour votre aide avec les composants organiques. Philippe je te remercie de m'avoir transmis ta passion pour la biologie. Merci pour toutes les discussions à mon endroit préféré, « Juliette et chocolat » et de tous tes efforts de me transformer en « biologiste ».

J'adresse aussi mes sincères remerciements à **Stéphane ARBAULT** pour toute son aide depuis le début du projet et pour avoir rapporté sur mon manuscrit de thèse. Je voudrais remercier **Wojtek WROBLEWSKI** d'avoir également accepté de rapporter sur ma thèse et pour toutes ses corrections pertinentes ainsi que **Rosaria FERRIGNO** et **Thierry CAMPS** d'avoir accepté de participer à mon jury de thèse et de tous leurs commentaires constructifs. Je tiens à remercier **Maurice Comtat** pour son regard critique, sa rigueur et sa disponibilité chaque fois que j'avais besoin de son aide.

Je voudrais particulièrement remercier **Céline et Fadhila** pour leur soutien inestimable. Je vous dois beaucoup car vous m'avez appris énormément, pas seulement au niveau scientifique. Un grand merci d'avoir su comment me rendre heureuse pendant des moments difficiles.

Un très grand merci à tous mes amis extraordinaires en France, **Laureine, Carlos, Adrian, Valentina, Hélène, Richard, Julie, Aude, Pattamon, Raphael, Sabrina, Aiva.** Merci pour tous les moments que nous avons passés ensemble dans tous les coins du monde. Vous étiez une des raisons principales pour laquelle j'avais hâte de venir au labo chaque matin. Merci de m'avoir aidé à trouver des solutions à tous mes problèmes (problèmes imaginaires parfois !). Sans vous, je n'aurais jamais pu imaginer l'existence du meilleur kit au monde, du « chicken kit » ! Un grand merci aussi à l'équipe volley/times-up, **Brieux, Ahmet, Gautier, Audrey, Nicolas** pour leur soutien et tous les moments drôles avec les fous rires (à cause des histoires d'Ahmet par rapport aux autres lyonnais… ou de Brieux qui tombait pour sauver le ballon après que le ballon soit tombé au sol !).

Je tiens également à remercier **Marie-Laure** pour toutes nos discussions, accompagnées toujours d'un « petit » bout de chocolat, **Boubou et Ludo** pour vos conseils, **Christian** pour ton « no worries » attitude qui nous faisait rire au pays des koalas, **Charline et Sandrine** pour votre aide infinie, **Vincent** pour nos moments algues et tous les moments drôles au bureau…

Je resterais aussi très reconnaissante à tous mes amis de l'ENSIACET, **Aneesha, Jon, Guillaume, Mariana, Roxana, Christophe, Koenrad** avec qui j'ai commencé mon voyage en France et mes amis au Canada, **Anubha, Philippe, Mathieu, Dave, Alexandre et Shiva**. Merci de m'avoir initié à la culture québécoise et de m'avoir permis de connaitre vos habitudes et votre accent magique (que j'avais du mal à comprendre…) !

Je ne pourrais jamais oublier l'aide de toute l'équipe TEAM sans laquelle nous n'aurions jamais pu fabriquer des dispositifs fonctionnels. **David, Laurent, Fabien, Samuel, David, Véronique, Monique, Éric, Bernard, Jean-Christophe, Benjamin, Ludo, Boubou, Boubinou, Christine, Monique, Pierre-François**, **Jean-Baptiste, Hugues** merci pour votre aide et vos réponses à mes questionnements infinis ! Un grand merci aussi à **Florent, Annie, Kui, Francis et Thibault** qui m'ont aidé à tester les dispositifs en terre canadienne.

Je voudrais maintenant faire un clin d'œil au plus beau pays du monde, la Grèce. Le début de ma thèse était le début d'une nouvelle époque pour eux, pendant laquelle ils passaient des heures infinies au téléphone avec beaucoup d'Alikostress. «Ένα τεράστιο ευχαριστώ στην **Κατερίνα, την Αθηνά, την Άσπα, τη Δανάη και τον Τάσο** για την υποστήριξή τους και όλες τις ώρες που πέρασαν στο τηλέφωνο. Ένα τεράστιο ευχαριστώ στο **Γιάννη**, που παρόλες τις δυσκολίες, με στήριξε και με βοήθησε. Θα ήθελα επίσης να ευχαριστήσω το **Γιώργο Δεληγιώργη** που έδινε μια χαρούμενη ελληνική νότα στην καθημερινότητα του LAAS. Το μεγαλύτερο, όμως, ευχαριστώ και ο

σημαντικότερος παράγοντας που συνέβαλε στο να φτάσω εώς εδώ είναι η οικογένειά μου. **Μαμά, μπαμπά, Αλεξάνδρα, Μαρίνα, γιαγιά, Σέμι, Ολγίτσα, Αντρέα, Βίβι** ευχαριστώ που είστε πάντα δίπλα μου... »

Merci à vous tous de m'avoir aidé à arriver au bout du chemin…

Table of contents

Preface

The ever-growing interest in assessing water quality in distinct and remote sites with high frequency and the stricter regulations implemented by governments have triggered the need for the development of rapid, portable and reliable detection systems for the detection of water pollutants. These devices are analytical tools that provide an early indication, serving at pointing out if implemented regulations are followed but also at identifying upcoming threats and decide whether it is urgent to respond accordingly.

This issue poses a considerable challenge that consists in developing reliable devices incorporating miniaturized sensors. This study is therefore aiming at addressing this issue by proposing a portable multisensor platform for water quality assessment. In order to attain the aforementioned objectives, a lab-on-chip platform will be composed of an electrochemical and an optical detection system integrated on a fluidic structure in order to combine the advantages of both detection systems. The detection principle lies in following alterations in metabolic response of algal cells serving as bioreceptors/biological sensing elements, induced by the presence of toxicants in water. These alterations are therefore representative of trace level pollution.

This project is a multidisciplinary approach and calls for chemistry, physics, biology, microtechnology and system engineering, with a final goal of yielding a complete and autonomous system for the detection of water pollutants. The development of the final system necessitates therefore the association of the skills, expertise and infrastructures of several research groups. The groups involved in the project are the following:

- The research team MICA (Microsystèmes d'Analyse) of the LAAS-CNRS (Laboratoire d'Analyse et d'Architecture des Systèmes) in Toulouse. More specifically the sub-groups involved are the MCEPL (MicroCapteurs Electrochimiques en Phase Liquide) group holding a significant potential in the development of electrochemical microsensors based on field-effect transistors and microelectrode systems as well as the Optics group, focused on the development of generic and organic optoelectronic devices.
- The group CoFaMic (Centre de Recherche sur la Conception et la Fabrication de Microsystems) at UQAM (Université du Québec à Montréal), holding a great expertise in the implementation of organic optoelectronic devices and microfluidic structures.
- The group of the "Laboratoire d'écotoxicologie des microorganismes aquatiques" at UQAM, with a great potential in biodetection based on monitoring of the physiology of phytoplancton.

The proposed methodology consists in validating separately each component of the platform (electrochemical sensor, optical sensor, bioreceptor) and subsequently integrating all components on the same lab-on-chip, validating simultaneously their compatibility.

The first part of the project, related to the optical detection system was developed through the PhD thesis of Florent Lefèvre, conducted exclusively in UQAM and completed in October 2013, under the supervision of Pr. Ricardo Izquierdo and Pr. Philippe Juneau. The present study will therefore present the development of the lab-on-chip electrochemical biodetection system that integrates upon its specifications the compatibility with optical, fluorescence-based measurements concerning materials and configurations employed for a further complete integration.

PhD research was conducted at LAAS-CNRS in Toulouse as far as the technological development, characterization and pre-validation tests are concerned. Bioassays using algal cells for the validation of toxicant detection in water samples were conducted at UQAM in Montreal.

The principal challenge lies in the complete system integration in order to construct a portable analysis tool, enabling on site measurements of water toxicants. The domains concerned are several, including the environmental, industrial, agricultural, public health and industrial/agricultural water treatment. The final cost-effective analysis device will therefore principally aim at validating if established standards are met and will be addressed in governmental institutions, laboratories, universities, food and agriculture industries, drinking water suppliers, independent organisms and individual consumers.

The present manuscript is presenting the implementation and characterization of this device as well as the first bioassays conducted and is divided in five chapters.

The first chapter deals with water contamination issue and the urge to find alternative ways for water quality assessment. An introduction to the existing biosensing systems is presented with a special emphasis on electrochemical and optical detection systems and algal cells used as biosensing elements (bioreceptors) and the main objectives of the study are established.

The second chapter presents the application context. A description of the targeted toxicants, followed by their mode of action on algae, serving as the biosensing element is presented. This chapter also includes an introduction to algal photosynthetic mechanism as well as the basic electrochemical principles applied through this study. Electroactive species having the role of toxicant indicators are then presented and the material selection for the implementation of the electrochemical cell is detailed.

The development of an electrochemical system, similar to the one intended for final application but involving simpler fabrication and characterization procedures, is shown in the third chapter. The fabrication and electrochemical characterization of the first prototypes on silicon chips using the

materials indicated by the previous bibliographic research is presented. In this way, materials and detection properties are validated using devices simpler than the final lab-on-chip.

The fourth chapter deals with the implementation of the lab-on-chip device. The final goal being an autonomous and portable sensor platform, the integration of the previously described electrochemical detection system consisting of three-electrode electrochemical cells on a sealed fluidic system is described. Selection of materials and techniques used for the fabrication of the device are detailed.

The fifth chapter demonstrates bioassays conducted using the fabricated device. The detection of herbicide-induced changes in algal photosynthetic activity is described. The response of the system in different samples and with different light source configurations is shown.

Finally, several perspectives presenting ways of improving the final detection system are demonstrated.

In summary, the present manuscript deals with the development and characterization of an electrochemical detection system and its integration on a fluidic platform. Bioassays performed with the fabricated sensor platform for the detection of herbicides, based on herbicide-induced modifications of algal photosynthetic activity are presented to validate the functionality of the device.

Chapter 1
Water quality assessment

Assessment of water quality is generating major interest over the past few years. There is an essential need to preserve freshwater sources such as lakes, rivers, water reservoirs and ground waters. Water contamination can be hazardous for human health, harmful for all living organisms in aquatic ecosystems and damaging for the environment. Governments therefore establish guidelines and implement strict legislations aiming at the sustainability of freshwater resources. Monitoring and management strategies have been developed at a national and international level. European Environment Agency, United States Environmental Protection Agency and World Health Organization are some of the bodies worldwide that provide technical guidance, set standards and review water quality reports. For instance, Global Environmental Monitoring System (GEMS)/Water is an important part of the United Nations Environment Program (UNEP), dealing with water quality monitoring worldwide and implemented by World Health Organization with the cooperation of the World Meteorological Organization (WMO) and UNESCO. It provides a global database for all country-members and establishes guidelines.

Water quality monitoring is an essential part of the environmental policies of most countries. As a matter of fact, the significant increase in agricultural and industrial activities during the last decades (Government of Canada, 2007) turned water monitoring into an increasingly important environmental aspect. Toxicants released from industrial plants, leach into ground water and are responsible for water quality degradation. Atmospheric pollution can also affect the quality of fresh waters. Deposition of airborne pollutants in water and acid rain principally caused by fossil fuel combustion, contribute to water contamination. Excess in nutrients leading to eutrophication as well as pesticide contamination mainly caused by agricultural activities and urban run-offs can also influence water quality (J. Bartram and Ballance, 1996).

However, human activities contaminating supplies are not the only cause that influences water composition. Water composition is also influenced by climate changes and depends on natural parameters such as weather conditions, geographic location and geological characteristics (J. Bartram and Ballance, 1996).

1.1 Indicators of water quality

It is important to assess water quality in order to decide if measures should be taken to protect human health and aquatic environment and define which will be the further use of each water resource. Depending on its characteristics, water is suitable for different uses such as drinking, irrigation, food, textile and paper industries, mining. Therefore, the variables selected to be monitored always depend on the purpose of the study and the further use of the specific water body. Several analyte groups can be identified and controlled in order to obtain information on the quality of a water sample (UNEP GEMS and IAEA, 2004)

- Physicochemical characteristics such as temperature, pH, conductivity, dissolved oxygen and transparency (color and turbidity) are among the parameters needed to be evaluated in water resources.
- Major inorganic ions such as cyanide, fluoride, sodium, magnesium, sulphate, chloride, potassium and calcium are monitored in order to define characteristics of water bodies. The sources of these ions can be rocks, minerals, clays or gases in the atmosphere dissolved in water. Higher concentrations of certain ions like sodium and chloride can indicate water contamination while others (calcium and magnesium) influence the hardness of water.
- Heavy metals concentration determination is an essential part of water quality assessment as they can pose severe threats to human health and aquatic organisms. Presence of higher concentration of heavy metals in water is mainly the result of water contamination through mining, industrial and domestic discharges and wastewaters. Although some of the heavy metals such as zinc and copper can be essential at trace levels to metabolic activities, they can be very toxic at higher levels. However, metals like lead, mercury, arsenic, cadmium can cause severe health problems even at low exposure levels (Järup, 2003).
- The amount of nutrients such as nitrogen, ammonia, silica, nitrate, nitrite, phosphorus and phosphate present in water should be controlled as high concentration of nutrients contributes to eutrophication phenomenon which is related to algal biomass bloom. Excess in nutrients in water is principally caused by fertilizers used in agricultural activities, municipal sewages, urban run-offs and domestic waste (Crouzet P. et al., 1999).
- Monitoring of microbiological parameters such as chlorophyll pigments is also essential in order to estimate algal biomass which is related to nutrients concentration and can indicate eutrophication (J. Bartram and Ballance, 1996). Furthermore, micro-organisms present in water should be monitored as some of them can be pathogenic and hazardous for human health.

- Organic matter level should be determined in water as it can give information on the effect of pollution of a water body. Biochemical oxygen demand (BOD) test is commonly performed to evaluate the total biodegradable organic matter present in water.
- Organic contaminants such as pesticides also need to be controlled in water as they represent a major source of pollution. Agricultural activities are mainly responsible for water contamination with pesticides. Pesticides are frequently used in agriculture to control targeted species of pests, protect crops, enhance crop yield or limit vegetation in non-crop areas. A particular interest has been placed on the detection of pesticides due to their ever-growing use but also the lack of instructions for their proper application and control of the post-application phase (Samuels and Obare, 2011). They leach into the soil and are transported to rivers and lakes through groundwater (Barbash et al., 2001). Some of them are stable, persistent with a long lifetime and can therefore be eventually detected in waters even long time after their application. Pesticides do not only affect the targeted species but can also affect other organisms, be harmful for the environment and have a severe impact on animals and humans.

In this study, special emphasis is placed on the determination of pesticides in water as they can be hazardous for humans and the environment and are identified as a crucial issue in many European countries.

1.2 Detection methods

1.2.1 Conventional techniques

Water contaminant determination is most commonly performed in laboratories. Conventional methods include advanced instrumental techniques such as gas and liquid chromatography coupled with different detection techniques as mass spectrometry, chemiluminescence or electrochemical detection (Schellin et al., 2004; Kim et al., 1998; M. E. Sánchez, 2007; Jáuregui et al., 1997; Shoup and Mayer, 1982). Chromatography is a separation technique which, when coupled with different detectors, can yield complete analysis systems. The analysis sample is separated into components through a stationary and a mobile phase and separation is based on the affinity of different components for the two phases (Bhadekar, 2011).

Spectrophotometric techniques, usually coupled with other methods, have also been used to determine pesticides in water samples. The operation principle consists in measuring the part of the light beam absorbed by the examined sample. The amount of light absorbed that corresponds to the difference in light intensities between the source beam and the final beam reaching the detector, depends on the

concentration of the analyte of interest (Bhadekar, 2011). Herbicides, like atrazine and dicamba have been detected using spectrophotometry (Amador-Hernández et al., 2005)

These techniques yield high sensitivity and accuracy and the methods followed are already validated and can be controlled by water quality programs (Bogue, 2003). Trace levels of toxicants can be identified and therefore very low limits of detection can be attained. High selectivity is also a positive feature of these methods as they can discriminate among different toxicant substances (Samuels and Obare, 2011). However, laboratory based analysis encounters considerable limitations as it implies complex procedures and requires not only qualified operators but also expensive equipment. Elevated cost and time consuming procedures are important deterrents in the frequent use of advanced instrumental methods (Bhadekar, 2011). What is more, the analysis is not conducted in situ which implies a delay in measurement and therefore a possible modification of the properties of the examined sample (Jang et al., 2011).

1.2.2 Alternative techniques

1.2.2.1 ***Electrochemical systems***

It is still essential to meet the ever-growing need for systems appropriate for rapid, on site analysis. Electroanalytical methods hold great potential for monitoring water samples as they are simple to carry on and sufficiently sensitive (Bhadekar, 2011; Navaratne and Priyanth, 2011). As a matter of fact, electrochemical detection systems are easily miniaturized and portable enabling on-site analysis and providing rapid, real-time feedback information on the presence of pesticides (Lagarde and Jaffrezic-Renault, 2011; Grieshaber et al., 2008; Li et al., 2013). Amperometric sensors were developed for the determination of electroactive organophosphate pesticides through cyclic and linear sweep voltammetry using glassy carbon electrodes modified with multi-wall carbon nanotubes/Nafion film (Li et al., 2005), hexadecane (Xu et al., 2002) and mercury film/polypyrrole (Hailin et al., 1997).

These electrochemical sensors are designed to measure pesticide's concentration in a direct way and not through the effect of the pesticide on living organisms. The only possible way to increase sensitivity and obtain lower detection limits is to use more efficient measurement techniques, such as square wave and differential pulse techniques (Bard and Faulkner, 2001).

1.2.2.2 ***Enzyme-linked immunosorbent assays (ELISA)***

It was therefore important to find alternative methods to existing analysis tools. Enzyme-linked immunosorbent assays (ELISA) have attracted wide attention (Casino et al., 2001). Antibodies are used to target the molecules of interest (Bhand et al., 2005). Chemiluminescent immunoassays are reported in literature for herbicide detection (Dzgoev et al., 1996; Surugiu et al., 2001). ELISA combined with flow injection analysis has been employed by Kumar et al. for the detection of methyl parathion and the method exhibited high sensitivity and accuracy (Kumar et al., 2006). As a matter of fact, high sensitivity can be achieved using high affinity antibodies. Furthermore, compared to instrumental methods, the ELISA technique provides rapidity and simplicity. However, ELISA is performed in laboratories and is therefore not appropriate for on-site analysis.

1.2.3 Biosensors

The demands remaining uncovered by previously developed systems triggered increasing research efforts centered on the development of biosensors. Biosensors are analytical detection devices that convert a biological phenomenon into a detectable and measurable signal which can be amplified and treated. Due to the fact that they can reflect the effect of pollution on living organisms, biosensors are capable of detecting substances and indicating pollution level that cannot be detected by other types of sensors. The fabricated devices can be low-cost and easy-to-use, offering the possibility of conducting on-site analysis. They consist of two principal parts, the biological sensing element, the so-called bioreceptor, and the physical transducer (Bogue, 2003). Different types of biosensors can be found, depending on the transduction system and the bioreceptor used.

1.2.3.1 ***Biological sensing element***

Biological sensing elements represent the part of the biosensor that interacts with the analyte of interest and responds in a specific way to different analytes. Different types of biological sensing elements have been integrated on biosensors for toxicity tests.

Important interest has been placed lately on the development of nucleic acid biosensors, oriented to the detection of pollutants, like carcinogens and mutagens. Nucleic acid biosensors are based on the interaction of pollutants with DNA. DNA hybridization is a technique commonly used. The single-stranded DNA which is complementary to the analyte of interest is immobilized on the surface of the biosensor. When the analyte of interest is present in the examined solution, a hybrid is formed. The

hybrid formation is electrochemically or optically detected through an indicator. Nucleic acid modified electrochemical biosensors have been developed for the detection of toxic substances (J. Wang et al., 1997).

Immunosensors are biosensors that use antibodies (Ab) or antigens (Ag) as the elements for the selective immunochemical interaction with the targeted pollutant (Karube and Suzuki, 1986). Atrazine and parathion have been detected using fiber-optic (Oroszlan et al., 1993) and piezoelectric crystals (Ngeh-Ngwainbi et al., 1986) immunosensors, respectively. As reported by Karube et al., it is more complicated to detect directly the antigen-antibody interaction and therefore many immunosensors use labels (enzymes, fluorescent substances) (Karube and Suzuki, 1986).

Enzymes are often used as biological sensing elements as they have high analytical specificity and can target specific classes of compounds (Updike and Hicks, 1967). Detection principle consists in measuring the activity of the enzymes towards a pollutant (they can contribute to the catalytic transformation of the pollutant) or the inhibition of their activity induced by pollutants. Their application in biosensors fabrication is limited by the fact that they sometimes require a coenzyme, activator or multiple enzymes to obtain a detectable signal. Furthermore, the costly and long procedures involved in the purification process hold back their wide industrial use (Lagarde and Jaffrezic-Renault, 2011).

Whole cells have also attracted wide attention given the fact that toxic substances can act as inhibitors or substrates of cellular respiratory and metabolic processes and generally modify cellular activities. Different types of microorganisms (D'Souza, 2001), such as bacteria, algae and fungal cells, like yeasts and mold, can be an interesting substitute for enzymes as they possess a large quantity of enzymatic activities and can therefore counterbalance the aforementioned limitations. In this case, enzymes carry on their activities while hosted in their natural environment and surrounded by activators and coenzymes making them more efficient towards toxic substances detection (Lagarde and Jaffrezic-Renault, 2011). Whole cell sensors exhibit many advantages such as rapid growth, simplicity in cultivation and manipulation (Baronian, 2004) and the possibility to detect multiple analytes as different enzymes can target different analytes and metabolize them either anaerobically or aerobically producing several detectable compounds (ammonia, carbon dioxide, acids, etc) (D'Souza, 2001; Lei et al., 2006).

- More specifically, fungal cells (Baronian, 2004) are often integrated on biosensors for the analysis of parameters associated with cellular respiration (Jia et al., 2003; Nakamura et al., 2007). Yeasts are robust microorganisms that can grow on several substrates. Their high pH and temperature tolerances assure sensor's efficiency under a wide range of operating conditions.

- Bacterial biosensors are commonly used for environmental monitoring (Karube et al., 1977, Farré et al., 2002; Farré et al., 2001; van der Meer and Belkin, 2010). Bacterial biosensors based on the inhibition of respiration process induced by toxic compounds are reported in literature (Farré et al., 2001). For some bacterial strains, bioluminescence inhibition can also be a pollution indicator (Farré et al., 2002).
- Microalgae (Figure 1.1) and photosynthetic cyanobacteria are used in biosensors industry for trace detection of environmental toxic compounds as they are sensitive to changes in their environment induced by the presence of toxicants and can therefore reflect the toxic effect of pollutants on living organisms (Giardi and Pace, 2005; Brayner et al., 2011; Moreno-Garrido, 2008; Carrilho et al., 2003). They are capable of providing information on pollution levels based on photosynthetic or metabolic activity inhibition (Brayner et al., 2011; Shitanda et al., 2005; Zamaleeva et al., 2011; Lagarde and Jaffrezic-Renault, 2011; Kasai and Hatakeyama, 1993).

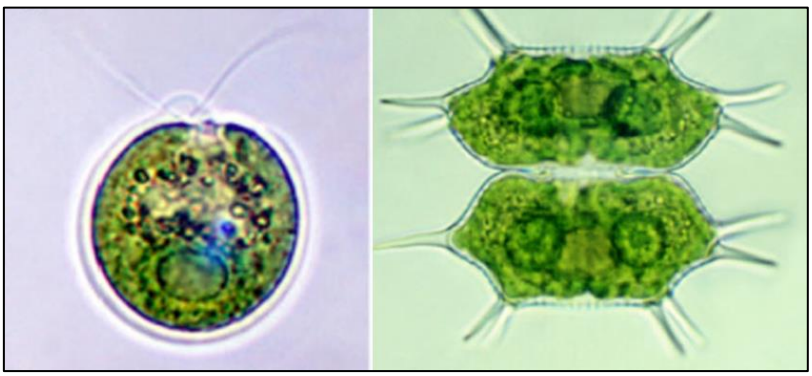

Figure 1.1. Images of isolated green algae taken through microscope (Brayner et al., 2011).

The objective of the present study being the development of a detection system which is easily implemented and simple to use for on-site measurements, algal cells were selected as the biological sensing element. As a matter of fact, the robustness of algal cells that enhances their stability is a very attractive characteristic of these microorganisms (Giardi and Piletska, 2006; Haigh-Flórez et al., 2014). Simple procedures related to their cultivation, isolation and manipulation can also be considered as a very important advantage that justifies this selection. Furthermore, as already mentioned the presence of pollutants influences distinct parts of algal physiology and in several ways (see Chapter 2). Different pollutant categories can thus be detected by observing the metabolic changes they bring about to one type of algal cells used as sensing element. Moreover, due to their high sensitivity to toxic substances, sufficiently low detection limits (LOD) can be reached (Brayner et al., 2011).

1.2.3.2 ***Physical transducer***

The physical transducer converts the biological activity into a signal related to the concentration of the analyte of interest (Lagarde and Jaffrezic-Renault, 2011). Several types of physical transducers can be integrated on a biosensor.

Piezoelectric biosensors

Piezoelectric biosensors are often used to detect toxicants present in water and are constructed by materials resonating when an external alternating electric field is applied, coated with a biological element on which the analyte will be adsorbed (Jiang et al., 2008). The operating principle consists in a modification of the oscillation frequency of the crystal, proportional to the increase in its mass due to binding of analytes on its surface (Mehrvar and Abdi, 2004; Chaubey and Malhotra, 2002). A schematic representation of a piezoelectric immunocrystal is shown in Figure 1.2 (Jiang et al., 2008). Piezoelectric immunosensors were developed for the detection of 2,4-D (Horáček and Skládal, 1997; Halamek et al., 2001) and atrazine (Přibyl et al., 2003) herbicides. Piezoelectric biosensors can assure real-time monitoring, are low-cost and simple to use. However, they are strongly influenced by temperature variations and require not very simple experimental set-up which can possibly deter their use for miniaturized systems.

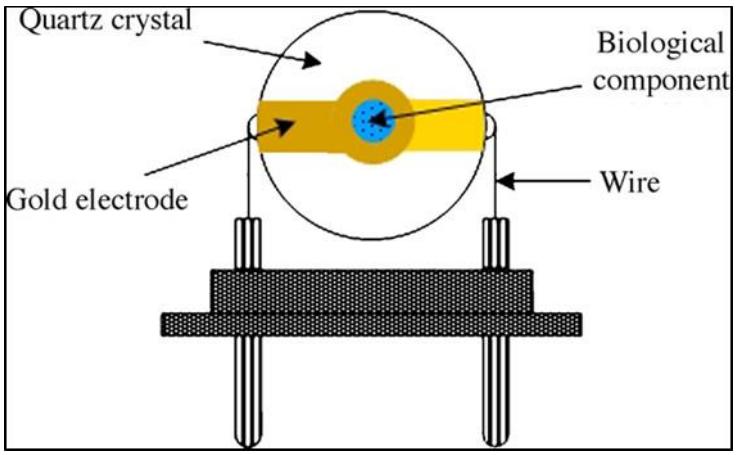

Figure 1.2. Schematic representation of a piezoelectric immunocrystal presented by (Jiang et al., 2008).

Thermal biosensors

Detection of toxicants can also be performed through thermal biosensors. Detection is based on the heat evolved through a biochemical reaction of the analyte of interest and the biological sensing element, which in most cases is an enzyme (Mehrvar and Abdi, 2004; Chaubey and Malhotra, 2002).

Thermal biosensors have been used for the detection of heavy metals (Mattiasson et al., 1978; Satoh, 1992). Despite the fact that they can be stable for a sufficiently long time period, one disadvantage associated with their use is the considerable fraction of heat losses due to irradiation that decrease sensitivity of the system (Eltzov and Marks, 2011).

Optical biosensors

Optical transducers are commonly used to assess water quality. Detection is based on the modification in optical properties of the sample examined caused by the interaction between the biological sensing element and the analyte of interest (Lei et al., 2006; Eltzov and Marks, 2011). UV–vis absorption, bioluminescence, chemiluminescence, reflectance, fluorescence, phosphorescence, Raman scattering, and refractive index can be found among the optical properties modified by the analyte. Optical transduction exhibits several advantages compared to other techniques such as the possibility of conducting multi-analysis based on different peaks that correspond to signals from different analytes (Liu et al., 2013). Furthermore, optical systems can be easily mass fabricated and miniaturized and are free of electric and magnetic signal interferences (Collings and Caruso, 1997; Eltzov and Marks, 2011). Transduction system is not in contact with the solution examined, eliminating biofouling issues. Fluorescence sensors measure the change in fluorescence which depends on the concentration of pesticides and are widely used due to their higher sensitivity compared to absorption methods (Liu et al., 2013). Bacterial biosensors based on the green fluorescent protein were developed for arsenic pollution (Stocker et al., 2003; Theytazi et al., 2009) and organic contaminants (Stiner and Halverson, 2002; Li et al., 2008) monitoring. Algal-based biosensors were also employed for the determination of herbicides based on chlorophyll fluorescence measurements (Frense et al., 1998; Védrine et al., 2003; Lefèvre et al., 2012). Figure 1.3 is a schematic representation of the algal optical biosensor used fo the detection of herbicides by Frense et al., 1998.

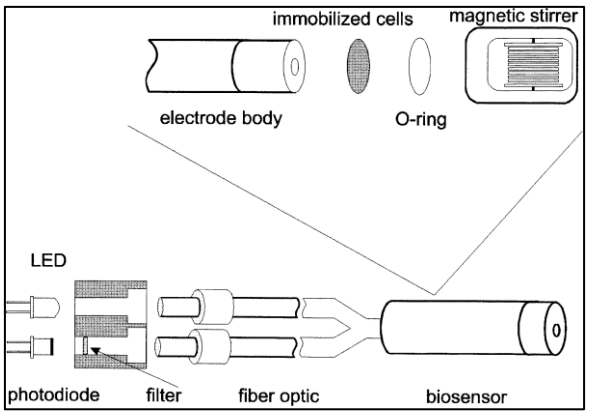

Figure 1.3. Optical biosensor based on algae for the detection of herbicides through fluorescence measurements (Frense et al., 1998).

Luminescence-based bacterial biosensors are reported for detection of toxicants in water samples (Bhattacharyya et al., 2005; Yin et al., 2005) using the ability of some enzymes to emit photons through certain reactions (Mehrvar and Abdi, 2004). Surface plasmon resonance biosensors, measuring changes in the refractive index induced by herbicides (Farré et al., 2007) or organophosphate pesticides (Mauriz et al., 2006) presence in water, were also developed (Figure1.4).

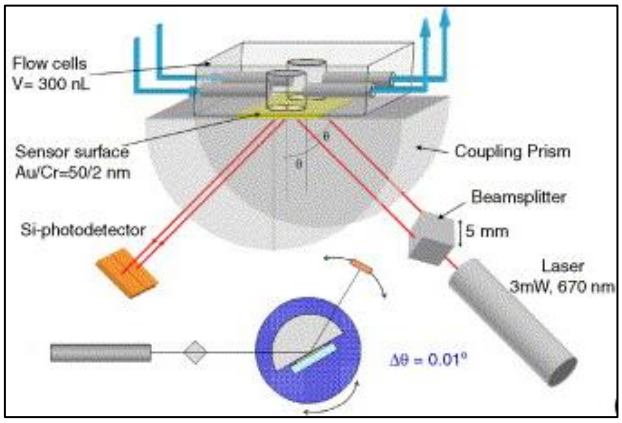

Figure 1.4. Portable β-SPR sensor system from SENSIA, S.L. (Madrid, Spain), used for pesticide detection (Farré et al., 2007; Mauriz et al., 2006).

Despite their numerous advantages, optical biosensors have still limitations such as light interference meaning that measurements need to be performed in dark chambers as well as their inadequacy in providing accurate results when examining turbid samples (Lagarde and Jaffrezic-Renault, 2011).

Electrochemical biosensors

Electrochemical biosensors represent an indispensable tool in water quality assessment as they meet the requirement for a cost-effective, accurate and sensitive analytical system and give information on water quality by detecting wide range of chemical species (Bogue, 2003). They enable higher sample analysis frequency as the measurement stabilization period is usually short. Another important advantage is that they are easily miniaturized. Moreover, noise which is proportional to electrode size, can be minimized when using microelectrodes (Amatore et al., 2008) and interferences by other electro-active species can be reduced by selecting the appropriate potential corresponding to the reaction of interest (Lagarde and Jaffrezic-Renault, 2011). In contrast with optical systems, electrochemical biosensors can be successfully employed for analysis in turbid samples and there is no light interference (Lagarde and Jaffrezic-Renault, 2011). Furthermore, the intensity of the signals generated depends on the concentration and not on the quantity of the analyte (Amatore et al., 2008) which is not the case for optical sensors. However, the use of electrochemical biosensors is limited to

applications involving electro-active species (Ben-Yoav et al., 2009). In addition, the direct contact of the sensor with the examined solution can cause surface deterioration resulting in modification of detection properties. This problem can yet be addressed by integrating membranes that minimize biofouling (Zhang et al., 2000).

Electrochemical biosensors convert a biochemical phenomenon into a detectable and measurable electrical signal which is correlated to the analyte concentration and can be potentiometric, conductimetric and amperometric.

Potentiometric biosensors are designed to measure the difference in potential between working electrode and a stable reference electrode with no current flowing through the system (Lagarde and Jaffrezic-Renault, 2011). Potential values are then correlated to the concentration of the analyte through a logarithmic relationship given by Nernst equation (Lei et al., 2006; Mehrvar and Abdi, 2004; Grieshaber et al., 2008). Although pH electrodes have been widely used for detection of pesticides in agriculture (Mulchandani et al., 2001; Gaberlein et al., 2000), other ion selective electrodes, such as chloride ion selective electrode, have also generated major interest in wastewater treatment domain (Han, 2002).

Conductimetric biosensors record variations in conductivity of the electrolyte containing charged species in contact with the electrode (Lagarde and Jaffrezic-Renault, 2011). These variations result from the production or consumption of charged species during different reactions and can therefore indicate a biological process taking place (Lawrence and Moores, 1972; (Jaffrezic-Renault and Dzyadevych, 2008). They have found various applications in environmental monitoring for detection of heavy metal ions, pesticides (Chouteau et al., 2005; Chouteau et al., 2004) and other toxicants (phenols, pentachlorophenate, potassium cyanide) degrading water quality (Figure 1.5) (Curtis et al., 2009).

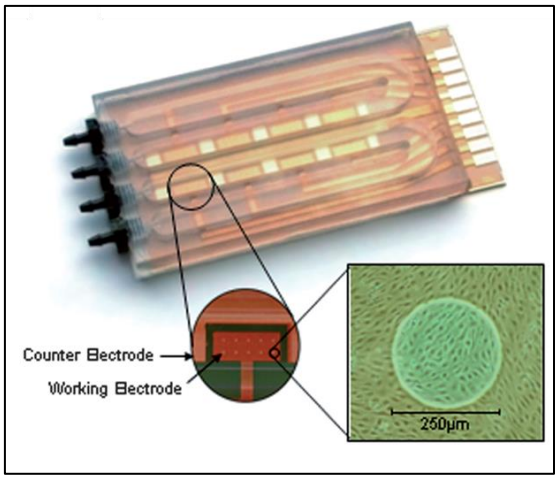

Figure 1.5. Electric Cell-substrate Impedance Sensing (ECIS) fluidic biochip (Agave Biosystems Inc., Ithaca, NY) for detection of water toxicants (Curtis et al., 2009).

The operating principle of amperometric biosensors lies in applying a potential and recording the current corresponding to oxidation and reduction of electroactive species on electrode surface. In amperometric systems, the faradaic current generated linearly depends on the concentration of the analyte of interest (Mehrvar and Abdi, 2004). Current variations result from variations in consumption-production rates of electroactive species and reflect the biochemical phenomenon taking place (Figure1.6) (Ben-Yoav et al., 2009). Amperometric biosensors have been widely used for the oxygen monitoring in wastewaters (Chan et al., 2000), detection of organophosphates (Mulchandani et al., 2001), phenols (Mulchandani et al., 2005), cyanide (Ikebukuro et al., 1996) and heavy metal ions (Figure 1.7) (Lehmann et al., 2000; Jang et al., 2011)

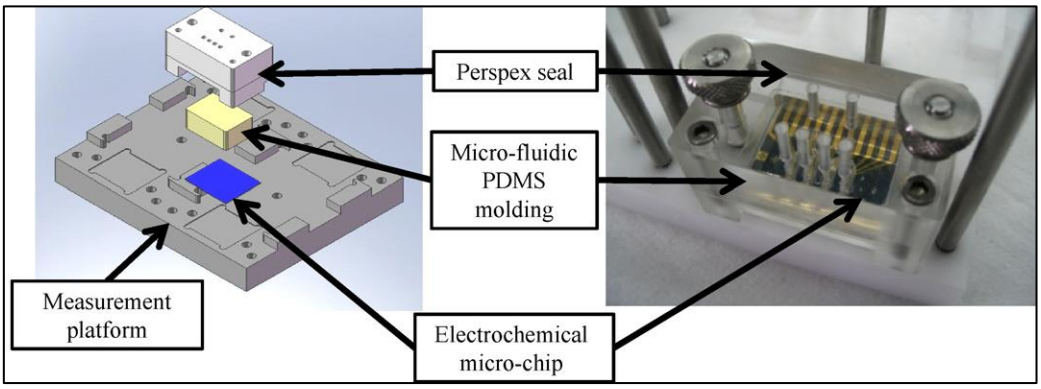

Figure 1.6. Micro-fluidic electrochemical chip system based on bacteria for the detection of two genotoxic substances (Ben-Yoav et al., 2009).

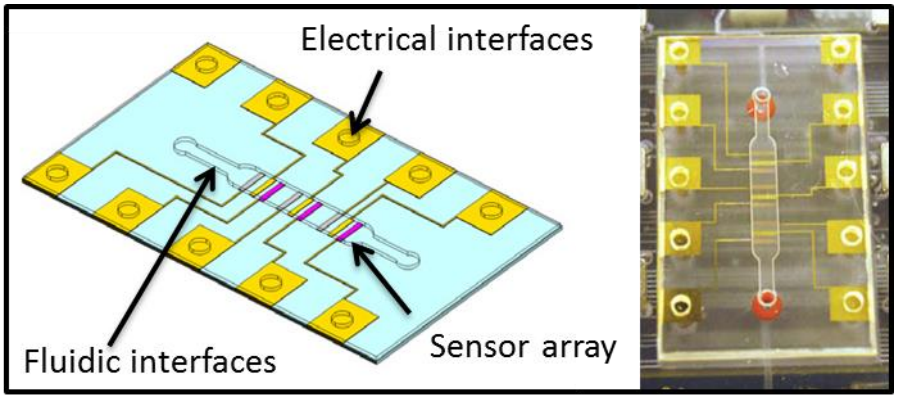

Figure 1.7. A polymer lab chip with an array of three amperometric sensors for heavy metal detection (Jang et al., 2011).

Given the fact that the final goal is to obtain a sufficiently sensitive detection system for rapid, simple and on-site measurements, the present study was oriented towards the implementation of an

electrochemical sensor which will be later coupled with the optical sensor. After considering all possibilities offered by available transduction systems, we converged to the development of the electrochemical sensor as it is easily miniaturized and involves simple procedures of development and further operation, providing, simultaneously, the sensitivity required for the particular application.

1.3 Axes of development

The objective of this project is the implementation of a multi-sensor platform for water quality assessment. The final goal is to deliver an enhanced detection system, by coupling the optical sensor, already developed by our collaborators in UQAM (Lefèvre et al., 2012), with an electrochemical sensor. Both sensors will be integrated on a lab-on-chip platform, offering the possibility of conducting double complementary detection: optical and electrochemical.

Given the fact that for the detection of different toxicants, one of the two techniques is more powerful than the other, the final device that combines electrochemical and optical detection can give the possibility of altering detection techniques depending on the sensitivity of each technique towards the detection of a specific toxicant. Another possibility is to combine both detection types in order to eliminate false positives and therefore increase system accuracy and reliability.

Algal cells are used as the biological sensing element and both sensor types aim at monitoring disturbances in algal physiology, caused by the presence of toxic substances. For the present study, algal cells are not immobilized on the surface of the biosensor but are mixed with the examined water sample before measurement. Immobilization of algae is the next step which will be carried out in the following part of the project.

As far as the optical sensor is concerned, fluorescence-based detection was employed as it is a sensitive and reliable technique to assess the effect of toxic substances on algal photosynthesis. Given the fact that we are aiming at providing a low-cost final device, organic optoelectronic components were used by our collaborators in UQAM, for the fabrication of the optical system. A blue organic light emitting diode (OLED) was used to stimulate algal photosynthesis and an organic photodetector (OPD) was used to measure the emitted algal fluorescence (Figure 1.8) (Lefèvre et al., 2012).

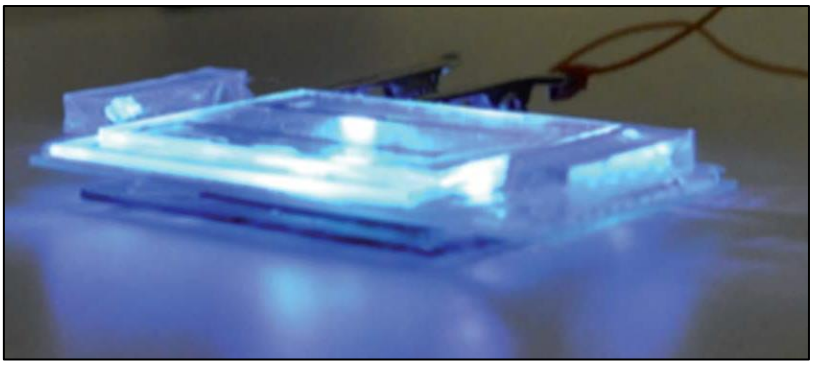

Figure 1.8. Fluorescence-based optical algal biosensor fabricated by Lefèvre et al. (Lefèvre et al., 2012).

The selection of the electrochemical transducer is driven by the need to obtain a system which is easily implemented and simple to use. As mentioned previously, electrochemical sensors are easily miniaturized, yielding solid and stable systems. They are therefore the appropriate tool for on-site analysis and meet the requirements of the targeted application that demands a portable system for on-site detection, providing an early indication by sorting the samples needed to be further analyzed by conventional techniques. Furthermore, electrochemical sensors can detect different compounds by employing different materials and methods (see Chapter 2) which is not necessarily the case for other transduction systems. They can therefore detect and dissociate different analytes produced by algae that are representative of the presence of different pollutants. A multi-parameter system, capable of rapidly providing parallel results can therefore be obtained.

This study is focused on the development of the electrochemical detection system integrated on a fluidic platform for the detection of toxicants based on algal physiology. However, the final platform that will be developed is a generic and versatile system that will eventually incorporate a fluorescence-based optical detection, coupled with a solid electrochemical system.

1.4 References

Amador-Hernández, J., Velázquez-Manzanares, M., Gutiérrez-Ortiz, M. del R., Hernández-Carlos, B., Peral-Torres, M., Alba, L.-, Luis, P., 2005. SIMULTANEOUS SPECTROPHOTOMETRIC DETERMINATION OF ATRAZINE AND DICAMBA IN WATER BY PARTIAL LEAST SQUARES REGRESSION. J. Chil. Chem. Soc. 50, 461–464. doi:10.4067/S0717-97072005000200004

Amatore, C., Arbault, S., Bouton, C., Drapier, J.-C., Ghandour, H., Koh, A.C.W., 2008. Real-time amperometric analysis of reactive oxygen and nitrogen species released by single immunostimulated macrophages. Chembiochem Eur. J. Chem. Biol. 9, 1472–1480. doi:10.1002/cbic.200700746

Amine, A., Mohammadi, H., Bourais, I., Palleschi, G., 2006. Enzyme inhibition-based biosensors for food safety and environmental monitoring. Biosens. Bioelectron. 21, 1405–1423. doi:10.1016/j.bios.2005.07.012

Arduini, F., Amine, A., Moscone, D., Palleschi, G., 2010. Biosensors based on cholinesterase inhibition for insecticides, nerve agents and aflatoxin B1 detection (review). Microchim. Acta 170, 193–214. doi:10.1007/s00604-010-0317-1

Bard, A.J., Faulkner, L.R., 2001. Electrochemical Methods: Fundamentals and Applications, New York: Wiley, 2001, 2nd ed. JOHN WILE SONS INC. doi:10.1023/A:1021637209564

Barbash, J.E., Thelin, G.P., Kolpin, D.W., Gilliom, R.J., 2001. Major herbicides in ground water: results from the National Water-Quality Assessment. J. Environ. Qual. 30, 831–845.

Baronian, K.H.R., 2004. The use of yeast and moulds as sensing elements in biosensors. Biosens. Bioelectron. 19, 953–962. doi:10.1016/j.bios.2003.09.010

Bartram J., Ballance, R., 1996. WHO | Water quality monitoring: A practical guide to the design and implementation of freshwater quality studies and monitoring programmes, in: Water Quality Monitoring - A Practical Guide to the Design and Implementation of Freshwater Quality Studies and Monitoring Programmes. UNEP/WHO.

Ben-Yoav, H., Biran, A., Pedahzur, R., Belkin, S., Buchinger, S., Reifferscheid, G., Shacham-Diamand, Y., 2009. A whole cell electrochemical biosensor for water genotoxicity bio-detection. Electroch. Acta 54, 6113–6118. doi:10.1016/j.electacta.2009.01.061

Bhadekar, R., 2011. Developments in Analytical Methods for Detection of Pesticides in Environmental Samples. Am. J. Anal. Chem. 02, 1–15. doi:10.4236/ajac.2011.228118

Bhand, S., Surugiu, I., Dzgoev, A., Ramanathan, K., Sundaram, P.V., Danielsson, B., 2005. Immuno-arrays for multianalyte analysis of chlorotriazines. Talanta, Evaluation/Validation of Novel Biosensors in Real Environmental and Food Samples 65, 331–336. doi:10.1016/j.talanta.2004.07.009

Bhattacharyya, J., Read, D., Amos, S., Dooley, S., Killham, K., Paton, G.I., 2005. Biosensor-based diagnostics of contaminated groundwater: assessment and remediation strategy. Environ. Pollut. 134, 485–492. doi:10.1016/j.envpol.2004.09.002

Bogue, R.W., 2003. Biosensors for monitoring the environment. Sens. Rev. 23, 302–310. doi:10.1108/02602280310496818

Brayner, R., Couté, A., Livage, J., Perrette, C., Sicard, C., 2011. Micro-algal biosensors. Anal. Bioanal. Chem. 401, 581–597. doi:10.1007/s00216-011-5107-z

Carrilho, E.N.V.M., Nóbrega, J.A., Gilbert, T.R., 2003. The use of silica-immobilized brown alga (Pilayella littoralis) for metal preconcentration and determination by inductively coupled plasma optical emission spectrometry. Talanta 60, 1131–1140. doi:10.1016/S0039-9140(03)00217-0

Casino, P., Morais, S., Puchades, R., Maquieira, Á., 2001. Evaluation of Enzyme-Linked Immunoassays for the Determination of Chloroacetanilides in Water and Soils. Environ. Sci. Technol. 35, 4111–4119. doi:10.1021/es010569f

Chaubey, A., Malhotra, B.D., 2002. Mediated biosensors. Biosens. Bioelectron. 17, 441–456. doi:10.1016/S0956-5663(01)00313-X

Chouteau, C., Dzyadevych, S., Chovelon, J.-M., Durrieu, C., 2004. Development of novel conductometric biosensors based on immobilised whole cell Chlorella vulgaris microalgae. Biosens. Bioelectron. 19, 1089–1096. doi:10.1016/j.bios.2003.10.012

Chouteau, C., Dzyadevych, S., Durrieu, C., Chovelon, J.-M., 2005. A bi-enzymatic whole cell conductometric biosensor for heavy metal ions and pesticides detection in water samples. Biosens. Bioelectron. 21, 273–281. doi:10.1016/j.bios.2004.09.032

Collings, A.F., Caruso, F., 1997. Biosensors: recent advances. Rep. Prog. Phys. 60, 1397–1445. doi:10.1088/0034-4885/60/11/005

Crouzet P., Leonard J., Nixon S., Rees Y., Parr W., Laffon L., Bogestrand J., Kristensen, Lallana C., Izzo G., Bokn T., Bak J., Lack T.J., 1999. Water quality and pollution by nutrients — European Environment Agency (EEA) (Page No. 4).

Curtis, T.M., Widder, M.W., Brennan, L.M., Schwager, S.J., Schalie, W.H. van der, Fey, J., Salazar, N., 2009. A portable cell-based impedance sensor for toxicity testing of drinking water. Lab. Chip 9, 2176–2183. doi:10.1039/B901314H

D'Souza, S.F., 2001. Microbial biosensors. Biosens. Bioelectron. 16, 337–353. doi:10.1016/S0956-5663(01)00125-7

Dzgoev, A., Mecklenburg, M., Larsson, P.-O., Danielsson, B., 1996. Microformat Imaging ELISA for Pesticide Determination. Anal. Chem. 68, 3364–3369. doi:10.1021/ac960129k

Eltzov, E., Marks, R.S., 2011. Whole-cell aquatic biosensors. Anal. Bioanal. Chem. 400, 895–913. doi:10.1007/s00216-010-4084-y

Farré, M., Gonçalves, C., Lacorte, S., Barceló, D., Alpendurada, M., 2002. Pesticide toxicity assessment using an electrochemical biosensor with Pseudomonas putida and a bioluminescence

inhibition assay with Vibrio fischeri. Anal. Bioanal. Chem. 373, 696–703. doi:10.1007/s00216-002-1313-z

Farré, M., Martínez, E., Ramón, J., Navarro, A., Radjenovic, J., Mauriz, E., Lechuga, L., Marco, M.P., Barceló, D., 2007. Part per trillion determination of atrazine in natural water samples by a surface plasmon resonance immunosensor. Anal. Bioanal. Chem. 388, 207–214. doi:10.1007/s00216-007-1214-2

Farré, M., Pasini, O., Carmen Alonso, M., Castillo, M., Barceló, D., 2001. Toxicity assessment of organic pollution in wastewaters using a bacterial biosensor. Anal. Chim. Acta 426, 155–165. doi:10.1016/S0003-2670(00)00826-6

Frense, D., Müller, A., Beckmann, D., 1998. Detection of environmental pollutants using optical biosensor with immobilized algae cells. Sens. Actuators B Chem. 51, 256–260. doi:10.1016/S0925-4005(98)00203-2

Gaberlein, S., Spener, F., Zaborosch, C., 2000. Microbial and cytoplasmic membrane-based potentiometric biosensors for direct determination of organophosphorus insecticides. Appl. Microbiol. Biotechnol. 54, 652–658. doi:10.1007/s002530000437

Giardi, M.T., Pace, E., 2005. Photosynthetic proteins for technological applications. Trends Biotechnol. 23, 257–263. doi:10.1016/j.tibtech.2005.03.003

Giardi, M.T., Piletska, E.V., 2006. Biotechnological Applications of Photosynthetic Proteins. Landes Bioscience, Springer Publishers, Church ST.Georgetown, USA.

Government of Canada, E.C., 2007. Environment Canada - Water - Water Availability [WWW Document]. URL https://www.ec.gc.ca/eau-water/default.asp?lang=En&n=2DC058F1-1 (accessed 5.3.14).

Grieshaber, D., MacKenzie, R., Vörös, J., Reimhult, E., 2008. Electrochemical Biosensors - Sensor Principles and Architectures. Sensors 8, 1400–1458. doi:10.3390/s8031400

Haigh-Flórez, D., de la Hera, C., Costas, E., Orellana, G., 2014. Microalgae dual-head biosensors for selective detection of herbicides with fiber-optic luminescent O2 transduction. Biosens. Bioelectron. 54, 484–491. doi:10.1016/j.bios.2013.10.062

Hailin, G., Ho, O.L., Xinhao, Y., 1997. Analysis of Pesticides Using a Polyppyrole Modified Electrode. Environ. Monit. Assess. 44, 361–367. doi:10.1023/A:1005799816175

Halamek, J., Hepel, M., Skladal, P., 2001. Investigation of highly sensitive piezoelectric immunosensors for 2,4-dichlorophenoxyacetic acid. Biosens. Bioelectron. 16, 253–260. doi:10.1016/S0956-5663(01)00132-4

Han, T., 2002. Flow injection microbial trichloroethylene sensor. Talanta 57, 271–276. doi:10.1016/S0039-9140(02)00027-9

Horáček, J., Skládal, P., 1997. Improved direct piezoelectric biosensors operating in liquid solution for the competitive label-free immunoassay of 2,4-dichlorophenoxyacetic acid. Anal. Chim. Acta, 347, 43–50. doi:10.1016/S0003-2670(97)00125-6

Ikebukuro, K., Honda, M., Nakanishi, K., Nomura, Y., Masuda, Y., Yokoyama, K., Yamauchi, Y., Karube, I., 1996. Flow-type cyanide sensor using an immobilized microorganism. Electroanalysis 8, 876–879. doi:10.1002/elan.1140081005

Jaffrezic-Renault, N., Dzyadevych, S.V., 2008. Conductometric Microbiosensors for Environmental Monitoring. Sensors 8, 2569–2588. doi:10.3390/s8042569

Jang, A., Zou, Z., Lee, K.K., Ahn, C.H., Bishop, P.L., 2011. State-of-the-art lab chip sensors for environmental water monitoring. Meas. Sci. Technol. 22, 032001. doi:10.1088/0957-0233/22/3/032001

Järup, L., 2003. Hazards of heavy metal contamination. Br. Med. Bull. 68, 167–182. doi:10.1093/bmb/ldg032

Jia, J., Tang, M., Chen, X., Qi, L., Dong, S., 2003. Co-immobilized microbial biosensor for BOD estimation based on sol–gel derived composite material. Biosens. Bioelectron. 18, 1023–1029. doi:10.1016/S0956-5663(02)00225-7

Jiang, X., Li, D., Xu, X., Ying, Y., Li, Y., Ye, Z., Wang, J., 2008. Immunosensors for detection of pesticide residues. Biosens. Bioelectron. 23, 1577–1587. doi:10.1016/j.bios.2008.01.035

Karube, I., Matsunaga, T., Mitsuda, S., Suzuki, S., 1977. Microbial electrode BOD sensors. Biotechnol. Bioeng. 19, 1535–1547. doi:10.1002/bit.260191010

Karube, I., Suzuki, M., 1986. Novel immunosensors. Biosensors 2, 343–362. doi:10.1016/0265-928X(86)85023-4

Kasai, F., Hatakeyama, S., 1993. Herbicide susceptibility in two green algae, Chlorella vulgaris and Selenastrum capricornutum. Chemosphere 27, 899–904. doi:10.1016/0045-6535(93)90019-2

Kim, D.H., Heo, G.S., Lee, D.W., 1998. Determination of organophosphorus pesticides in wheat flour by supercritical fluid extraction and gas chromatography with nitrogen–phosphorus detection. J. Chromatogr. A 824, 63–70. doi:10.1016/S0021-9673(98)00629-3

Kumar, M.A., Chouhan, R.S., Thakur, M.S., Amita Rani, B.E., Mattiasson, B., Karanth, N.G., 2006. Automated flow enzyme-linked immunosorbent assay (ELISA) system for analysis of methyl parathion. Anal. Chim. Acta 560, 30–34. doi:10.1016/j.aca.2005.12.026

Lagarde, F., Jaffrezic-Renault, N., 2011. Cell-based electrochemical biosensors for water quality assessment. Anal. Bioanal. Chem. 400, 947–964. doi:10.1007/s00216-011-4816-7

Lawrence, A.J., Moores, G.R., 1972. Conductimetry in Enzyme Studies. Eur. J. Biochem. 24, 538–546. doi:10.1111/j.1432-1033.1972.tb19716.x

Lefèvre, F., Chalifour, A., Yu, L., Chodavarapu, V., Juneau, P., Izquierdo, R., 2012. Algal fluorescence sensor integrated into a microfluidic chip for water pollutant detection. Lab. Chip 12, 787–793. doi:10.1039/C2LC20998E

Lehmann, M., Riedel, K., Adler, K., Kunze, G., 2000. Amperometric measurement of copper ions with a deputy substrate using a novel Saccharomyces cerevisiae sensor. Biosens. Bioelectron. 15, 211–219. doi:10.1016/S0956-5663(00)00060-9

Lei, Y., Chen, W., Mulchandani, A., 2006. Microbial biosensors. Anal. Chim. Acta 568, 200–210. doi:10.1016/j.aca.2005.11.065

Li, C., Wang, C., Ma, Y., Bao, W., Hu, S., 2005. A novel amperometric sensor and chromatographic detector for determination of parathion. Anal. Bioanal. Chem. 381, 1049–1055. doi:10.1007/s00216-004-2978-2

Li, Y., Sella, C., Lemaître, F., Guille Collignon, M., Thouin, L., Amatore, C., 2013. Highly Sensitive Platinum-Black Coated Platinum Electrodes for Electrochemical Detection of Hydrogen Peroxide and Nitrite in Microchannel. Electroanalysis 25, 895–902. doi:10.1002/elan.201200456

Li, Y.-F., Li, F.-Y., Ho, C.-L., Liao, V.H.-C., 2008. Construction and comparison of fluorescence and bioluminescence bacterial biosensors for the detection of bioavailable toluene and related compounds. Environ. Pollut. 152, 123–129. doi:10.1016/j.envpol.2007.05.002

Liu, S., Zheng, Z., Li, X., 2013. Advances in pesticide biosensors: current status, challenges, and future perspectives. Anal. Bioanal. Chem. 405, 63–90. doi:10.1007/s00216-012-6299-6

Mallat, E., Barceló, D., Barzen, C., Gauglitz, G., Abuknesha, R., 2001. Immunosensors for pesticide determination in natural waters. TrAC Trends Anal. Chem. 20, 124–132. doi:10.1016/S0165-9936(00)00082-0

Mattiasson, B., Danielsson, B., Hermansson, C., Mosbach, K., 1978. Enzyme thermistor analysis of heavy metal ions with use of immobilized urease. FEBS Lett. 85, 203–206. doi:10.1016/0014-5793(78)80455-4

Mauriz, E., Calle, A., Lechuga, L.M., Quintana, J., Montoya, A., Manclús, J.J., 2006. Real-time detection of chlorpyrifos at part per trillion levels in ground, surface and drinking water samples by a portable surface plasmon resonance immunosensor. Anal. Chim. Acta 561, 40–47. doi:10.1016/j.aca.2005.12.069

Mehrvar, M., Abdi, M., 2004. Recent developments, characteristics, and potential applications of electrochemical biosensors. Anal. Sci. 20, 1113–1126.

Moreno-Garrido, I., 2008. Microalgae immobilization: Current techniques and uses. Bioresour. Technol. 99, 3949–3964. doi:10.1016/j.biortech.2007.05.040

Mulchandani, A., Chen, W., Mulchandani, P., Wang, J., Rogers, K.R., 2001. Biosensors for direct determination of organophosphate pesticides. Biosens. Bioelectron. 16, 225–230. doi:10.1016/S0956-5663(01)00126-9

Mulchandani, P., Hangarter, C.M., Lei, Y., Chen, W., Mulchandani, A., 2005. Amperometric microbial biosensor for p-nitrophenol using Moraxella sp.-modified carbon paste electrode. Biosens. Bioelectron. 21, 523–527. doi:10.1016/j.bios.2004.11.011

Nakamura, H., Suzuki, K., Ishikuro, H., Kinoshita, S., Koizumi, R., Okuma, S., Gotoh, M., Karube, I., 2007. A new BOD estimation method employing a double-mediator system by ferricyanide and menadione using the eukaryote Saccharomyces cerevisiae. Talanta 72, 210–216. doi:10.1016/j.talanta.2006.10.019

Navaratne, A., Priyanth, N., 2011. Chemically Modified Electrodes for Detection of Pesticides, in: Stoytcheva, M. (Ed.), Pesticides in the Modern World - Trends in Pesticides Analysis. InTech.

Ngeh-Ngwainbi, J., Foley, P.H., Kuan, S.S., Guilbault, G.G., 1986. Parathion antibodies on piezoelectric crystals. J. Am. Chem. Soc. 108, 5444–5447. doi:10.1021/ja00278a012

Oroszlan, P., Duveneck, G.L., Ehrat, M., Widmer, H.M., 1993. Fiber-optic Atrazine immunosensor. Sens. Actuators B Chem. 11, 301–305. doi:10.1016/0925-4005(93)85268-F

Přibyl, J., Hepel, M., Halámek, J., Skládal, P., 2003. Development of piezoelectric immunosensors for competitive and direct determination of atrazine. Sens. Actuators B Chem. 91, 333–341. doi:10.1016/S0925-4005(03)00107-2

Samuels, T., Obare, S., 2011. Advances in Analytical Methods for Organophosphorus Pesticide Detection, in: Stoytcheva, M. (Ed.), Pesticides in the Modern World - Trends in Pesticides Analysis. InTech.

Satoh, I., 1992. Use of immobilized alkaline phosphatase as an analytical tool for flow-injection biosensing of zinc(II) and cobalt(II) ions. Ann. N. Y. Acad. Sci. 672, 240–244.

Schellin, M., Hauser, B., Popp, P., 2004. Determination of organophosphorus pesticides using membrane-assisted solvent extraction combined with large volume injection-gas chromatography-mass spectrometric detection. J. Chromatogr. A 1040, 251–258.

Shitanda, I., Takada, K., Sakai, Y., Tatsuma, T., 2005. Compact amperometric algal biosensors for the evaluation of water toxicity. Anal. Chim. Acta 530, 191–197. doi:10.1016/j.aca.2004.09.073

Shoup, R., Mayer, G., 1982. Determination of Environmental Phenols by Liquid-Chromatography Electrochemistry. Anal. Chem. 54, 1164–1169.

Stiner, L., Halverson, L.J., 2002. Development and Characterization of a Green Fluorescent Protein-Based Bacterial Biosensor for Bioavailable Toluene and Related Compounds. Appl. Environ. Microbiol. 68, 1962–1971. doi:10.1128/AEM.68.4.1962-1971.2002

Stocker, J., Balluch, D., Gsell, M., Harms, H., Feliciano, J., Daunert, S., Malik, K.A., van der Meer, J.R., 2003. Development of a Set of Simple Bacterial Biosensors for Quantitative and Rapid Measurements of Arsenite and Arsenate in Potable Water. Environ. Sci. Technol. 37, 4743–4750. doi:10.1021/es034258b

Surugiu, I., Danielsson, B., Ye, L., Mosbach, K., Haupt, K., 2001. Chemiluminescence Imaging ELISA Using an Imprinted Polymer as the Recognition Element Instead of an Antibody. Anal. Chem. 73, 487–491. doi:10.1021/ac0011540

UNEP GEMS, IAEA, 2004. Analytical Methods for Environmental Water Quality. United Nations Environment Programme Global Environment Monitoring System/Water Programme and International Atomic Energy Agency.

Updike, S.J., Hicks, G.P., 1967. The Enzyme Electrode. Nature 214, 986–988. doi:10.1038/214986a0

Van der Meer, J.R., Belkin, S., 2010. Where microbiology meets microengineering: design and applications of reporter bacteria. Nat. Rev. Microbiol. 8, 511–522. doi:10.1038/nrmicro2392

Védrine, C., Leclerc, J.-C., Durrieu, C., Tran-Minh, C., 2003. Optical whole-cell biosensor using Chlorella vulgaris designed for monitoring herbicides. Biosens. Bioelectron. 18, 457–463. doi:10.1016/S0956-5663(02)00157-4

Wang, J., Rivas, G., Cai, X., Palecek, E., Nielsen, P., Shiraishi, H., Dontha, N., Luo, D., Parrado, C., Chicharro, M., Farias, P.A.M., Valera, F.S., Grant, D.H., Ozsoz, M., Flair, M.N., 1997. DNA electrochemical biosensors for environmental monitoring. A review. Anal. Chim. Acta 347, 1–8. doi:10.1016/S0003-2670(96)00598-3

Xu, C., Wu, K., Hu, S., Cui, D., 2002. Electrochemical detection of parathion at a glassy-carbon electrode modified with hexadecane. Anal. Bioanal. Chem. 373, 284–288. doi:10.1007/s00216-002-1325-8

Yin, J.Q., Li, X.Z., Zhou, C., Zhang, Y.H., 2005. Luminescent bacterial sensors made from immobilized films of photobacterium phosphoreum. Chem. Res. Chin. Univ. 21, 44–47.

Zamaleeva, A.I., Sharipova, I.R., Shamagsumova, R.V., Ivanov, A.N., Evtugyn, G.A., Ishmuchametova, D.G., Fakhrullin, R.F., 2011. A whole-cell amperometric herbicide biosensor based on magnetically functionalised microalgae and screen-printed electrodes. Anal. Methods 3, 509–513. doi:10.1039/C0AY00627K

Zhang, S., Wright, G., Yang, Y., 2000. Materials and techniques for electrochemical biosensor design and construction. Biosens. Bioelectron. 15, 273–282. doi:10.1016/S0956-5663(00)00076-2

Chapter 2
Theory and context

Chapter 1 indicated the type of biosensors needed to be constructed and is best adapted to the targeted application. Given the fact that the optical part was validated by our collaborators in Canada (Lefèvre et al., 2012), special emphasis was placed on the development of the algal-based, electrochemical biosensor aiming at yielding a multisensor platform at the end of the project.

This chapter describes the application context towards which this study is oriented. Despite the fact that the final goal is to implement a generic, versatile device for water quality assessment, a case study dealing with the electrochemical detection of two types of herbicides, serving as proof of concept, was carried out.

The herbicides examined are firstly presented, followed by a brief description of the way they affect algal physiology and more particularly, photosynthetic mechanisms. The effect of herbicides on algal physiology is evident through disturbances in photosynthetic activities. These disturbances are represented by variations in consumption-production rates of specific electro-active species such as dissolved oxygen (O_2) (extracellular level), hydrogen peroxide (H_2O_2) and hydroxide ion (OH^-) (intracellular level) by algae and can therefore be detected by the electrochemical sensor. The electro-active species to be monitored indicate the working electrode materials that will be used to fabricate the sensor. The state of the art of the electrode materials used for the detection of each of the three electroactive species will therefore be detailed in this chapter. Theoretical electrochemical concepts implemented through the present study will also be briefly presented.

2.1 Herbicides

Herbicides represent a category of pesticides that are used to protect crops and non-crop areas and prevent growth of undesired weeds. According to Bhadekar et al., they can be classified in several groups based on their composition, such as: triazines, substituted-urea, bipyridyl compounds, chlorophenoxy compounds, carbamate herbicides (Bhadekar, 2011). Herbicides can easily penetrate the soil, be transported to rivers through groundwater paths and be often detected in different water bodies such as lakes and rivers. In this way, they can potentially affect non-targeted living organisms

and pose possible threats on the environment and human health. It is therefore a major challenge to monitor the quantities of different toxicants present in water.

Special emphasis was placed on herbicides as they represent 65% of the pesticides used (USDA, 1999). The research was oriented towards the detection of two different herbicides, Diuron and Paraquat that were selected due to their highly toxic effects on aquatic organisms and human health, in order to validate the detection principle.

Diuron, or 3-(3,4-dichlorophenyl)-1,1-dimethylurea is an urea-based herbicide, employed for total, non-selective vegetation control (Fedtke and Duke, 2004; Tasmin et al., 2014). It is mainly used upon non-crop areas, in irrigation or drainage canals (Government of Canada, 1997) but has also found applications in paints to protect from fouling (Tasmin et al., 2014). According to conducted surveys, Diuron has been found in 70% of European rivers and is also ranked high upon water contaminants for Australian, Canadian and U.S agencies (Tasmin et al., 2014), posing considerable threats to aquatic microorganisms. Diuron can also affect human respiratory and gastrointestinal systems. It is not found upon the compounds monitored in food surveys in Canada and U.S. (Government of Canada, 1997), which is reinforcing the interest of monitoring it directly in water bodies, such as river and lakes.

Paraquat, or 1,1′-dimethyl 4-4′bipyridinium dichloride is a bipyridyl compound used to control total vegetation and eliminate undesired weeds among crops. It is applied directly on the leafs of the targeted vegetation, as it is only active on leafs and not through the soil (Fuerst and Vaughn, 1990). Paraquat is used before planting annual crops, before crop harvesting or is selectively sprayed to eliminate undesired vegetation among seed crops, vineyards and orchards (Fedtke and Duke, 2004; Fuerst and Vaughn, 1990; Rodriguez Jr et al., 2002). It induces respiratory problems and can affect nervous systems (Rodriguez Jr et al., 2002). Paraquat affects photosynthesis, can damage non-photosynthesizing tissues in high concentrations and has moderate to high toxicity to aquatic organisms. It is a restricted use pesticide and its application has been prohibited in several countries. Due to its high water solubility, it can be transported through runoffs and it is therefore important to be capable of detecting it in waters bodies (Fuerst and Vaughn, 1990).

2.2 Algal physiology: Herbicide-induced changes in metabolism

Herbicides can act on the targeted vegetation in different ways. They can inhibit, for instance, cell growth and photosynthesis depending on their molecular structure and site of action (Ross and Childs DJ, 1996). The two herbicides selected to be monitored, Diuron and Paraquat, are inhibiting photosynthesis, targeting two different sites of plants photosynthetic apparatus.

The two herbicides were chosen as they are representative of widely used groups of herbicides that are soluble to water and have different sites of action at the photosynthetic apparatus of targeted weeds (Fuerst and Vaughn, 1990; Malato et al., 2002). As a matter of fact, 50% of herbicides inhibit photosynthesis acting at vital systems of the photosynthetic apparatus (USDA, 1999).

Therefore, the sensors that will be implemented should be designed to monitor photosynthetic activity. As stated by Davison, 1991, given the fact that algal physiology resembles to the one of the targeted vegetation, microalgae are directly affected by herbicides. They are thus suitable indicators of the presence of herbicides and can be successfully used as biological recognition elements among herbicide biosensors. Based on previously reported ecotoxicological studies on monitoring the effect of herbicides on living organisms (Schubnell et al., 1999; Lefèvre et al., 2012), *Chlamydomonas reinhardtii*, wild type microalgae were selected as biological recognition elements as they are extensively studied and characterized.

Prior to presenting the toxic mode of action of herbicides on algal photosynthesis, it is important to introduce the parts and functions of photosynthetic apparatus that will be the center of our interest.

2.2.1 Photosynthetic apparatus

Photosynthesis takes place in particular organelles of the cells of photosynthetic organisms, the so-called chloroplasts. Chloroplasts contain the stroma and the thylakoids that are organized in stacks, called grana (Figure 2.1).

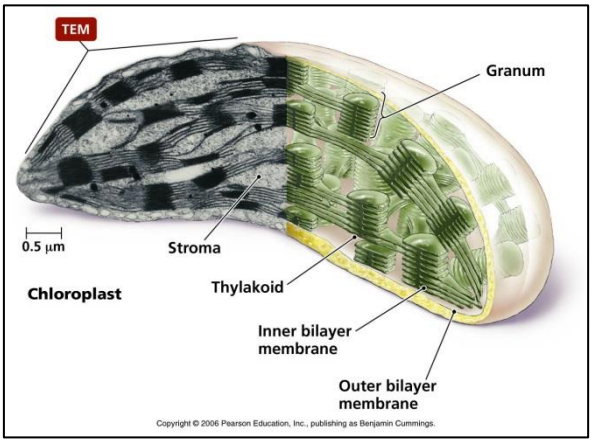

Figure 2.1. Schematic view of a chloroplast, containing the stroma and thylakoid (Pearson Education, Inc., publishing as Benjamin Cummings.)

Photosynthesis consists in two main stages associated with light-based and carbon-based reactions. The entire process, from light reactions to carbon fixation reactions, is resumed through the following equation (Equation 1):

$$6\,CO_2 + 6\,H_2O \xrightarrow{light} C_6H_{12}O_6 + 6\,O_2 \qquad (Equation\ 1)$$

2.2.1.1 ***Light reactions***

Light reactions are taking place in the thylakoids through photosynthetic pigments that are organized in photosystems.

Light energy is collected by chlorophylls that are light-absorbing pigments present in the thylakoids. Photosynthetic pigments absorb light mainly in blue and red region (Taiz and Zeiger, 2006). When chlorophyll absorbs a high energy, blue photon, it gets into the excited, high energy, unstable state. In order to make the transition to an excited, lower energy state, chlorophyll transfers heat to its surroundings. The excess energy remaining after heat transfer or the energy gained after the absorption of a red photon needs still to be transferred so that chlorophyll will return to its initial stable state. This can occur through several pathways such as fluorescence, which consists in the emission of a photon of lower energy by chlorophyll. However, the main way for releasing the excess energy upon functional chloroplasts is by transferring it to another molecule or by using it through chemical reactions, known as photochemistry. The latter involves a series of oxidation and reduction reactions of several compounds and electron transfer carried out by molecules having the role of electron carriers. Two photochemical complexes, Photosystem I and II (PSI and PSII), situated in the membrane of the thylakoids, are mainly responsible for these reactions. PSI and PSII are clusters of pigments in protein lattices that operate one after the other for the eventual production of NADPH (Nicotinamide adenine dinucleotide phosphate) and ATP (Adenosine triphosphate). PSII reaction center, being associated to the oxygen evolving complex, is mainly responsible for oxidizing water and providing electron to the transport chain, while PSI is responsible for reducing $NADP^+$ (Figure 2.2). PSII reaction center uses light of shorter wavelength, around 680 nm compared to PSI that uses light in the far-red region, greater than 700 nm.

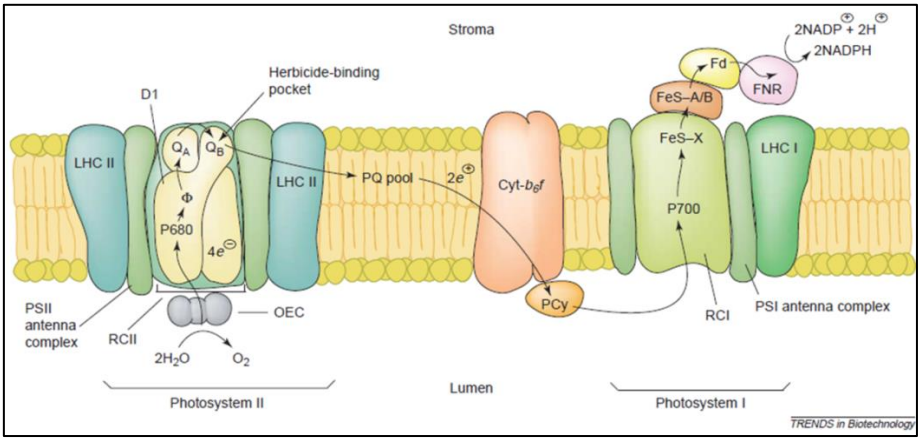

Figure 2.2. Schematic representation of the photochemical complexes situated in the thylakoid membrane and their cooperation for NADPH and ATP production (Giardi and Pace, 2005).

Light reactions are carried out through a *Z scheme* as presented in Figure 2.3.

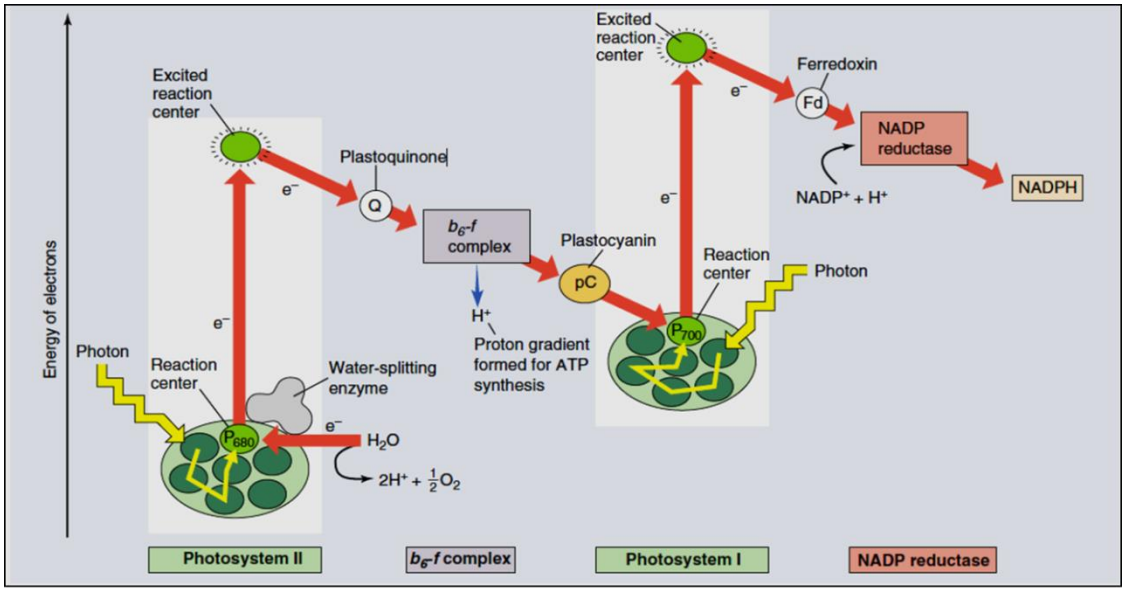

Figure 2.3. *Z-scheme* representing the light-dependent reactions of photosynthesis procedure (Raven and Johnson, 2002).

Firstly, the antenna pigments of PSII absorb light and transfer it from one pigment to the other, simply through energy transferring and not through electron transferring, until the reaction center where a special chlorophyll pigment P_{680} is embedded in a matrix of proteins.

The absorbed light energy is therefore used to excite the chlorophyll P_{680} of the reaction center, which is then transferring the excited electrons to the associated proteins and more particularly to molecules serving as primary acceptors, the quinones. In order to return to its initial condition after transferring the excited electron, chlorophyll takes an electron from water. Water oxidation is taking place in the oxygen-evolving complex that is found inside an enzyme. The complex is a cluster of four manganese ions that converts water to oxygen, releasing at the same time protons and electrons.

Protons produced by water oxidation are passed to the lumen (the inner space of the thylakoid membrane) and then transferred by ATP synthase to the stroma following the ATP production.

The quinones that receive the electrons from the excited chlorophyll are therefore reduced and turned into plastoquinones (Q_A and Q_B) which are strong electron donors. The plastoquinone is transferring the electron to a protein complex, the b6-f complex. This complex is also contributing to passing protons to the lumen of the thylakoids and subsequently to the stroma for the formation of ATP. Another protein, the plastocyanin (PCy) transfers the electrons from the b6-f complex to PSI. At PSI, the absorbed light excites the special chlorophyll molecule P_{700}. The excited chlorophyll transfers the excited electrons to the acceptors that are the iron-sulfur proteins FeS-X, FeS-A and FeS-B and then to

the ferredoxin (Fd), which is then passing electrons to a molecule of $NADP^+$ to produce NADPH in the stroma, with the help of an enzyme. After passing the excited electron to the electron acceptors, the chlorophyll needs to return to initial state and therefore takes the electron transferred via the plastocyanin (PCy).

Overall, through light reactions, oxygen is released and NADPH and ATP are eventually formed, that will be further used in reactions of carbon fixation and other metabolic pathways.

2.2.1.2 ***Carbon fixation reactions***

The previously formed ATP and NADPH are used for sugar synthesis by reducing CO_2. This procedure, taking place in the stroma, is known as the Calvin-cycle and is independent of light (in a direct way) when ATP and NADPH are available. In reality, these reactions are light dependent in an indirect way, as the enzymes involved in Calvin cycle are activated by light. Figure 2.4 shows Calvin cycle as presented by Raven and Johnson, 2002.

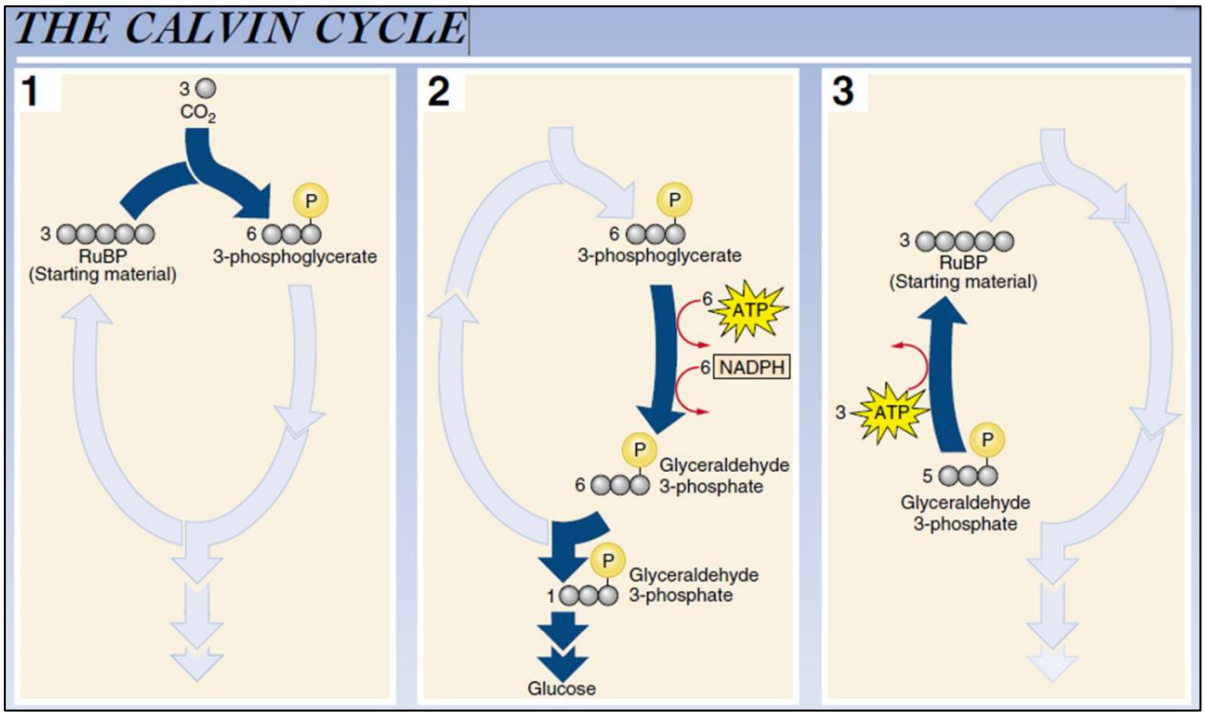

Figure 2.4. The Calvin cycle (adapted from Raven and Johnson, 2002)

Several reactions are taking place during the Calvin cycle to eventually produce glucose. Firstly, the carbon atoms of three CO_2 are fixed on three organic molecules, called ribulose1,5-bisphosphate (RuBP) that already contains five atoms of carbon, yielding three unstable carbon molecules. Carbon

fixation on RuBP is performed through an enzyme called ribulose bisphosphate carboxylase/oxygenase, the so-called rubisco. The unstable carbon molecules produced split in three-carbon molecules, called the 3-phosphoglycerates (3-PGA). The produced 3-PGA are reduced using the ATP and NADPH of the light reactions in order to produce six molecules of glyceraldehyde 3-phosphate (G3P). Five molecules of the produced G3P are then used for the regeneration of ribulose1,5-bisphosphate (RuBP) using also ATP, and one G3P molecule is the final product of the Calvin cycle that will be further used for the production of glucose.

2.2.2 Mode of action of herbicides

After introducing the basic principles of the photosynthetic procedure, the mode of action on photosynthesis of the selected herbicides will be presented. Diuron and Paraquat act on photosynthetic organisms by interfering in photosynthetic electron flow during light reactions.

2.2.2.1 ***Diuron***

Diuron blocks the electron flow from PSII to PSI causing total or partial inhibition of photosynthetic activity. This works by replacing plastoquinone Q_B that normally serves as electron carrier along the electron transport chain. Indeed, Diuron binds to the site of the D1 reaction center protein where normally Q_B is binding (Figure 2.2) (Giardi and Pace, 2005). In this way, Diuron inhibits electron transfer from the primary acceptor Q_A of PSII to the secondary plastoquinone Q_B (Scognamiglio et al., 2009). The latter results in accumulation of energy in PSII, as electrons cannot be anymore transferred forward in the chain, which is therefore damaged (Fedtke and Duke, 2004). As the electron flow is blocked, oxygen production through water oxidation is partially or totally blocked and consequently, the excess energy is released in the form of fluorescence.

Thus, the presence of this type of herbicides has a visible impact on the photosynthetic oxygen production and the emitted fluorescence. The majority of microalgal biosensors that aim at detecting Diuron are therefore either based on fluorescence or photosynthetic oxygen production monitoring (Brayner et al., 2011). These two approaches are effective alternatives to the conventional method which is the standard growth test, where the inhibition of algal growth is measured (Ma et al., 2002). As a matter of fact, although this method yields good results in terms of limit of detection and sensitivity, long assay duration is an important issue when rapid results are desired.

Fluorescence biosensors are based on optical transduction system in order to detect the emitted photons, while the transducer for oxygen monitoring is performed through electrochemical measurement.

It is demonstrated in literature that fluorescence-based biosensors employed for the detection of Diuron have high performances with low limits of detection (Podola and Melkonian, 2005, Rodriguez Jr et al., 2002, Naessens et al., 2000). However, they often demand high stabilization times and can only be effective when optically clear, not turbid samples are examined (Haigh-Flórez et al., 2014).

Among previous experimental works based on algal photosynthetic activity as an indicator of the presence of Diuron, amperometric monitoring is reported several times as the detection technique (Shitanda et al., 2005; Shitanda et al., 2009; Koblízek et al., 2002). Figure 2.5 shows the electrochemical algal-based biosensor developed by Shitanda et al. for the detection of Diuron (Shitanda et al., 2009).

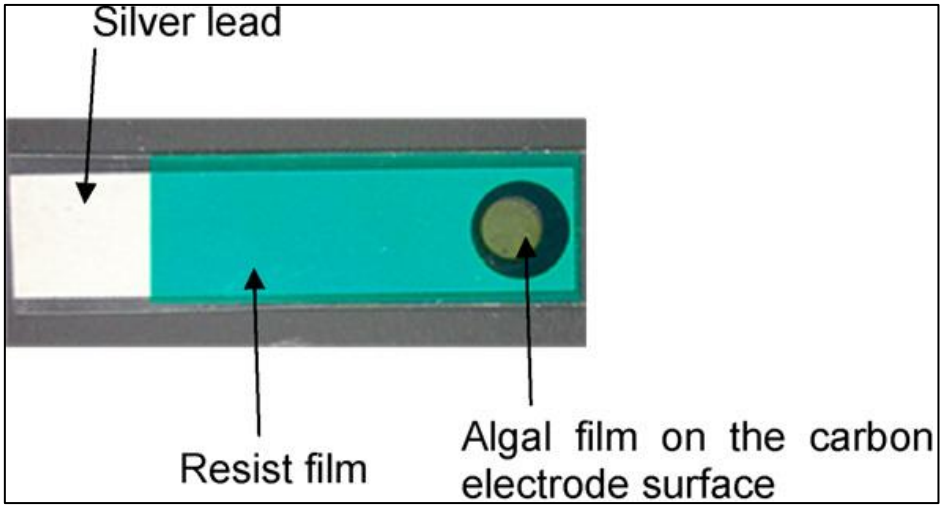

Figure 2.5. Algal based biosensor developed by Shitanda et.al for the detection of Diuron. (Shitanda et al., 2009)

The inhibiting effect on photosynthetic activity of algae is evaluated by monitoring electrochemically the photosynthetically produced oxygen and the concentration inhibiting 50% of the activity (IC_{50}) is estimated. Therefore, this value corresponds to the Diuron concentration that gives 50% inhibition of oxygen reduction current. Shitanda et al. mention that the performance of the sensor strongly depends on the immobilization technique used (Shitanda et al., 2005). Koblízek et al. present a sensor that attains very low detection limits due to the use of artificial electron acceptors and isolated PS II complexes as biological sensing element instead of whole algal cells (Koblízek et al., 2002). The system yet shows lower stability compared to whole cell biosensors.

The following table reports different systems reported for the detection of Diuron.

Table 2-1. Different systems reported in literature for Diuron detection.

	Detection method	Biological sensing element	Limit of detection	Measurement time
Del Mar Parrilla Vázquez et al., 2014	Liquid chromatography with mass spectroscopy	-	4-20pM	n.d
Schneider et al., 1994	ELISA	Diuron haptens	0.2nM	n.d
Podola and Melkonian, 2005	Fluorescence measurement	Tetraselmis cordiformis -Scherffelia dubia	2nM	20 min exposure
Védrine et al., 2003	Fluorescence measurement	Chlorella vulgaris	0.1nM	14h stabilization time
Lefèvre et al., 2012	Fluorescence measurement	Chlamydomonas reinhardtii	7.5nM	n.d
Tibuzzi et al., 2008	Amperometric O_2 measurement	Isolated PSII	0.7nM	
Shitanda et al., 2009	Amperometric O_2 measurement	Chlorella vulgaris	30nM	4 min measurement

2.2.2.2 ***Paraquat***

Compared to Diuron, Paraquat targets photosynthetic electron flow at PSI level (Eullaffroy and Vernet, 2003). Paraquat receives the electrons that are normally transferred from PSI to ferredoxin, preventing the formation of NADPH. After receiving the electrons, Paraquat is reduced to the paraquat radical which then transfers one electron to oxygen (O_2) to form the superoxide anion ($O_2^{\cdot -}$) (Equation 2). The superoxide anion produced is transformed, through the superoxide dismutase, to H_2O_2 that can then be transformed to H_2O by peroxidases (Fuerst and Vaughn, 1990; Fedtke and Duke, 2004) (Equations 3, 4). Therefore a high concentration of H_2O_2 in the interior of the cell can indicate the presence of Paraquat and could be monitored with a sensor.

When the amounts of superoxide anions produced are very big, they cannot be effectively processed by the ROS protective, scavenging system of algae. As already stated, the electron acceptors after PSI consist in a series of three membrane-associated iron-sulfur proteins (FeS-X, FeS-A and FeS-B) and the ferredoxin (Fd). The toxic forms of oxygen created after Paraquat application, can damage the membrane of the thylakoids, giving accessibility to Fe^{3+} ions. Superoxide anion therefore gives electrons to Fe^{3+} that is reduced to Fe^{2+} (Equation 5). When the latter reacts with H_2O_2 it produces the hydroxyl ion (OH^-) and the highly toxic hydroxyl radical ($OH^{\cdot}$) (Fedtke and Duke, 2004) (Equation 6). Monitoring of the hydroxyl ion (OH^-) with a pH sensor can therefore be an efficient indicator of the presence of Paraquat.

The equations describing the previously mentioned mechanism through which Paraquat affects photosynthesis are presented in the following part and are found in Chapter 7 of Plant Toxicology (Fedtke and Duke, 2004):

$$2\ Paraquat^{+} + 2\ O_2 \rightarrow\ 2\ Paraquat^{2+} + 2\ O_{\dot{2}}{}^{-} \qquad (Equation\ 2)$$

$$2\ O_{\dot{2}}{}^{-} + 2\ H^{+} \xrightarrow{superoxide\ dismutase} H_2O_2 + O_2 \qquad (Equation\ 3)$$

$$H_2O_2 + RH_2 \xrightarrow{peroxidase} 2\ H_2O + R \qquad (Equation\ 4)$$

$$O_{\dot{2}}{}^{-} + \ [Fe^{3+}] \xrightarrow{iron\ complex} O_2 + [Fe^{2+}] \qquad (Equation\ 5)$$

$$[Fe^{2+}] + H_2O_2 \xrightarrow{Fenton\ reaction} [Fe^{2+}] + \cdot OH + OH^{-} \qquad (Equation\ 6)$$

In literature, when Paraquat is detected through bioassays, the most common methods applied are conventional growth tests and optical-based techniques using fluorescent molecules as markers to measure Paraquat-induced changes in intracellular produced H_2O_2 or pH level (Zhang, 2010; Prado et al., 2012a). These molecules enter the cell and form fluorescent compounds when reacting with the produced H_2O_2 or depending on the pH ; for instance, fluorescent emission increases with increasing pH for the fluorochrome 2′,7′-bis(2-carboxyethyl)-5(6)-carboxyfluorescein (BCECF AM) (Prado et al., 2012a). The fluorescent compounds emit fluorescence when excited with light of a particular wavelength. Inverted fluorescent microscope (Zhang, 2010) as well as flow cytometry (Prado et al., 2012b) have therefore been used to monitor fluorescent signals resulting from the reaction between the fluorescent molecules and H_2O_2 or modifications in pH. To the best of our knowledge, electrochemical detection of H_2O_2 and pH that indicate the presence of Paraquat through bioassays, are not reported in literature. Since the final goal is to develop a simple, easily integrated and portable system, aspects not covered by the techniques mentioned, it is important to orient the study towards monitoring of these electroactive species with the electrochemical sensor.

2.2.3 Electroactive species to be monitored

The aforementioned information on the mode of action of the Diuron and Paraquat on photosynthetic activity can point out the electroactive species that can be monitored in order to detect the two herbicides. In the presence of Diuron, the production rate of oxygen (O_2) is modified and can be observed even at extracellular level while in the presence of Paraquat, production of hydrogen peroxide (H_2O_2) and pH related ions (H_3O^+/ OH^-) in the intracellular level is modified. Measuring modifications in their concentration in a polluted sample compared to a non-polluted, control sample can therefore reflect the presence of the herbicides.

Monitoring of these electroactive species, possibly coupled with fluorescence-based sensor already developed in UQAM, can possibly provide a complete image on the presence of the two types of herbicides, representing groups of widely used herbicides and therefore provide the versatile tool, needed for the application.

The electrochemical detection of each electroactive species requires specific, appropriate materials. As a matter of fact, different sensors have been developed for the detection of the species mentioned above (O_2, H_2O_2, H_3O^+/OH^- ions). Two basic detection methods, amperometry and potentiometry have been discussed and various electrode materials have been mentioned. A literature review will be presented in the following paragraph, after introducing the basic electrochemical principles.

2.3 Electrochemistry: Basic principles and methods

Prior to introducing electrode materials that will be used for the detection of the three electroactive elements (O_2, H_2O_2, H_3O^+/OH^- - pH related ions), it is necessary to present the basic electrochemical concepts and methods that are employed throughout the present study (Bard and Faulkner, 2001).

2.3.1 Amperometry

The basic measurement principle of amperometric techniques lies in applying a particular potential difference which initiates the desired electrochemical reaction, i.e an oxidation or reduction. There are two types of reactions taking place: faradaic and non-faradaic.

Faradaic reactions are the reactions during which electrons are transferred at the interface electrode-solution. The signal produced by these reactions is the signal that needs to be eventually measured for the species of interest.

The electrochemical reaction can be an oxidation or a reduction and results to an electron transfer. The oxidant is the species giving electrons while the reductant is the species receiving electrons (Equation 7).

$$v_{Ox}\, Ox + n\, e^{-} \leftrightarrow v_{Red}\, Red \qquad (Equation\ 7)$$

These reactions follow Faraday's law (Equation 8) and indicate that the current circulating in the system is proportional to the quantity of electroactive species chemically transformed and is a function of their concentration in the solution examined.

$$Q = I\, t = n\, F\, N \qquad (Equation\ 8)$$

Where:

Q: corresponding charge passing through the electrode/electrolyte interface

I: the generated current

n: the number of electrons exchanged per mole

F: the Faraday constant (96500 C.mol^{-1})

N: the moles of the reactant species consumed

The reaction generating the current at a particular potential is representative of the presence of a particular electroactive species, considering a particular electrode material.

Non-faradaic reactions, such as adsorption and desorption of ionic species on the surface, are taking place at the interface of the electrode with the solution.

2.3.1.1 ***Electrochemical cell***

An electrolytic cell typically is a setup of two or three electrodes, the working, the reference and the counter electrode. The working electrode (WE) is the electrode of interest, where we observe the reactions taking place as they give information on the analytical characteristics of the solution examined. The reference electrode (RE) is an electrode of fixed electrochemical potential which is not changed when current flows through the system. A potential difference is applied between the two electrodes in order to initiate the electrochemical reaction. The generated current flows between the working and the counter/auxiliary electrodes (CE). This current is the result of the electrochemical reaction taking place. The entire system is directed by a potentiostat consisting principally in an operational amplifier. The potentiostat enables to maintain the potential difference between working

and reference electrodes at a constant value, independently of the current circulating through the cell Ruffien-Ciszak, 2005. It is possible to omit the counter electrode and let current flow between working and reference electrode, when current is sufficiently low, yielding a two-electrode system. However, when the current is of large amplitude (typically larger than pA), a three-electrode system is used so that the current will not pass through the reference electrode and will not cause a change in its potential.

2.3.1.2 ***Microelectrodes***

The introduction of microelectrodes in electrochemical measurements has opened new areas of applications since around 1980. According to Bard et al. (Bard and Faulkner, 2001), there is still no widely accepted definition of the ultramicroelectrodes (UMEs). However, in this reference (Bard and Faulkner, 2001), the term "ultramicroelectrodes" is referring to electrodes having a critical dimension smaller than 25µm.

Various types of microelectrodes have been used in different applications with the most common being disk-shaped microelectrodes, followed by spherical, bands and cylindrical.

We will now focus on disk microelectrodes as they are most commonly used. Planar diffusion is occurring towards the plane of the microelectrode, similar to conventional electrodes of bigger size (presented in Figure 2.6 a), and radial diffusion from the edges of the microelectrode is also a prominent phenomenon (Figure 2.6 b). Mass transport towards microelectrode surface is therefore taking place in two dimensions, compared to conventional sized electrodes, where only planar diffusion has a significant effect.

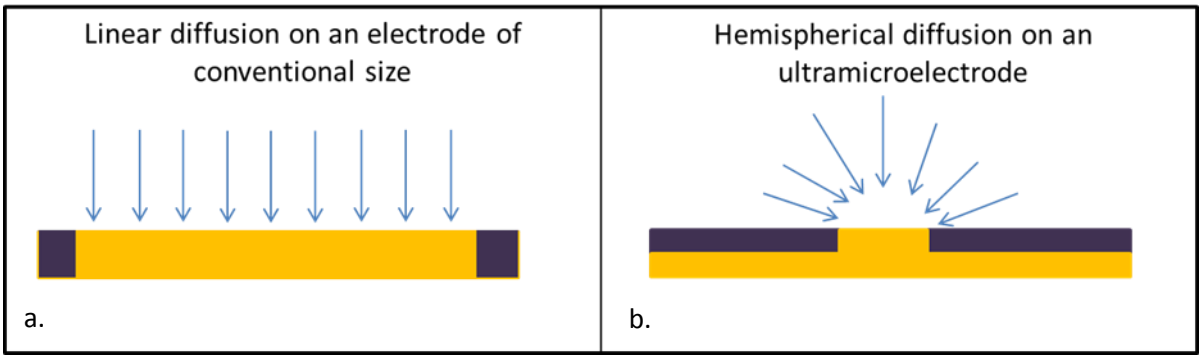

Figure 2.6. Diffusion profiles depending on electrode size: (a) linear diffusion on an electrode of conventional size. (b) hemispherical diffusion on a microelectrode.

The simplified expression of the current (Equation 9) at the steady state, called I_{lim}, obtained at a constant potential, at planar, disk-shaped microelectrode was reported by Saito (Saito, 1968) and gives the relationship between recorded current and concentration of analyte, for a given electrode surface.

$$I_{lim} = 4\,nFDC^{sol}r_d \qquad (Equation\ 9)$$

Where:

n: the number of electrons exchanged per mole

F: Faraday constant

D: diffusion coefficient

C^{sol}: analyte concentration in the solution

r_d: microelectrode radius

Microelectrodes present several advantages due to their small size:

- Mass transport is enhanced due to the non-negligible diffusion from the edges resulting in greater current density and better signal-to-noise ratio. Steady-state regimes of diffusion are therefore achieved in shorter time (Amatore et al., 2012), producing currents independent of time. This behavior is similar to the one obtained with a rotating disk electrode or a solution under mechanical agitation.

- When an electrode comes into contact with the solution, the interface resembles to a capacitor. An array of charged, oriented species is formed at the interface electrode-solution which is called electrical double-layer and is characterized by a capacitance. The capacitive current, associated to the double layer depends on the geometry and the size of the electrode. Therefore, one more significant advantage is the smaller double-layer capacitance, which is related to the smaller surface of the microelectrodes. The current recorded throughout an experiment is the sum of the faradaic, representative of the electroactive species to be detected, and capacitive currents. This feature is important when lower concentrations of species need to be detected and the faradaic current generated is low and comparable to the capacitive current. When using microelectrodes, the capacitive current is small and therefore the ratio faradaic-to-capacitive current is high, yielding higher sensitivity.

- Furthermore, given the fact that the faradaic current intensity is proportional to the electrode surface, microelectrodess yield low currents. Ohmic drop is the product of the resistance of the solution and the current flowing in the system. Highly resistive solutions or high currents induce a modification of the potential applied. Therefore, the ohmic drop in microelectrodes is not important and measurements can even be conducted in highly resistive electrolytes (Devynck and Chivot, 1991).

- Finally, as the electroactive area is limited, the consumption of analyte species is low in quantity. The composition of the analyte sample is therefore not significantly modified.

Figure 2.7 a presents a handmade fabricated platinum microelectrode sealed in a glass capillary developed by Ruffien-Ciszak, 2005, while Figure 2.7 b presents an electrochemical microcell fabricated using microfabrication technology by Popovtzer et al., 2008.

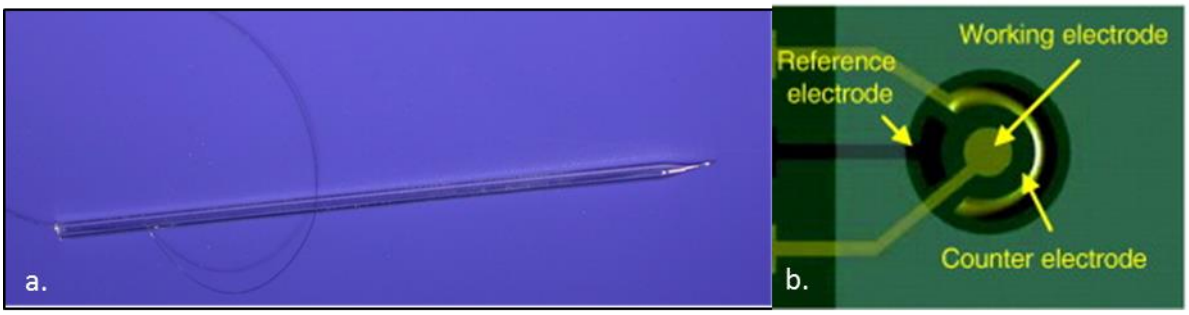

Figure 2.7. (a) Handmade platinum microelectrode (d=120 µm) sealed in a glass capillary (Ruffien-Ciszak, 2005). (b) an electrochemical 100 nL microcell fabricated using microfabrication technology (Popovtzer et al., 2008)

2.3.1.3 ***Ultramicroelectrode arrays***

One important limitation of microelectrodes is the low current obtained with a single microelectrode which calls for sophisticated instrumentation. This issue can be circumstanced with by using arrays of microelectrodes connected in parallel. In this way, favorable properties of microelectrodes are exploited and the total current recorded is of higher magnitude. It is however important to place the electrodes at a sufficient distance from each other so that diffusion zones of adjacent electrodes do not overlap (Davies and Compton, 2005). In case of overlapping, the array will act as a single macroelectrode and radial diffusion due to edge effects will be negligible compared to planar, linear diffusion (Figure 2.8). Eventually, the diffusion profile has an impact on the form of courant versus potential curves (Guo and Lindner, 2009).

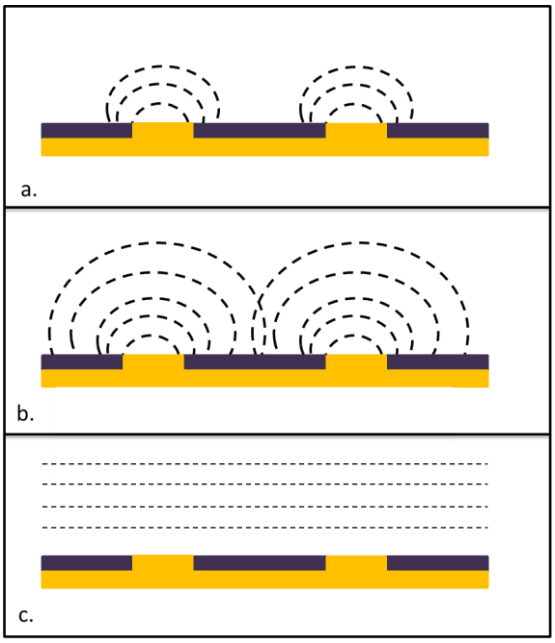

Figure 2.8. Diffusion profiles for an ultramicroelectrode array : (a) not overlapping, individual diffusion zones. (b) Overlapping diffusion zones. (c) Highly overlapping diffusion zones that lead to a linear diffusion.

For an array of disk microelectrodes where there is no overlapping of diffusion layers, the expression of the current at steady state is given by Equation 10. With *z* being the number of microelectrodes in the array, I_{lim} represents the sum of currents obtained for all ultramicroelectrodes as they are connected in parallel.

$$I_{lim} = 4\, nFDC^{sol} r_d\, z \qquad (Equation\ 10)$$

2.3.1.4 ***Amperometric methods***

For the study of the electrochemical phenomena taking place in the interface of the electrode-electrolyte, several techniques can be implemented. The electrochemical techniques employed in this study for the deposition of materials, characterization of the fabricated devices and during the bioassays are summarized.

Cyclic voltammetry

Cyclic voltammetry is one of the most commonly used techniques due to its simplicity and the big quantity of information it provides on the electrochemical phenomena taking place. It consists in varying linearly with time the potential of the working electrode and recording the current produced. Once a potential scan between two values is performed, the direction is switched and the reverse

potential scan is recorded. The potential is given as a function of the scan rate (v) and is shown in Equation 11 (where E_i is the initial potential):

$$E = E_i \pm vt \qquad (Equation\ 11)$$

By potential scanning, oxidation and reduction reactions take place. When scanning the potential towards anodic values, the reductant is oxidized and when the scan is reversed, the previously oxidized species is now reduced. The initiation of the reaction at a particular potential results in an increase in the anodic or cathodic current. The whole phenomenon is firstly limited by thermodynamics and then by the diffusion of the species from the bulk solution to the electrode's surface, when the overpotential applied is sufficiently high ($E>E_{pa}$ in figure 2.9). In the case of a macroelectrode and a non-agitated solution, current starts decreasing after attaining a maximum value since the concentration of the electroactive species on the surface of the electrode starts decreasing. The voltammogram therefore shows peaks corresponding to the oxidation and reduction reactions and the peak currents reflect the quantity of the species oxidized or reduced (Figure 2.9 a). On the other hand, in the case of an microelectrodes, diffusion is increased up to the maximum concentration gradient and concentration of species on the electrode surface remains constant with time. Provided that the scan rate is not high ($r > 1V.s^{-1}$), oxidation and reduction reactions are therefore represented by plateaus on the voltammogram, and the plateau current value is proportional to the concentration of the species in the solution (Figure 2.9 b).

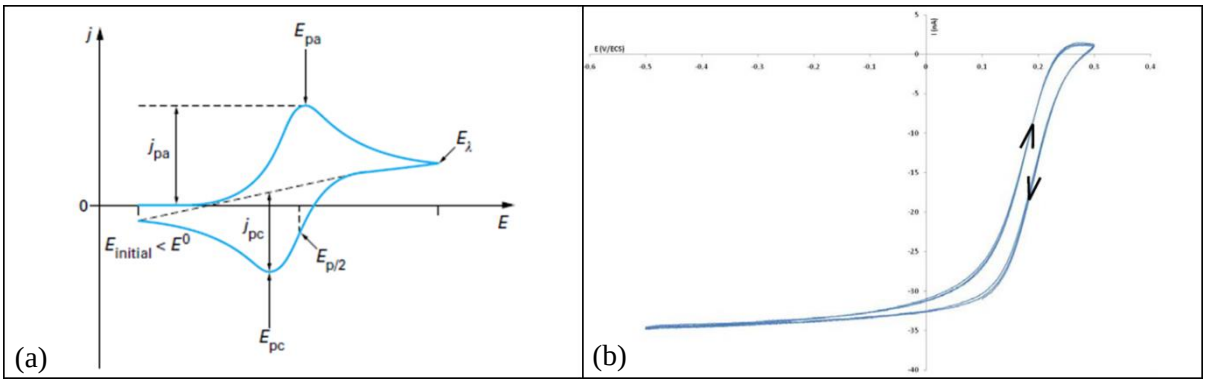

Figure 2.9. Cyclic voltammograms obtained with (a) a macroelectrode (Bedioui, 1999) and (b) microelectrode (Christophe, 2010).

Chronoamperometry

Chronoamperometry is a simple method that consists in applying a constant potential and recording the current produced over time. The potential is shifted from the equilibrium potential to the potential where the desired electrochemical reaction can take place.

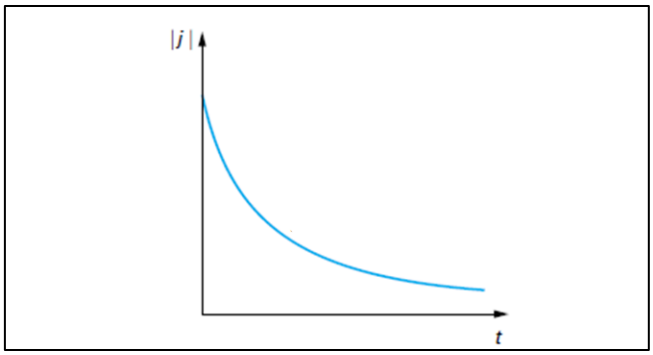

Figure 2.10. Current versus time plot on a disk microelectrode at constant potential presented by Bedioui, 1999.

Current variation as function of time follows Cottrell equation (Equation 12) when there is an electrochemical reaction and when the reaction is not limited by diffusion:

$$i(t) = \frac{nFSD^{1/2}C^{sol}}{\pi^{1/2}\, t^{1/2}} \qquad (Equation\ 12)$$

Where C_o^{sol} is the concentration in the bulk solution of the electrochemical species that is reduced or oxidized and *S* is the electroactive surface.

For microelectrodes, since diffusion is enhanced, the current reaches rapidly a steady-state value corresponding to the I_{lim} (Figure 2.10). The recorded I_{lim} current is proportional to the concentration of electroactive species in the solution and for a disk-shaped microelectrode, is given by Saito's equation (Equation 9,10).

2.3.2 Potentiometry-Open circuit potential

Potentiometry was already introduced in Chapter 1 (c.f. potentiometric biosensor) and is applied to follow the electrode potential in an equilibrium state, where no current flows through the system. The system which can be a redox couple, reacting at the electrode, is at equilibrium; no faradaic reactions occur, as no current flows. The reaction taking place is an equilibrated charge transfer between the oxidant and the reductant of the same redox couple (Equation 7).

The potential recorded in this case is called open circuit voltage (or open circuit potential or equilibrium potential) and is related to the concentration of the analyte of interest through Nernst equation (Equation 13):

$$E_{eq} = E^{o} + \frac{RT}{nF} \ln \frac{(a_{ox})^{v_{Ox}}}{(a_{red})^{v_{Red}}} \qquad \text{(Equation 13)}$$

Where:

E_{eq}: equilibrium potential

E^{o}*:* standard potential of the ion vs NHE (Normal Hydrogen electrode) reference electrode

R: universal gas constant

T: temperature

n: number of electrons exchanged for one mole

F: Faraday constant

a_i*:* activity of oxidant or reductant which is the product of their activity coefficient γ_i (cm^3. mol^{-1}) and their concentration C_i (mol. cm^{-3}). For sufficiently diluted solutions, $\gamma_i = 1$.

v_i: stoichiometric coefficients of oxidant or reductant

2.4 Electrode materials: State of the art

In order to develop the final detection systems for monitoring of the electrochemical species (O_2, H_2O_2, H_3O^+/OH^- pH related ions), serving as indicators of the presence of the two pollutants, detection materials and methods should be elaborated.

In general, the most commonly used electrode materials are metals and carbon as they are mechanically stable, chemically inert, very good electrical conductors and yield solid systems. Carbon is often found in the form of graphite, carbon black and carbon fiber while concerning metals, platinum, gold, silver and stainless steel are the most appropriate candidates for electrode structuring (Zhang et al., 2000; Grieshaber et al., 2008).

A literature review is presented that will eventually indicate the appropriate materials to be used for the detection of each electroactive species and their implementation on the final device. This review is mostly focused on materials that are easily integrated on microsystems.

2.4.1 O_2 detection

As far as oxygen monitoring is concerned, amperometry is the most commonly used method.

Noble metals (platinum or gold) are primarily used in literature as working electrode materials so that the electrode surface does not participate in the chemical reaction (Lee et al., 2007). Clark-type electrodes are the electrodes the most commonly used and were initially presented by Leland C.Clark in 1953 for oxygen measurements in blood (L. C. Clark et al., 1953). A typical Clark-type cell consists of an electrode system where the working electrode is a platinum surface (L. C. Clark et al., 1953), an oxygen permeable, selective membrane and the electrolyte (Figure 2.11).

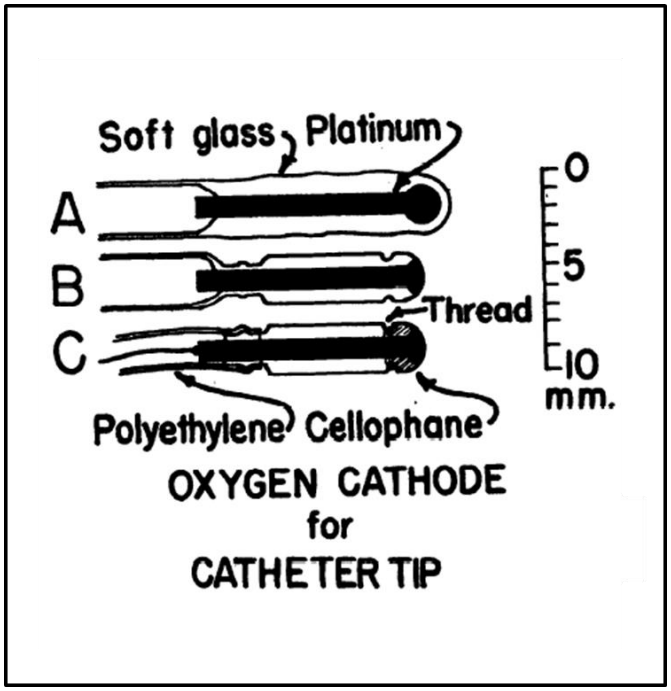

Figure 2.11. Fabrication procedure followed by Clark et al. for the implementation of the first Clark electrode. (A) A 2 mm platinum wire was first sealed in a glass tube. (B) The diameter of the glass was reduced and a recess was formed near the edge of the electrode so that the cellophane, oxygen permeable membrane can be held on the glass. (C)Cellophane membrane was placed on the tip of the electrode and a copper wire was soldered so that electrical connection will be assured. (Leland C. Clark et al., 1953).

M. Koudelka was the first to fabricate a planar, two-electrode, Clark-type sensor through thin-film fabrication technology in order to determine oxygen levels (Koudelka, 1986). Suzuki et al. reported in numerous of their works the fabrication of miniature Clark-type oxygen electrodes for biological assessments (Suzuki et al., 1990a; Suzuki et al., 1990b; Suzuki et al., 2000; Suzuki et al., 2001).

Platinum microdiscs (Sosna et al., 2007) and array of platinum microelectrodes (L. C. Clark et al., 1953) have been employed as dissolved oxygen sensors in environmental monitoring. Different

techniques, such as platinization that yields platinum black (Pt-Bl) electrodes, have been followed to enhance sensitivity by increasing electro-active surface area and porosity of platinum electrodes and therefore enhancing mass transport of species towards electrode surface (Qiang et al., 2010; Lee and Park, 2011). Indeed, sensors with platinized working electrodes yield greater sensitivity due to their nanoscale structure (Vaddiraju et al., 2010) and the large number of electroactive sites that facilitates electron transfer (Li et al., 2013).

Although platinum is the most commonly applied material in oxygen sensors, gold electrodes have been designed to measure dissolved oxygen in environmental samples (Liu et al., 2007), bacterial films (Lee et al., 2007) or during cell culture (Pereira Rodrigues et al., 2008). Carbon nanotubes integrated on a screen-printed algal biosensor have also been used to detect oxygen produced by algae (Shitanda et al., 2009).

Platinum (Pt) and platinum black (Pt Bl) are the electrode material selected for oxygen monitoring through this study as it is the most suitable candidate for oxygen detection since it is physically stable (Zhang and Wilson, 1993), mechanically robust (Ben-Amor et al., 2013), and compared to gold and other metals, is the best electrocatalyst for the oxygen reduction reaction (Maja N. Desic, 2005).

2.4.2 H_2O_2 detection

Similarly to O_2 monitoring, H_2O_2 measurement is performed through amperometry. As already stated, hydrogen peroxide is an essential species to monitor as it is taking part in various biological processes (Li et al., 2013). Biosensors containing enzyme modified electrodes (Ruzgas et al., 1996) have been widely used for H_2O_2 detection due to their high sensitivity and selectivity. Gold (Brett et al., 1997), platinum (Zhang and Wilson, 1993; Yokoyama et al., 1997), carbon based (Cho et al., 2010; Nowall and Kuhr, 1997) and Prussian Blue modified (Karyakin et al., 2009) electrodes are also situated in the main stream of research interest towards suitable working electrode materials for the detection of H_2O_2.

Platinum is still the preferred option when a simple system needs to be implemented, as it provides a good catalytic surface for H_2O_2 oxidation (Arbault et al., 1995) and it is even possible to increase active surface area of the electrodes by platinization (Pt-Bl) (Figure 2.12).

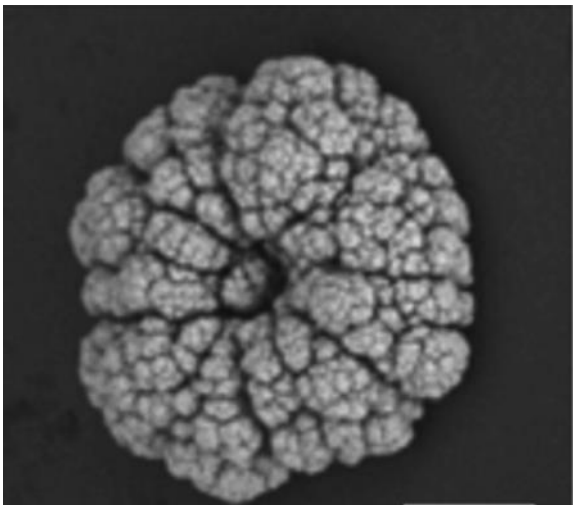

Figure 2.12. Highly porous structure of a platinized (Pt-Bl) ultramicroelectrode fabricated by Ben-Amor et al., 2013.

Furthermore, on platinum black (Pt-Bl) microelectrodes, H_2O_2 oxidation is taking place at a lower potential compared to bare Pt electrodes, minimizing interferences induced by other electroactive species (Arbault et al., 1995). Platinum black microelectrodes have been widely used to study ROS (reactive oxygen species) released during cellular oxidative bursts (Li et al., 2013) and monitor the production of H_2O_2 by mitochondria during aerobic metabolism (Ben-Amor et al., 2013). They have also found various applications as amperometric glucose sensors (De Corcuera et al., 2005).
Consequently, in our study, special emphasis was placed on the implementation of platinum (Pt) and platinum black (Pt-Bl) electrodes for H_2O_2 monitoring.

2.4.3 pH monitoring

Class electrodes have been commonly used for pH monitoring. However, glass fragility and size limitation impede in situ measurement in complex configurations and media (Ruffien-Ciszak et al., 2008; Huang et al., 2011). A considerable interest has been placed on other types of ion sensitive electrodes. Potentiometric electrodes containing electroactive polymeric membranes as ion-sensitive receptor layers have been often used (Wróblewski, 2004). An example of a pH sensitive membrane is the aminated PVC (PVC-NH_2) containing an ion carrier and a solvent plasticizer used for pH measurement in the beating heart (Cosofret et al., 1995). A drawback identified for ion-exchange membrane electrodes is their physical and chemical instability due to the use of a polymer layer as the sensitive layer.
Ion-sensitive field-effect transistor (ISFET) have also been widely used for pH monitoring and were first presented by Bergveld (Bergveld, 1970). The basic principle consists in measuring changes in the double layer capacity at the interface between the gate and the solution that results in a variation in threshold voltage of the transistor. Although ISFET devices are commonly applied, they involve

complicated fabrication procedures. Ion sensitive materials used for ISFETs are SiO_2 (Bergveld, 1970), Si_3N_4 (Matsuo and Wise, 1974), Al_2O_3 (Bousse et al., 1983) and Ta_2O_5 (Bergveld, 1970).

A powerful alternative to previously mentioned electrodes are metal/metal oxide or simply metal oxide based pH sensors that are easily miniaturized and robust (Daomin Zhou, 2008). RuO_2, OsO_2, Ta_2O_5, TiO_2 (Fog and Buck, 1984), Bi_2O_3 (Einerhand et al., 1989) and nanoporous PtO_2 (Park et al., 2005) have been reported in literature as candidates for pH monitoring with W/WO_3 (Lale et al., 2014) and IrO_x (Yamanaka, 1989) being the most commonly used. More specifically, iridium oxide films can be formed by various physical and chemical methods (Ges et al., 2005) and exhibit many advantages among which high pH sensitivity, biocompatibility, chemical stability and fast response time (Daomin Zhou, 2008; Marzouk et al., 1998). IrO_x films have therefore found applications in cell metabolism monitoring in cell cultures (Ges et al., 2005) and microenvironmental studies (Bezbaruah and Zhang, 2002). Tungsten/tungsten oxide (W/WO_3) sensors represent another attractive alternative for pH monitoring as tungsten is cheaper compared to other metals such as Pt or Au (Lale et al., 2014). Additionally, stable tungsten oxides can be easily formed by electrochemical oxidation of the metal at low potential (Ruffien-Ciszak et al., 2008). W/WO_3 sensors have been developed for skin pH monitoring (Ruffien-Ciszak et al., 2008), determination of extracellular pH values for cultured cells (Yamamoto et al., 2003) and pH measurement of environmental water samples (Dimitrakopoulos et al., 1998).

As stated by Lale et al., 2014, the W/WO_3 sensor yielded lower sensitivity towards pH monitoring compared to the IrO_x sensor. IrO_x was therefore the electrode material selected for the development of pH sensors through this work.

2.5 Conclusion

The application context was described in this chapter. The two types of herbicides, Diuron and Paraquat, that will be detected with the final device were presented with a brief description of their use, mode of application and effect on humans and other organisms. Basic parts of algal photosynthetic procedure were then introduced so that the mode of action of the aforementioned herbicides on photosynthesis could be explained. Emphasis was placed on two photosynthetic complexes, Photosystems I and II (PSI and PSII), situated in algal chloroplasts and playing a vital role in electron transport through the photosynthetic chain. Diuron targets the electron flow after PSII blocking partially or totally oxygen production while Paraquat targets electron flow after PSI resulting in ROS production and therefore a modification in the level of hydrogen peroxide and pH. The electroactive species that will serve as indicators of the presence of these two types of herbicides were therefore determined and are O_2, H_2O_2 and H_3O^+/OH^- pH related ions. A literature review, related to

the appropriate working electrode materials for the detection of the aforementioned electroactive species was then presented after a brief introduction to the basic electrochemical concepts and methods that will be needed throughout this work. This review eventually led to the selection of the electrode materials: platinum (Pt) and platinum black (Pt-Bl) were identified as the most suitable materials for the detection of O_2 and H_2O_2 while IrO_x was chosen for pH monitoring.

In order to validate the bibliographic research, the first prototypes were developed on silicon chips using the materials stated above and will be presented in the following chapter. In this way, their detection properties could be validated with the final goal to integrate them in the lab-on-chip structure.

2.6 References

Amatore, C., Pebay, C., Sella, C., Thouin, L., 2012. Mass Transport at Microband Electrodes: Transient, Quasi-Steady-State, and Convective Regimes. ChemPhysChem 13, 1562–1568. doi:10.1002/cphc.201100942

Arbault, S., Pantano, P., Jankowski, J.A., Vuillaume, M., Amatore, C., 1995. Monitoring an oxidative stress mechanism at a single human fibroblast. Anal. Chem. 67, 3382–3390.

Bard, A.J., Faulkner, L.R., 2001. Electrochemical Methods: Fundamentals and Applications, New York: Wiley, 2001, 2nd ed. JOHN WILE SONS INC. doi:10.1023/A:1021637209564

Bedioui, F., 1999. Voltampérométrie. Théorie et mise en œuvre expérimentale, in: Techniques de L'ingénieur Méthodes Électrochimiques. Editions T.I.

Ben-Amor, S., Devin, A., Rigoulet, M., Sojic, N., Arbault, S., 2013. Oxygen Plasma Treatment of Platinized Ultramicroelectrodes Increases Sensitivity for Hydrogen Peroxide Detection on Mitochondria. Electroanalysis 25, 656–663. doi:10.1002/elan.201200409

Bergveld, P., 1970. Development of an Ion-Sensitive Solid-State Device for Neurophysiological Measurements. IEEE Trans. Biomed. Eng. BME-17, 70–71. doi:10.1109/TBME.1970.4502688

Bezbaruah, A.N., Zhang, T.C., 2002. Fabrication of anodically electrodeposited iridium oxide film pH microelectrodes for microenvironmental studies. Anal. Chem. 74, 5726–5733.

Bhadekar, R., 2011. Developments in Analytical Methods for Detection of Pesticides in Environmental Samples. Am. J. Anal. Chem. 02, 1–15. doi:10.4236/ajac.2011.228118

Bousse, L., De Rooij, N.F., Bergveld, P., 1983. Operation of chemically sensitive field-effect sensors as a function of the insulator-electrolyte interface. IEEE Trans. Electron Devices 30, 1263–1270. doi:10.1109/T-ED.1983.21284

Brayner, R., Couté, A., Livage, J., Perrette, C., Sicard, C., 2011. Micro-algal biosensors. Anal. Bioanal. Chem. 401, 581–597. doi:10.1007/s00216-011-5107-z

Brett, A.M.O., Matysik, F.-M., Vieira, M.T., 1997. Thin-film gold electrodes produced by magnetron sputtering. Voltammetric characteristics and application in batch injection analysis with amperometric detection. Electroanalysis 9, 209–212. doi:10.1002/elan.1140090304

Cho, S.-H., Jang, A., Bishop, P.L., Moon, S.-H., 2010. Kinetics determination of electrogenerated hydrogen peroxide (H2O2) using carbon fiber microelectrode in electroenzymatic degradation of phenolic compounds. J. Hazard. Mater. 175, 253–257. doi:10.1016/j.jhazmat.2009.09.157

Christophe, C., 2010. Thesis. Intégration de microcapteurs électrochimiques en technologies "Silicium et Polymères" pour l'étude du stress oxydant. Application à la biochimie cutanée. Université Paul Sabatier - Toulouse III.

Cosofret, V.V., Erdosy, M., Johnson, T.A., Buck, R.P., Ash, R.B., Neuman, M.R., 1995. Microfabricated Sensor Arrays Sensitive to pH and K+ for Ionic Distribution Measurements in the Beating Heart. Anal. Chem. 67, 1647–1653. doi:10.1021/ac00106a001

Daomin Zhou, D., 2008. Chapter 10 - Microelectrodes for in-vivo determination of pH, in: Zhang, X., Ju, H., Wang, J. (Eds.), Electrochemical Sensors, Biosensors and Their Biomedical Applications. Academic Press, San Diego, pp. 261–305.

Davies, T.J., Compton, R.G., 2005. The cyclic and linear sweep voltammetry of regular and random arrays of microdisc electrodes: Theory. J. Electroanal. Chem. 585, 63–82. doi:10.1016/j.jelechem.2005.07.022

Davison, I.R., 1991. Environmental Effects on Algal Photosynthesis: Temperature. J. Phycol. 27, 2–8. doi:10.1111/j.0022-3646.1991.00002.x

De Corcuera, J.I.R., R.P. Cavalieri, Powers, J.R., 2005. Improved platinization conditions produce a 60-fold increase in sensitivity of amperometric biosensors using glucose oxidase immobilized in poly-o-phenylenediamine. J. Electroanal. Chem. 575, 229–241. doi:10.1016/j.jelechem.2004.09.015

Devynck, J., Chivot, J., 1991. Voltampérométrie aux ultramicroélectrodes, in: Techniques de L'ingénieur Méthodes Électrochimiques. Paris. Editions T.I.

Dimitrakopoulos, L.T., Dimitrakopoulos, T., Alexander, P.W., Logic, D., Hibbert, D.B., 1998. A tungsten oxide coated wire electrode used as a pH sensor in flow injection potentiometry. Anal. Commun. 35, 395–398. doi:10.1039/A807697I

Einerhand, R.E.F., Visscher, W.H.M., Barendrecht, E., 1989. pH measurement in strong KOH solutions with a bismuth electrode. Electrochimica Acta 34, 345–353. doi:10.1016/0013-4686(89)87010-0

Eullaffroy, P., Vernet, G., 2003. The F684/F735 chlorophyll fluorescence ratio: a potential tool for rapid detection and determination of herbicide phytotoxicity in algae. Water Res. 37, 1983–1990. doi:10.1016/S0043-1354(02)00621-8

Fedtke, C., Duke, S., 2004. Plant Toxicology, Fourth Edition.

Fog, A., Buck, R.P., 1984. Electronic semiconducting oxides as pH sensors. Sens. Actuators 5, 137–146. doi:10.1016/0250-6874(84)80004-9

Fuerst, E.P., Vaughn, K.C., 1990. Mechanisms of Paraquat Resistance. Weed Technol. 4, 150–156.

Ges, I.A., Ivanov, B.L., Schaffer, D.K., Lima, E.A., Werdich, A.A., Baudenbacher, F.J., 2005. Thin-film IrOx pH microelectrode for microfluidic-based microsystems. Biosens. Bioelectron. 21, 248–256. doi:10.1016/j.bios.2004.09.021

Giardi, M.T., Pace, E., 2005. Photosynthetic proteins for technological applications. Trends Biotechnol. 23, 257–263. doi:10.1016/j.tibtech.2005.03.003

Government of Canada, H.C., 1997. Diuron [Technical document - Chemical/Physical Parameters] [WWW Document]. URL http://www.hc-sc.gc.ca/ewh-semt/pubs/water-eau/diuron/index-eng.php (accessed 10.30.14).

Grieshaber, D., MacKenzie, R., Vörös, J., Reimhult, E., 2008. Electrochemical Biosensors - Sensor Principles and Architectures. Sensors 8, 1400–1458. doi:10.3390/s8031400

Guo, J., Lindner, E., 2009. Cyclic Voltammograms at Coplanar and Shallow Recessed Microdisk Electrode Arrays: Guidelines for Design and Experiment. Anal. Chem. 81, 130–138. doi:10.1021/ac801592j

Haigh-Flórez, D., de la Hera, C., Costas, E., Orellana, G., 2014. Microalgae dual-head biosensors for selective detection of herbicides with fiber-optic luminescent O2 transduction. Biosens. Bioelectron. 54, 484–491. doi:10.1016/j.bios.2013.10.062

Huang, W.-D., Cao, H., Deb, S., Chiao, M., Chiao, J.C., 2011. A flexible pH sensor based on the iridium oxide sensing film. Sens. Actuators Phys. 169, 1–11. doi:10.1016/j.sna.2011.05.016

Karyakin, A.A., Kuritsyna, E.A., Karyakina, E.E., Sukhanov, V.L., 2009. Diffusion controlled analytical performances of hydrogen peroxide sensors: Towards the sensor with the largest dynamic range. Electrochimica Acta 54, 5048–5052. doi:10.1016/j.electacta.2008.11.049

Koblízek, M., Malý, J., Masojídek, J., Komenda, J., Kucera, T., Giardi, M.T., Mattoo, A.K., Pilloton, R., 2002. A biosensor for the detection of triazine and phenylurea herbicides designed using Photosystem II coupled to a screen-printed electrode. Biotechnol. Bioeng. 78, 110–116.

Koudelka, M., 1986. Performance characteristics of a planar “clark-type” oxygen sensor. Sens. Actuators 9, 249–258. doi:10.1016/0250-6874(86)80025-7

Lale, A., Tsopela, A., Civelas, A., Salvagnac, L., Launay, J., Temple-Boyer, P., 2014. Integration of tungsten layers for the mass fabrication of WO3-based pH-sensitive potentiometric microsensors. Sens. Actuators B Chem. 206, 152–158.

Lee, J.-H., Lim, T.-S., Seo, Y., Bishop, P.L., Papautsky, I., 2007. Needle-type dissolved oxygen microelectrode array sensors for in situ measurements. Sens. Actuators B Chem. 128, 179–185. doi:10.1016/j.snb.2007.06.008

Lee, Y.J., Park, J.Y., 2011. A Highly Miniaturized Dissolved Oxygen Sensor Using a Nanoporous Platinum Electrode Electroplated on Silicon. J. Korean Phys. Soc. 58, 1505. doi:10.3938/jkps.58.1505

Lefèvre, F., Chalifour, A., Yu, L., Chodavarapu, V., Juneau, P., Izquierdo, R., 2012. Algal fluorescence sensor integrated into a microfluidic chip for water pollutant detection. Lab. Chip 12, 787–793. doi:10.1039/C2LC20998E

Leland C. Clark, J.R., Wolf, R., Granger, D., Taylor, Z., 1953. Continuous Recording of Blood Oxygen Tensions by Polarography. J. Appl. Physiol. 6, 189–193.

Li, Y., Sella, C., Lemaître, F., Guille Collignon, M., Thouin, L., Amatore, C., 2013. Highly Sensitive Platinum-Black Coated Platinum Electrodes for Electrochemical Detection of Hydrogen

Peroxide and Nitrite in Microchannel. Electroanalysis 25, 895–902. doi:10.1002/elan.201200456

Liu, S.-Y., Liu, G., Tian, Y.-C., Chen, Y.-P., Yu, H.-Q., Fang, 2007. An Innovative Microelectrode Fabricated Using Photolithography for Measuring Dissolved Oxygen Distributions in Aerobic Granules. Environ. Sci. Technol. 41, 5447–5452. doi:10.1021/es070532g

Ma, J., Zheng, R., Xu, L., Wang, S., 2002. Differential Sensitivity of Two Green Algae, Scenedesmus obliqnus and Chlorella pyrenoidosa, to 12 Pesticides. Ecotoxicol. Environ. Saf. 52, 57–61. doi:10.1006/eesa.2002.2146

MAJA N. DESIC, M.M.P., 2005. Study of gold-platinum and platinum-gold surface modification and its influence on hydrogen evolution and oxygen reduction. J. Serbian Chem. Soc.

Malato, S., Blanco, J., Cáceres, J., Fernández-Alba, A.R., Agüera, A., Rodríguez, A., 2002. Photocatalytic treatment of water-soluble pesticides by photo-Fenton and TiO2 using solar energy. Catal. Today 76, 209–220. doi:10.1016/S0920-5861(02)00220-1

Marzouk, S.A., Ufer, S., Buck, R.P., Johnson, T.A., Dunlap, L.A., Cascio, W.E., 1998. Electrodeposited iridium oxide pH electrode for measurement of extracellular myocardial acidosis during acute ischemia. Anal. Chem. 70, 5054–5061.

Matsuo, T., Wise, K.D., 1974. An Integrated Field-Effect Electrode for Biopotential Recording. IEEE Trans. Biomed. Eng. BME-21, 485–487. doi:10.1109/TBME.1974.324338

Naessens, M., Leclerc, J.C., Tran-Minh, C., 2000. Fiber Optic Biosensor Using Chlorella vulgaris for Determination of Toxic Compounds. Ecotoxicol. Environ. Saf. 46, 181–185. doi:10.1006/eesa.1999.1904

Nowall, W.B., Kuhr, W.G., 1997. Detection of hydrogen peroxide and other molecules of biologicl importance at an electrocataltic surface on a carbon fiber microelectrode. Electroanalysis 9, 102–109. doi:10.1002/elan.1140090203

Park, S., Boo, H., Kim, Y., Han, J.-H., Kim, H.C., Chung, T.D., 2005. pH-Sensitive Solid-State Electrode Based on Electrodeposited Nanoporous Platinum. Anal. Chem. 77, 7695–7701. doi:10.1021/ac050968j

Pereira Rodrigues, N., Sakai, Y., Fujii, T., 2008. Cell-based microfluidic biochip for the electrochemical real-time monitoring of glucose and oxygen. Sens. Actuators B Chem. 132, 608–613. doi:10.1016/j.snb.2007.12.025

Podola, B., Melkonian, M., 2005. Selective real-time herbicide monitoring by an array chip biosensor employing diverse microalgae. J. Appl. Phycol. 17, 261–271. doi:10.1007/s10811-005-4945-5

Popovtzer, R., Neufeld, T., Popovtzer, A., Rivkin, I., Margalit, R., Engel, D., Nudelman, A., Rephaeli, A., Rishpon, J., Shacham-Diamand, Y., 2008. Electrochemical lab on a chip for high-throughput analysis of anticancer drugs efficiency. Nanomed. Nanotechnol. Biol. Med. 4, 121–126. doi:10.1016/j.nano.2008.03.002

Prado, R., Rioboo, C., Herrero, C., Cid, Á., 2012a. Screening acute cytotoxicity biomarkers using a microalga as test organism. Ecotoxicol. Environ. Saf. 86, 219–226. doi:10.1016/j.ecoenv.2012.09.015

Prado, R., Rioboo, C., Herrero, C., Suárez-Bregua, P., Cid, A., 2012b. Flow cytometric analysis to evaluate physiological alterations in herbicide-exposed Chlamydomonas moewusii cells. Ecotoxicol. Lond. Engl. 21, 409–420. doi:10.1007/s10646-011-0801-3

Qiang, L., Vaddiraju, S., Rusling, J.F., Papadimitrakopoulos, F., 2010. Highly sensitive and reusable Pt-black microfluidic electrodes for long-term electrochemical sensing. Biosens. Bioelectron. 26, 682–688. doi:10.1016/j.bios.2010.06.064

Raven, P., Johnson, G., 2002. Photosynthesis, in: Biology. London. Mc Graw Hill.

Rodriguez Jr, M., Sanders, C.A., Greenbaum, E., 2002. Biosensors for rapid monitoring of primary-source drinking water using naturally occurring photosynthesis. Biosens. Bioelectron. 17, 843–849. doi:10.1016/S0956-5663(02)00059-3

Ross, M., Childs DJ, 1996. Herbicide Mode-of-Action Summary. Purdue Univ. Dep. Bot. Plant Pathol. West Lafayette Rep. No WS-23-W.

Ruffien-Ciszak, A., 2005. Thesis. Potentialités des microélectrodes pour une évaluation directe et non invasive des propriétés antioxydantes du stratum corneum. Toulouse 3.

Ruffien-Ciszak, A., Baur, J., Gros, P., Questel, E., Comtat, M., 2008. Electrochemical microsensors for cutaneous surface analysis: Application to the determination of pH and the antioxidant properties of stratum corneum. IRBM 29, 162–170. doi:10.1016/j.rbmret.2007.11.020

Ruzgas, T., Csöregi, E., Emnéus, J., Gorton, L., Marko-Varga, G., 1996. Peroxidase-modified electrodes: Fundamentals and application. Anal. Chim. Acta 330, 123–138. doi:10.1016/0003-2670(96)00169-9

Saito, Y., 1968. A Theoretical Study on the Diffusion Current at the Stationary Electrodes of Circular and Narrow Band Types. Rev. Polarogr. 15, 177–187. doi:10.5189/revpolarography.15.177

Schubnell, D., Lehmann, M., Baumann, W., Rott, F.G., Wolf, B., Beck, C.F., 1999. An ISFET-algal (Chlamydomonas) hybrid provides a system for eco-toxicological tests. Biosens. Bioelectron. 14, 465–472. doi:10.1016/S0956-5663(99)00025-1

Scognamiglio, V., Raffi, D., Lambreva, M., Rea, G., Tibuzzi, A., Pezzotti, G., Johanningmeier, U., Giardi, M.T., 2009. Chlamydomonas reinhardtii genetic variants as probes for fluorescence sensing system in detection of pollutants. Anal. Bioanal. Chem. 394, 1081–1087. doi:10.1007/s00216-009-2668-1

Shitanda, I., Takada, K., Sakai, Y., Tatsuma, T., 2005. Compact amperometric algal biosensors for the evaluation of water toxicity. Anal. Chim. Acta 530, 191–197. doi:10.1016/j.aca.2004.09.073

Shitanda, I., Takamatsu, S., Watanabe, K., Itagaki, M., 2009. Amperometric screen-printed algal biosensor with flow injection analysis system for detection of environmental toxic compounds. Electrochim. Acta 54, 4933–4936. doi:10.1016/j.electacta.2009.04.005

Sosna, M., Denuault, G., Pascal, R.W., Prien, R.D., Mowlem, M., 2007. Development of a reliable microelectrode dissolved oxygen sensor. Sens. Actuators B Chem. 123, 344–351. doi:10.1016/j.snb.2006.08.033

Suzuki, H., Arakawa, H., Karube, I., 2001. Fabrication of a sensing module using micromachined biosensors. Biosens. Bioelectron. 16, 725–733.

Suzuki, H., Hirakawa, T., Sasaki, S., Karube, I., 2000. An integrated module for sensing pO2, pCO2, and pH. Anal. Chim. Acta 405, 57–65. doi:10.1016/S0003-2670(99)00748-5

Suzuki, H., Kojima, N., Sugama, A., Takei, F., Ikegami, K., 1990a. Disposable oxygen electrodes fabricated by semiconductor techniques and their application to biosensors. Sens. Actuators B Chem. 1, 528–532. doi:10.1016/0925-4005(90)80266-3

Suzuki, H., Sugama, A., Kojima, N., 1990b. Miniature Clark-type oxygen electrode with a three-electrode configuration. Sens. Actuators B Chem. 2, 297–303. doi:10.1016/0925-4005(90)80157-U

Taiz, L., Zeiger, E., 2006. Photosynthesis: The Light Reactions, in: Plant Physiology. Sinauer.

Tasmin, R., Shimasaki, Y., Tsuyama, M., Qiu, X., Khalil, F., Okino, N., Yamada, N., Fukuda, S., Kang, I.-J., Oshima, Y., 2014. Elevated water temperature reduces the acute toxicity of the widely used herbicide diuron to a green alga, Pseudokirchneriella subcapitata. Environ. Sci. Pollut. Res. Int. 21, 1064–1070. doi:10.1007/s11356-013-1989-y

USDA, 1999. Agricultural Chemical Usage: 1998 Field Crop Summary. US Department of Agriculture, Washington, DC.

Vaddiraju, S., Tomazos, I., Burgess, D.J., Jain, F.C., Papadimitrakopoulos, F., 2010. Emerging synergy between nanotechnology and implantable biosensors: A review. Biosens. Bioelectron. 25, 1553–1565. doi:10.1016/j.bios.2009.12.001

Wittkampf, M., Chemnitius, G.-C., Cammann, K., Rospert, M., Mokwa, W., 1997. Silicon thin film sensor for measurement of dissolved oxygen. Sens. Actuators B Chem. 43, 40–44. doi:10.1016/S0925-4005(97)00138-X

Wróblewski, W., 2004. Towards advanced chemical microsensors—an overview. Talanta 63, 33–39. doi:10.1016/j.talanta.2003.11.020

Yamamoto, K., Shi, G., Zhou, T., Xu, F., Zhu, M., Liu, M., Kato, T., Jin, J.-Y., Jin, L., 2003. Solid-state pH ultramicrosensor based on a tungstic oxide film fabricated on a tungsten nanoelectrode and its application to the study of endothelial cells. Anal. Chim. Acta 480, 109–117. doi:10.1016/S0003-2670(02)01602-1

Yamanaka, K., 1989. Anodically Electrodeposited Iridium Oxide Films (AEIROF) from Alkaline Solutions for Electrochromic Display Devices. Jpn. J. Appl. Phys. 28, 632. doi:10.1143/JJAP.28.632

Yokoyama, H., Tsuchihashi, N., Kasai, N., Matsue, T., Uchida, I., Mori, N., Ohya-Nishiguchi, H., Kamada, H., 1997. Hydrogen peroxide augmentation in a rat striatum after

methamphetamine injection as monitored in vivo by a Pt-disk microelectrode. Biosens. Bioelectron. 12, 1037–1041.

Zhang, S., Wright, G., Yang, Y., 2000. Materials and techniques for electrochemical biosensor design and construction. Biosens. Bioelectron. 15, 273–282. doi:10.1016/S0956-5663(00)00076-2

Zhang, W.-H., 2010. Antioxidant attenuation of ROS-involved cytotoxicity induced by Paraquat on HL-60 cells. Health (N. Y.) 02, 253–261. doi:10.4236/health.2010.23036

Zhang, Y., Wilson, G.S., 1993. Electrochemical oxidation of H2O2 on Pt and Pt + Ir electrodes in physiological buffer and its applicability to H2O2-based biosensors. J. Electroanal. Chem. 345, 253–271. doi:10.1016/0022-0728(93)80483-X

Chapter 3
Silicon-based devices: First prototype

Prior to the development of the final lab-on-chip device, the detection principle as well as the electrode materials that were going to be integrated needed to be validated using a simpler device. An electrochemical system, similar to the one intended for final application was fabricated on silicon substrate by means of silicon-based microfabrication technology, involving already validated and standard microfabrication procedures. Furthermore, the fact that fluidic structure is not yet integrated on the device provides many advantages regarding pre-validation tests. Indeed, fabrication and packaging procedures are simple and can therefore yield a great number of reduced-size chips that can be used in numerous tests. Moreover, characterization and validation of detection principle are easier to perform as the device is simpler. The autonomous electrochemical cell consisted in three electrodes integrated on the same silicon chip. Platinum (Pt), platinum black (Pt-Bl) and iridium oxide (Pt/IrO_x) working microelectrodes were developed. Ag/AgCl and Pt electrodes were used as quasi-reference and counter integrated electrodes, respectively. The microelectrodes were employed for the detection of O_2, H_2O_2 and pH related ions H_3O^+/OH^-, species taking part in photosynthetic and metabolic activities of algae. Fabricated microelectrodes were electrochemically characterized to validate the characteristics of deposited electrode materials and calibrated to determine their detection properties.

3.1 Device conception

Electrochemical microcells designed for this work consist of a three-electrode electrochemical system comprised of a working microelectrode, a pseudo-reference electrode and a counter electrode. In order to determine the arrangement and form of the three integrated electrodes, different electrode configurations were patterned. Based on previous works (Nassi et al., 2012; Christophe, 2010), concentric arrangements were tested for single microelectrodes and UME arrays (Figure 3.1 a, b respectively).

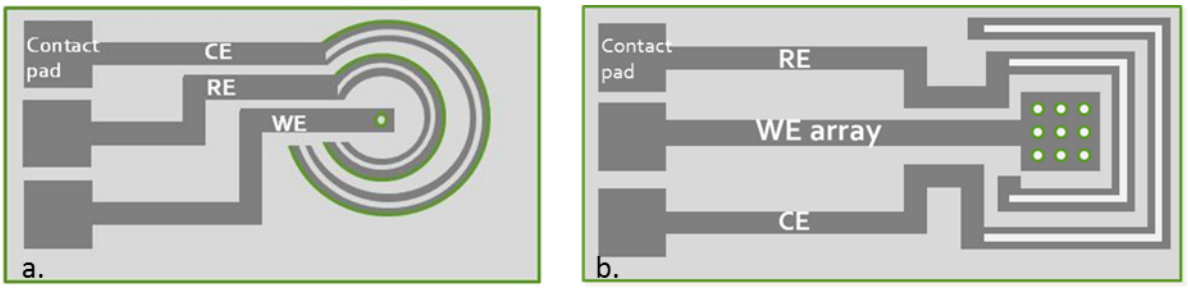

Figure 3.1. Schematic representation of concentric configurations tested: a) single microelectrode b) UME array.

Concentric configuration was preferred to parallel due to its symmetry and homogeneity concerning its electric field lines. Working microelectrode was placed in the middle of the structure and was encircled by the reference and counter electrodes.

As far as working microelectrode dimensions are concerned, the diameter of the single microelectrode was 50 µm while each UME forming the 5 x 5 UME array had a diameter of 10 µm. Distance between ultraelectrodes in the array was determined so that diffusion profiles of adjacent electrodes will not overlap and yield planar diffusion profiles similar to the ones obtained with macroelectrodes. There have been many studies dealing with the required distance so that each UME of the array acts as a unique UME (Davies and Compton, 2005). Berduque et al. (Berduque et al., 2007) consider that a sufficient distance is 33 times the disk diameter whereas Gardner et al. and Wittkampf et al. (Gardner et al., 2009, Wittkampf et al., 1997) consider that a 10 times ratio is acceptable. Given the fact that there is currently no actual limitation concerning the size of the array, a large centre-to-centre spacing of 500 µm was selected.

Reference and counter electrodes were designed with surfaces much more important than the surface of working microelectrode so that polarization can be properly applied and the total current of the circuit will not be limited by the counter electrode. Concerning the configuration including the single microelectrode, the surfaces of the reference and counter electrodes were 2.10^4 µm^2 and 1.10^6 µm^2, respectively. For the configuration including the array, the surfaces of the reference and counter electrodes were 6.10^5 µm^2 and 7.10^5 µm^2, respectively. In both cases (single-array), the total surface of working microelectrode is approximately 2.10^3 µm^2. It is therefore obvious that a minimum ratio of 10-fold between counter and reference to working microelectrode surfaces was always respected.

3.2 Fabrication of electrochemical microcells

The three–electrode electrochemical cell was basically comprised of a platinum (Pt) working microelectrode, a platinum (Pt) counter electrode and a silver (Ag) based quasi-reference electrode and was fabricated using clean-room facilities. The development of the electrochemical microcell was based on previous work completed by C. Christophe in the framework of her PhD thesis carried out at LAAS-CNRS (Christophe, 2010).

Thin-film microfabrication technology was employed for the successive depositions and patterning of different electrode layers as well as the deposition of the passivation layer.

3.2.1 Substrate

Silicon wafers were used as substrates for the development of the first device prototype, serving simply as a mechanical support. Standard silicon wafers of P type (boron doped) with a crystallographic orientation (100) were selected due to their low cost and compatibility with the equipment available in the clean room. Wafer diameter was 4 inches and the thickness was 525 µm.

3.2.2 Wafer preparation

A cleaning step was firstly applied in order to remove impurities from wafer surface. Wafers were immersed in a solution of sulfuric acid (96%) and hydrogen peroxide (30%) in a volumetric ratio of 1/1 and a thin silicon oxide layer was formed. Wafers were next immersed in hydrofluoric acid solution (10%) so that the previously formed oxide layer and all impurities will be removed.

3.2.3 Silicon oxidation

Given the fact that silicon is a semiconductor, it is important to electrically isolate it by forming a dielectric layer on the surface. A 1 µm layer of silicon oxide (SiO_2) was thermally grown on the surface of the silicon wafer. The oxidation was performed in an oxygen atmosphere and the temperature was 1070 °C.

Figure 3.2 presents a schematic view of the wafer after the first step of the fabrication procedure.

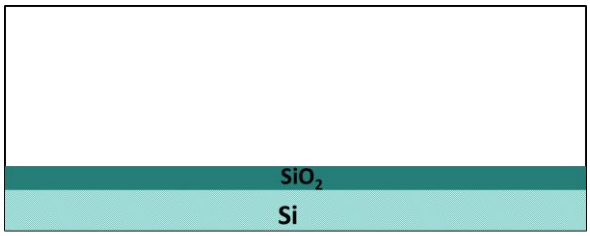

Figure 3.2. Schematic representation of the first step of fabrication procedure: oxidation of the silicon wafer.

3.2.4 Electrode structuring

3.2.4.1 ***Photolithography***

Photolithography is a very important tool used for electrode patterning which is most often followed by either lift-off or etching (Suzuki, 2000). A mask with the desired patterns and a photoresist are required through photolithographic processes. Photoresist is a UV sensitive resist that is comprised of the organic polymer, the solvent and photoactive substances (Fiaccabrino and Koudelka-Hep, 1998). For the fabrication of the systems used in this study, lift-off technique was used. The sequence of steps comprising the complete photolithography procedure and metal deposition is presented in Figure 3.3.

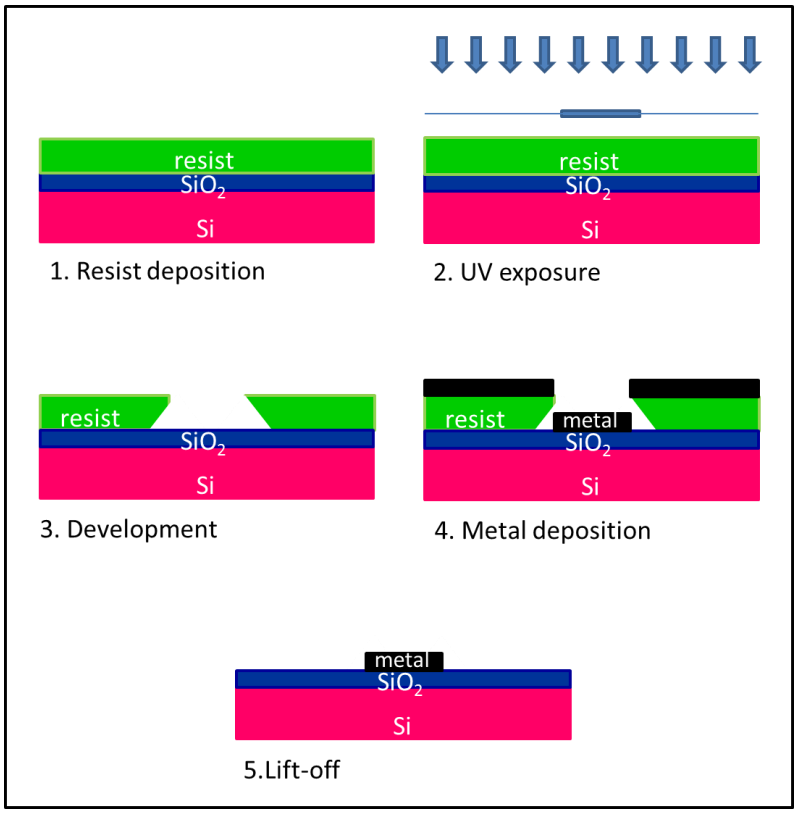

Figure 3.3. Lift-off technique for electrode patterning using a negative photoresist.

Selective deposition of the metallic layers is achieved by creating on the wafer the inverse pattern of what is eventually desired through photolithography (Fiaccabrino and Koudelka-Hep, 1998). The photoresist is spin-coated on the wafer level and soft-baked in order to eliminate the solvent and promote adhesion (Christophe, 2010). The wafer is then exposed to UV radiation through the mask with the desired patterns. Depending on whether the photoresist is positive or negative, the irradiated part will be either dissolved and removed or stay (Suzuki, 2000). Post-exposure bake is then carried out to eliminate any solvent left and increase adhesion. Development is the next step during which the parts of the photoresist that are soluble in the developer solution can be removed. Once the inverse patterns are formed, metallic films are deposited through evaporation on top of the photoresist patterns. Lift-off follows metal deposition. The undesired metallic regions are eliminated by dissolving the underlying photoresist in a stripper solution (Fiaccabrino and Koudelka-Hep, 1998). It is important to assure discontinuity of the metallic layer so that the stripper solution can access the underlying photoresist and eliminate it (Suzuki, 2000). The thickness and the sidewall profile of the photoresist are very critical parameters that determine the result of the lift-off. A pronounced undercut (Figure 3.3, step 3) after development facilitates lift-off process.

Metal layers patterning was performed using a bi-layer lift-off procedure. A LOR 3A lift-off resist (MicroChem Inc.) was used as the undercut layer followed by the application of AZ NLof (AZ Electronic Materials) negative photoresist, well-suited for lift-off procedures due to its inverted sidewall profile. The LOR 3A is not photosensitive but dissolves in conventional developer solutions. The thickness of the resist depends on the desired resolution and pattern precision. Given the fact that high precision and resolution are not critical parameters for the actual process, a high aspect ratio of resist to metal thickness was applied.

3.2.4.2 ***Deposition of electrode materials***

All electrode materials were deposited through physical vapor deposition (PVD) and layer thicknesses were selected so that no mechanical stress is exerted on the silicon wafer. Platinum (Pt) is the material corresponding to working microelectrodes, counter electrodes and conduction trails. In order to assure adhesion of platinum on SiO_2 substrate, a thin (20 nm) adhesion layer of titanium (Ti) was firstly deposited by electron beam PVD on the already photoresist-patterned wafer (through the procedure described in the 'Photolithography' paragraph), followed by the deposition of the platinum (Pt) layer of 150 nm through the same way. After lift-off, annealing was carried out during 20 minutes at 250°C in order to decrease mechanical stress and improve adhesion of metallic layers on the underlying layers (Christophe, 2010). Figure 3.4 shows the schematic representation of the Ti/Pt deposition which corresponds to the second step of the fabrication procedure.

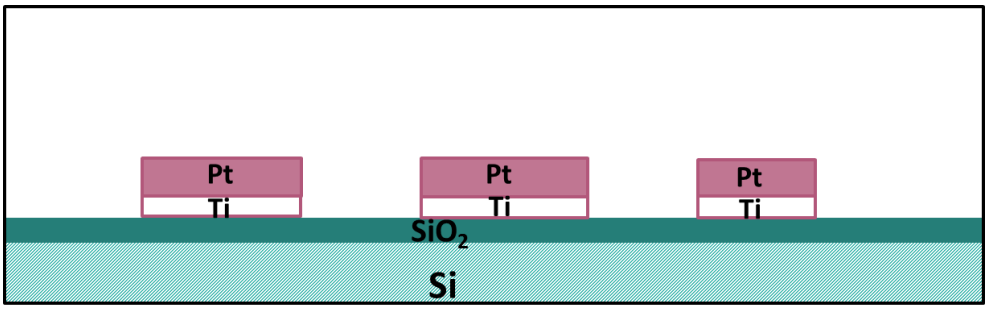

Figure 3.4. Schematic representation of the second step of fabrication procedure: Ti/Pt deposition.

A 400 nm silver layer which represents the future reference electrode was next deposited by PVD by Joule effect. The underlying platinum layer serves as a barrier layer, in order to avoid diffusion of titanium atoms in the silver layer. In this way, the future reference electrode will not have Ti atoms on the surface that can influence its stability. The technique followed to pattern the Ag layer was the same as the one followed for Ti/Pt patterning and described through the 'Photolithography' paragraph. After the silver layer was deposited, neither heat treatment at high temperature nor plasma oxidation should be carried out as these would have an impact on the quality and stability of later reference electrode given the fragility of silver (Suzuki et al., 1998). Figure 3.5 is a schematic representation of the Ag deposition, the third step of fabrication procedure.

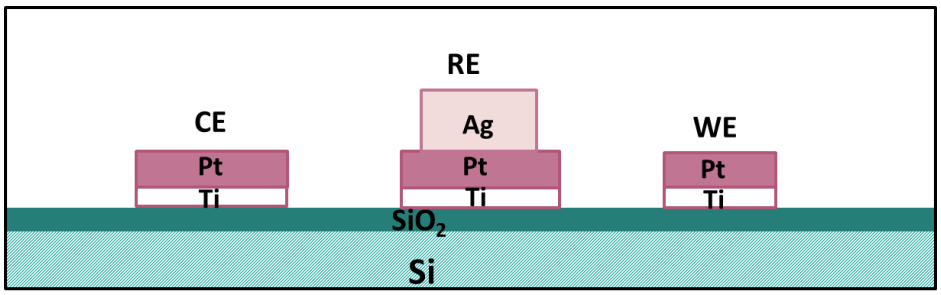

Figure 3.5. Schematic representation of the third step of fabrication procedure: Ag deposition.

3.2.4.3 ***Passivation layer***

Following the development of all metal layers, a passivation layer should be deposited in order to expose the active surface of all electrodes and the connection pads as well as provide good insulation to the rest of the structure when in contact with test solutions. Indeed, electrode active surface area needed to be precisely defined as it will be later used to correlate current intensity recorded to the quantity of species to be detected.

The passivation layer should therefore exhibit good dielectric properties, be chemically inert and contribute to long-term stability of electrochemical microcells that will be used in possibly corrosive mediums (Fiaccabrino and Koudelka-Hep, 1998). Organic (Meng et al., 2011) and inorganic (Schmitt et al., 1999, Zorman et al., 2011) passivation layers are found in literature. Organic layers do not provide sufficient stability through time in complex, corrosive mediums and inorganic layers call for harsh etching procedures and are usually taking place at high temperatures (Vanhove et al., 2013). In order to avoid these drawbacks, a low temperature deposition process of high quality silicon nitride (Si_3N_4) was selected for the development of the passivation layer used for the electrochemical cells. The procedure was developed by E. Vanhove during her post-doctoral activity in LAAS-CNRS (Vanhove et al., 2013). Si_3N_4 passivation layer (100 nm) was therefore deposited at low temperature through inductively coupled plasma chemical vapour deposition (ICP-CVD). ICP-CVD process yields conformal deposition that enables perfect covering of the whole structure, even the lateral parts of metal layers. However, in order to enable patterning of a conformal coating, a specific bi-layer lift-off process has been developed and the thickness of the Si_3N_4 film was optimized accordingly (Vanhove et al., 2013). The LOR 3A resist was used, combined this time with the positive AZ ECI 3012 photoresist (AZ Electronic Materials). The desired discontinuities of the deposited Si_3N_4 layer can be achieved by the creation of T-shaped resist profiles in order to prevent Si_3N_4 deposition on the bottom part of the T cap, leaving it accessible to the stripper lift-off solution (Figure 3.6).

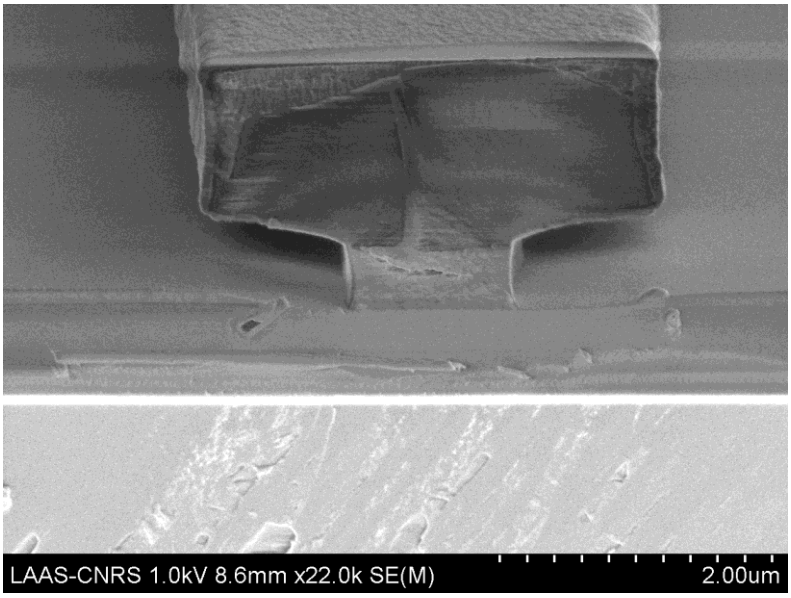

Figure 3.6. SEM image of the T-shaped bi-layer resist profile after Si_3N_4 deposition.

The electroactive surface area obtained after deposition of Si_3N_4 and resist removal is presented in Figure 3.7 and represents the platinum single microelectrode of 50 µm diameter.

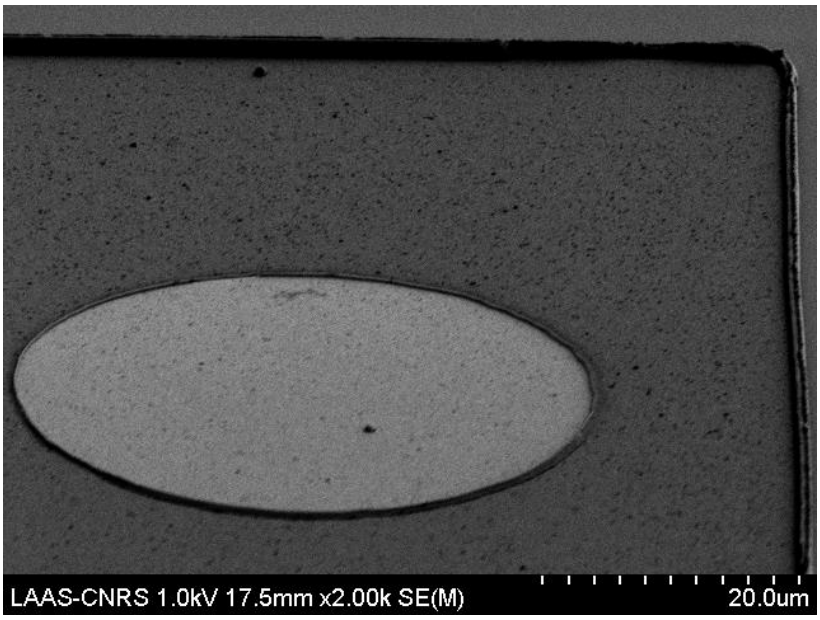

Figure 3.7. SEM image of a 50 µm diameter single microelectrode obtained after Si_3N_4 deposition and resist removal.

Figure 3.8 demonstrates a schematic representation of the cross-section view of all layers comprising the fabricated electrochemical sensor.

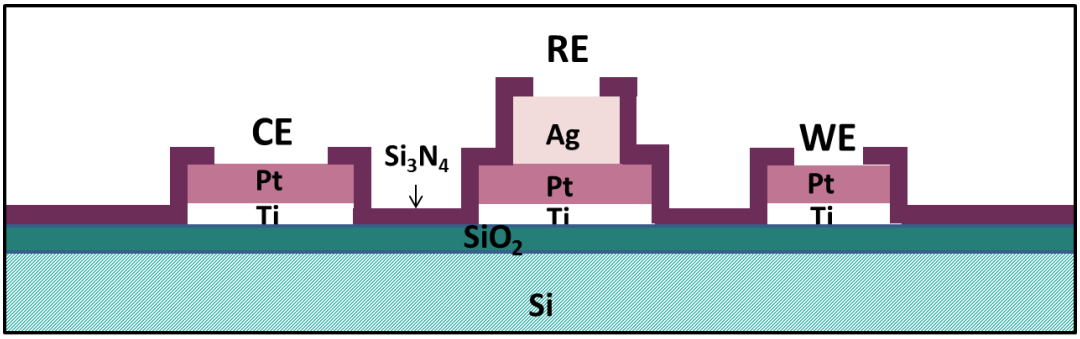

Figure 3.8. Schematic representation of all layers comprising the fabricated electrochemical sensor.

3.2.5 Packaging

After fabrication, the wafer was diced into individual chips. Each device was then mounted on a printed circuit board (PCB). Wedge bonding was subsequently carried out to complete packaging procedure and wire bonds were encapsulated in glob-top to ensure mechanical protection and avoid electrical short circuit. Figure 3.9 presents the autonomous electrochemical three-electrode microcell obtained.

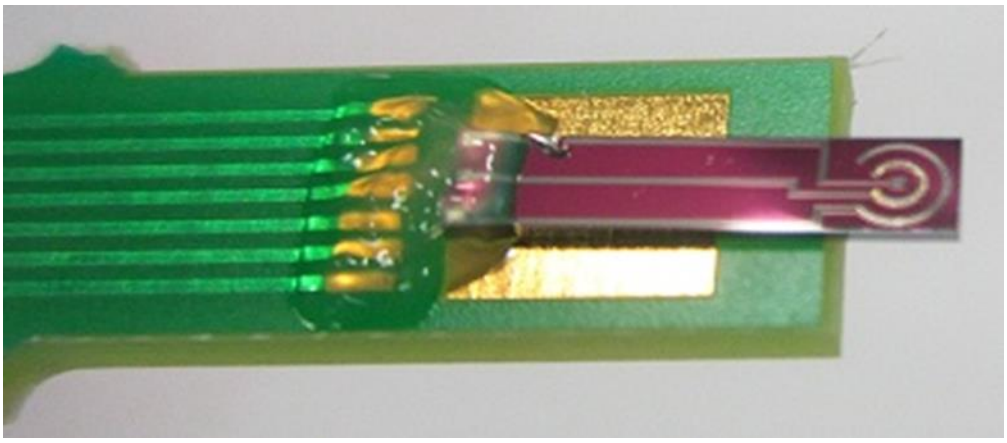

Figure 3.9. Autonomous electrochemical micro-sensor obtained, comprised of the single working, reference and counter electrodes.

3.3 Functionalization-Electrochemical validation

Following fabrication, electrode materials were further functionalized in order to obtain a film adapted to each detection type or to enhance their detection properties. Integrated materials were electrochemically characterized in model solutions in order to verify that their electrochemical properties are similar to the ones of bulk materials. Different steps of microfabrication procedure (surface preparation, deposition, lift-off, cleaning) can induce a surface pollution modifying the classic electrochemical behavior of pure materials.

All electrochemical experiments were conducted using a potentiostat (VMP3, BioLogic) with a low-current option controlled by EC-Lab software, at room temperature. The electrochemical set-up consisted in a standard three-electrode system. An external Ag/AgCl/KCl_{sat} or saturated calomel electrode (SCE) served as the reference electrode (indicated each time), while a platinum wire was the counter electrode. Working microelectrode was one of the electrodes of the future autonomous device that was examined through each test.

3.3.1 Working microelectrodes

As stated in Chapter 2, working electrode materials were determined according to electro-active species needed to be detected. Platinum (Pt) and functionalized Platinum Black (Pt-Bl) working microelectrodes were fabricated for H_2O_2 and dissolved O_2 measurements whereas iridium oxide (Pt/IrO_x) microelectrodes were used for pH monitoring.

3.3.1.1 ***Platinum and Platinum Black microelectrodes***

Electrodeposition of Platinum Black (Pt-Bl)

In order to attain high sensitivity of platinum working microelectrodes, porosity and surface area were enhanced by forming "platinum black" microelectrodes (Arbault et al., 1995).

Prior to platinization, electroactive surface was cleaned and activated by performing cyclic voltammetry in a solution of 0.5 M H_2SO_4, through the potential range of -0.2 to +1.1 V vs $Ag/AgCl/KCl_{sat}$. This anodic-cathodic treatment is important, especially after fabrication procedure, in order to prepare the surface of the metal for following operations as it serves as cleaning step removing impurities and enhances electrocatalytic properties of platinum (Rand and Woods, 1972). Platinization procedure was carried out by reducing a solution of hexachloroplatinic acid (32 mM in phosphate buffer solution) which contains lead acetate (1.23 mM) at -60 mV versus $Ag/AgCl/KCl_{sat}$ (Ben-Amor et al., 2013). The amount of Pt deposited was controlled by the coulometric charge recorded during platinization so that a nanostructured surface could be obtained reproductibly. When increasing charge deposited, the diameter of the platinized microelectrodes obtained increases while mechanical stability is declining. The increase in the initial diameter of the microelectrodes after platinization should be taken into account especially when dealing with UME arrays so that overlapping of the diffusion layers between adjacent microelectrodes in the array can be avoided. Therefore, platinization charge deposited on single Pt microelectrodes (d = 50 µm) was 0.5 $\mu C.\mu m^{-2}$ compared to 0.25 $\mu C.\mu m^{-2}$ on the arrays of Pt ultramicroelectrodes (25 disks of 10 µm diameter).

Figure 3.10 shows the nanostructured, highly porous structure of the functionalized single microelectrode obtained after depositing platinum black on platinum surface.

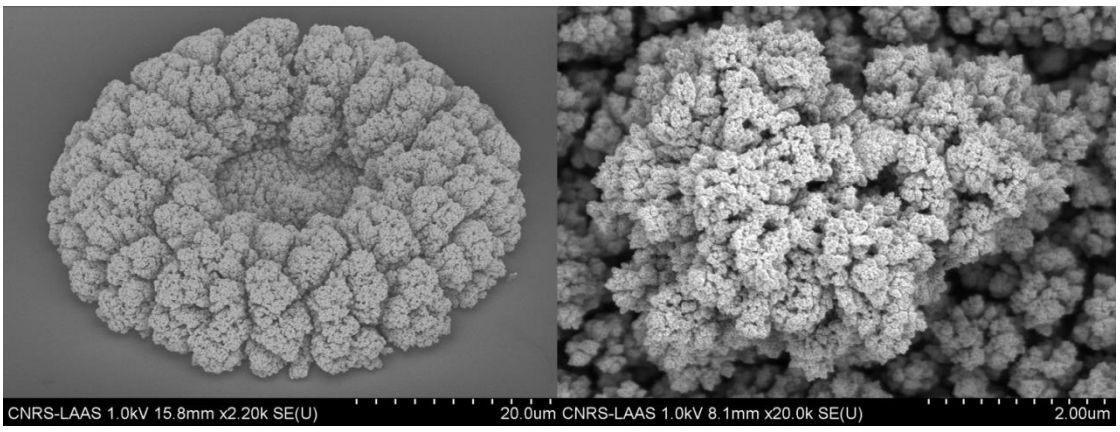

Figure 3.10. SEM images of the porous structure of Pt-Bl microelectrode.

Electrochemical characterization

Platinum (Pt) and platinum black (Pt-Bl) microelectrodes were then electrochemically characterized in order to verify that their behavior is similar to the one classically obtained with a pure platinum microwire commonly used through experiments.

Cyclic voltammetry in a degazed 0.5 M H_2SO_4 solution was conducted to characterize the quality of fabricated Pt and Pt-Bl microelectrodes (Figure 3.11). Potential range scanned was -0.2 to +1.1 V versus Ag/AgCl/KCl_{sat} at a scan rate of 100 $mV.s^{-1}$.

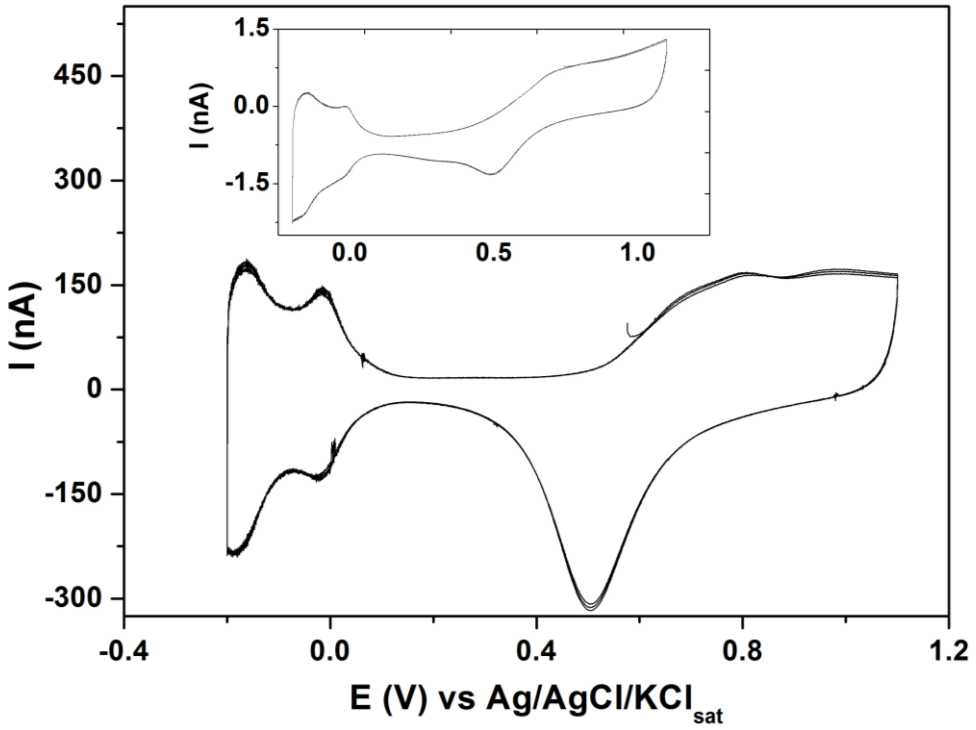

Figure 3.11. Cyclic voltammograms obtained for Pt-Bl and Pt (inset) integrated single microelectrodes (d=50 µm) fabricated through microfabrication technologies, in 0.5 M H_2SO_4 solutions. Scan rate: 100$mV.s^{-1}$.

The voltammograms obtained for Pt-Bl (Figure 3.11) and Pt single microelectrodes of 50 µm diameter (Figure 3.11, inset) correspond to typical cyclic voltammograms (CV) of Pt bulk material (Tilak et al., 1973).

The waves in the anodic part of the CV represent the formation of platinum oxides (above 0.6 V versus Ag/AgCl/KCl_{sat}). According to Angerstein-Kozlowska et al., the formation of oxides on Pt surface can be described as following (Angerstein-Kozlowska et al., 1973):

$$4\,Pt + H_2O \rightarrow Pt_4OH + H^+ + e^- \quad (Equation\ 14)$$
$$Pt_4OH + H_2O \rightarrow 2Pt_2OH + H^+ + e^- \quad (Equation\ 15)$$
$$Pt_2OH + H_2O \rightarrow 2PtOH + H^+ + e^- \quad (Equation\ 16)$$
$$PtOH \rightarrow PtO + H^+ + e^- \quad (Equation\ 17)$$

The first peak (around 0.5 V versus Ag/AgCl/KCl_{sat}), appearing at the reverse scan corresponds to the reduction of the previously formed oxides. Following the oxide reduction peak, the reduction of the adsorbed protons is obvious with the two peaks appearing below 0 V versus Ag/AgCl/KCl_{sat}. Adsorbed protons desorb when the potential scan is inverted (from -0.2 to slightly above 0 versus Ag/AgCl/KCl_{sat}).

When comparing voltammograms of Pt-Bl (Figure 3.11) and Pt microelectrodes (Figure 3.11, inset) in sulfuric acid solution, it is important to notice the difference in current level recorded. Platinum black surface provides a higher geometric area and more active sites for electrochemical reactions and therefore yields greater current intensities.

Active surface area of Pt and Pt-Bl working microelectrodes was experimentally determined by linear sweep voltammetry in solutions of potassium hexacyanoferrate (II) trihydrate ($Fe(CN)_6^{4-}$) (10 mM) in 0.1 M KCl used as a supporting electrolyte (Figure 3.12). The radius of fabricated single and array Pt and Pt-Bl microelectrodes was evaluated through a standard electrochemical couple ($Fe(CN)_6^{4-}$ /$Fe(CN)_6^{3-}$) and compared to the dimensions initially designed.

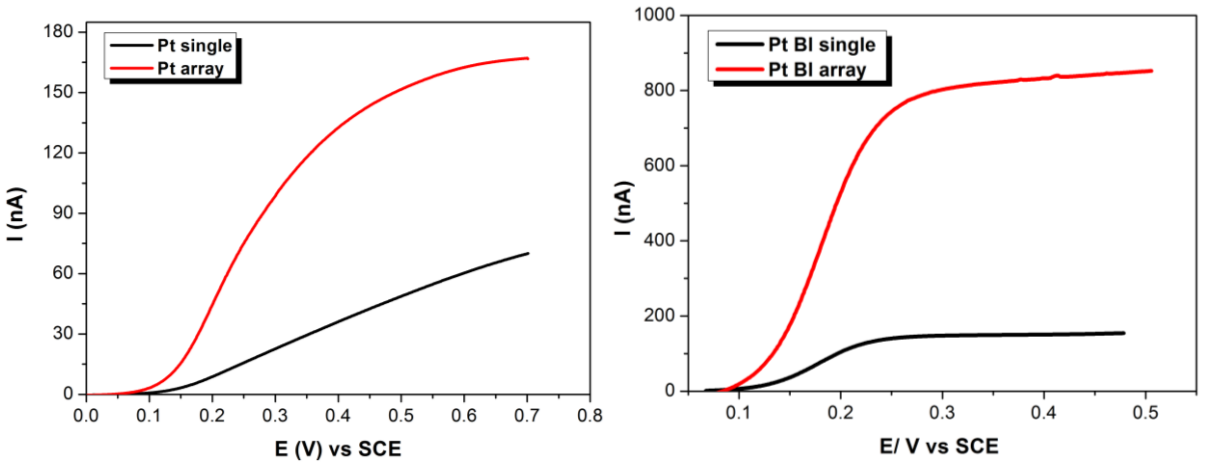

a. b.

Figure 3.12. Linear sweep voltammograms obtained for (a) Pt and (b) Pt-Bl single microelectrodes (black lines) and microelectrode arrays (red lines) in 10 mM of $Fe(CN)_6^{4-}$ in KCl solution. Scan rate: 4 $mV.s^{-1}$.

Potential range was scanned from 0 to 0.7 V versus SCE and scan rate was 4 mV. s^{-1}. The oxidation of $Fe(CN)_6^{4-}$ yielded typical sigmoidal voltammograms. Steady state responses, that are demonstrated through the oxidation plateau and provide the limiting current value (I_{lim}), were obtained around 0.6 V versus SCE for platinum microelectrodes and around 0.3 V versus SCE for platinum black microelectrodes (Figure 3.12).

Pt single microelectrode exhibited a not well-defined plateau in comparison with Pt ultramicroelectrode array that gave a plateau at 0.6 V versus SCE. Although the plateau was not well-defined for Pt single microelectrode, an approximate value of limiting current was considered for both configurations at 0.6 V versus SCE.

The value of the electrode radius was determined through the theoretical equation relating I_{lim} current (value of the oxidation plateau) to the radius of the microelectrode (Equations 9 and 10 of Chapter 2) (Saito, 1968). Equation 10 is given for an array of microdisk electrodes widely spaced where there is no overlapping of diffusion layers and I_{lim} represents the sum of currents obtained for each ultramicroelectrode as they are connected in parallel.

After applying the equations for Pt single microelectrode and array, the values obtained for the radius of each ultramicroelectrode of the array was approximately 3 μm and the one of the single microelectrode approximately 25 μm, when initially designed radii were 5 μm and 25 μm respectively. The comparison between the real values obtained and the values initially designed revealed a limitation associated to fabrication procedure and focused on the definition of low values of ultramicroelectrode radius (5μm) through the application of the passivation layer.

As far as platinum black porous structures are concerned, they yielded steeper waves indicating rapid electron transfer reactions. The system appeared to be faster compared to platinum microelectrodes demonstrating the improved electrocatalytic activity of Pt-Bl microelectrodes towards $Fe(CN)_6^{4-}$ oxidation. Both platinum black configurations exhibited well-defined oxidation plateaus and limiting currents were estimated at 0.3 V versus SCE. For the calculation of the microelectrode radius, the microelectrodes were approximately considered as disks in order to be able to compare with Pt configurations and equations applied were then Equations 9 and 10. The concentration (C) of $Fe(CN)_6^{4-}$ ion was 0.01 M and the diffusion coefficient (D) was 6.3 x 10^{-6} $cm^2.s^{-1}$ (Konopka and McDuffie, 1970). The value obtained for the radius of each ultramicroelectrode of the array was approximately 14 μm and the one of the single microelectrode 65 μm.

Aforementioned results are summarized in the following table (Table 3.1):

Table 3-1. Limiting current, radius and total electroactive surface values obtained for Pt and Pt-Bl single microelectrodes and ultramicroelectrode arrays.

		Single µelectrode	UME array
Pt	I_{lim} (nA)	60	165
	$r_{each\ electrode}$ (µm)	25	3
	S_{total} (µm^2)	19 10^2	6 10^2
Pt-Bl	I_{lim} (nA)	150	850
	$r_{each\ electrode}$ (µm)	60	14
	S_{total} (µm^2)	1.2 10^4	1.5 10^4

By comparing values obtained for platinum and platinum black microelectrodes, it was estimated that platinization of Pt arrays induces a 5-fold increase in electrode I_{lim} value whereas platinization of Pt single microelectrode induces a 2.5-fold increase the I_{lim} value. A possible explanation for this can be the more important radial diffusion from the edges of the ultramicroelectrodes comprising the array, considering their smaller radius compared to the radius of the single microelectrode. Mass transport during platinization procedure is enhanced for the array configuration as the latter is comprised of 25 microelectrodes with small radius compared to the single microelectrode configuration that consists of one microelectrode with bigger radius.

3.3.1.2 ***Iridium oxide microelectrode (IrO_x)***

Electrodeposition of IrO_x

Anodically electrodeposited iridium oxide films (AEIROF) were prepared on previously fabricated platinum microelectrodes. Electrodeposition was the technique selected over different techniques frequently used such as thermal oxidation of iridium substrates (Sato, 1989), reactive sputtering (Klein et al., 1989), electrochemical oxidation of iridium microelectrodes (Olthuis et al., 1990), due to its advantages including the low cost of fabrication process, compatibility with microfabrication procedures as well as the fact that it is a low-temperature process.

An iridium tetrachloride based alkaline solution was prepared (Yamanaka, 1989). The solution contained iridium tetrachloride, hydrogen peroxide, potassium carbonate and oxalic acid in distilled water. The final pH was adjusted at 10.5 and the solution was left stabilize one week before use (Remita, 2007).

Different deposition protocols have been proposed in literature, including galvanostatic (Ges et al., 2005), potentiostatic (Hull et al., 2008) and potential cycling methods (Yang et al., 2004). Ges et al. report greater results when deposition is carried out through galvanostatic mode. However, as reported by Elsen et al., concerning thick IrO_x films, when deposition is carried out by applying a controlled potential, adhesion of IrO_x on substrate is higher and the formed layer is more uniform compared to galvanostatic methods. For the anodic electrodeposition of IrO_x on Pt microelectrodes in this study, a constant potential (0.6 V/SCE) was applied and the duration of the deposition was indicated by the total charge transferred (0.5 $C.cm^{-2}$) (Elsen et al., 2009).

Iridium oxide on the surface is formed through the oxidation of the Ir(IV) compound. Iridium exists as a complex in the solution and the mechanism proposed by Yamanaka et al. for the deposition is the following (Equation 18):

$$[Ir(COO)_2(OH)_4]^{2-} = IrO_2 + 2CO_2 + 2H_2O + 2e^- \qquad (Equation\ 18)$$

Anodic electrodeposition yielded rough, blue-black films as shown in Figure 3.13, in agreement with what is reported in literature (Yamanaka, 1989).

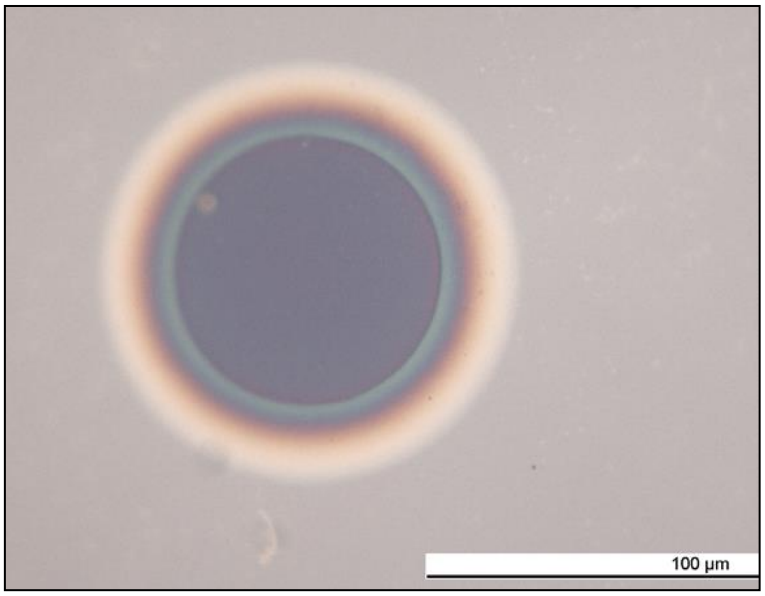

Figure 3.13. IrO_x film deposited on Pt single microelectrode of 50 µm diameter.

Electrochemical characterization

Once the electrodeposition process was completed, the microelectrodes were characterized electrochemically through cyclic voltammetry in 0.5 M sulfuric acid solution (Figure 3.14).

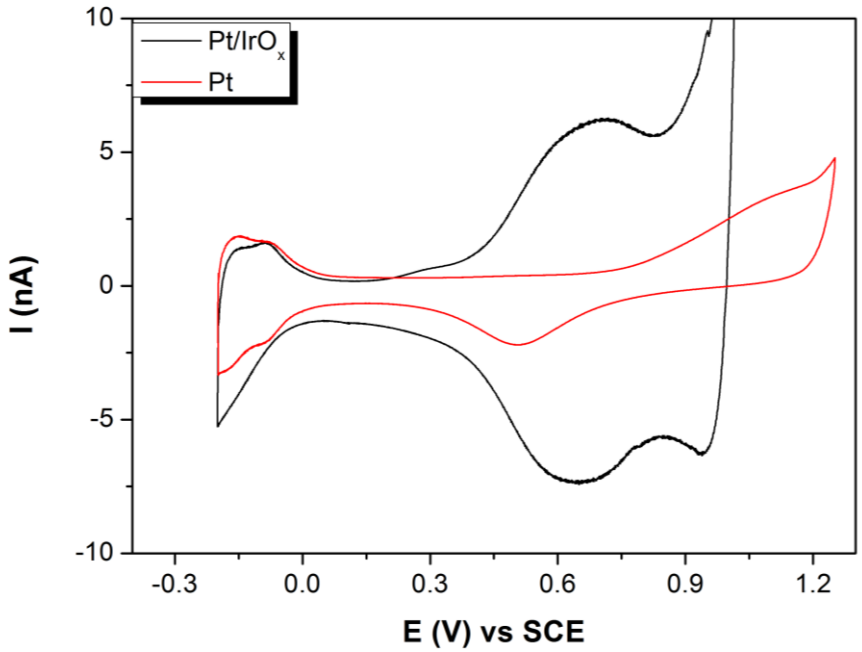

Figure 3.14. Cyclic voltammogram recorded before and after the deposition of IrO_x on Pt microelectrode in 0.5 M H_2SO_4 solution. Scan rate: 100 $mV.s^{-1}$.

The voltammogram presented in Figure 3.14 shows the characteristic response of the IrO_x layer in 0.5 M H_2SO_4 solution with the characteristic oxidation peaks corresponding to the oxidation of Ir(III) to Ir (IV) and the associated reduction peaks (Kieninger, 2011). However, the characteristic behavior of Pt electrodes is also evident indicating that Pt is also exposed and the surface is not fully covered with IrO_x. This characterization technique involves current flow and redox reactions in acidic solutions and is therefore pointing out the mechanical instability of the IrO_x layer. After the first cycles the characteristic response of IrO_x is less evident and the layer seems to be deteriorated.

This was confirmed through SEM observations. Figure 3.15 shows the IrO_x layer deteriorated after potential cycling in 0.5 M H_2SO_4 solution. The cracks that appeared on the surface explain the characteristic peaks of Pt exhibited on the cyclic voltammogram presented above (Figure 3.15). Therefore, this characterization method should be avoided when this layer has to be used as detection surface due to its low stability.

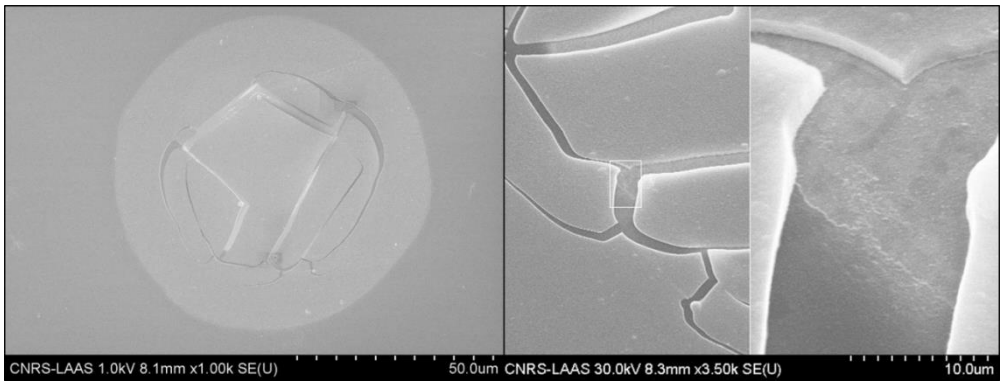

Figure 3.15. Pt/IrO_x microelectrode deteriorated after potential cycling in 0.5 M H_2SO_4 solution.

3.3.2 Reference electrode

The integration of a reference electrode in the structure was necessary in order to obtain an autonomous detection system. It is important to have a stable reference electrode as in the opposite case the potential applied on the working electrode which is set with respect to the reference, will be shifted and the generated current can be altered (Suzuki et al., 1998). Different techniques have been reported for the fabrication of silver/silver chloride reference electrodes. Ag/AgCl is often formed from a silver layer through either a spontaneous chemical reaction in a solution of $FeCl_3$ (Parker et al., 2009) or a controlled electrochemical reaction (Schwake et al., 1998, Popovtzer et al., 2006). The formation of Ag/AgCl through electrochemical –galvanostatic or potentiostatic- processes provides the advantage of a controlled growth of the silver chloride on the silver surface, which is not the case for the formation through spontaneous chemical reaction (Christophe, 2010).

Due to problems associated with the stability and dissolution of Ag/AgCl in the solution as well as the fact that the potential of the reference electrode depends on the concentration of chloride ions in the analyte solution according Nernst equation, many efforts have been made to integrate KCl doped resins (Desmond et al., 1997), polymeric membranes based on ionic liquids (Toczyłowska-Mamińska et al., 2008) as well as Nafion coatings (Kounaves et al., 1994). Electrodes that do not contain any internal electrolyte and are in direct contact with the examined solution are called "quasi-reference electrodes" (Simonis et al., 2004). In this study, provided the short measurement time and considering that the Cl^- concentration of analyte solutions will be almost similar, no internal liquid reservoir, gel or membrane was integrated in the reference electrode structure and therefore a "quasi reference electrode" was obtained.

Prior to Ag/AgCl formation, silver surface was electrochemically characterized by conducting cyclic voltammetry in a zero-oxygen, acidified potassium nitrate (KNO_3) solution of 0.1 M with a scan rate

of 50 mV.s^{-1} (Figure 3.16). This step also serves as a cleaning procedure in order to prepare/activate the surface and remove impurities remaining on silver surface after fabrication.

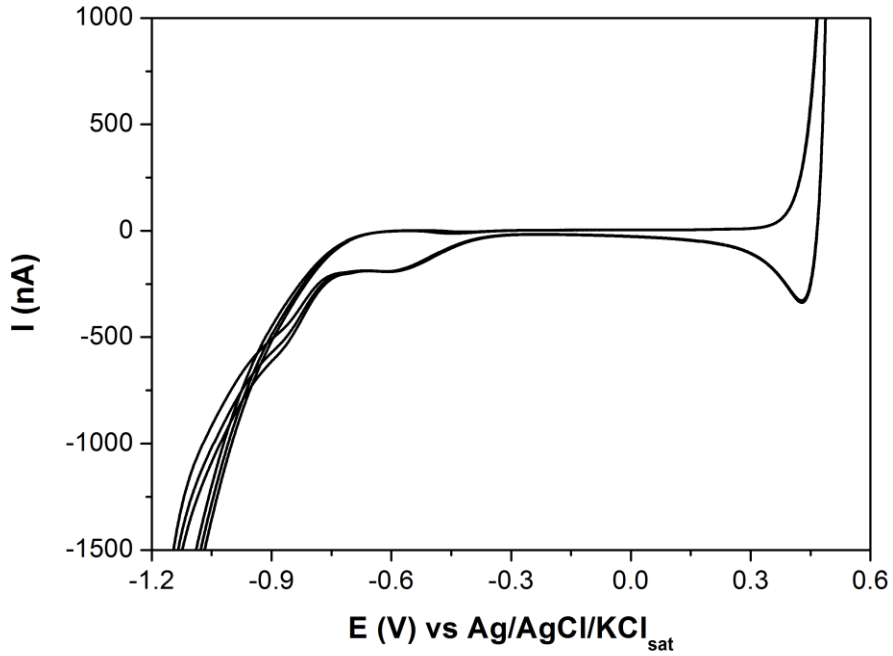

Figure 3.16.Cyclic voltammogram of Ag surface obtained in zero-oxygen 0.1M KNO_3 solution with a scan rate of 50mV.s^{-1}.

The voltammogram obtained is similar to the ones obtained for a bulk silver material and we can discern the exponential current increase after 0.3 V versus Ag/AgCl/KCl$_{sat}$ corresponding to the beginning of silver oxidation as well as the reduction of the proton below –0.45 V versus Ag/AgCl/KCl$_{sat}$.

In order to form the Ag/AgCl reference electrode, the previously deposited Ag surface was electrochemically oxidized. The electrode was then oxidized in 10^{-2} M potassium chloride solution (KCl) by linear sweep voltammetry within the potential range of 0.1- 0.25 V/SCE and a low scan rate of 1 mV.s^{-1} which yields stable and homogeneous Ag/AgCl structure. Indeed, higher scan rates could result in porous layers and electroactive species trapped between pores induce changes in reference electrode potential (Christophe et al., 2013).

Quasi-reference electrode stability was evaluated in 0.01 M KCl solution. Ag/AgCl electrode potential compared to external Ag/AgCl/KCl$_{sat}$ electrode was plotted versus time (Figure 3.17).

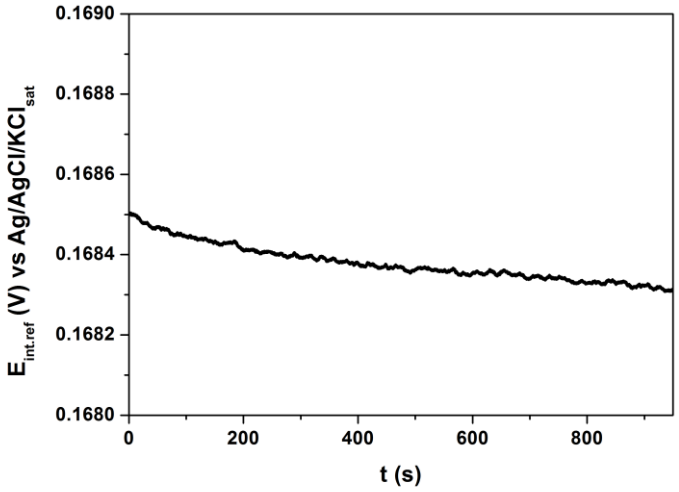

Figure 3.17. Potential variation in time of the integrated Ag/AgCl reference electrode versus an external commercial reference electrode in 0.01 M KCl solution (open circuit value).

It was observed that the deviation in time is more important during the first seconds of the first immersion in the solution. For following immersions, this transient phenomenon is not observed. Potential deviation in time was estimated around 0.6 $mV.h^{-1}$, which is an acceptable value for the present application given the fact that short-time measurements are conducted through bioassays (5-10min).

3.4 Sensors calibration

Following validation of electrochemical performance of the different electrode materials, micro-electrochemical cells were used to detect electroactive species of interest (H_2O_2, O_2, pH related ions H_3O^+/OH^-).

3.4.1 pH monitoring

The equilibrium equations proposed in literature for the anhydrous (Equation19 and 20) and hydrated (Equation 21) iridium oxide films are the following (Ges et al., 2005):

$$IrO_2 + H^+ + e^- \leftrightarrow IrO \cdot OH \qquad \text{(Equation 19)}$$

$$2IrO_2 + 2H^+ + 2e^- \leftrightarrow Ir_2O_3 + 2H_2O \qquad \text{(Equation 20)}$$

$$2[IrO_2(OH)_2 \cdot 2H_2O]^{2-} + 3H^+ + 2e^- \leftrightarrow [Ir_2O_3(OH)_3 \cdot 3H_2O]^{3-} + 3H_2O \qquad \text{(Equation 21)}$$

The equilibrium potential is given by Nernst equation (Equation 13 of Chapter 2) and for metal/metal oxide electrodes depends only on the pH of the solution (Equation 22).

$$E_{eq} = E^o + \frac{RT}{nF}\ln[H^+]^a \qquad \text{(Equation 22)}$$

$[H^+]$ corresponds to the concentration of protons and indicates the pH of the solution and a to the stoicheiometric coefficient of H^+.

For the calibration of the pH sensors, the equilibrium potential of the metal oxide electrode was monitored in solutions of different pH through open circuit potential (OCP) (or OCV: open circuit voltage) mode at room temperature (Figure 3.18).

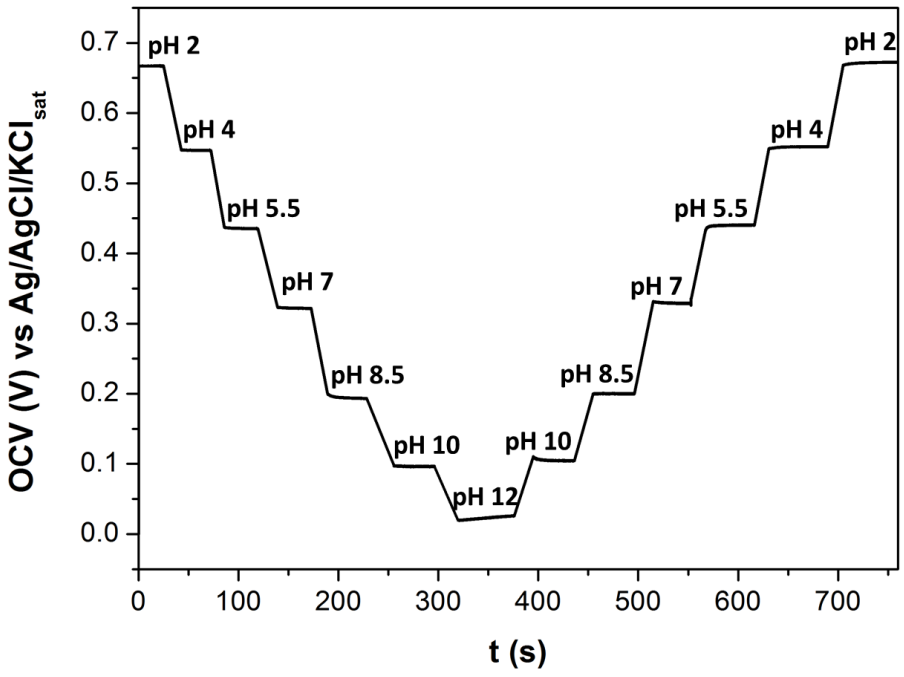

Figure 3.18. Pt/IrO$_x$ microelectrode response for different pH values.

Hysteresis was first examined in order to verify that the Pt/IrO$_x$ microelectrode can follow pH transitions no matter the direction they are made (Figure 3.18). Potential drift was evaluated for the acid/basic/acid transition by measuring open-circuit voltage values for solutions of different pH. After immersing the Pt/IrO$_x$ microelectrode and the external Ag/AgCl/KCl$_{sat}$ reference in each pH solution for several seconds, potential recording was carried out until stabilization and was then paused in order to change solution.

As shown in Figure 3.18 the response time of the fabricated sensor is fast as equilibrium plateau values were reached immediately after immersion. As far as the hysteresis of the system is concerned, a low value of potential drift (around 5 mV) was obtained for each buffer solution.

By plotting potential values obtained versus pH (Figure 3.19), it was shown that the microelectrode demonstrated an almost linear response over a wide pH range (2.0–12.0).

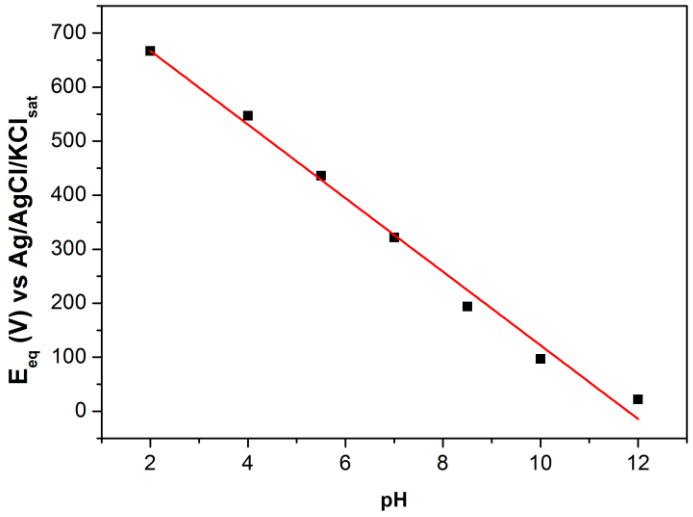

Figure 3.19. Calibration curve obtained for Pt/IrO_x microelectrode.

The theoretical value of the sensitivity of the sensors at room temperature can be deduced from Nernst equation (Equation 22). The experimental value of sensitivity is calculated from the response plot of open circuit voltage versus pH. The sensitivity of Pt/IrO_x microelectrode obtained by the graph presented in Figure 3.19 was around 68 mV/pH, similarly to the response of the AEIROF (anodically electrodeposited iridium oxide film) electrodes developed by Marzouk et al., 1998, Bezbaruah and Zhang, 2002 and Wu et al., 2011. However, higher sensitivity values are also often reported in literature for AEIROF (Prats-Alfonso et al., 2013, Ges et al., 2005) and are usually attributed to variations in the oxidation state of the iridium oxide present on the surface (Kim and Yang, 2014, Olthuis et al., 1990). On the other hand, Nernstian values of approximately 59 mV/pH were obtained for anhydrous iridium oxide film electrodes fabricated through different deposition methods, like sputtering (Klein et al., 1989; Katsube et al., 1981).

As reported by Kieninger, 2011, both types of iridium oxide (hydrated and anhydrous), coexisting on the surface of real electrodes can contribute to the final measured potential and can therefore explain the value (68 mV/pH) obtained with the present sensor. Elsen et al. also reported that the slope of the calibration curves depends on the thickness and the form of the created IrO_x film. It increases from 49

to 76 mV/pH unit when increasing the deposition time. Smaller values reflect a non-continuous film that is not covering the whole surface of the underlying layer and higher values correspond to full, continuous, thick films (Elsen et al., 2009).

The stability of the fabricated Pt/IrO_x microelectrode was finally tested in a pH 7 standard buffer solution, using an external Ag/AgCl/KCl_{sat} electrode at room temperature. A temporal drift of approximately 6 $mV.h^{-1}$, e.g. 0.09 $pH.h^{-1}$ was observed (Lale et al., 2014). Such high values can be related to the weak mechanical stability of the fabricated microelectrode.

3.4.2 H_2O_2 detection

Calibration curves for H_2O_2 measurements were then obtained by recording current responses to different concentrations through chronoamperometry.

Prior to chronoamperometry, it was important to determine the potential corresponding to the oxidation of H_2O_2 on platinum and platinum black microelectrodes with respect to an external Ag/AgCl reference electrode which corresponds to the plateau potential of the oxidation wave.

The oxidation of hydrogen peroxide is taking place as described in the following equation:

$$H_2O_2 \rightarrow O_2 + 2H^+ + 2e^- \qquad \text{(Equation 23)}$$

Cyclic voltammetry was conducted in a solution of 10 mM H_2O_2 in phosphate buffer (PBS) (10 mM) and the voltammograms obtained for Pt and Pt-Bl microelectrodes are presented in Figure 3.20. Potential range scanned was from 0.05 to 0.8 V and from 0.05 to 0.4 vs Ag/AgCl for Pt and Pt-Bl microelectrodes respectively. Scan rate was 20 $mV.s^{-1}$.

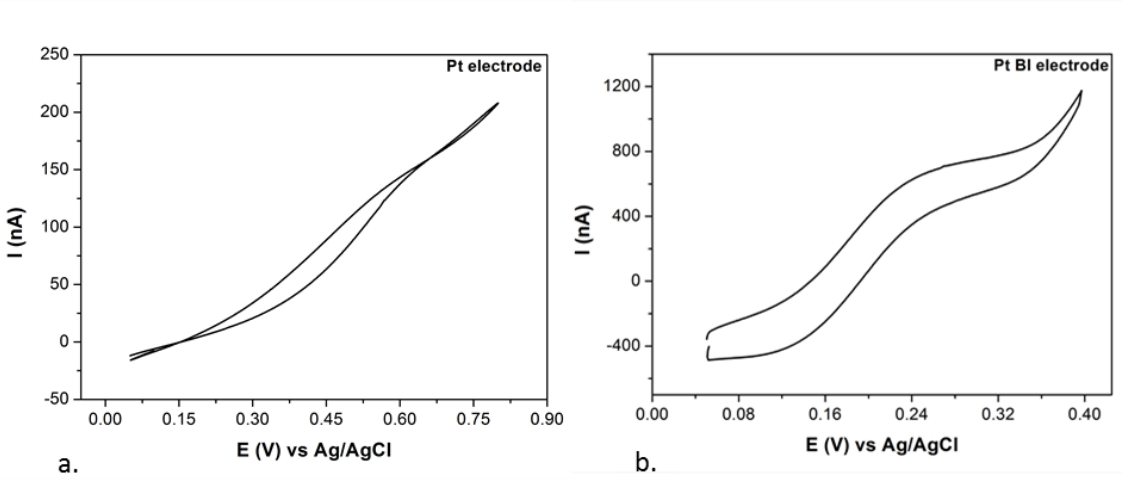

Figure 3.20. Cyclic voltammograms recorded in 10 mM H_2O_2 in PBS solutions with a scan rate of 20 $mV.s^{-1}$ for (a) Pt and (b) Pt-Bl microelectrodes.

Although Pt microelectrodes did not display a well-defined plateau, H_2O_2 oxidation took place around 0.6 V vs Ag/AgCl. On the other hand, Pt-Bl microelectrodes exhibited a plateau around 0.3 V. The lower potential value of H_2O_2 oxidation on Pt-Bl microelectrodes compared to the one of Pt microelectrodes is ascribed to electrocatalytic activity of platinum black towards H_2O_2 reactions and provides a significant advantage, minimizing interferences induced by other electroactive species (Arbault et al., 1995).

Consequently, an anodic potential of 0.6 V and 0.3 V vs Ag/AgCl was applied upon chronoamperometric determination of hydrogen peroxide in order to initiate the oxidation of H_2O_2 present in the solution for Pt and Pt-Bl microelectrodes, respectively.

Concentration range tested was between 10 nM and 10 µM so that it can be verified that the detection of low H_2O_2 quantities (range of interest in biological applications) is feasible. H_2O_2 detection was performed by following current increase after successive injections of H_2O_2 in PBS (10 mM) solution. Figure 3.21 shows the chronoamperometric curve recorded using Pt array configuration, focusing on the significant injections that yielded a measurable current increase. Figure 3.22 a presents the chronoamperometric curve obtained with Pt-Bl array, including all different injections, in order to stress out the remarkable detection properties of the functionalized configuration.

In Figure 3.22 b, special emphasis was placed on lower concentrations of H_2O_2 in order to validate that a variation of 10 nM can also be detected, through more spaced injections so that plateau values can be easily determined.

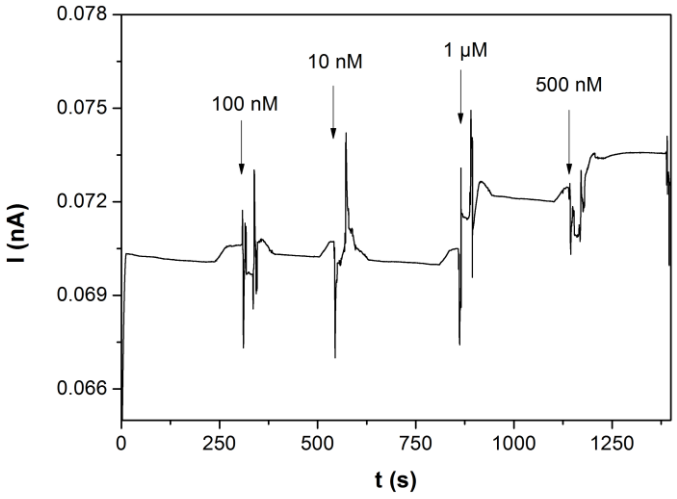

Figure 3.21. Current measurement after successive injections of H_2O_2 for a Pt ultramicroelectrode array. The potential applied is 0.6 V vs Ag/AgCl.

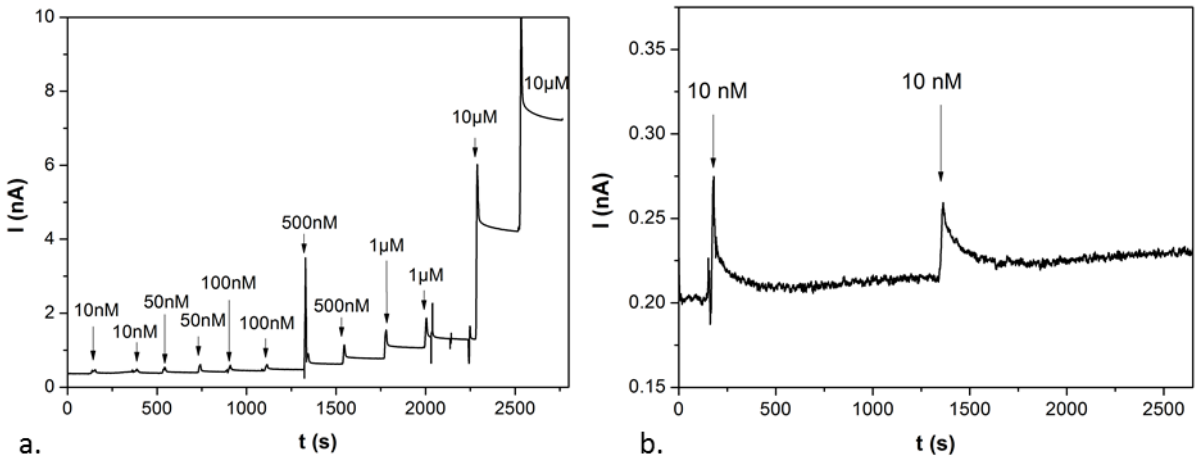

Figure 3.22. (a) Current measurement after successive injections of H_2O_2 for a Pt-Bl ultramicroelectrode array. The potential applied is 0.3 V vs Ag/AgCl (b) Current response for 10 nM H_2O_2 injections.

Calibration curves for H_2O_2 microsensors were obtained by plotting current increase recorded for each injection (Figure 3.23). Platinum and platinum black single microelectrodes and arrays were compared in terms of sensitivity.

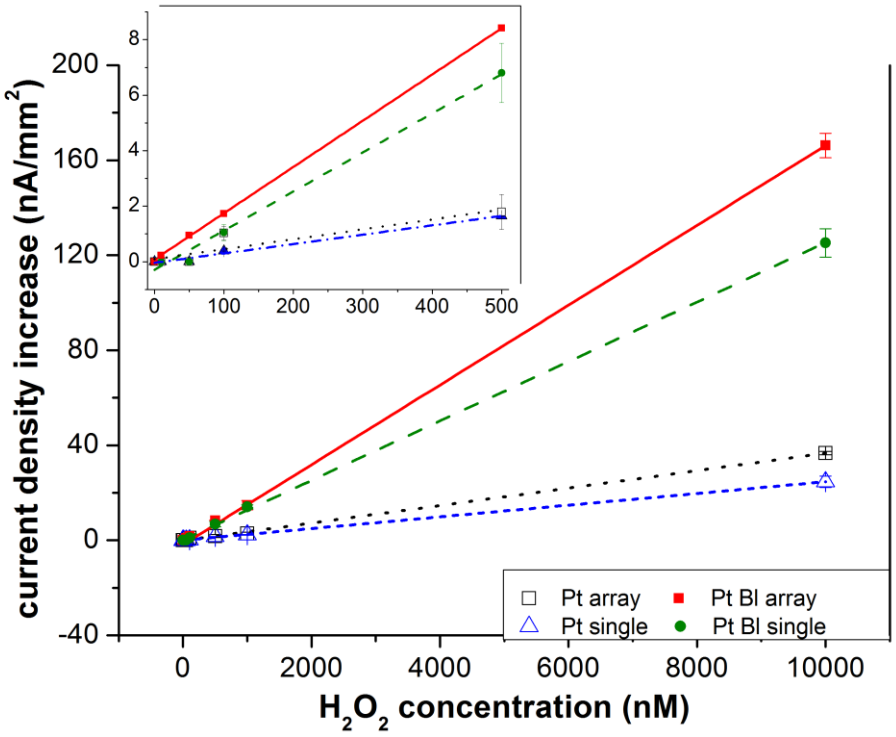

Figure 3.23. H_2O_2 calibration curves obtained for Pt-Bl and Pt single microelectrodes and arrays. Inset: zoom in lower concentration range.

Linear response was observed through the entire concentration range tested ($R^2 \geq 0.99$) for all Pt and Pt-Bl single microelectrodes and arrays. Reproducibility was not thoroughly evaluated but the curves obtained represent the results obtained for at least three measurements.

Table 3-2 summarizes the results obtained for H_2O_2 detection with all microelectrodes, regarding sensitivities.

Table 3-2. Sensitivities obtained for H_2O_2 monitoring with Pt and Pt-Bl single microelectrodes and arrays in the range of 0-10 µM.

		Single microelectrode	**UME array**
Pt	Sensitivity ($pA.mm^{-2}.nM^{-1}$)	2.4	3.7
Pt-Bl	Sensitivity ($pA.mm^{-2}.nM^{-1}$)	12.4	17

By comparing sensitivity results, it can be concluded that passing from single microelectrodes to ultramicroelectrode arrays, brings about a 1.5-fold increase in sensitivities whereas passing from Pt to Pt-Bl brings about a 5-fold increase in sensitivity. This conclusion demonstrates the impact of Pt-Bl functionalization on the properties of the microelectrodes towards H_2O_2 detection. Indeed, Pt-Bl microelectrodes exhibit increased electro-active surface area and porosity compared to platinum microelectrodes and therefore enhanced mass transport of species towards electrode surface. Their nanoscale structure (Vaddiraju et al., 2010) and large number of electroactive sites enhance electron transfer (Li et al., 2013).

As expected, black platinum ultramicroelectrode arrays exhibited the greatest sensitivity for H_2O_2 detection with a slope of 17 $pA.mm^{-2}.nM^{-1}$ and it was demonstrated that 10 nM of H_2O_2 can be detected. The high electrocatalytic activity of platinum black surface combined with the high signal-to-noise ratio of array configurations lead to enhanced electrode performance regarding detection properties, detection limits and sensitivities. Pl Bl single microelectrodes yielded higher sensitivity than both Pt microelectrode configurations, single and array, with a slope of 12.4 $pA.mm^{-2}.nM^{-1}$.

As far as detection limits are concerned, 10 nM were detected using Pt-Bl ultramicroelectrode arrays whereas the limit of detection for the other configurations was not lower than 100 nM.

Overall, it was demonstrated that Pt-Bl ultramicroelectrode arrays demonstrated the best results in terms of sensitivity and detection limits and will therefore be used through following experiments.

3.4.3 O_2 detection

Calibration of dissolved oxygen sensors is a complicated procedure and requires not only fully controlled gas flows (oxygen and nitrogen) but also a commercial oxygen sensor to verify the amount of oxygen in the solution. Nevertheless, a simpler calibration method consists in measuring the current generated in a saturated and zero-oxygen solution (Rodriguez-López et al., 1992).

The performance of the O_2 sensors used in this study was pre-validated by comparing current values obtained by the reduction of dissolved oxygen on the electrode surface in saturated oxygen and zero oxygen High Salt Medium solutions (HSM, pH 6.8) (cf. chapter 5). This solution is the medium which will be later used through the tests in algal solutions. What is more, the potential for O_2 reduction that should be applied through chronoamperometric experiments for bioassays was determined.

In order to establish optimal conditions for detection of O_2 as it will be the center of our interest, platinum black ultramicroelectrode arrays were used for the tests as it was validated through H_2O_2 calibration experiments that they have better detection properties. As reported also in literature, Pt-Bl ultramicroelectrode arrays present the greatest sensitivity for O_2 and H_2O_2 reactions due to the electrocatalytic activity of platinum black towards these reactions (Arbault et al., 1995, Ben-Amor et al., 2014). Therefore special emphasis was placed through the following tests on oxygen measurements by Pt-Bl ultramicroelectrode arrays.

Oxygen reduction on platinum electrodes follows a one-step reduction reaction pathway involving four electrons described by Equation 24:

$$O_2 + 4H^+ + 4e^- \rightarrow 2H_2O \qquad \text{(Equation 24)}$$

As reported in literature, the potential range of -0.6 to -0.8 V is appropriate for oxygen reduction reaction in saline solutions on Pt electrodes (Clark et al., 1953). It strongly depends though on the surface state of the electrode. Cyclic voltammetry was conducted in the potential range of 0 to -1 V (vs Ag/AgCl integrated) in order to determine the suitable potential for the reduction of oxygen on Pt-Bl microelectrodes in solutions of HSM (Figure 3.24).

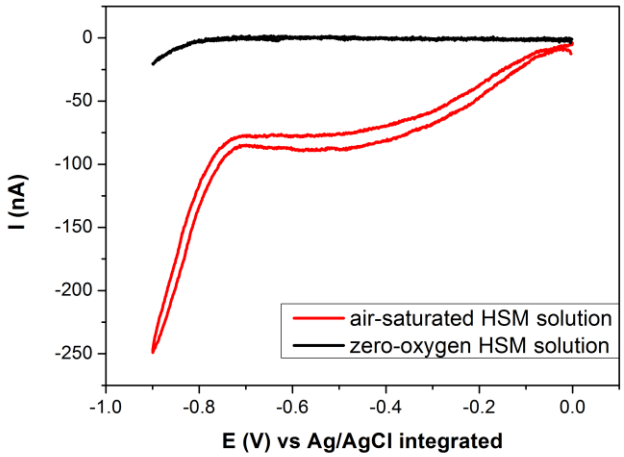

Figure 3.24. Cyclic voltammograms recorded in saturated and zero-oxygen HSM solutions with a Pt-Black UME array. Scan rate: 50 $mV.s^{-1}$.

Cyclic voltammogram was first recorded in air-saturated HSM solutions in order to identify the limiting current region which was observed from -0.6 to -0.7 V. The shape of the voltammogram including only one wave confirms that oxygen reduction on platinum surfaces takes place in one step through the exchange of four electrons. Then, the same voltammogram was recorded in a zero-oxygen solution to demonstrate that the current generated is mainly the result of the oxygen reduction and therefore depends on the oxygen concentration in the solution. The limiting current region indicated the suitable potential to be applied for chronoamperommetry which was -0.7 V versus Ag/AgCl integrated electrode. The output current recorded for a saturated and a zero oxygen HSM solution at room temperature demonstrated that O_2 concentration variation induces a variation in current intensity generated by the O_2 reduction reaction on platinum black electrodes. The current variation between saturated and zero-oxygen solution is 86 nA. The sensitivity of the sensor was calculated by correlating the measured current difference with the oxygen concentration in saturated water and considering the solubility coefficient of oxygen in the medium used similar to the one in water. Oxygen concentration in saturated water solutions at room temperature (25°C) is given by Truesdale and Downing and is 253 nmol/mL (Truesdale and Downing, 1954). The sensitivity value obtained is 19 $pA.mm^{-2}.nM^{-1}$.

3.5 Conclusion

The development of the autonomous electrochemical systems used through prevalidation tests is presented above. Electrochemical microcells were fabricated for the detection of O_2, H_2O_2 and H_3O^+/OH^- ions, species taking part in metabolic activities of algae. Electrochemical microcells consist

of three integrated electrodes (working, reference and counter) on silicon chip. Electrode materials were chosen according to the species to be detected: Pt and black Pt microelectrodes were therefore used for O_2 and H_2O_2 detection while Pt/IrO_x microelectrodes were selected for pH monitoring. The prototype was developed on a silicon substrate by means of microfabrication technology using clean room facilities. Microelectrodes were functionalized and characterized in model solutions. The integrated Ag/AgCl electrode demonstrated sufficient stability with a temporal drift of 0.6 $mV.h^{-1}$, which is an acceptable value for bioassays involving short-time measurements conducted for the present application. As far as working microelectrodes are concerned, Pt/IrO_x microelectrodes yielded satisfying performances towards pH monitoring in the range of 2 to 12, in accordance with literature. Calibration results indicated that platinum black UME arrays present great properties towards O_2 and H_2O_2 detection due to the enhanced electrocatalytic activity combined with favorable features of array configurations. Therefore, the aforementioned materials and configurations will be further used through bioassays with lab-on-chip devices for O_2, H_2O_2 and pH monitoring.

Following are the final detection properties obtained that validate the further use of the selected materials (Table 3-3):

Table 3-3. Sensitivity values obtained for H_2O_2 and O_2 detection as well as for pH monitoring using Pt-Bl arrays and Pt/IrO_x microelectrodes.

	Sensitivity
H_2O_2 detection (Pt-Bl arrays)	17 $pA.mm^{-2}.nM^{-1}$
O_2 detection (Pt-Bl arrays)	19 $pA.mm^{-2}.nM^{-1}$
pH monitoring (Pt/IrO_x)	68 $mV.pH^{-1}$

3.6 References

Angerstein-Kozlowska, H., Conway, B.E., Sharp, W.B.A., 1973. The real condition of electrochemically oxidized platinum surfaces: Part I. Resolution of component processes. J. Electroanal. Chem. Interfacial Electrochem. 43, 9–36. doi:10.1016/S0022-0728(73)80307-9

Arbault, S., Pantano, P., Jankowski, J.A., Vuillaume, M., Amatore, C., 1995. Monitoring an oxidative stress mechanism at a single human fibroblast. Anal. Chem. 67, 3382–3390.

Ben-Amor, S., Devin, A., Rigoulet, M., Sojic, N., Arbault, S., 2013. Oxygen Plasma Treatment of Platinized Ultramicroelectrodes Increases Sensitivity for Hydrogen Peroxide Detection on Mitochondria. Electroanalysis 25, 656–663. doi:10.1002/elan.201200409

Ben-Amor, S., Vanhove, E., Sékli Belaïdi, F., Charlot, S., Colin, D., Rigoulet, M., Devin, A., Sojic, N., Launay, J., Temple-Boyer, P., Arbault, S., 2014. Enhanced Detection of Hydrogen Peroxide with Platinized Microelectrode Arrays for Analyses of Mitochondria Activities. Electrochimica Acta, BIOELECTROCHEMISTRY 2013 Selection of papers from the 12th ISE Topical Meeting17-21 March 2013, Bochum, Germany 126, 171–178. doi:10.1016/j.electacta.2013.11.104

Berduque, A., Lanyon, Y.H., Beni, V., Herzog, G., Watson, Y.E., Rodgers, K., Stam, F., Alderman, J., Arrigan, D.W.M., 2007. Voltammetric characterisation of silicon-based microelectrode arrays and their application to mercury-free stripping voltammetry of copper ions. Talanta 71, 1022–1030. doi:10.1016/j.talanta.2006.05.090

Bezbaruah, A.N., Zhang, T.C., 2002. Fabrication of anodically electrodeposited iridium oxide film pH microelectrodes for microenvironmental studies. Anal. Chem. 74, 5726–5733.

Christophe, C., 2010. Intégration de microcapteurs électrochimiques en technologies “Silicium et Polymères” pour l’étude du stress oxydant. Application à la biochimie cutanée. Université Paul Sabatier - Toulouse III.

Christophe, C., Sékli Belaidi, F., Launay, J., Gros, P., Questel, E., Temple-Boyer, P., 2013. Elaboration of integrated microelectrodes for the detection of antioxidant species. Sens. Actuators B Chem. 177, 350–356. doi:10.1016/j.snb.2012.11.032

Clark, L.C., Jr, Wolf, R., Granger, D., Taylor, Z., 1953. Continuous recording of blood oxygen tensions by polarography. J. Appl. Physiol. 6, 189–193.

Davies, T.J., Compton, R.G., 2005. The cyclic and linear sweep voltammetry of regular and random arrays of microdisc electrodes: Theory. J. Electroanal. Chem. 585, 63–82. doi:10.1016/j.jelechem.2005.07.022

Desmond, D., Lane, B., Alderman, J., Glennon, J.D., Dermot Diamond, Arrigan, D.W.M., 1997. Evaluation of miniaturised solid state reference electrodes on a silicon based component. Sens. Actuators B Chem. 44, 389–396. doi:10.1016/S0925-4005(97)00231-1

Elsen, H.A., Monson, C.F., Majda, M., 2009. Effects of Electrodeposition Conditions and Protocol on the Properties of Iridium Oxide pH Sensor Electrodes. J. Electrochem. Soc. 156, F1. doi:10.1149/1.3001924

Fiaccabrino, G.C., Koudelka-Hep, M., 1998. Thin-Film Microfabrication of Electrochemical Transducers. Electroanalysis 10, 217–222. doi:10.1002/(SICI)1521-4109(199804)10:4<217::AID-ELAN217>3.0.CO;2-W

Gardner, R.D., Zhou, A., Zufelt, N.A., 2009. Development of a Microelectrode Array Sensing Platform for Combination Electrochemical and Spectrochemical Aqueous Ion Testing. Sens. Actuators B Chem. 136, 177–185. doi:10.1016/j.snb.2008.10.031

Ges, I.A., Ivanov, B.L., Schaffer, D.K., Lima, E.A., Werdich, A.A., Baudenbacher, F.J., 2005. Thin-film IrOx pH microelectrode for microfluidic-based microsystems. Biosens. Bioelectron. 21, 248–256. doi:10.1016/j.bios.2004.09.021

Hull, E., Piech, R., Kubiak, W.W., 2008. Iridium Oxide Film Electrodes for Anodic Stripping Voltammetry. Electroanalysis 20, 2070–2075. doi:10.1002/elan.200804295

Katsube, T., Lauks, I., Zemel, J.N., 1981. pH-sensitive sputtered iridium oxide films. Sens. Actuators 2, 399–410. doi:10.1016/0250-6874(81)80060-1

Kieninger, J., 2011. Electrochemical microsensor system for cell culture monitoring. Universität Freiburg.

Kim, T.Y., Yang, S., 2014. Fabrication method and characterization of electrodeposited and heat-treated iridium oxide films for pH sensing. Sens. Actuators B Chem. 196, 31–38. doi:10.1016/j.snb.2014.02.004

Klein, J.D., Clauson, S.L., Cogan, S.F., 1989. Morphology and charge capacity of sputtered iridium oxide films. J. Vac. Sci. Technol. Vac. Surf. Films 7, 3043–3047. doi:10.1116/1.576313

Konopka, S.J., McDuffie, B., 1970. Diffusion coefficients of ferri- and ferrocyanide ions in aqueous media, using twin-electrode thin-layer electrochemistry. Anal. Chem. 42, 1741–1746. doi:10.1021/ac50160a042

Kounaves, S.P., Deng, W., Hallock, P.R., Kovacs, G.T.A., Storment, C.W., 1994. Iridium-based ultramicroelectrode array fabricated by microlithography. Anal. Chem. 66, 418–423. doi:10.1021/ac00075a017

Lale, A., Tsopela, A., Civelas, A., Salvagnac, L., Launay, J., Temple-Boyer, P., 2014. Integration of tungsten layers for the mass fabrication of WO3-based pH-sensitive potentiometric microsensors. Sens. Actuators B Chem. 206, 152–158.

Li, Y., Sella, C., Lemaître, F., Guille Collignon, M., Thouin, L., Amatore, C., 2013. Highly Sensitive Platinum-Black Coated Platinum Electrodes for Electrochemical Detection of Hydrogen Peroxide and Nitrite in Microchannel. Electroanalysis 25, 895–902. doi:10.1002/elan.201200456

Marzouk, S.A., Ufer, S., Buck, R.P., Johnson, T.A., Dunlap, L.A., Cascio, W.E., 1998. Electrodeposited iridium oxide pH electrode for measurement of extracellular myocardial acidosis during acute ischemia. Anal. Chem. 70, 5054–5061.

Meng, E., Zhang, X., Benard, W., 2011. Additive Processes for Polymeric Materials, in: Ghodssi, R., Lin, P. (Eds.), MEMS Materials and Processes Handbook, MEMS Reference Shelf. Springer US, pp. 193–271.

Nassi, A., Kim, L.T.T., Girard, A., Griscom, L., Razan, F., Griveau, S., Thouin, L., Bedioui, F., 2012. Comparison of three different configurations of dual ultramicroelectrodes for the decomposition of S-Nitroso-L-glutathione and the direct detection of nitric oxide. Microchim. Acta 179, 337–343. doi:10.1007/s00604-012-0860-z

Olthuis, W., Robben, M.A.M., Bergveld, P., Bos, M., van der Linden, W.E., 1990. pH sensor properties of electrochemically grown iridium oxide. Sens. Actuators B Chem. 2, 247–256. doi:10.1016/0925-4005(90)80150-X

Parker, C.O., Lanyon, Y.H., Manning, M., Arrigan, D.W.M., Tothill, I.E., 2009. Electrochemical immunochip sensor for aflatoxin M1 detection. Anal. Chem. 81, 5291–5298. doi:10.1021/ac900511e

Popovtzer, R., Neufeld, T., Ron, E. z., Rishpon, J., Shacham-Diamand, Y., 2006. Electrochemical detection of biological reactions using a novel nano-bio-chip array. Sens. Actuators B Chem. 119, 664–672. doi:10.1016/j.snb.2006.01.037

Prats-Alfonso, E., Abad, L., Casañ-Pastor, N., Gonzalo-Ruiz, J., Baldrich, E., 2013. Iridium oxide pH sensor for biomedical applications. Case urea–urease in real urine samples. Biosens. Bioelectron. 39, 163–169. doi:10.1016/j.bios.2012.07.022

Rand, D.A.J., Woods, R., 1972. A study of the dissolution of platinum, palladium, rhodium and gold electrodes in 1 m sulphuric acid by cyclic voltammetry. J. Electroanal. Chem. Interfacial Electrochem. 35, 209–218. doi:10.1016/S0022-0728(72)80308-5

Remita, E., 2007. Thesis. Etude de la corrosion d'un acier faiblement allié en milieu confiné contenant du CO2 dissous. Paris 6.

Rodriguez-López, J.N., Ros-Martínez, J.R., Varón, R., García-Cánovas, F., 1992. Calibration of a Clark-Type oxygen electrode by tyrosinase-catalyzed oxidation of 4-tert-butylcatechol. Anal. Biochem. 202, 356–360.

Saito, Y., 1968. A Theoretical Study on the Diffusion Current at the Stationary Electrodes of Circular and Narrow Band Types. Rev. Polarogr. 15, 177–187. doi:10.5189/revpolarography.15.177

Sato, Y., 1989. Electrochromis in Thermally Oxidized Iridium Oxide Films in LiClO4/Propylene Carbonate. Jpn. J. Appl. Phys. 28, 1290. doi:10.1143/JJAP.28.1290

Schmitt, G., Schultze, J.-W., Faßbender, F., Buß, G., Lüth, H., Schöning, M.J., 1999. Passivation and corrosion of microelectrode arrays. Electrochim. Acta 44, 3865–3883. doi:10.1016/S0013-4686(99)00094-8

Schwake, A., Ross, B., Cammann, K., 1998. Chrono amperometric determination of hydrogen peroxide in swimming pool water using an ultramicroelectrode array. Sens. Actuators B Chem. 46, 242–248. doi:10.1016/S0925-4005(98)00124-5

Simonis, A., Lüth, H., Wang, J., Schöning, M.J., 2004. New concepts of miniaturised reference electrodes in silicon technology for potentiometric sensor systems. Sens. Actuators B Chem. 103, 429–435. doi:10.1016/j.snb.2004.04.072

Suzuki, H., 2000. Microfabrication of chemical sensors and biosensors for environmental monitoring. Mater. Sci. Eng. C 12, 55–61. doi:10.1016/S0928-4931(00)00158-2

Suzuki, H., Hiratsuka, A., Sasaki, S., Karube, I., 1998. Problems associated with the thin-film Ag/AgCl reference electrode and a novel structure with improved durability. Sens. Actuators B Chem. 46, 104–113. doi:10.1016/S0925-4005(98)00043-4

Tilak, B.V., Conway, B.E., Angerstein-Kozlowska, H., 1973. The real condition of oxidized pt electrodes: Part III. Kinetic theory of formation and reduction of surface oxides. J. Electroanal. Chem. Interfacial Electrochem. 48, 1–23. doi:10.1016/S0022-0728(73)80290-6

Toczyłowska-Mamińska, R., Ciosek, P., Ciok, K., Wróblewski, W., 2008. Development of a miniaturised electrochemical cell integrated on epoxy-glass laminate. Microchim. Acta 163, 89–95. doi:10.1007/s00604-008-0959-4

Truesdale, G.A., Downing, A.L., 1954. Solubility of Oxygen in Water. Nature 173, 1236–1236. doi:10.1038/1731236a0

Vaddiraju, S., Tomazos, I., Burgess, D.J., Jain, F.C., Papadimitrakopoulos, F., 2010. Emerging synergy between nanotechnology and implantable biosensors: A review. Biosens. Bioelectron. 25, 1553–1565. doi:10.1016/j.bios.2009.12.001

Vanhove, E., Tsopéla, A., Bouscayrol, L., Desmoulin, A., Launay, J., Temple-Boyer, P., 2013. Final capping passivation layers for long-life microsensors in real fluids. Sens. Actuators B Chem. 178, 350–358. doi:10.1016/j.snb.2012.12.088

Wittkampf, M., Chemnitius, G.-C., Cammann, K., Rospert, M., Mokwa, W., 1997. Silicon thin film sensor for measurement of dissolved oxygen. Sens. Actuators B Chem. 43, 40–44. doi:10.1016/S0925-4005(97)00138-X

Wu, C.-C., Lin, W.-C., Fu, S.-Y., 2011. The open container-used microfluidic chip using IrOx ultramicroelectrodes for the in situ measurement of extracellular acidification. Biosens. Bioelectron. 26, 4191–4197. doi:10.1016/j.bios.2011.04.034

Yamanaka, K., 1989. Anodically Electrodeposited Iridium Oxide Films (AEIROF) from Alkaline Solutions for Electrochromic Display Devices. Jpn. J. Appl. Phys. 28, 632. doi:10.1143/JJAP.28.632

Yang, H., Kang, S.K., Choi, C.A., Kim, H., Shin, D.-H., Kim, Y.S., Kim, Y.T., 2004. An iridium oxide reference electrode for use in microfabricated biosensors and biochips. Lab. Chip 4, 42–46. doi:10.1039/b309899k

Zorman, C.A., Roberts, R.C., Chen, L., 2011. Additive Processes for Semiconductors and Dielectric Materials, in: Ghodssi, R., Lin, P. (Eds.), MEMS Materials and Processes Handbook, MEMS Reference Shelf. Springer US, pp. 37–136.

Chapter 4
Lab-on-chip devices: technology

After validating suitable electrode materials and detection properties through simple devices and procedures, the final device intended for the environmental application was developed. The final device consists in a portable system for on-site detection capable of providing an early indication and meeting the requirement for simple, rapid, cost-effective and portable techniques for the detection of pollutants.

As a matter of fact, system integration and miniaturization gives the possibility of performing on-site analysis providing rapid, real-time feedback information on the presence of pollutants and enabling higher analysis frequency of samples directly in the field (Lagarde and Jaffrezic-Renault, 2011; Grieshaber et al., 2008; Li et al., 2013). Lab-on-chip systems are environmentally and economically affordable as they require samples and reagents of smaller volume, therefore producing wastes of smaller quantities (Jang et al., 2011). Moreover, samples can be tested directly after collection which is advantageous considering the fact that their composition can rapidly change after storage (Manz et al., 1990).

It was therefore essential to integrate the previously described electrochemical detection system consisting of three-electrode electrochemical cells on a sealed fluidic system in order to obtain an autonomous and portable sensor. The selection of materials and techniques used for the fabrication and packaging of the lab-on-chip device is based on the desired characteristics of the final device and are described in this chapter.

4.1 Lab-on-chip design

The lab-on-chip platform developed through this project is intended to give the possibility of conducting double complementary detection, electrochemical and optical (Lefèvre et al., 2012) and will be used in environmental applications and more specifically water toxicity analysis. All different sensors, electrochemical and optical, will be assembled on a fluidic matrix.

The main characteristics of the final device were indicated by the requirements of the electrochemical and optical detection system, as well as the major objectives of the targeted application:

- All components of the lab-on-chip should be compatible with optical technology in order to enable optical measurements requiring materials of high optical transmission.

- The final device needs to be compact and fragile components should be avoided given the fact that a solid device can be easily handled by any operator.

- The system should be biocompatible as it will be hosting algal cells, the biological recognition element of the sensors.

- Detection chambers, large enough to accommodate the three-electrode electrochemical cells, consisting of a working ultramicroelectrode array, encircled by the reference and counter electrodes are required. What is more, large chambers can facilitate optical measurements. Indeed, an important prerequisite for optical detection is to ensure a sufficiently high number or concentration of algal cells in the chamber in order to produce a large signal.

- Large channels that enable easy reagent loading are also important for the implementation of an easy-to-use device.

- All procedures and structures used should not be detrimental for fragile electrode materials.

All these requirements should be taken into account upon the implementation of the lab-on-chip, described through this chapter.

Six independent detection chambers were designed on each platform enabling the simultaneous processing of different assays. The platform designed is presented in Figure 4.1.

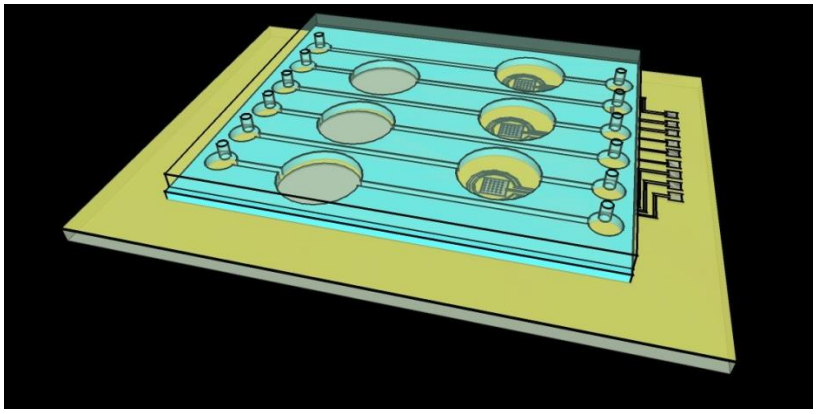

Figure 4.1. 3D model of lab-on-chip platform including 6 independent chambers. The three chambers on the left are dedicated to optical detection whereas the chambers on the right to electrochemical.

Three chambers are dedicated to the optical detection while the complete electrochemical cells were integrated on the other three chambers. This matrix of channels and measurement chambers could serve different purposes, for instance:

- Increase analysis frequency by conducting parallel analysis of several samples in order to reduce false alarms.

- Give the possibility of calibrating the sensor by using one of the chambers for control measurement with a non-polluted sample and compare with the values obtained for the polluted samples.

- Enable future integration of different algal species in order to increase sensor selectivity as each algae species will be sensitive to different pollutant giving the possibility of conducting multi-analysis.

- Concerning the electrochemical part, the detection of the three species of interest (O_2, H_2O_2, pH related ions) can be performed at the same time by integrating each sensor in one independent chamber. Monitoring of each species can indicate the presence of different herbicides type. Indeed, herbicides like Diuron and Atrazine target Photosystem II, with a direct impact on O_2 production, while herbicides like Paraquat target Photosystem I by causing an increase in H_2O_2 and OH^- production (see Chapter 2). Monitoring of each of the three elements indicating the presence of herbicides should be performed in separate chambers. A different fluidic chamber should be dedicated for the detection of each species as detection protocols are different: extracellular O_2 variation measurement can be directly performed after adding algae cells whereas intracellular H_2O_2 and pH variation monitoring needs cell lysis prior to measurement. Moreover, dissociation of measurement chambers is important as not only electrochemical methods conducted for detection are different (chronoamperometry or potentiometry) but also detection of one species can produce elements that interfere with the measurement of the other species (i.e O_2 reduction can produce H_2O_2).

4.2 Fabrication procedure

The process followed for the development of the prototype consisted in the following steps:

a. Substrate selection and preparation
b. Electrode structuring

c. Fluidic system implementation
d. Device packaging

Each step of the process is detailed in the following part.

4.2.1 Substrate

Silicon substrates used through the development of the first prototype described in Chapter 3 could not be used for the fabrication of the final lab-on-chip device given the fact that optical sensors will be integrated on the final structure. Compatibility with optical technology is therefore one of the basic criteria to be satisfied through the selection of the suitable substrate. Glass has been widely used as a substrate due to good electric insulation properties, chemical resistance to reagents used through assays and optical transparency (Henares et al., 2008). Flexible films, such as PET (Polyethylene terephthalate), could also be a potential alternative and have been previously developed through research projects of the LAAS laboratory, as substrates for the integration of electrode cells on fluidic structures intended to humidity measurements (NanoComm ANR research project). Nevertheless, given the fact that the application does not require flexible devices, glass substrates were preferred for the development of the lab-on-chip device due to their rigidity and compatibility with procedures available in clean room.

BOROFLOAT®33 glass wafers were purchased from Schott. Their thickness is 500 µm and their diameter four inches. This material is suitable for chemical analysis as it is highly resistant to attack of several chemical substances. What is more, its high optical transmission and low fluorescence intensities over the entire light spectrum make it suitable for the integration of optical technology (BOROFLOAT®33, SCHOTT Technical Glass Solutions GmbH, Germany).

4.2.2 Electrode structuring

The electrochemical sensors consisted in the three-electrode cells presented in Chapter 3. The results detailed previously (Chapter 3) indicated the materials and configurations that gave good detection properties and should be used through the following tests. Platinum black UME arrays were integrated on the electrochemical part for O_2 and H_2O_2 detection while Pt/IrO_x ultramicroelectrodes for pH monitoring. The fabrication process for electrode structuring consisted in deposition and patterning of Ti/Pt and Ag layers, followed by deposition and patterning of the Si_3N_4 passivation layer (see Chapter 3: Fabrication of electrochemical microcells).

Among the key points of the fabrication strategy followed, was the transfer of the previously described silicon-based fabrication technology used for electrode structuring on glass substrates. Photolithography parameters previously applied needed now to be adapted to the properties of the glass wafer. These parameters for resists deposited on silicon wafers are already determined, given the fact that silicon is the substrate most often used among research projects developed in the clean room of LAAS, as it is a semiconductor. Thermal properties and transparency of glass have a direct impact on resist baking procedures as well as time of exposure to UV radiation.

4.2.2.1 ***Baking procedures***

Soft bake and post exposure bake are crucial steps (see Chapter 3: Fabrication of electrochemical microcells), as they determine the stress adhesion of the resist on the underlying layer and their duration is modified according to the thermal properties of the material. More precisely, during soft bake, the solvent in the resist layer is reduced, yielding a stable film and improving adhesion of the resist on the underlying layer. Post-exposure bake serves at completing the crosslinking mechanism of negative photoresists initiated through exposure as well as reducing mechanical stress and therefore enhancing resist adhesion.

The efficiency of these steps depends on the temperature applied through the hot plate and the baking duration. Since these parameters were already determined for silicon wafers, they now needed to be adapted to the different thermal properties of the glass. Thermal capacitance and thermal resistance are known to influence transient heat transfer in the wafer volume and determine the time the wafer needs to reach the desired temperature. The greater these values are, the more time the system will take to respond to changes in its thermal environment (Incropera et al., 2006). The glass wafer used has higher thermal resistance and capacitance than the silicon wafer (for the same thickness) and therefore needs more time to attain the suitable temperature.

Baking time needed consequently to be increased compared to silicon-based procedure for all resists used. At this point it is important to remind that a double layer of LOR 3A lift-off resist and AZ NLof negative photoresist was used for patterning of all metallic layers, while a double layer of LOR 3A and AZ ECI 3012 positive photoresist was used for Si_3N_4 passivation layer patterning (see Chapter 3: Fabrication of electrochemical microcells). The appropriate time increase was determined empirically and eventually (final values are presented in Table 4-1):

- 25% increase in soft-bake duration was applied for AZ NLof and AZ ECI 3012 photoresists and the dissolution rate in the developer could be effectively controlled.

- 100% increase in soft-bake duration was applied LOR 3A lift-off resist in order to get optimal adhesion so that the resist film will be sufficiently resistant to etching by the developer solution. For shorter baking times, dissolution rate of the LOR 3A film during development could not be controlled and the etching was not uniform along the film (Figure 4.2).

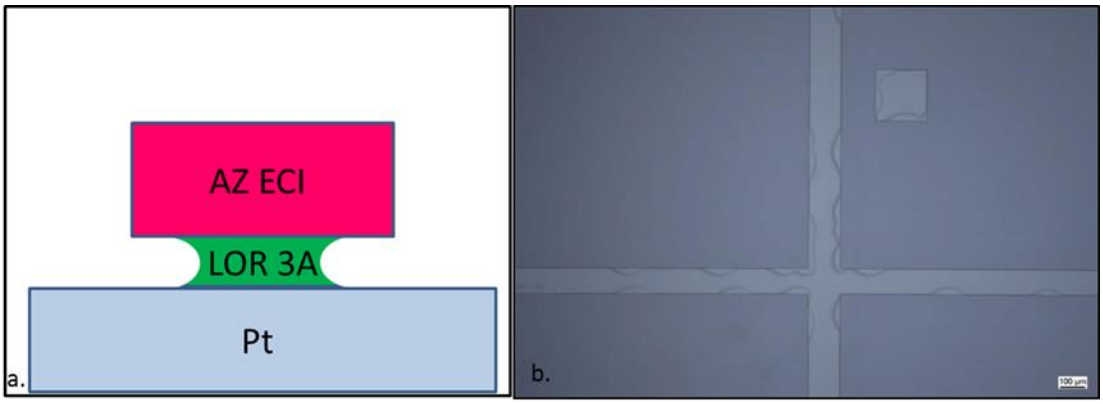

Figure 4.2. Bi-layer resist patterns obtained after development, (a) schematic view of the cross section (b) microscope image: When baking time was not sufficiently long, the underlying LOR 3A layer was not uniformly etched by the developer while the profile of the upper AZ ECI 3012 resist layer was well-defined.

4.2.2.2 ***Exposure to UV irradiation***

The second photolithography parameter needed to be modified for the glass-based fabrication process was the exposure time to UV irradiation. In the case of silicon wafers, the surface is reflecting the UV light, increasing the total dose of light received by the resist. On the other hand, glass is transparent, allowing light to pass through its volume. The total dose of light received by the resist is less compared to the one received when Si substrates are used, calling for an increase in the exposure time so that homogeneous illumination of the entire resist film can be achieved.

The exposure time required for resists deposited on glass wafers was determined experimentally, through several tests carried out by the technical team of the clean room of LAAS. 20% increase was eventually introduced in the exposure time of the photoresist during the glass-based procedure compared to the one during Si-based.

After integrating the aforementioned modifications in the photolithography parameters and following the fabrication procedure described in Chapter 3, the three-electrode electrochemical cells comprised of platinum working and counter electrodes and silver-based reference electrodes were formed on the glass wafers. A 3D model of the electrochemical cells obtained after electrode and passivation layer structuring is shown in Figure 4.3.

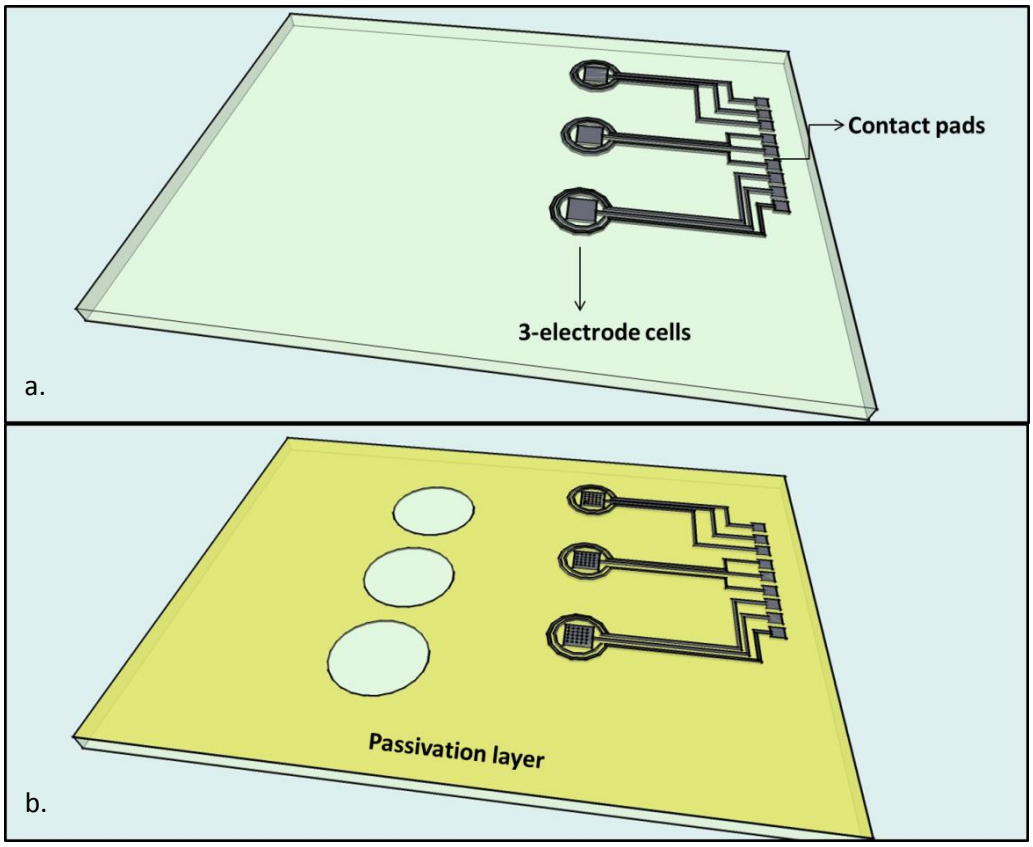

Figure 4.3. 3D model of the (a) first and (b) second level of the lab-on-chip fabrication procedure: (a) electrode material deposition and pattering and (b) Si_3N_4 passivation layer deposition and pattering for the creation of the electrochemical cells.

The unjustified presence of the passivation layer on the left part of the device dedicated to the optical detection will be explained in the following section as it is related to the definition of the fluidic structure.

At this point it is important to mention a problem encountered during photolithography for patterning of the passivation layer. Distortion of the desired resist pattern was occasionally observed after UV exposure. This distortion only occurred for the circular, bi-layer resist patterns that were intended to form the electroactive surface area of the ultramicroelectrodes of 10 µm diameter after lift-off. Instead of obtaining a compact circular stack of the bi-layer LOR 3A and AZ ECI after development, a donut-shaped stack of the two resists with a hole in the middle is formed, making lift-off impossible. In Figure 4.4 a, the donut-shaped stack of resists is shown after the deposition of Si_3N_4. The resist bi-layer could not be reached by the stripping solution during lift-off as the original shape was modified and the underlying platinum electroactive electrode surface could not be liberated (the desired result shown in Figure 4.4 b).

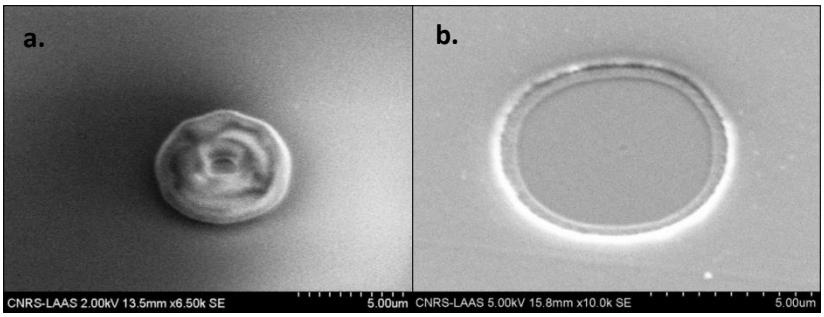

Figure 4.4. (a) The donut-shaped stack of resists after the deposition of Si_3N_4. (b) The desired shape of the electrode obtained after resist lift-off.

One possible assumption is that this interference pattern is created by the diffraction of the UV light after encountering the disk pattern on the mask and probably caused by a gap between the mask and the resist surface on the wafer due to edge beads, bubbles or particles in the resist film. What is more, diffraction and therefore interference patterns are more pronounced with high exposure dose. Consequently, vacuum contact between mask and wafer was always verified so that any proximity gap will be avoided and UV irradiation time was decreased in order to minimize optical interference. After applying the above modifications, interference patterns were no longer observed and lift-off was successfully carried out.

The following table (Table 4-2) presents important photolithography parameters that had to be modified when the silicon substrate was changed to a glass substrate (all other deposition and passivation processes were left unchanged).

Table 4-1. Comparison of photolithography parameters applied for resists deposited on silicon and glass substrates.

		Silicon substrate		**Glass substrate**	
Photolithography for metal layers patterning		LOR 3A	AZ NLof	LOR 3A	AZ NLof
	Baking Soft Bake Post exposure bake	2min(170°C) -	1min(105°C) 1min(110°C)	5min(170°C) -	1min15sec(105°C) 1min15sec(110°C)
	Exposure (405nm, 25mW.cm^{-2})	-	4sec	-	4.8sec
Photolithography for passivation layer patterning		LOR 3A	AZ ECI	LOR 3A	AZ ECI
	Baking Soft Bake Post exposure bake	2min(170°C) -	1min(90°C) 1min(110°C)/ 1min(105°C)	5min(170°C) -	1min15sec(90°C) 1min15sec(110°C)/ 1min15sec(105°C)
	Exposure (405nm, 25mW.cm^{-2})	-	8sec	-	8sec

4.2.3 Fluidic system implementation

As mentioned at the beginning of the chapter, the fluidic matrix consists of six independent chambers and channels. Dimensions of the chambers were indicated by the dimensions of the electrochemical cells as well as the requirements related to the optical detection system. Consequently, sufficiently large, circular-shaped fluidic chambers were designed with a diameter of 8 mm. The height of the fluidic structure was set at 250 µm which means that each chamber can receive a maximum volume of test solution of 12.5 µL. Fluidic channel width was 500 µm so that reagent loading can be relatively easy.

Different possible alternatives of fluidic matrix structuring were considered. Techniques and materials used for prototyping of fluidic systems depend on the dimensions of channels and chambers, the desired resolution, the selected substrate material and the biocompatibility required for the specific application (Johnson et al., 2008).
Limitations related to bonding of the fluidic structure on the glass substrate or the general sealing procedure are also significant factors that should be considered for the final selection. For instance, the sensitivity of previously deposited electrode materials towards several steps of bonding procedure is another factor that will determine the appropriate sealing technique.

4.2.3.1 ***Glass***

Devices consisting of a fluidic structure made of glass have been already reported in literature. Wet chemical etching has been used to create channels and chambers on a glass substrate which were then sealed with a glass cover (Harrison et al., 1992). Bonding was carried out in a furnace at high temperature (620°C).

This technique involves high temperature procedures and cannot be used for the fabrication of our device as the latter contains temperature-sensitive electrode materials.

In order to avoid this high temperature bonding, Sayah et al. proposed a simple process using an epoxy glue to bond the two glass surfaces (Sayah et al., 2000) while Wang et al. used a thin layer of sodium silicate as an adhesive (H. Wang et al., 1997). In both cases, a heating curing procedure at 90°C is required which is not detrimental for previously deposited electrode materials. However, a possible risk coming along with these procedures is that adhesive materials used could flow into channels and chambers when squeezed during bonding process and block the channels or create interferences to following electrochemical measurements. Leatzow et al. reported that double stick tape could be alternatively applied but its use could also result in eventual leaks as it can easily delaminate in aqueous solutions (Leatzow et al., 2002).

4.2.3.2 ***Polydimethylsiloxane (PDMS)***

Polydimethylsiloxane (PDMS) fluidic systems have been widely used upon lab-on-chip devices due to their simple and low cost fabrication procedure through a replica molding process (Pittet et al., 2007, Brun et al., 2012). The structures made of this elastomeric polymeric are transparent and biocompatible making them suitable for optical systems and biological studies (Sia and Whitesides, 2003, Fujii, 2002). Another significant advantage is the simple sealing procedure followed to bond PDMS on surfaces such as glass, plastic or other polymers (Becker, 2002).

PDMS was the material used to construct the microfluidic chip (Figure 4.5) dedicated exclusively to algal fluorescence measurement for water toxicity evaluation developed in UQAM (Lefèvre et al., 2012).

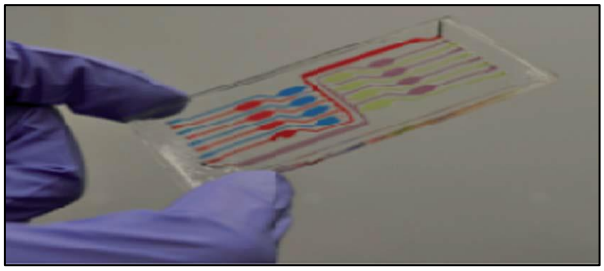

Figure 4.5. Microfluidic chip dedicated to fluorescence measurements (Lefèvre et al., 2012).

A possible alternative for the fluidic system described in this study could thus be to fabricate a PDMS structure through a simple molding procedure and attach it on the glass substrate, which is already patterned with electrodes. The limitation related to the implementation of a fluidic structure made of PDMS on the present device is the plasma oxidation required before bonding. As a matter of fact, a plasma oxygen treatment of high power is necessary to activate both surfaces and form a permanent bond between the PDMS and the substrate surface (Duffy et al., 1998) but on the same time it is detrimental for the silver-based reference electrode (Christophe, 2010). A potential solution to this problem could have been the use of an adhesive layer between the PDMS and the glass substrate but the risks of this technique that are presented in the previous paragraph make this solution not optimal for the implementation of the present device.

Leaks caused by the non-optimal adhesion of the PDMS on the substrate is another problem occasionally encountered with this type of material (Pourciel-Gouzy et al., 2008) and acts as a deterrent in the construction of PDMS fluidic system for the present case.

4.2.3.3 ***SU-8 photoresist***

SU-8 epoxy type, negative photoresist has attracted wide attention upon the construction of fluidic systems as it is biocompatible, has very good mechanical properties, high optical transparency and requires simple fabrication procedures (Yun-Ju Chuang, 2003, Shaw et al., 2003, Heuschkel et al., 1998). What is more, fluidic structure implementation can be performed massively on a wafer level compared to PDMS replica moulding fabrication procedure performed individually on each device. SU-8 is a photo-definable epoxy-based polymer that can be spin or spray coated on the substrate and then patterned through conventional photolithography (Abgrall et al., 2007). After cross-linking, SU-8 films have high physical stability and are chemically inert at room temperature (Kieninger, 2011).
Although the mechanical stress of thick SU-8 films can cause poor adhesion of the fluidic structure on the substrate and result in leaks (Kieninger, 2011), this problem can be solved by optimizing photolithography parameters.
The construction of the SU-8 fluidic structure is therefore an option worth considering for the implementation of the fluidic system. Although the implementation of an open SU-8 fluidic structure is relatively simple, sealing of the channels and chambers is still a challenging issue. Several techniques have been examined:

- The first option consists in creating embedded SU-8 chambers and channels by performing a double-exposure photolithography procedure already reported by Pourciel-Gouzy et al. (Pourciel-Gouzy et al., 2008). A thick layer of SU-8 is deposited and initially exposed to UV light of a wavelength of 365 nm. At this wavelength, the transmission of the SU-8 is very high (Yun-Ju Chuang, 2003) and therefore the entire layer is exposed and therefore cross-linked. The resist layer is then exposed to another wavelength using a filter (280-320 nm) at which the transmission of the resist is lower and therefore the UV cannot access the bottom part of the layer. By partial UV exposure, only the top part is cross-linked, forming the top wall of the structure while the bottom part is dissolved in the developer solution. The only drawback of this procedure is the size limitation yielding chambers of width ranging from 100 to 1000 μm and is therefore not compatible with the dimensions of the desired chambers (d=8 mm).

- Another solution is to seal SU-8 tanks with a cover SU-8 layer coated on a flexible film (Abgrall et al., 2006). The flexible film with the coated, not yet cross-linked SU-8 is laminated on the underlying SU-8 structure. The flexible film is then peeled off and the SU-8 cover layer is exposed to UV light in order to form apertures for liquid injection and extraction. One drawback of this approach is the need of plasma oxygen treatment on both surfaces to perform

bonding. What is more, big dimensions of detection chamber call for a rigid cover that will not bend and fall in the chambers and this cannot be assured using a thin SU-8 cover.

- The third option is to seal SU-8 tanks with either a glass piece or a PDMS structure using a glue in order to obtain a more solid and stable cover that will not fall in the chambers. However this sealing technique requires either the use of UV glue as adhesive between the glass and the underlying SU-8, that can create interferences during electrochemical experiments, or the use of a long plasma O_2 treatment of high power on the PDMS and SU-8 structure before bonding.

- Another option consists in sealing SU-8 tanks with a glass cover using a thin SU-8 layer as glue, so that a mechanically rigid structure can be obtained on which optical parts can later be integrated. Although both PDMS and SU-8 are permeable to gases, a glass cover prevents exchanges with atmospheric oxygen and therefore minimizes the influence of the latter on monitoring of photosynthetically produced oxygen which is the analyte of interest. A thin SU-8 film is deposited on the glass cover before bonding. The first possibility is that the top, thin SU-8 film is already cross-linked before bonding. In this case, high pressure and temperature are required for bonding procedure (Truong and Nguyen, 2004). The second possibility is to use an uncross-linked SU-8 layer as a glue in order to facilitate bonding procedure which is carried out using the wafer bonder (Jackman et al., 2001).

After considering all possible options for the implementation of the fluidic system, the solution that meets the requirements of the desired system was the construction of an SU-8 structure which will be sealed by a glass cover coated with a thin layer of SU-8. The fabrication part concerning fluidic system implementation can therefore be described through two steps:

i. SU-8 fluidic structure deposition and patterning
ii. Bonding of glass cover on fluidic structure

Fabrication procedure of each step is detailed in the following part.

SU-8 fluidic structure deposition and patterning

SU-8 layer structuring followed the formation of the electrochemical cells on the glass wafer (3-electrode systems defined through the Si_3N_4 passivation layer) (Figure 4.6).

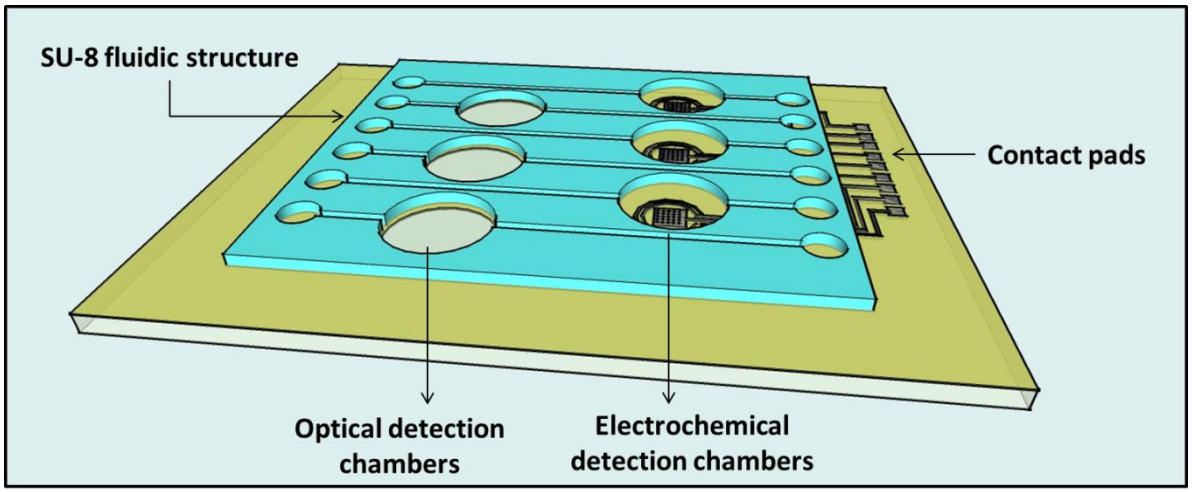

Figure 4.6. 3D model of the third step of the fabrication procedure: SU8 fluidic structure patterning.

Sufficient adhesion of the SU-8 layer on the glass substrate is normally assured through a plasma oxygen treatment of 15 minutes at 800 W, on the glass substrate just before deposition. However, such a long plasma O_2 treatment would have been detrimental for silver electrodes and was therefore replaced by a plasma O_2 treatment of 1 min at 800 W during which electrodes were protected through a positive resist pad. A photolithography step was carried out, prior to plasma, in order to deposit the AZ ECI 3012 photoresist on the electrode cells and it was verified that after plasma treatment, the resist film was not totally etched and was still covering the electrodes. Figure 4.7 shows a schematic cross-section view of the different layers.

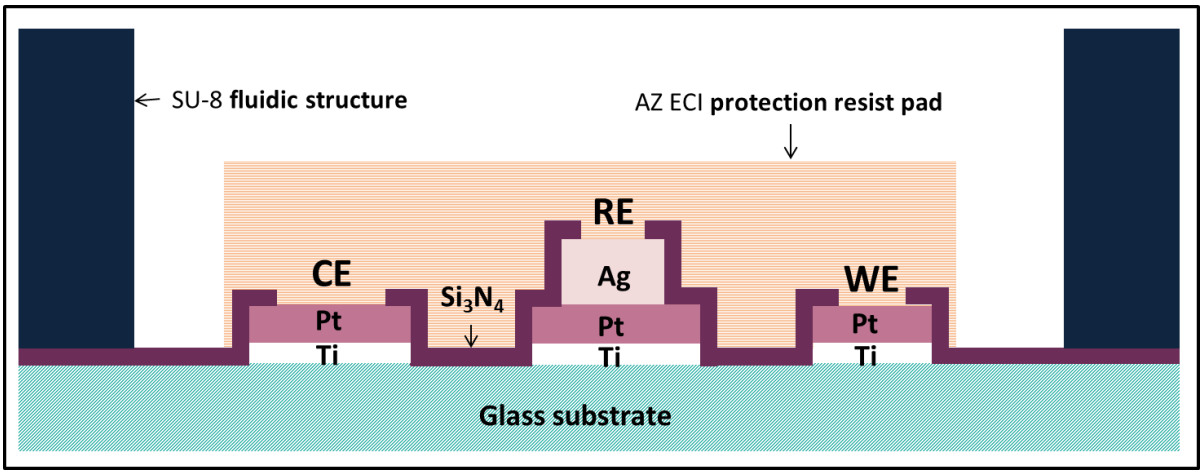

Figure 4.7. Schematic cross section view of deposited layers.

SU-8 photolithography process and more particularly UV exposure and baking parameters, were also optimised in order to assure adhesion of the SU-8 layer on the substrate.

A 250 µm layer of SU-8 3050 (MicroChem Inc.) was spin coated on the already electrode-patterned, glass wafer through a two-step deposition process followed by two soft-bakes overnight. Baking steps are very crucial. Optimised and glass-adapted baking procedures were used in order to reduce high stress and avoid cracking of the resist (Hammacher et al., 2008) and wafer bending (Abgrall et al., 2007). This stress is induced by the big difference in the thermal expansion coefficients of SU-8 and glass that correspond to 52 ppm.K^{-1} (Lorenz et al., 1998) and 3.2 ppm.K^{-1} (value provided by the supplier), respectively. All baking steps were therefore carried out on a hot plate using a progressive temperature ramp to reach a particular temperature, at which the wafer was kept for a sufficient time period and then ramped down again until room temperature. Figure 4.8 presents the temperature variation through time during the two SU-8 soft-bakes.

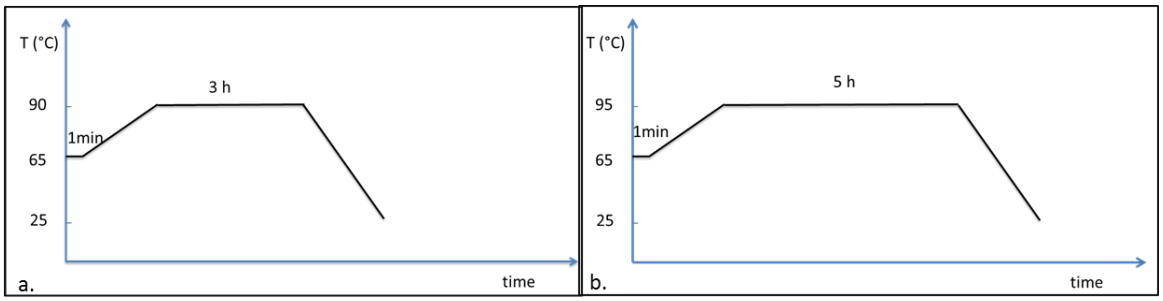

Figure 4.8. Temperature variation through time for both soft-bakes of the 250 µm SU-8 structure.

UV exposure time had to be optimized in order to compensate the absence of the long plasma oxygen treatment required before the deposition of the SU-8 layer to promote adhesion. Considering the thickness of the SU-8 film, if exposure time is not sufficient, the bottom part of the film will not be cross-linked, leading to weak adhesion and therefore potential leaks of the liquid from one chamber to the other (Figure 4.9).

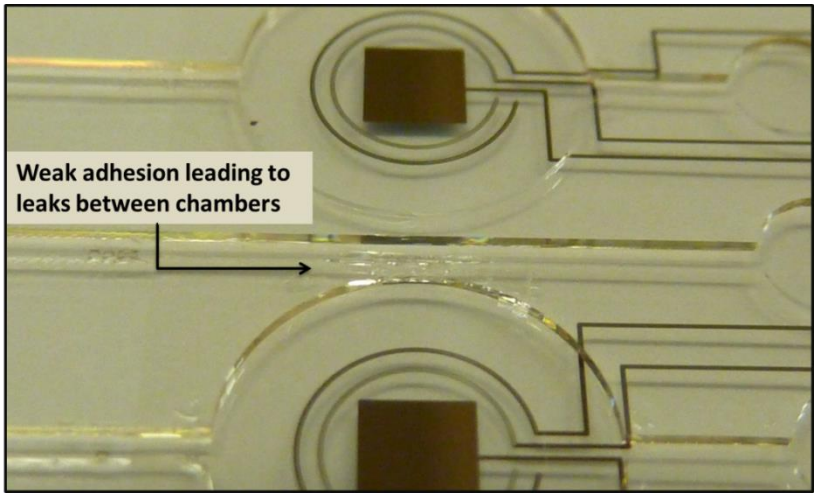

Figure 4.9. Weak adhesion of SU-8 film on glass substrate.

The wafer and the optical mask were placed in hard contact in a MA6 Optical aligner (Suss Microtec) using a filter (λ=365 nm) and different exposure durations, ranging from 20 to 125 seconds, were tested. The optimal exposure time was found to be 100 seconds, for a power of 20 $mW.cm^{-2}$, corresponding to a two-fold increase in the standard time required (power was kept constant).

Post-exposure bake was then performed in order to complete cross-linking procedure (Hammacher et al., 2008) and the temperature variation through baking time is presented in Figure 4.10 a.

The development of the thick film in the SU-8 developer solution was the next step. During the development, the non-exposed SU-8 part is dissolved in the developer, followed by the dissolution of the positive resist pad, deposited previously to protect electrodes during plasma O_2, by the same developer.

Hard bake was then performed to complete SU-8 structuring procedure and enhance chemical and physical stability of the resist film (Figure 4.10 b).

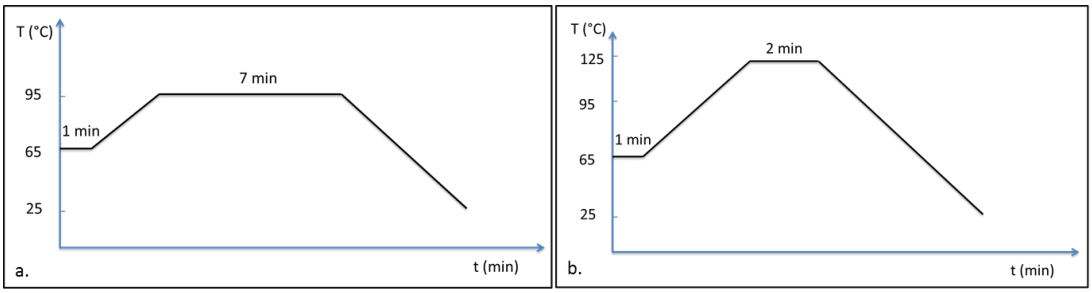

Figure 4.10. Temperature variation through time for (a) post-exposure bake and (b) hard bake of the 250 µm SU-8 structure.

Despite the progressive temperature ramp applied through baking procedures to reach time to reach a particular temperature, residual stress of SU-8 layer was still evident. Given the fact that SU-8 film thickness (250 µm) is comparable to the thickness of the glass substrate (500 µm) and due to the big difference in the two thermal expansion coefficients, the stress at the interface is not negligible, leading to bending of the wafer. This issue can be problematic through bonding procedure, presented below, but can be compensated by optimizing bonding parameters.

After optimising photolithography parameters, it was important to focus on patterning of the underlying layer in order to improve adhesion of SU-8. It was observed that adhesion of SU-8 was better on Si_3N_4 rather than glass. For the first devices, Si_3N_4 passivation layer was not deposited on the left part of the device and the SU-8 film of this part was detached (Figure 4.11).

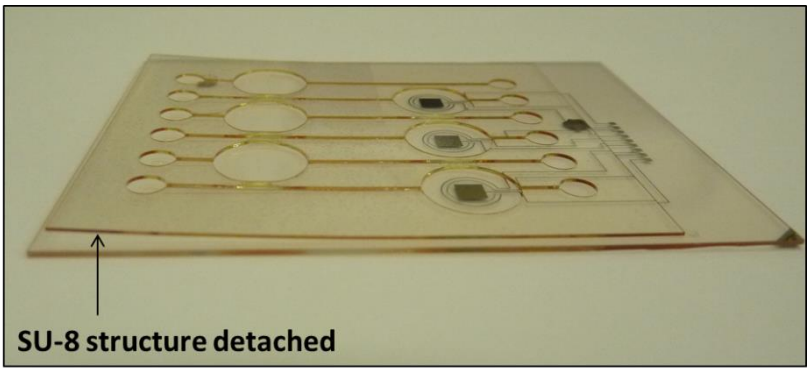

Figure 4.11. SU-8 film detached on the part of the device where it is in contact with glass (left part) and not with Si_3N_4 (right part).

Therefore, in order to assure adhesion of SU-8, Si_3N_4 was even deposited on the left part of the device. Nevertheless, the chambers dedicated to optical measurements were left uncovered, given the fact that Si_3N_4 is semi-transparent and can impede optical measurements.

Once all parameters were optimised and SU-8 structuring was completed, a resist was deposited through spray coating to protect the wafer during dicing procedure. The devices obtained after dicing and protection resist elimination, had dimensions of 5.5 cm length and 4 cm width and are shown in Figure 4.12.

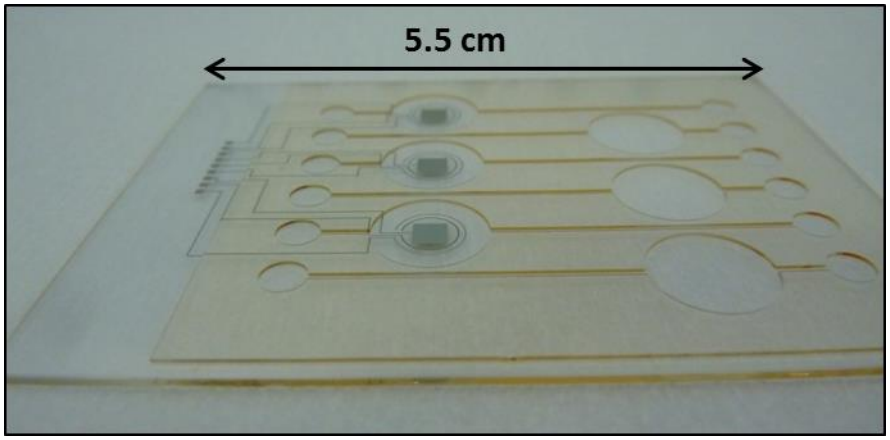

Figure 4.12. SU-8 structure on the sensor platform.

Bonding of glass cover on fluidic structure

The fluidic platforms had now to be sealed with the glass cover. BOROFLOAT®33 glass wafers of 500 µm thickness were diced to form the glass covers and apertures for the injection and extraction of

liquids were drilled through sand blasting, before bonding. Figure 4.13 presents a 3D model of the component assembly.

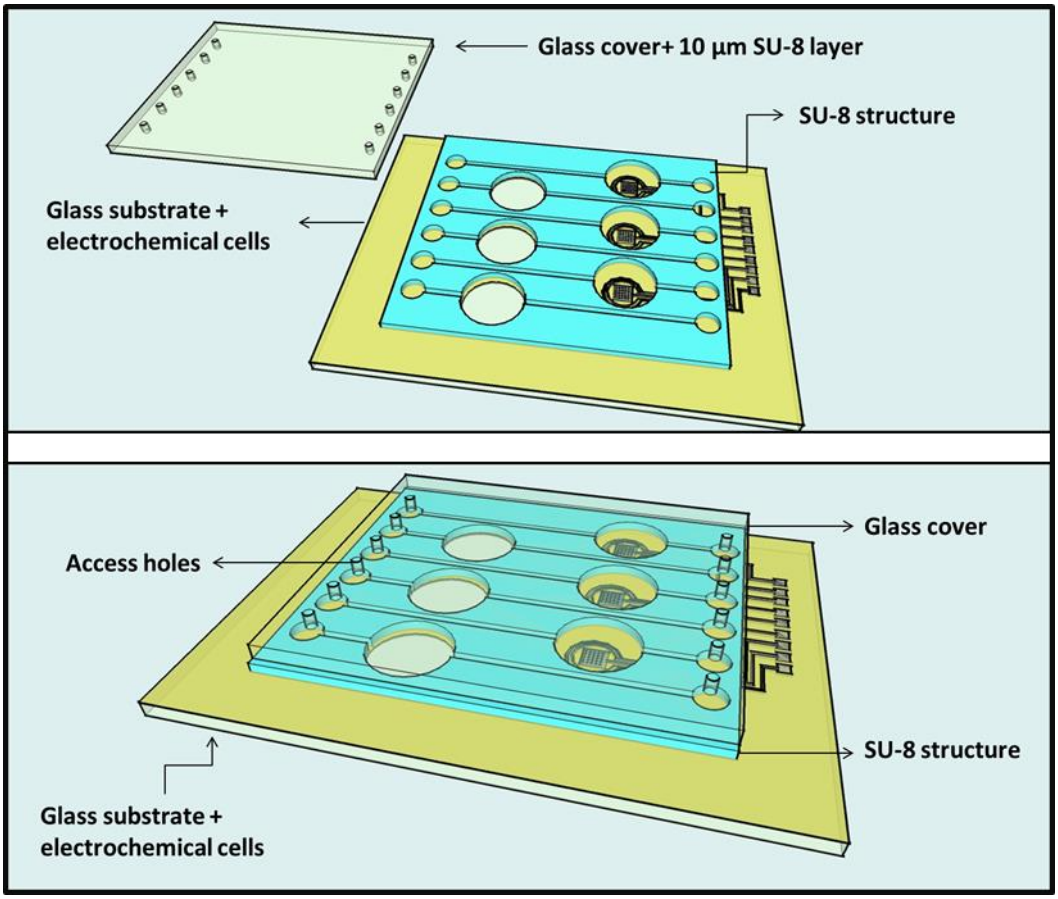

Figure 4.13. 3D model of the component assembly: Bonding of glass cover on underlying fluidic structure.

Sand blasting was the technique used to drill the access holes. Prior to drilling, a dry photosensitive film was laminated on both surfaces of the wafer using Shipley laminator (The Rohm and Haas Electronic Materials, Italy). The role of the film is to allow patterning of the glass cover as it changes its color from light blue to dark blue after UV exposure and protect during drilling. Drilling was performed using the Micro Blaster (Comco Inc.). Powder flow, air pressure and blasting duration were optimized in order to drill access holes of 1 mm diameter.

Once the wafer was cut and apertures on the cover were drilled, a 10 µm thin film of SU-8 3005 was spin coated on the cover. The SU-8 was soft baked at 95°C for 7 minutes in order to remove the solvents, but not exposed to UV so that it will not cross-link and act as a glue to facilitate bonding. One problem coming along with the use of a non-cross-linked resist is that resist post-exposure patterning is complicated, as the accessibility of the film by the developer is limited. However, for the present device patterning of the thin SU-8 cover layer is not necessary, given the fact the channels and

chambers are already formed on the underlying SU-8 structure. The only remaining challenging issue related to this technique, which is becoming more prominent when increasing thickness of SU-8 film, is the possibility that the non-cross-linked resist could flow in the chambers and cover the electrodes or block the channels.

Component assembly was performed using the Aligner Wafer bonder (AML-Applied Microengineering Ltd, UK). The two components were brought into contact and placed between two heating platens in the wafer bonding chamber. The stack was placed with the glass cover being in touch with the bottom platen in order to reduce the risk of SU-8 flowing in the electrode structure. A schematic cross section view illustrating the fabricated device is presented in Figure 4.14.

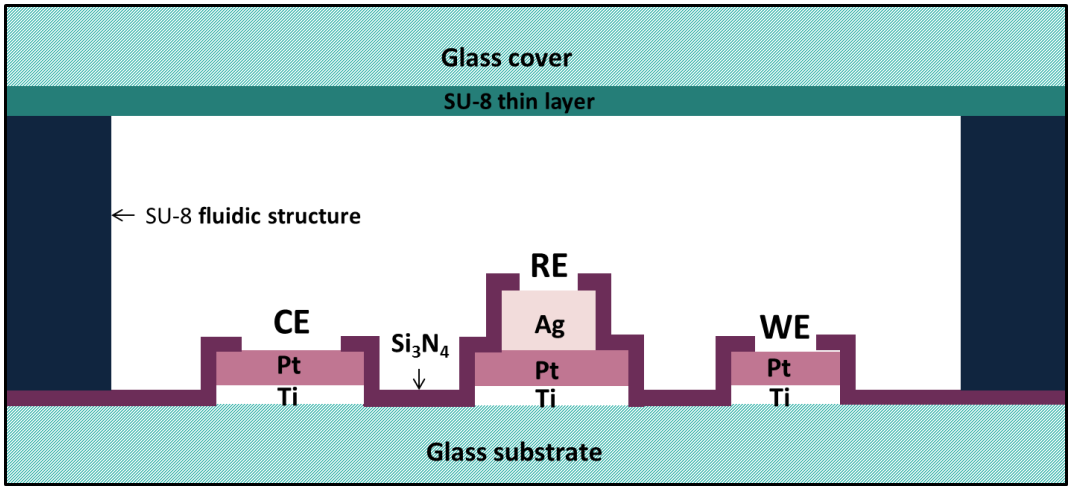

Figure 4.14. Schematic cross section view of the fabricated device.

After reaching 10^{-4} mbar vacuum in the bonding chamber, a specific temperature was set on upper and lower platens in order to heat the device; pressure was applied during a certain time period. Temperature, applied pressure and duration were the three parameters that had to be considered in order to optimize bonding procedure.

Given the thermal properties of the glass substrate, bonding duration should be long enough so that the thin SU-8 layer can be effectively heated and get into the molten state. The optimal bonding time for the present device was determined at 7 minutes.

It is important to apply a sufficiently high pressure in order to minimize voids between the two components needed to be assembled (Sayah et al., 2000). The range of pressure values tested was from 600 to 1200 N and the final value selected was 1200 N as it could compensate the initial bending of the platform with the underlying thick SU-8 structure.

Different bonding temperatures were tested, ranging from 65 to 110 °C. 65°C corresponds to the glass transition temperature of SU-8 (Jackman et al., 2001), above which, SU-8 films become pliable and can be used as glue. Certain studies report 75°C to be the optimum heating temperature during bonding (Jackman et al., 2001, Carlier et al., 2004). However, in the present study, temperatures below 95°C were not sufficient to perform a successful bonding and temperatures above 95°C increased the risk of SU-8 flowing and covering the electrodes or blocking channels (Figure 4.15 a). The optimal temperature used through bonding procedure was 95°C ; bonding was successfully performed, fraction of SU-8 flowing in the chambers was negligible and channels were not blocked.

As a matter of fact, if temperature and pressure applied during bonding are not sufficiently high, a lack of proper sealing and leaks between chambers can be observed upon the fabricated final devices (Figure 4.15 b). Relatively high values of temperature and pressure were required as the underlying fluidic platform containing electrode systems was already slightly bent, due to residual stress at the interface between the glass substrate and the thick SU-8 structure.

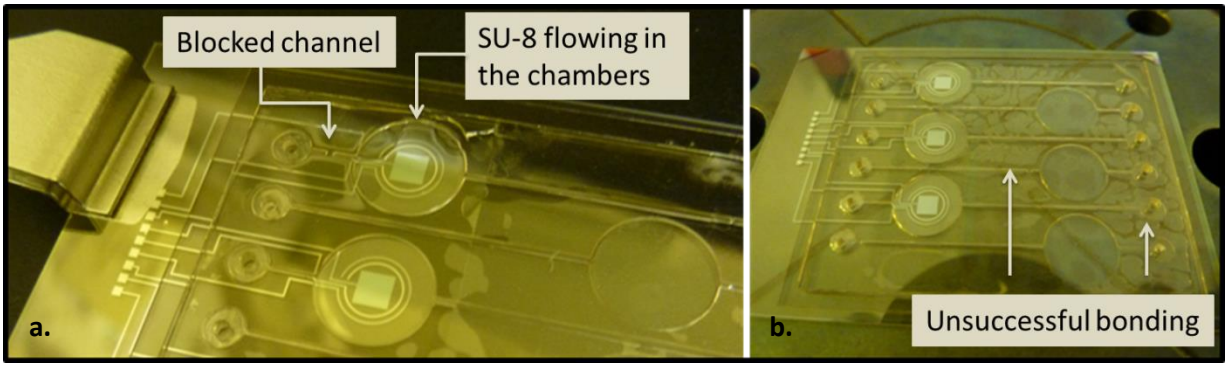

Figure 4.15. Final devices obtained after wafer bonding: (a) High temperature of 110°C was applied during bonding and SU-8 flowed in the first chamber, covering a part of the electrodes and blocked the channel. (b) Applied temperature (65°C) and pressure (600 N) were not sufficiently high and could not counteract the initial bending of the underlying platform, yielding an unsuccessful sealing, leading to potential leaks.

The device was then exposed to UV light through a blanket exposure during 25 seconds, followed by post-exposure bake and hard bake in order to crosslink the thin SU-8 layer so that sealing is completed.

4.2.4 Device packaging

Device packaging followed component assembly. The connection system selected was the flexible flat cable (FFC) system (RS Components SAS, France) in order to obtain a plug-in, easy to use device (Figure 4.16).

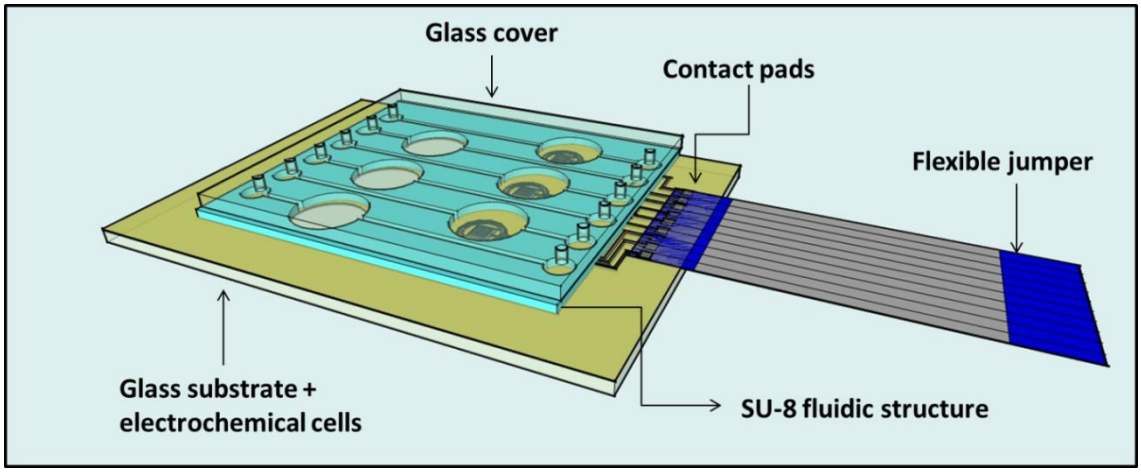

Figure 4.16. 3D model of the last step of the fabrication procedure: packaging.

The flexible jumper had to meet the needs of the electrochemical system. A ten-contact cable, with 0.5 mm pitch was selected. Since the three electrochemical cells of the platform contain a total of nine electrodes, only nine of the ten contacts of the flexible cable were eventually used.

Concerning mounting of the flexible jumper on the device, conductive glue and UV-curable adhesive were used. Electrically conductive, silver epoxy glue (EPO-TEC H20E, Epoxy Technology, INC, USA) was applied on the nine contacts of the jumper, to connect it with the contact pads of the device, followed by the application of the UV-curable adhesive (UV625, Permabond UK), to stick both components together. A Tresky-3000 (Dr. TRESKY AG, Switzerland) bonding platform was used to transfer and join the flexible jumper on the device. The device was then placed in a furnace at 80°C for 90 minutes, to cure the electrically conductive glue. The part where the flexible jumper was connected to the contact pads of the device was encapsulated in a glob–top of E505 epoxy adhesive (Epotecny Sarl, France) in order to assure mechanical stability. The device obtained is presented in Figure 4.17 a.

A ZIF (zero insertion force) electrical connector (RS Components SAS, France) was used to eventually connect the flexible jumper to the measurement apparatus as it enables insertion and removal of the flexible jumpers in a simple way (Figure 4.17 b).

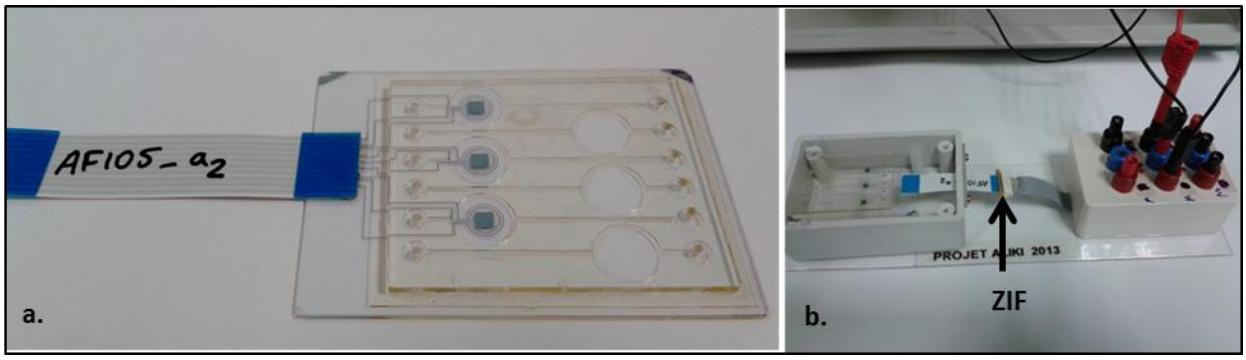

Figure 4.17. (a) Final device obtained after packaging. (b) Connection system of the lab-on-chip device with the potentiostat.

The entire fabrication procedure is resumed in Figure 4.18.

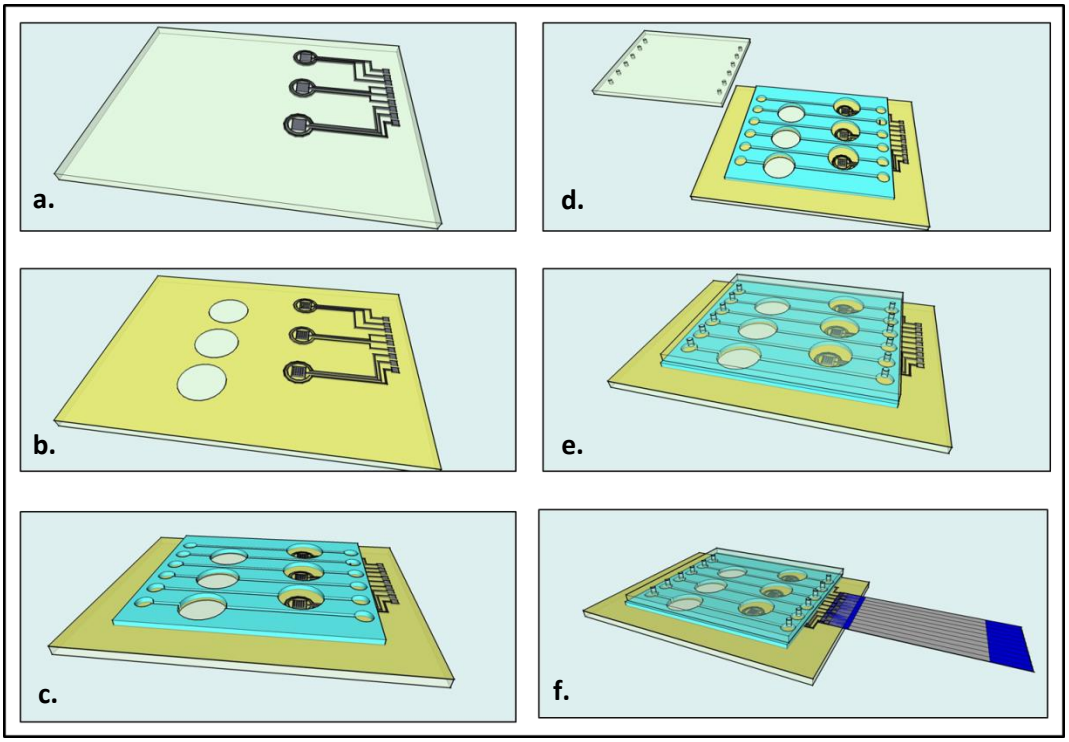

Figure 4.18. Fabrication procedure process flow: (a) electrode materials deposition and patterning. (b) passivation layer deposition and patterning. (c) fluidic structure implementation. (d)-(e) bonding procedure. (f) packaging.

Once fabrication procedure was completed, reagent loading conditions were tested. External pumping system was not necessary and the test solution was manually delivered by simply using a syringe (Figure 4.19). Although SU-8 and Si_3N_4 layers are hydrophobic, sample loading was easy and no surface modification was needed to yield hydrophilic surfaces.

System packaging and reagent loading were therefore verified in order to start validation assays using algal solutions for herbicide detection. These assays will be thoroughly presented in the following chapter.

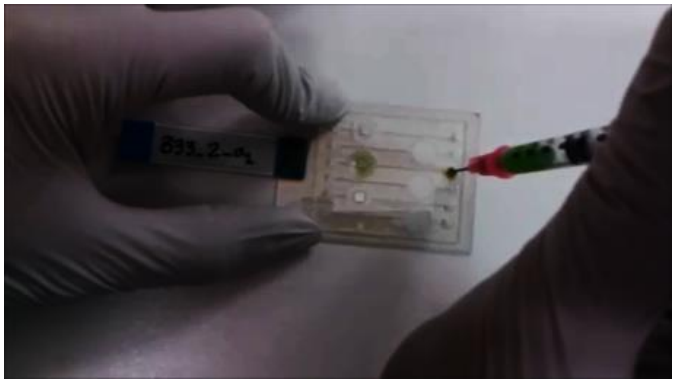

Figure 4.19. Test solution injection in lab-on-chip device.

4.3 Conclusion

The technology followed for the fabrication of the biosensor system is described in this chapter. A portable system for in-situ detection was developed that will provide an early indication by sorting the samples needed to be further analysed by conventional techniques. The fabricated lab-on-chip platform offers the possibility of conducting double complementary detection: optical and electrochemical. It therefore consists in three fluidic chambers dedicated to electrochemical detection and three chambers to optical detection.

A glass substrate of high optical transmission was used in order to assure compatibility with optical technologies. In the first place, the electrode structures were patterned on the glass substrate. Three electrochemical cells were fabricated on the substrate. Each cell was comprised of one silver and two platinum ultramicroelectrodes which will be later functionalized, as described in chapter 3, in order to form the final integrated working (Pt-Bl for O_2 and H_2O_2 and Pt/IrO_x for pH) and reference (Ag/AgCl) electrodes. Photolithography parameters applied for the fabrication on silicon substrates had to be adapted to the different thermal properties and the transparency of the glass wafers.

The next step was the implementation of the fluidic system. A thick SU-8 fluidic structure was first deposited and patterned. The key parameters that had to be optimised in order to improve adhesion and minimize residual stress were the UV exposure time and baking conditions, respectively. In order to seal the system, a glass cover was bonded on the underlying thick SU-8 structure. A thin, non-cross-linked SU-8 was used as the bonding layer and bonding procedure took place in the Aligner Wafer

Bonder, using optimised values for bonding temperature, pressure and duration. A flexible flat cable (FFC) system and a ZIF (zero insertion force) electrical connector (RS Components SAS, France) were used to eventually connect the flexible jumper to the measurement apparatus.

The designed fluidic system allows easy reagent loading through a syringe and needs no further surface modification. Each device could be used through numerous tests without leaks, giving the possibility of establishing a generic prototype that can also target applications requiring repetitive measurements.

The system provides a significant versatility as it can be used in various ways. It enables parallel analysis of different samples and gives the possibility of integrating different algal strains sensitive to different pollutants in each chamber, increasing in this way the selectivity of the sensor. Concerning the electrochemical part, the detection of the three species of interest (O_2, H_2O_2, pH related ions), indicators of the presence of pollutants, can be performed at the same time by integrating each specific electrochemical sensor in one independent chamber.

4.4 References

Abgrall, P., Conedera, V., Camon, H., Gue, A.-M., Nguyen, N.-T., 2007. SU-8 as a structural material for labs-on-chips and microelectromechanical systems. Electrophoresis 28, 4539–4551. doi:10.1002/elps.200700333

Abgrall, P., Lattes, C., Conederal, V., Dollat, X., Colin, S., Gue, A.M., 2006. A novel fabrication method of flexible and monolithic 3D microfluidic structures using lamination of SU-8 films. J. Micromechanics Microengineering 16, 113–121. doi:10.1088/0960-1317/16/1/016

Becker, H., 2002. Polymer microfluidic devices. Talanta 56, 267–287. doi:10.1016/S0039-9140(01)00594-X

Brun, M., Frenea-Robin, M., Chateaux, J.F., Haddour, N., Deman, A.L., Ferrigno, R., 2012. A new microfluidic device for electric lysis and separation of cells, in: 2012 Annual International Conference of the IEEE Engineering in Medicine and Biology Society (EMBC). Presented at the 2012 Annual International Conference of the IEEE Engineering in Medicine and Biology Society (EMBC), pp. 6281–6284. doi:10.1109/EMBC.2012.6347430

Carlier, J., Arscott, S., Thomy, V., Fourrier, J.C., Caron, F., Camart, J.C., Druon, C., Tabourier, P., 2004. Integrated microfluidics based on multi-layered SU-8 for mass spectrometry analysis. J. Micromechanics Microengineering 14, 619–624. doi:10.1088/0960-1317/14/4/024

Christophe, C., 2010. Intégration de microcapteurs électrochimiques en technologies “Silicium et Polymères” pour l’étude du stress oxydant. Application à la biochimie cutanée. Université Paul Sabatier - Toulouse III.

Duffy, D.C., McDonald, J.C., Schueller, O.J.A., Whitesides, G.M., 1998. Rapid Prototyping of Microfluidic Systems in Poly(dimethylsiloxane). Anal. Chem. 70, 4974–4984. doi:10.1021/ac980656z

Fujii, T., 2002. PDMS-based microfluidic devices for biomedical applications. Microelectron. Eng., Micro- and Nano-Engineering 2001 61–62, 907–914. doi:10.1016/S0167-9317(02)00494-X

Grieshaber, D., MacKenzie, R., Vörös, J., Reimhult, E., 2008. Electrochemical Biosensors - Sensor Principles and Architectures. Sensors 8, 1400–1458. doi:10.3390/s8031400

Hammacher, J., Fuelle, A., Flaemig, J., Saupe, J., Loechel, B., Grimm, J., 2008. Stress engineering and mechanical properties of SU-8-layers for mechanical applications. Microsyst. Technol. 14, 1515–1523. doi:10.1007/s00542-007-0534-7

Harrison, D.J., Manz, A., Fan, Z., Luedi, H., Widmer, H.M., 1992. Capillary electrophoresis and sample injection systems integrated on a planar glass chip. Anal. Chem. 64, 1926–1932. doi:10.1021/ac00041a030

Henares, T.G., Mizutani, F., Hisamoto, H., 2008. Current development in microfluidic immunosensing chip. Anal. Chim. Acta 611, 17–30. doi:10.1016/j.aca.2008.01.064

Heuschkel, M.O., Guérin, L., Buisson, B., Bertrand, D., Renaud, P., 1998. Buried microchannels in photopolymer for delivering of solutions to neurons in a network. Sens. Actuators B Chem. 48, 356–361. doi:10.1016/S0925-4005(98)00071-9

Incropera, F.P., DeWitt, D.P., Bergman, T.L., Lavine, A.S., 2006. Fundamentals of Heat and Mass Transfer, 6th edition. ed. John Wiley & Sons, Hoboken, NJ.

Jackman, R.J., Floyd, T.M., Ghodssi, R., Schmidt, M.A., Jensen, K.F., 2001. Microfluidic systems with on-line UV detection fabricated in photodefinable epoxy. J. Micromechanics Microengineering 11, 263–269. doi:10.1088/0960-1317/11/3/316

Jang, A., Zou, Z., Lee, K.K., Ahn, C.H., Bishop, P.L., 2011. State-of-the-art lab chip sensors for environmental water monitoring. Meas. Sci. Technol. 22, 032001. doi:10.1088/0957-0233/22/3/032001

Johnson, R.D., Gavalas, V.G., Daunert, S., Bachas, L.G., 2008. Microfluidic ion-sensing devices. Anal. Chim. Acta 613, 20–30. doi:10.1016/j.aca.2008.02.041

Kieninger, J., 2011. Electrochemical microsensor system for cell culture monitoring. Universität Freiburg.

Lagarde, F., Jaffrezic-Renault, N., 2011. Cell-based electrochemical biosensors for water quality assessment. Anal. Bioanal. Chem. 400, 947–964. doi:10.1007/s00216-011-4816-7

Leatzow, D.M., Dodson, J.M., Golden, J.P., Ligler, F.S., 2002. Attachment of plastic fluidic components to glass sensing surfaces. Biosens. Bioelectron. 17, 105–110.

Lefèvre, F., Chalifour, A., Yu, L., Chodavarapu, V., Juneau, P., Izquierdo, R., 2012. Algal fluorescence sensor integrated into a microfluidic chip for water pollutant detection. Lab. Chip 12, 787–793. doi:10.1039/C2LC20998E

Li, Y., Sella, C., Lemaître, F., Guille Collignon, M., Thouin, L., Amatore, C., 2013. Highly Sensitive Platinum-Black Coated Platinum Electrodes for Electrochemical Detection of Hydrogen Peroxide and Nitrite in Microchannel. Electroanalysis 25, 895–902. doi:10.1002/elan.201200456

Lorenz, H., Laudon, M., Renaud, P., 1998. Mechanical characterization of a new high-aspect-ratio near UV-photoresist. Microelectron. Eng., International Conference on Micro- and Nanofarbication 41–42, 371–374. doi:10.1016/S0167-9317(98)00086-0

Pittet, P., Lu, G.-N., Galvan, J.-M., Ferrigno, R., Blum, L.J., Leca-Bouvier, B., 2007. PCB-based integration of electrochemiluminescence detection for microfluidic systems. The Analyst 132, 409. doi:10.1039/b701296a

Pourciel-Gouzy, M., Assié-Souleille, S., Mazenq, L., Launay, J., Temple-Boyer, P., 2008. pH-ChemFET-based analysis devices for the bacterial activity monitoring. Sens. Actuators B Chem. 134, 339–344. doi:10.1016/j.snb.2008.04.029

Sayah, A., Solignac, D., Cueni, T., Gijs, M.A.., 2000. Development of novel low temperature bonding technologies for microchip chemical analysis applications. Sens. Actuators Phys. 84, 103–108. doi:10.1016/S0924-4247(99)00346-5

Shaw, M., Nawrocki, D., Hurditch, R., Johnson, D., 2003. Improving the process capability of SU-8. Microsyst. Technol. 10, 1–6. doi:10.1007/s00542-002-0216-4

Sia, S.K., Whitesides, G.M., 2003. Microfluidic devices fabricated in Poly(dimethylsiloxane) for biological studies. ELECTROPHORESIS 24, 3563–3576. doi:10.1002/elps.200305584

Truong, T.Q., Nguyen, N.T., 2004. A polymeric piezoelectric micropump based on lamination technology. J. Micromechanics Microengineering 14, 632–638. doi:10.1088/0960-1317/14/4/026

Wang, H.., Foote, R.., Jacobson, S.., Schneibel, J.., Ramsey, J.., 1997. Low temperature bonding for microfabrication of chemical analysis devices. Sens. Actuators B Chem. 45, 199–207. doi:10.1016/S0925-4005(97)00294-3

Yun-Ju Chuang, F.-G.T., 2003. A novel fabrication method of embedded micro-channels by using SU8 thick-film photoresists. Sens. Actuators -Phys. - Sens. ACTUATOR -PHYS 103, 64–69. doi:10.1016/S0924-4247(02)00325-4

Chapter 5
Biological application

In this chapter, the results of electroactive species (O_2, H_2O_2, H_3O^+/OH^- pH related ions) monitoring in algal solutions will be demonstrated. Herbicide-induced changes in photosynthetic activity were detected. Pre-validation tests using silicon-based devices are first shown, followed by the results obtained with the lab-on-chip devices using as light sources for the stimulation of algal cells either a standard, halogen white light source where light is transmitted through an optical fiber or a blue OLED. Special emphasis was placed on the detection of oxygen as it is largely influenced by the presence of herbicides. Traces of Diuron herbicide in water samples were detected by evaluating disturbances in photosynthetic and metabolic activities of algae caused by this herbicide.

5.1 Pre-validation using silicon-based sensors in algal solutions

5.1.1 Green algae cell culture

Green micro algae *Chlamydomonas reinhardtii (CC-125)* were cultivated in an incubator (Model: MIR-154, SANYO Electronic Co., Ltd) at 25°C with time-regulated light/dark (16h/8h) cycles in Erlenmeyer flasks containing High Salt Medium (HSM) (N Sueoka, 1967) with pH adjusted at 6.8 (Figure 5.1), this algal strain is considered as a model algal strain and was selected as it is extensively studied and characterized (Schubnell et al., 1999).

Figure 5.1. Culture flasks containing algal cells in HSM medium.

Culture flasks were covered by porous stoppers that permit air exchange. Algal solutions in flasks were re-diluted once per week in fresh HSM culture medium so that the initial solution used for measurements will be in an exponential growth phase of approximately 1 x 10^6 cells/mL (Lefèvre et al., 2012). Cell concentration measurements were conducted using Multisizer 3 Coulter Counter particle analyzer (Beckman Coulter Inc., USA). Provided that the quantity of electroactive species produced or consumed depends on the concentration of cells in the solution, initial algal solutions were centrifuged and re-suspended in HSM medium to obtain a 6-fold concentration increase (final concentration: 6 x 10^6 cells/mL).

The main goal of the preliminary study being to determine the relation between the change in metabolic activities of algae and the presence of herbicides, measurements were first conducted in model HSM solution in order to eliminate possible interferences found in real water samples. Nevertheless, for final application, this concept will be validated in consumption water obtained from groundwater, rivers or lakes with lab-on-chip devices and is presented in a following section.

Bioassays using the fabricated electrochemical microsensors were performed in the dense algal solutions and current evolution was observed during light and dark periods in the presence and absence of the toxic chemical to be detected. Despite the fact that the fabricated device can be used as a generic platform for the assessment of total water toxicity, the detection principle was tested by monitoring two herbicides. Diuron (3(3,4-dichlorophenyl)-1,1-dimethylurea) is a herbicide targeting the electron flow from PSII to PSI, having therefore a direct impact on the quantity of oxygen produced through photosynthesis. On the other hand, Paraquat belongs to the other type of herbicides accepting electrons from PSI and therefore contributing to the production of ROS (Fedtke and Duke, 2004).

5.1.2 Oxygen detection with silicon-based devices

Oxygen was the center of our interest as it is the element giving more information on the presence of the most widely used pollutants. Indeed, O_2 evolution reflects photosynthetic activity of algae and is largely altered by pollutants existence. As already stated it can be measured at extracellular level as it is diffusing through the cellular membrane therefore demanding simpler measurement protocols, in contrast to the other two electroactive species, H_2O_2 and pH related ions that are produced inside the cell and need a membrane lysis protocol in order to be monitored.

During photosynthesis, light energy is captured by light harvesting complexes in PSII and transferred to the part of PSII where photochemical reactions take place. These reactions result in the oxidation of

water to molecular oxygen in the oxygen-evolving complex (OEC) described through the following reaction (Equation 25) (Giardi and Piletska, 2006):

$$2H_2O \rightarrow 4e^- + 4H^+ + O_2 \qquad (Equation\ 25)$$

On the other hand, during respiration (Raven and Beardall, 2003) oxygen is used as the substrate for catabolic reactions in order to produce cellular energy and release CO_2 and water (Wu et al., 2010).

It is therefore evident that oxygen is an element taking part in both procedures either as a product or a substrate. The reduction current of dissolved oxygen was measured through time during light and dark periods. As already stated, the current produced is directly proportional to the concentration of the analyte, in this case oxygen. The theoretical equation relating current to the concentration of oxygen, for a given electroactive surface, is presented in Chapter 2 (Equation 9 and 10). Therefore, current recorded through time reflects oxygen evolution through different processes of algal metabolism.

The electrochemical technique selected to follow oxygen evolution through photosynthesis and respiration was chronoamperometry. This method was used for its simplicity even though it is less sensitive compared to other electrochemical techniques, such as pulse voltammetric techniques that can be considered in the future if sensitivity properties need to be improved. Figure 5.2 presents the silicon-based electrochemical sensor immersed in algal solution for O_2 measurements.

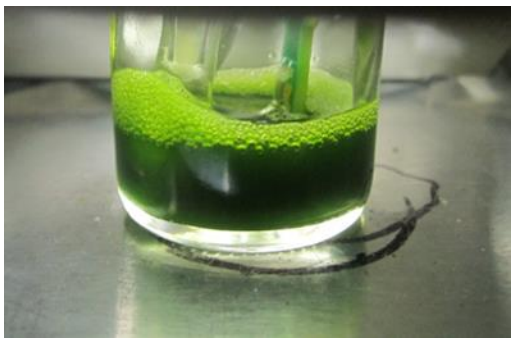

Figure 5.2. Silicon-based oxygen sensor in algal solution.

Oxygen reduction reaction is a one-step reaction on platinum surface as described in Chapter 3 (Equation 24). The suitable potential for the reaction in the culture medium solution of pH 6.8 was determined previously and the selected potential was -0.7 V versus integrated Ag/AgCl reference electrode. Platinum black working electrode arrays were used through tests as it was validated that they give the best results.

A cleaning step was applied before each series of measurements in order to reactivate the electrode surface and recycle the system. The cleaning step consists in cycling (cyclic voltammetry) the already used electrode in 0.5 M H_2SO_4 for 20 cycles through the potential range of -0.2 to +1.1 V vs

$Ag/AgCl/KCl_{sat}$ with a scan rate of 100 $mV.s^{-1}$. After potential cycling, the voltammogram was similar to the one recorded before measurements in algal solutions which implies a similar surface and allows a further utilization of the device.

At first, the performance of the sensor for O_2 detection was evaluated with algae in the absence of toxicants in order to demonstrate the relationship between photosynthetic activity and current signal measured. Light and dark periods were therefore altered to obtain periods of daylight illumination and darkness and current variations were recorded.

Variations in photosynthetic activity of algae were then determined in presence of Diuron herbicide (Figure 5.3). As ethanol 70% is the solvent used to prepare Diuron solutions, its concentration was kept constant through different injections to prevent solvent influence on algal response. Current evolution through respiration and photosynthesis with and without Diuron is presented in Figure 5.3. The impact of the herbicide on electron flow and therefore photosynthetic O_2 production is confirmed by comparing the steep slope corresponding to oxygen production rate ($nA.s^{-1}$) during photosynthesis obtained for the control algal solution with the smoother one obtained for Diuron contaminated algal solution. It is should be mentioned that Diuron has a principal effect on PSII as it is an inhibitor of photosynthetic electron flow (Fedtke and Duke, 2004) and it can therefore be assumed that the effect on respiration is negligible.

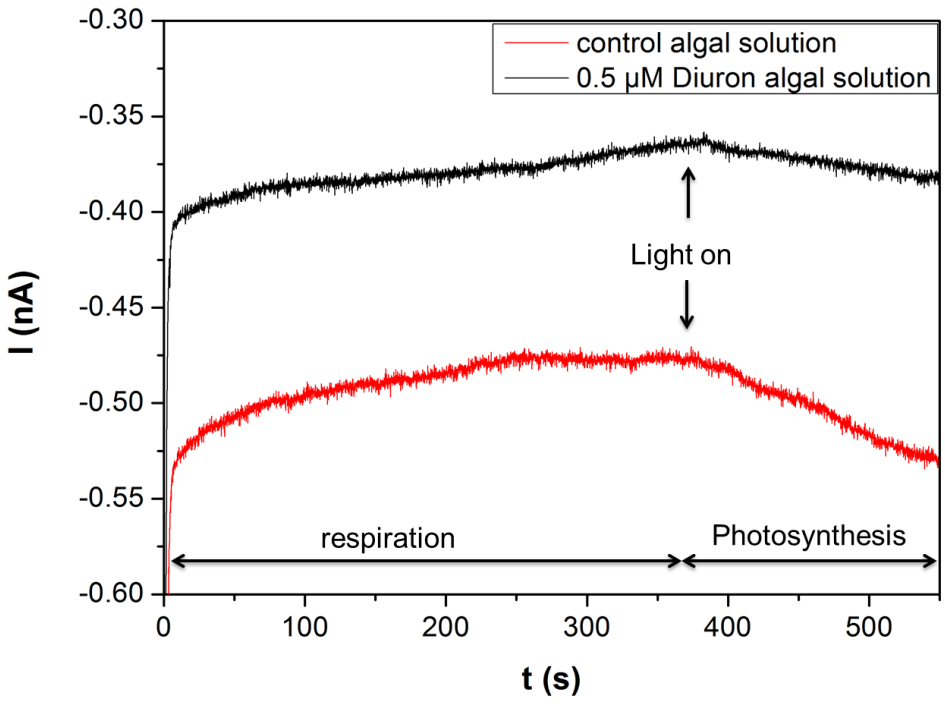

Figure 5.3. Algal response to 0.5 µM Diuron herbicide measured with a Pt-Bl working ultramicroelectrode array.

A difference in the initial current value and therefore oxygen level was observed for the two experiments, nevertheless given the fact that a temporal current/oxygen variation is used to evaluate Diuron effect, this current level difference is not considered problematic for the detection.

Oxygen evolution rates on illumination were compared for different pollutant concentrations, starting with a non-polluted/control solution and going up to a 1 µM Diuron solution (control-1µM), in order to demonstrate concentration dependent inhibition effect of the herbicide on photosynthesis (Figure 5.4). The response of a control algal solution was first compared to the one of a control algal solution with ethanol to validate that ethanol has no inhibitory effect on O_2 production.

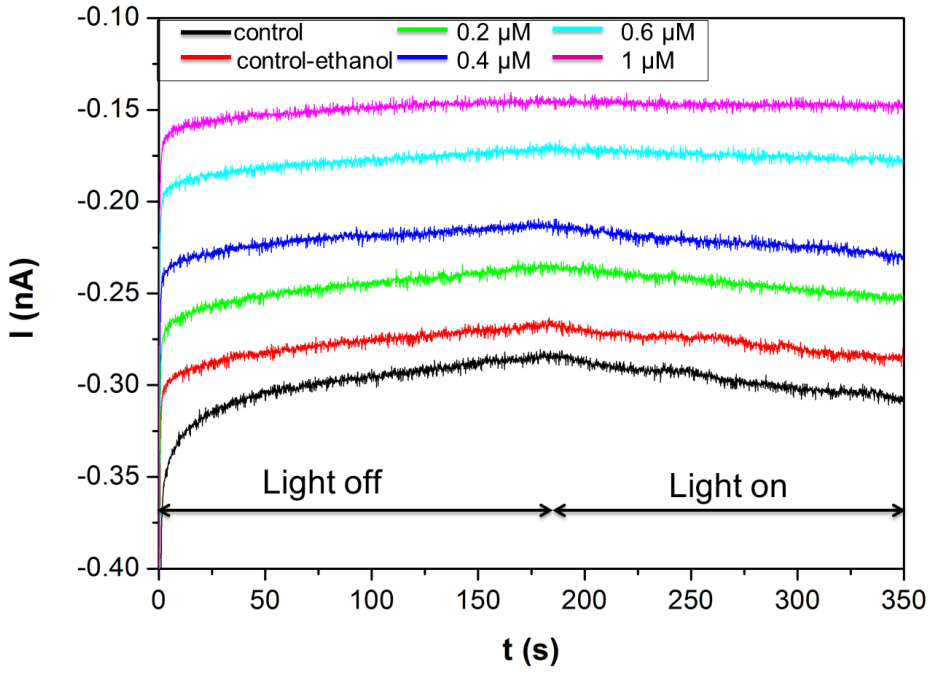

Figure 5.4. Algal response to various concentrations of Diuron herbicide measured with a Pt-Bl working ultramicroelectrode array.

Figure 5.5 shows the decrease in the rate recorded under illumination with the increase in Diuron concentration. It is therefore demonstrated that the fabricated electrochemical biosensor can effectively follow the change in photosynthetic activity induced by Diuron herbicide and can be an efficient indicator of water pollution. The concentration range tested was 0-1 µM of Diuron so that it would embrace the limit of maximum acceptable concentration implemented by Canadian government (0.64 µM).

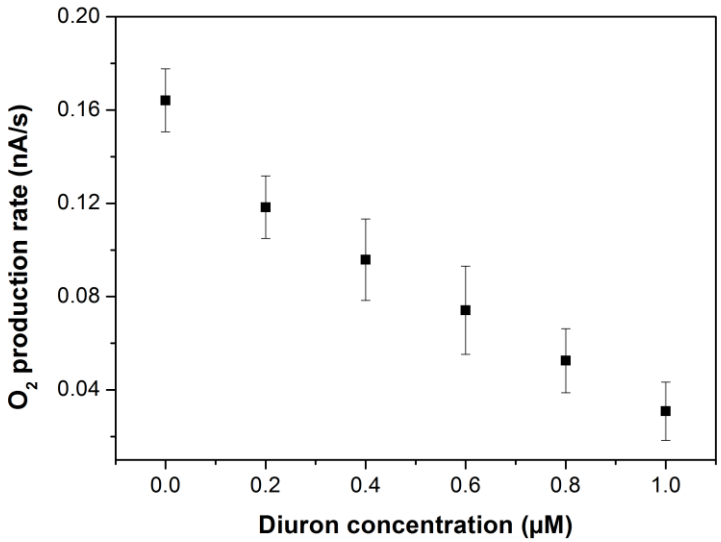

Figure 5.5. Calibration curve (recorded oxygen production rate during photosynthesis versus Diuron concentration) for Pt-Bl ultramicroelectrode array fabricated on silicon substrates.

5.1.3 Hydrogen peroxide-pH monitoring with silicon-based devices

As stated in Chapter 2, herbicides like Paraquat influence photosynthesis and cause the production of ROS (reactive oxygen species) like superoxide anion and hydrogen peroxide (Fedtke and Duke, 2004). If there is an overload of ROS, the scavenging system cannot efficiently deal with it, resulting in an accumulation of H_2O_2 inside algal cells.

Given the fact that H_2O_2 production takes place in the cell, algal cells need to be lysed prior to measurement. Cell lysis was achieved through ultrasonication. A commonly used protocol was followed including ultrasonication three times for 30 seconds each time, with 30 seconds cooling intervals. A dense algal solution of 40 x 10^6 cells.mL^{-1} was used so that H_2O_2 production could be high enough to be measured.

The potential for H_2O_2 oxidation was set at 0.3 V (determined previously) and chronoamperometry was conducted under continuous illumination. Given the fact that Paraquat induces an increase in the amount of H_2O_2 produced by algae, it can be detected by comparing the current level generated through H_2O_2 oxidation on the electrode surface, for a control algal solution and a 1 mM Paraquat algal solution. The quantity of herbicide added was big enough for these first tests so that the induced variation will be as visible as possible. Paraquat herbicide was added under illumination and before cell lysis. In this way, it will affect the electron transfer when photosynthetic apparatus is still completely functional and all protein complexes are intact. Lysis should serve in liberating and

therefore making accessible the already produced H_2O_2 after the injection of the herbicide. At the same time, current recording was also carried out under illumination so that photosynthetic activity of protein complexes that are still active after cell lysis and continue producing H_2O_2, could also contribute to the current level recorded.

After carrying out the experiment with the two solutions (control and 1 mM Paraquat), no Paraquat-induced variation was evidenced as no difference was observed upon the current levels. Experimental protocol should be improved and measurement parameters should be reconsidered in order to effectively monitor intracellular H_2O_2 production. In particular, ultrasonication parameters should be optimized so that cell membrane can get decomposed, giving access to the intracellular level but at the same time protein complexes should stay intact so that the scavenging system will continue working. What is more, provided that H_2O_2 is an intermediate product of scavenging system reactions, it should be monitored rapidly after production and therefore measurement time should be minimized.

All in all, Paraquat-induced variation in H_2O_2 production was not detected but further work will be dedicated on this matter through this project. Similarly, the influence of Paraquat on pH could not be observed, since the pH, associated to the quantity of OH^- produced by algae, is influenced in the same way as H_2O_2 by Paraquat herbicide and its variation is associated with the variation in H_2O_2 (mentioned in Chapter 2).

5.2 Validation of lab-on-chip sensor in algal solutions

5.2.1 Application in solutions without herbicide

The response of the sensor was firstly evaluated in control algal solutions that do not contain any herbicide. Oxygen evolution was followed through photosynthesis and respiration process similarly to previously used sensors.

5.2.1.1 ***Operation protocol***

All experiments were carried out in a dark Faraday cage using an external, halogen white light source as the excitation source for algae photosynthesis similarly to previous prevalidation experiments. The potentiostat used was Bio-Logic SP-200 equipped with a low current option. The Faraday cage was used at this stage in order to establish optimal experimental conditions and avoid noise problems even though the use of the cage may not be obligatory, considering the sufficiently high current intensity obtained as well as the potenstiotat used that is equipped with a low current option. The algal test

solution re-suspended in HSM medium was injected in the detection chamber (Figure 5.6) by simply using a syringe. Chronoamperometry was conducted and the potential applied corresponds to the O_2 reduction potential which was estimated before through cyclic voltammetry and is -0.7 V versus integrated Ag/AgCl.

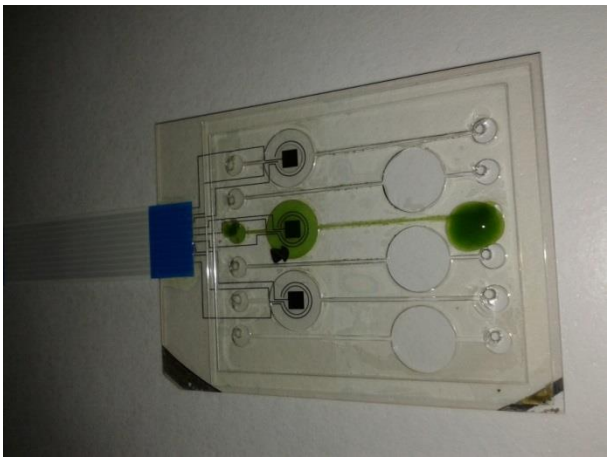

Figure 5.6. Algal test solution inserted in one of the chambers of the lab-on-chip device.

5.2.1.2 ***Oxygen measurement in algal solutions***

Dark and light periods were altered so that changes in O_2 level can be registered as shown in Figure 5.7. Algae were first left in dark (not presented in graph). The onset of photosynthesis is indicated by a current increase which represents the oxygen production when light is on. On the other hand, when light is off, algae are consuming oxygen for the respiration procedure. Through the 5 first cycles of light on-off, illumination and dark periods were equally long (1 cycle: 1 minute illumination + 1 minute dark).

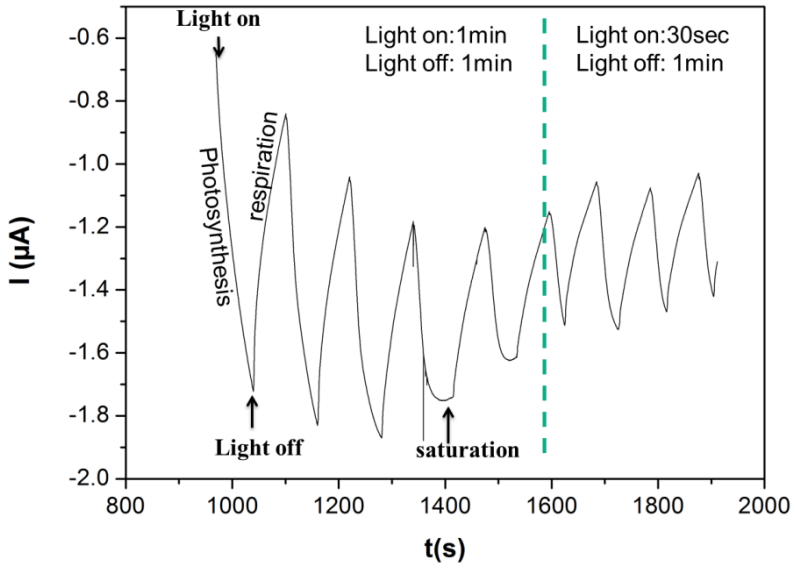

Figure 5.7.Current measurement through algal respiration and photosynthesis with Pt-Bl ultramicroelectrode array integrated on lab-on-chip device.

A saturation effect is more and more evident through cycles and is particurarly observed on the fourth cycle when light is on. This effect is probably caused by the depletion of CO_2 substrate needed for O_2 production in the area around the cells. Given the fact that gas exchanges of the test solution with the environment are limited, the closed chamber will be rapidly deprived of CO_2. It is important to mention that during the first part of photosynthesis, light energy is used to eventually produce ATP and NADPH (along with O_2 production), which are then used in the second part, during Calvin cycle, to produce sugar glucose using CO_2 as substrate (Raven and Johnson, 2002). A CO_2 limitation has therefore an impact on the Calvin cycle level. Calvin cycle needs less ATP and NADPH and there is an accumulation of these two products which leads to limited electron transfer and therefore limited O_2 production.

It was thus necessary to increase the amount of CO_2 substrate for photosynthesis in order to eliminate the saturation effect and obtain a measurement time long enough that allows the estimation of the slope of a curve considered linear. Illumination time was reduced to 30 seconds while dark time was kept at 1 minute (evident after the dashed line presented on the graph of Figure 5.7). In this way, during respiration, algae were able to produce a sufficient amount of CO_2, use it for photosynthesis when light was turned on so that saturation effect will be eliminated.

This limitation influences the protocol that should be followed for measurements in herbicide solutions as it was important to obtain a well-defined, linear oxygen production slope for a sufficient time period.

In order to verify that changes in recorded current (increase-decrease) were not related to light interferences but only caused by algal photosynthesis, the same experiment was conducted in water solutions that do not contain algal cells (Figure 5.8).

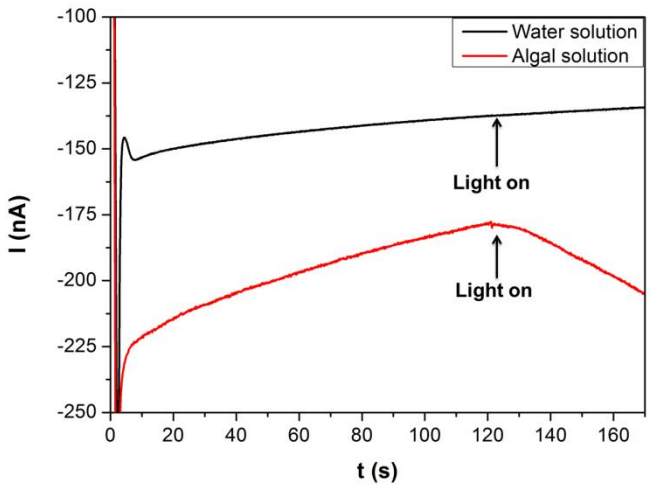

Figure 5.8. Current measurement through illumination and dark periods for an algal solution and a water solution using a halogen white light source.

For water solution, when light was switched on, no modification was observed in the reduction current demonstrating that the current increase observed with light for algal solutions reflects O_2 production by algal cells.

On the other hand, a slight decrease in the reduction current with a rate of approximately 0.15 $nA.s^{-1}$ is observed even for the solution that does not contain algal cells. In theory, as described in Chapter 2, mass transport is enhanced for ultramicroelectrodes and steady state response is achieved. The absence of algal cells implies that there is no oxygen consumption for algae respiration and therefore current should maintain a constant value in dark.

However, the diffusion limited oxygen reduction can explain this current decrease in time. Even though spherical diffusion can be achieved when using ultramicroelectrodes, the rate at which the species are consumed on the surface can be greater than the rate at which species diffuse towards the surface. What is more, given the fact that interfering species can be present at the solution that are reduced before -0.7 V, the decrease in current can also be due to the diffusion limited reduction of these interfering species.

The assumption that this decrease can be due to the depletion of O_2 in the confined environment of the detection chamber (μvolume) was eliminated after calculating the number of O_2 moles consumed for 2 minutes current measurement in dark by applying Faraday's law (Equation 8).

Oxygen reduction reaction is given by equation (24). The charge was easily calculated as the product of time and current intensity (black curve, Figure 5.8) at 24 μC, which finally yielded the number of O_2 moles consumed during measurement which was 0.06 nmoles.

According to Truesdale and Downing, 1954, oxygen concentration of a saturated solution at 22°C is approximately 266 $nmol.mL^{-1}$ and considering the volume of the detection chamber (12.5μL), the calculated number of moles contained in the test solution was 3.3 nmoles. Therefore, the amount of O_2 consumed represents only approximately 1.5 % of the total quantity of O_2 contained in the chamber.

Another possible explanation can be competing reactions taking place on the electrode surface. Non-faradaic processes such as adsorption and desorption of different interfering species present in the solution can modify the electrode surface and therefore influence the generated current (Bard and Faulkner, 2001).

As described by Li et al., reactive oxygen species (ROS) passivate metallic surfaces. It is yet mentioned that surface passivation on platinum black ultramicroelectrodes is not as prominent as the one on platinum ultramicroelectrodes as the number of active sites of platinum black is greater compared to bare platinum ultramicroelectrodes (Li et al., 2013). A potential reason for the current decrease can therefore be the diminution of electroactive sites during oxygen reduction that is due to surface poisoning by the ROS.

As far as the solution containing algae is concerned, the decrease in reduction current with a rate of approximately 0.35 $nA.s^{-1}$ is demonstrated in Figure 5.8 (red line). The O_2 consumption rate for the solution containing algae is greater than the rate recorded for the solution without algae. It can therefore be concluded that the current versus time slope obtained in dark reflects three phenomena taking place: O_2 consumption for algal respiration, diffusion limited O_2 consumption on electrode surface and faradaic and non-faradaic electrochemical reactions of interfering species. These three phenomena are taking place not only during dark period but also during illumination and should therefore be subtracted in order to obtain only the signal corresponding to the real photosynthetic oxygen production as will be presented in the following section.

Normalization protocol

At this point, it is important to note that the current slope recorded during illumination corresponds to the so-called net photosynthesis. Respiration and photosynthesis are two independent processes in algal cells. Respiration is a constant metabolic process and therefore during illumination period, photosynthesis and respiration are taking place simultaneously (Stoy, 1969). Net photosynthesis (solid line of Figure 5.9) represents the oxygen production rate that is eventually decreased due to the oxygen consumption related to respiration as both processes occur at the same time. Gross photosynthesis, presented in the following scheme by a dashed line, is the oxygen production rate that would have been recorded if photosynthesis was the only process taking place. Consequently, in order to calculate gross photosynthesis which is the parameter usually monitored through physiological applications, oxygen consumption rate during respiration should be subtracted from apparent oxygen production rate (net photosynthesis).
Respiratory activity was considered similar during dark and illumination periods and gross oxygen production rate was calculated through the following equation:

$$O_2\ production\ rate_{\ gross} = O_2\ evolution_{\ photos.net} - O_2\ evolution_{\ respir.} \quad \text{(Equation 26)}$$

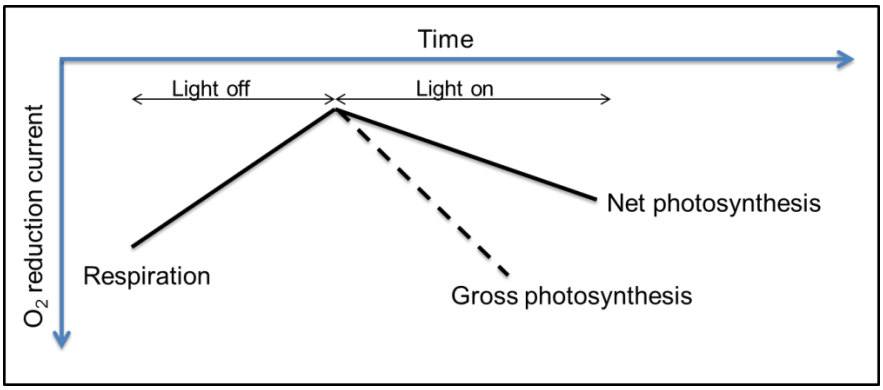

Figure 5.9. Slopes corresponding to gross and net photosynthesis.

By subtracting respiration slope from net photosynthesis slope, phenomena that are constantly present during both illumination and dark periods can be eliminated: O_2 consumption due to diffusion limited reduction reaction as well as interferences caused by species that are reduced at any potential before -0.7 V.

However, prior to optimization of actual device, an additional normalization step needed to be conducted in order to compare results obtained regarding photosynthetic activity. As a matter of fact, by recording current during photosynthesis and respiration, variability in O_2 consumption rates during respiration was noticed for similar algal solutions. Variability is typically observed when dealing with biosystems since there can be a biofouling effect due to the deposition of algal cells on the surface of the electrodes. This variability should be dealt with by setting an average "reference value" for respiration in order to be able to compare all gross photosynthesis values obtained for different pollutant concentrations.

A difference was observed even among algal test solutions that were loaded consecutively in the chamber and originated from the same initial algal concentrated solution. It is difficult to determine the causes of this variability but certain assumptions have been made. As stated previously in this chapter, slope recorded through dark period reflects three possible phenomena taking place: O_2 consumption for algal respiration, O_2 consumption on electrode surface and electrochemical reactions of interfering species.

One of the most important parameters inducing this variability in slope values is the fact that algae are not yet integrated on the device but are introduced in the detection chamber by a syringe for each measurement. The protocol followed to load algal solutions can inevitably introduce variations in number of active cells injected each time as well as variability in their activity.

Moreover, provided that the slope also reflects O_2 electrochemical reduction on electrode surface, electrode surface variation can also explain this variability. One of the causes of surface variation is the biofouling which can be avoided by integrating a membrane (Wu et al., 2010). Algal cells get

attached and then detached from the porous surface of Pt-Bl ultramicroelectrodes through consecutive measurements in a random way that cannot be controlled.
Cleaning protocol of the detection chamber and channels between measurements can also induce variability in slope values. The actual design of the device should be optimized in order to eliminate particular zones of the chambers that cannot easily be cleaned as fluid flow is not optimal and reduce the bubbles that can modify the surface. In this way, the concentration of algal cells in each test solution cannot be controlled.

It is therefore crucial to normalize photosynthetic oxygen production rate with respect to respiratory activity in order to eliminate this variability. Photosynthetic activity is considered proportional to respiratory activity as both represent cellular activity, taking place only in active living cells even though slight differences may be observed as they are occurring in different organelles of the cell. Respiration slope reflects not only oxygen consumption that can be representative of cellular activity and number, electroactive surface available but also interfering species activity. All these parameters are also present during photosynthetic activity and should be considered when determining gross oxygen production rate. This approach therefore, compensates interferences as well as variations induced by differences in cellular activity, number and available active surface.

In order to compare gross photosynthetic oxygen production rates y_i, respiration slopes for O_2 consumption x_i of each test solution should be made equal to the average O_2 consumption slope $\overline{x}$. They were therefore multiplied by the correction factor ($\overline{x} / x_i$).
In this way, the same correction factor should be applied on the gross photosynthetic oxygen production rates y_i, in order to obtain normalized gross O_2 production rates y_i^* (Equation 27).

$$y_i^* = y_i \left(\frac{\bar{x}}{x_i}\right) \qquad (Equation\ 27)$$

Thus, the effect of Diuron on photosynthetic activity of different algal test solutions was evaluated for all measurements by comparing normalized gross O_2 production rates y_i^*.

5.2.2 Application in herbicide solutions

Any stress exerted on algae is reflected by a variation in its usual response in normal, healthy conditions. As already stated in Chapter 2, Diuron herbicide partially or entirely inhibits the electron flow after PSII and consequently blocks O_2 production (Xue et al., 1996). Toxicity bioassays based on inhibition in photosynthetic activity caused by Diuron toxicant was then performed in detection

chambers of lab-on-chip devices. Quantitative analyses were conducted by monitoring oxygen levels during photosynthesis. As a matter of fact, by recording oxygen production rate for various concentrations of Diuron, it is possible to evaluate the effect of the pollutant on algal photosynthetic activity and therefore calibrate the sensor regarding Diuron detection.

5.2.2.1 ***Operation protocol***

Ethanol solutions containing Diuron herbicide were mixed in an Eppendorf with algal test solutions re-suspended in either HSM culture medium or lake water in order to prepare final solutions of various Diuron concentrations. Final solutions were injected in the detection chamber with a syringe.

For the determination of measurement protocol, several parameters had to be considered:

Algal concentration

Concentration of algal cells has an effect on the oxygen production rate and therefore the slope of the current versus time graph. When the concentration is high, the total production of O_2 and therefore the slope is more prominent. Given the fact that oxygen production rate corresponds to the output signal measured by the sensor, a sufficiently high concentration of algae (Shitanda et al., 2009) is required in order to yield a high signal (rate), avoid limitations imposed by measurement apparatus and obtain a well-defined difference between respiration and photosynthesis slopes. On the other hand, cell concentration should not be too high so that the signal-to-noise ratio will be optimal. Indeed, Deblois et al. reported that the effect of atrazine, a herbicide that targets PSII in the same way as Diuron, on algal metabolism is less visible when the availability of total binding sites is high compared to the number of sites that can actually be blocked by the herbicide (Deblois et al., 2013a). A high cell concentration can therefore relatively reduce the apparent toxic effect of a specific quantity of the herbicide as the slope corresponding to O_2 production is important and therefore the slope variation related to presence of Diuron appears to be negligible. Signal-to-noise ratio is therefore not optimal.
As a matter of fact, preliminary experiments with silicon chips demonstrated that through the concentration range of Diuron tested (control solution to 1µM), total inhibition of photosynthetic activity is not occurring when using $6x10^6$ cells/mL HSM as algal concentration. Thus, not all binding sites of electron carriers are attacked by herbicide molecules. What is more, Lefèvre et al. demonstrated that the Diuron detection is not limited by the concentration of algae even when using $1x10^6$ cells/mL HSM (Lefèvre et al., 2012). In the above cases, it can therefore be assumed that Diuron targets a limited number of cells no matter if the cell concentration is high or low.

Concentration was optimized since the first tests with the silicon chips in order to get a significant difference between photosynthesis and respiration slopes but up to the point where an acceptable signal-to-noise ratio can be obtained. Concentration of cells per mL of solution was always kept constant through different experiments and was measured by Multisizer Coulter Counter (Beckman Coulter).

Measurement duration

Oxygen production rates should always be compared referring to the same cycle (respiration-photosynthesis) as parameters should be similar for all tests (Smith, 1936). At the same time, it is important to keep protocol simple for final application and measurement time short. The first cycle (respiration-photosynthesis) was therefore recorded and observed for each experiment with different Diuron concentrations. Furthermore, oxygen production rate is calculated through the linear part of the temporal curve of the reduction current when light is on. As already stated, a linear well-defined oxygen production slope needs to be obtained before saturation effect related to CO_2 depletion is observed. Algae should therefore be left in dark for a sufficiently long time period and produce the necessary amount of CO_2.

Light intensity

Light intensity has an important role in photosynthesis procedure. In general, for relatively low light intensity levels, photosynthesis is enhanced when light intensity is increased as more photons are captured by the pigments and processed through the reaction centers and therefore oxygen production rate is increased (Cho et al., 2008). However, when increasing photon flux density, a critical point is observed when all reaction centers of chloroplasts are saturated and there is no photosynthesis enhancement with absorption of additional photons (Raven and Johnson, 2002). If photon flux density is higher than the saturation point, photons arrive in too large amounts to be processed and photosynthetic activity is decreased (Leverenz et al., 1990; Shapira et al., 1997). This phenomenon is known as photoinhibition and consists in a light–induced damage of the reaction center subunits of PSII (Barber and Andersson, 1992).

Cho et al. checked the effect of light intensity on photosynthesis of freshwater microalgal strain, *Selenastrum capricornutum* in the absence and presence of a particular toxicant (Cho et al., 2008). O_2 production during photosynthesis increased with increasing light intensity but reached a constant value for light intensities of 1000 to 1200 $\mu E.m^{-2}.s^{-1}$. They therefore decided to use this light intensity to monitor oxygen production of their particular system. Deblois et al. demonstrated that for a different

unicellular algal strain, *Chlamydomonas Snowii*, the maximum growth rate was reached for 600 $\mu E.m^{-2}.s^{-1}$ (Deblois et al., 2013b). However, the effect of photoinhibition on algae as well as the general algal response strongly depends on physiological state of algae and varies among different algal strains (Aro et al., 1993).

It was therefore important to evaluate photosynthetic capacity for different light intensities of algal strain *Chlamydomonas reinhardtii*. Two values of light intensity were tested for following tests, yet the estimation of optimal light intensity should be completed through further studies when the system will be autonomous and an OLED will be fully integrated on the device as light source for algae photosynthesis. In this way, by varying operational voltage of OLED, light intensity can be varied and optimal value can be determined based on algae response.

All parameters listed above were considered for the measurements that followed. Calibration tests were conducted by mixing algal solutions of identical cell concentration with different concentrations of Diuron (control-non polluted solution -1µM Diuron algal solution) in an Eppendorf and directly loading the prepared test solution in the detection chamber of the lab-on-chip device. Similarly to O_2 detection tests carried out in control algal solutions, working electrode potential was set at -0.7 V vs Ag/AgCl integrated reference electrode. Temperature variations were not taken into account through measurements and a value of 22°C was considered.

Although fabricated systems aim for environmental applications that require disposable devices in compliance with regulations, the characteristics of the prototypes were tested in order to examine their repeatability. The devices were used through several tests (around 60 tests) with algae and different concentrations of Diuron pollutant after applying a cleaning step in 0.5 M H_2SO_4 before each series of measurements in order to reactivate the electrode surface and recycle the system. The results gave comparable surfaces before and after each series of measurements which means that after some slight improvements, other applications that require repetitive and/or online measurements can be targeted.

5.2.2.2 ***Diuron detection in culture medium algal solutions***

Optimal concentration of algal cells selected for tests was $10x10^6$ cells/mL HSM. A dark period of 10 minutes was introduced for first measurements in HSM medium before the onset of illumination. Artificial illumination was supplied through the halogen white light source where light is transmitted through an optical fiber (Hansatech instruments Ltd., UK). Two different light intensities were tested: 1800 $\mu E.m^{-2}.s^{-1}$ and 600 $\mu E.m^{-2}.s^{-1}$. Light intensity was measured using the WATER-Pulse-Amplitude-Modulated (WATER-PAM) fluorometer (Heinz Walz GmbH, Effeltrich, Germany).

Figure 5.10 presents algal response to Diuron concentrations varying from control solution to 1μM Diuron, illustrated through the current versus time graph. As already stated, the temporal curve of reduction current reflects oxygen evolution through time. Light-induced oxygen evolution was measured for approximately 2 minutes and changes in oxygen production rates point out the toxicant effect. Oxygen production rate corresponds to the slope obtained for reduction current through time during illumination. Oxygen production rate decreased upon the addition of Diuron and varies in a concentration-dependent way. In particular, when increasing Diuron concentration, the slope and consequently the rate are decreasing confirming the inhibition in algal photosynthetic activity induced by the toxicant. The diminution in the rate of O_2 production was evident immediately after injection of herbicide.

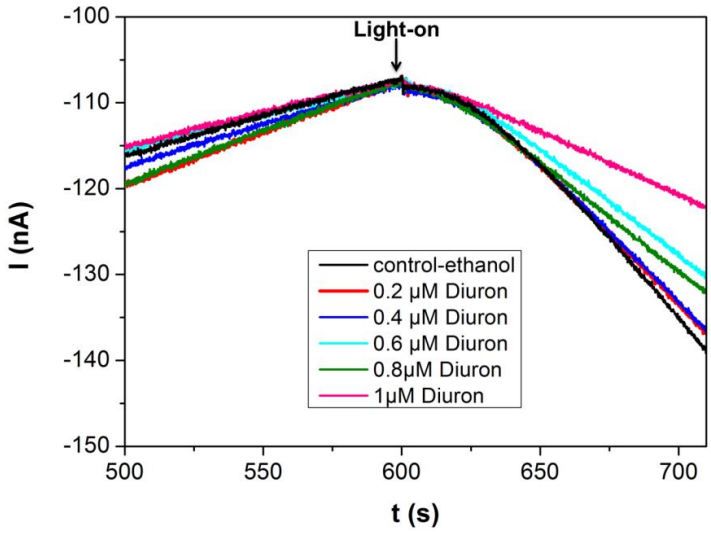

Figure 5.10. Not-normalized algal response to various Diuron concentrations for Pt-Bl ultramicroelectrode array integrated on lab-on-chip device.

Diuron is a herbicide targeting only photosynthetic activity (Fedtke and Duke, 2004), so the effect on respiration is considered negligible. However, similarly to previous observations with control algal solutions, respiration slopes registered are not identical for various pollutant concentrations. Therefore, gross photosynthetic oxygen production rates were normalized according to normalization protocol described previously in order to evaluate the real impact of Diuron on photosynthetic activity (cf. Chapter 2). Given the fact that obtained slopes are compared, curves corresponding to current evolution are considered linear. The normalized photosynthetic curves obtained are presented in Figure 5.11.

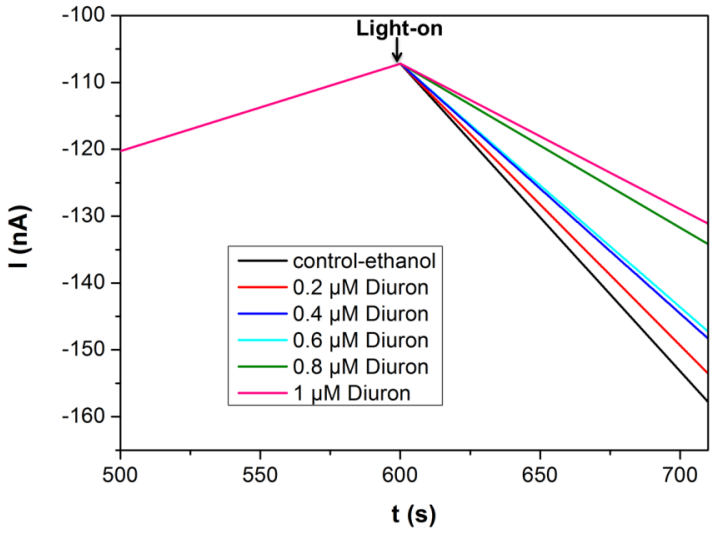

Figure 5.11. Normalized algal response to various Diuron concentrations for Pt-Bl ultramicroelectrode array integrated on lab-on-chip device.

The classic approach most often found in literature for the evaluation of the effect of Diuron on produced oxygen lies in estimating inhibition effect on photosynthetic activity and comparing the IC_{50} value that corresponds to the Diuron concentration that gives 50% inhibition of oxygen reduction current. This approach suggests therefore the presentation of the biosensor response as inhibition ratio (Shitanda et al., 2005, Shitanda et al., 2009) or similarly residual activity (Koblízek et al., 2002).

Inhibition in photosynthetic activity is calculated through the following equation (Equation 28) (Shitanda et al., 2009):

$$Inhibition\ ratio\% = \frac{I_1 - I_2}{I_1}\ 100\ (\%) \qquad (Equation\ 28)$$

Where, I_1 and I_2 represent the increase in photosynthetic oxygen reduction current through a constant time period before and after injection of Diuron respectively.
By following the classic approach and applying a similar equation including rates instead of increases in current, inhibition ratio can be presented by Equation 29:

$$Inhibition\ ratio\% = \frac{rate_{control} - rate_i}{rate_{control}} \qquad (Equation\ 29)$$

Where $rate_{control}$ represents gross oxygen production rate during photosynthesis for control algal solution and $rate_i$ represents the rate for different concentrations of Diuron injected in algal solutions.

After applying Equation 29 on results obtained for each Diuron concentration at both light intensities and plotting inhibition ratios versus Diuron concentration, the results obtained are similar to the ones presented by Shitanda et al. (Shitanda et al., 2009) (Figure 5.12). The biosensor used by Shitanda et al. consists in an algal ink screen-printed on a carbon electrode. The algal ink contains *Chlorella vulgaris* cells, carbon nanotubes and sodium alginate solution and the reference and counter electrodes are not integrated on the sensor device.

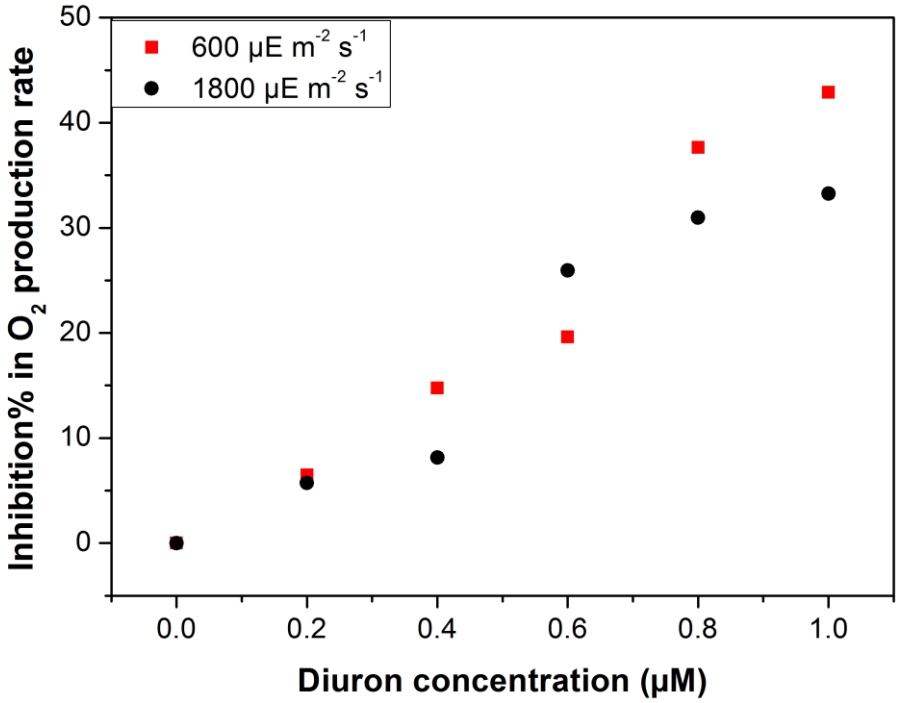

Figure 5.12. Calibration curves presented in inhibition ratio for the same sensor under two different light intensities in HSM algal solutions.

Similar ratios and IC_{50} values were obtained for both light intensities. IC_{50} value is a given value and should be the same no matter the sensor (transduction system) as it is a characteristic of the particular algal strain and represents its response to a specific concentration of herbicide. Therefore IC_{50} value can measure how sensitive the algal strain is to the particular herbicide but in this study, since the same algal strain under the same conditions is used through all the experiments, comparison of inhibition ratios is not rich in information purely in terms of the electrochemical sensor properties.

Through the approach proposed here, the sensitivity of the electrochemical sensor is examined and the evaluation is based on the comparison of the rates of oxygen production for different Diuron concentrations. By plotting the normalized gross oxygen production rate (y_i^*) versus Diuron concentration the concentration-response curve was obtained (Figure 5.13). A concentration-

dependent decrease in the rate was confirmed for both light intensities tested and the sensitivity of the fabricated sensor was evaluated.

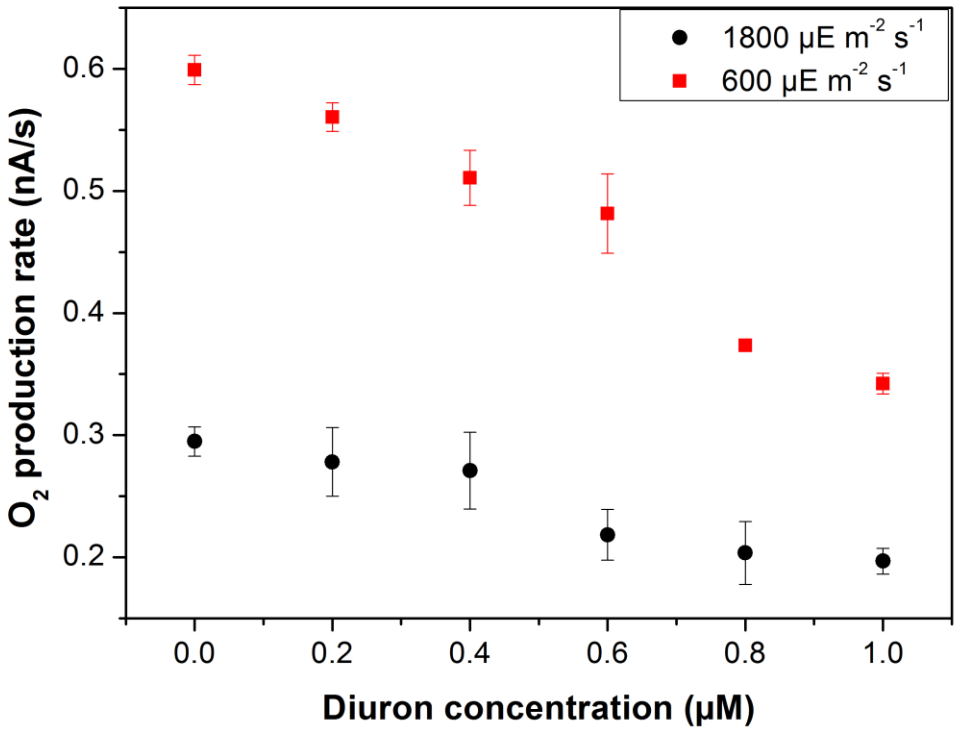

Figure 5.13. Calibration curves (normalized gross oxygen production rates versus Diuron concentrations) for the same sensor under two different light conditions in HSM algal solutions using halogen white light source.

Photosynthetic activity for control algal solutions was higher for light intensity of 600 $\mu E.m^{-2}.s^{-1}$ (red points) compared to the one obtained for 1800 $\mu E.m^{-2}.s^{-1}$ (black points), demonstrating that photosynthetic apparatus is more efficient in the first case. This result is in accordance with the results presented by Deblois et al. on *Chlamydomonas snowii* indicating the light intensity for maximal growth rate, mentioned earlier (Deblois et al., 2013b). It is important to precise that this optimal value is given for a halogen white source, the spectrum of which is presented later (Figure 5.18). It can therefore be deduced that for this particular algal strain and its physiological state, a light intensity of 1800 $\mu E.m^{-2}.\ s^{-1}$ introduces an additional stress that has an impact on algal physiology and consequently on the sensitivity of the device regarding herbicide detection. Sensitivity was determined by estimating the variation in the O_2 production rates between control and 1µM solutions. A value of 0.26 $nA.s^{-1}.\mu M^{-1}$ was calculated for the measurement performed at 600 $\mu E.m^{-2}.s^{-1}$ compared to the value of 0.1 $nA.s^{-1}.\mu M^{-1}$ at 1800 $\mu E.m^{-2}.s^{-1}$.

Indeed, for measurement conducted under 1800 $\mu E.m^{-2}.s^{-1}$, inhibition in photosynthetic activity is demonstrated as a combined effect between Diuron-induced and light-induced stresses and the real effect of the herbicide on photosynthesis cannot be evaluated accurately.
This result demonstrates that for an optimal light intensity, the photosynthetic activity is enhanced and the sensitivity is greater. The strong contribution of light conditions to photosynthetic activity, already highlighted in bibliography, is also outlined here and suggests that further work should be carried out for optimization of light intensity when the OLED will be integrated on the device in order to stimulate algal photosynthesis.

5.2.2.3 ***Diuron detection in lake water algal solutions-external light***

Measurements for herbicide determination were also performed using lake water instead of culture medium as the test solution into which different Diuron quantities were injected. Given the fact that fresh water will be the solution to be analyzed for final application, it was important to verify that the different properties (conductivity, CO_2 content) of fresh water compared to culture medium and the possible biofouling of the electrode surface will not impede measurements.

Algae were cultivated in HSM medium, centrifuged and the pellet was then re-suspended in lake water sample obtained from Lac Kelly, Sutton, QC, Canada. The non-polluted lake water sample was filtered before use through a filter with pore size of 0.45 µm in order to eliminate other microorganisms and suspended solids.
Oxygen reduction potential was determined for the new lake water solution through cyclic voltammetry and the value of -0.8 V was selected. This slight variation in the potential value can be explained because of the change in the solution examined that can induce a slight difference in pH. Measurements were conducted using light intensity of 600 $\mu E.m^{-2}.s^{-1}$.
Measurement time was reduced compared to experiments carried out with algae in HSM medium. Shorter dark incubation time was required as lake water is naturally richer in CO_2 than HSM medium. As a matter of fact, there is no carbon source among the ingredients of HSM medium and CO_2 needed by algae is assured through gas exchanges with air (N. Sueoka, 1967). However, fresh water of lakes or rivers contains dissolved inorganic and organic carbon as it is in contact with soil and rocks (Tranvik et al., 2009). A study was carried out to determine the time needed to leave algae in dark so that O_2 production slope can be measured for a sufficiently long time before CO_2 saturation during photosynthesis occurs in order to obtain a linear slope (Figure 5.14).

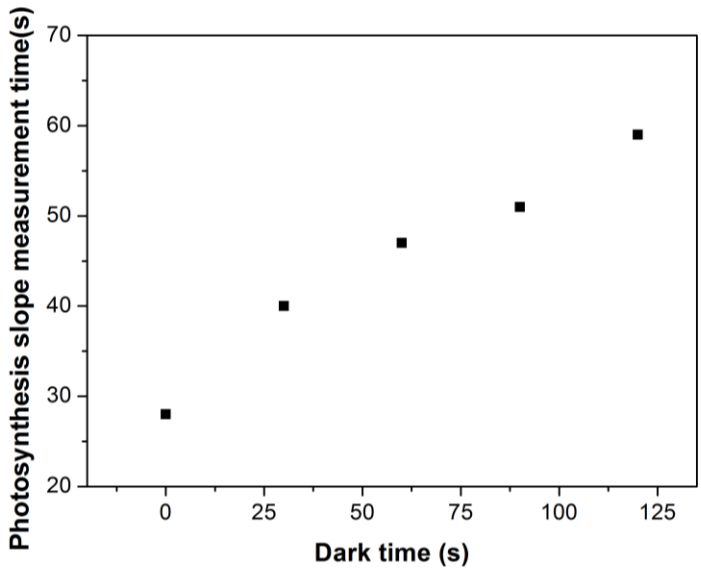

Figure 5.14. Influence of dark time duration prior to photosynthesis on the duration of the linear photosynthesis slope.

As presented in Figure 5.14, the results gave reasonable agreement with trends stated when operation protocol was described. By increasing dark incubation, algae produce more CO_2 that can be used in photosynthesis. Upon illumination, linear O_2 production lasts longer as saturation caused by depletion of CO_2 occurs later and the slope can be easily determined. A dark incubation time of two minutes was selected as it represents a duration, long enough to allow a precise estimation of the photosynthetic slope value. The total assay time therefore was four minutes, two minutes of dark followed by two minutes of illumination.

The influence of Diuron herbicide on the signal was quantified by plotting the O_2 production rate obtained for different Diuron concentrations versus the concentrations introduced. The concentration-response curve obtained for river water measurements is demonstrated in Figure 5.15. According to the Guidelines implemented for Canadian Drinking Water Quality, the maximum acceptable concentration for Diuron in drinking water is 0.15 mg/L or 0.64 µM. In order to verify that this limit can be detected, the concentration range of 0 to 0.6 µM Diuron was examined.

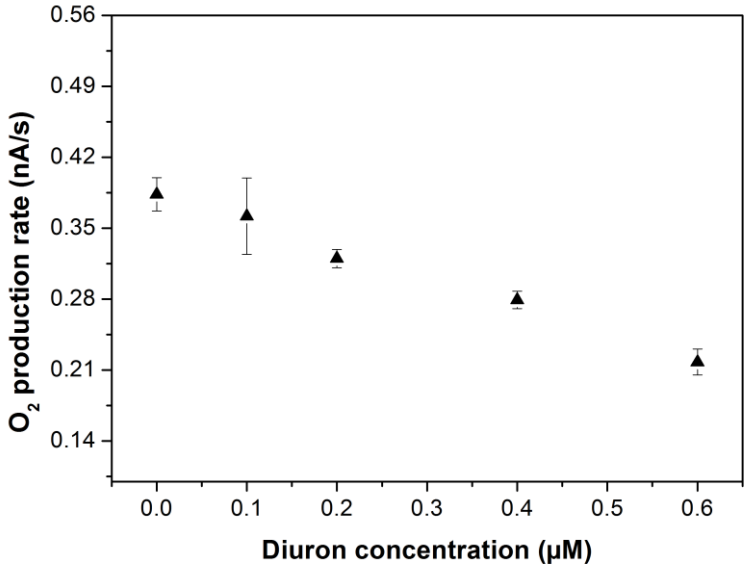

Figure 5.15. Calibration curve (normalized gross oxygen production rates versus Diuron concentrations) in lake water algal solutions using halogen white light source.

The curve obtained illustrates the toxic effect of Diuron on algal activity. The oxygen production rate decreased when Diuron concentration increased. Standard deviation is still large indicating that further work needs to be carried out in order to improve repeatability. Various assumptions have been made that may lead to this variability. Respiratory activity was considered proportional to photosynthetic in order to be able to normalize results and suppress non-regularities induced by the difference in the number of cells loaded in the chamber. It is assumed that both respiration and photosynthesis represent the average cellular activity and slight differences that may be observed as they are taking place in different organelles of the cell were not taken into account. Another reason explaining this variability can be the biofouling that implies the attachment and detachment of algal cells on the porous electrode surface in a random way. As already highlighted in literature, membrane integration improves the stability of the devices and the lack of membrane induces changes in surface as cells adhere and metabolic products are adsorbed on the surface (Wu et al., 2010).

By examining the concentration-response curve, it is obvious that the limit of maximum acceptable concentration implemented by the Canadian Government is detectable by the actual device. The sensitivity obtained in the range of 0 to 0.6 µM Diuron is of 0.26 nA s^{-1} μM^{-1}. Even though further improvements need to be carried out to enhance repeatability, the results are overall satisfying and the system can serve as an efficient tool in preliminary water toxicity tests. Moreover, it is validated that the detection properties of the sensor in real lake water samples are similar to the ones in HSM.

At this point it is important to mention that the fabricated sensor is a generic device that can be used through water quality assessment. Diuron herbicide was used as an example of toxicant in order to

prove the detection concept. If greater sensitivity needs to be achieved, several modifications can be considered related for instance to the functionalization of the electrode sensitive area, the electrochemical technique applied for the detection or the algal strain used as biological element.

5.2.2.4 ***Diuron detection in lake water algal solutions-OLED***

The final goal being an autonomous system and therefore the integration of the electrochemical and optical sensor on one single device, the light source used for the stimulation of algal photosynthetic apparatus should be integrated on the final system. Furthermore, through previous studies, it was highlighted that illumination methods and parameters need to be controlled in order to assure the accurate monitoring of metabolic processes of algae related to photosynthesis and respiration. The integration of the light source on the system will therefore be necessary. It was decided to make use of the technological platform established in LAAS dedicated to the development of Organic Light Emitting Diodes (OLED) (cf. works of Mme. Isabelle Séguy, researcher at LAAS and M. Ludovic Salvagnac, engineer in the technical team of the clean room of LAAS).

The absorption spectrum of green algae that contain chlorophyll *a* pigment to harvest light shows two peaks situated in the blue (near 430 nm) and red (near 675 nm) regions (Yun and Park, 2001). It is therefore possible to excite algae either by using red or blue light. This was also demonstrated by the absorption spectrum of *Chlamydomonas reinhardtii* measured in LAAS-CNRS using the NanoDrop 2000c Spectrophotometer of Thermo Scientific, USA (Figure 5.18).

Given the fact that the OLED will also be used in the optical sensor of the device, the color of the OLED was selected according to the system used by Lefèvre et al. who used a blue OLED in order to excite algae and lead to the measurement of the fluorescence produced (Lefèvre et al., 2012).

A low-cost, blue OLED was thus fabricated using the dedicated technological platform developed at LAAS. The design of the OLED was predefined in a form of six rectangles (Ossila Ltd). Even though the design is not adapted to measurement chambers of the present lab-on-chip device, the fabricated OLED were used for the pre-tests in order to validate the possibility of initiating photosynthesis with a blue organic light source, the wavelength of which corresponds to the absorption band of algae.

The OLED was fabricated on ITO coated glass substrates (Ossila Ltd.) and consisted of the following layers (Cho et al., 2011):

Poly(3,4-ethylenedioxythiophene) Polystyrene sulfonate (PEDOT:PSS) (40 nm)\ N,N′-bis(naphthalen-1-yl)-N,N′-bis(phenyl)-benzidine (NPB) (20 nm)\ 9-(9-phenylcarbazole-3-yl)-10-(naphthalene-1-

yl)anthracene PCAN (40 nm)\ Tris(8-hydroxy-quinolinato) aluminium (Alq3) (20 nm)\ Aluminium (Al) (150 nm).

The material stack and the final design obtained is presented in Figure 5.16.

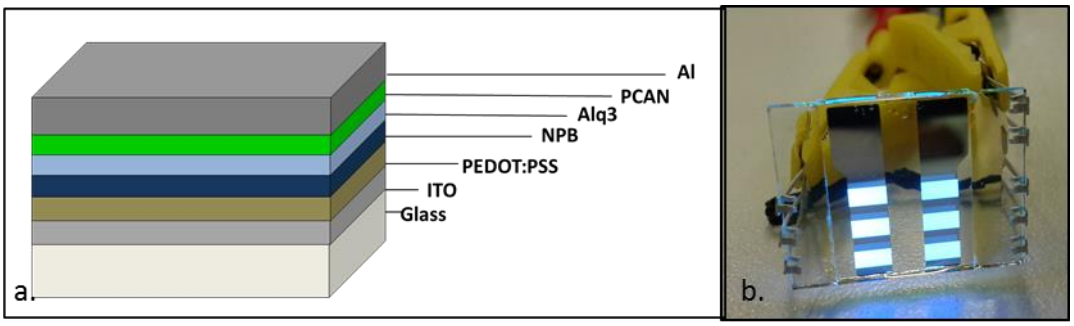

Figure 5.16. (a) OLED composition. (b) Fabricated OLED.

A sufficient OLED stability throughout measurement duration is essential so that deviations in light intensity are negligible. When increasing the operation voltage, the performance of the OLED is deteriorating (Lefèvre et al., 2012). The OLED were biased at 9V using a Keithley 2450 Sourcemeter (KEITHLEY Instruments Inc.), so that the decrease in light intensity will not be important for the duration of the measurement.

Current and power were measured through time in order to test the performance of the fabricated OLED during 10 minutes (Figure 5.17). Measurement of the power was performed using the Thorlabs power meter PM200 equipped with an integrating sphere (THORLABS, Inc).

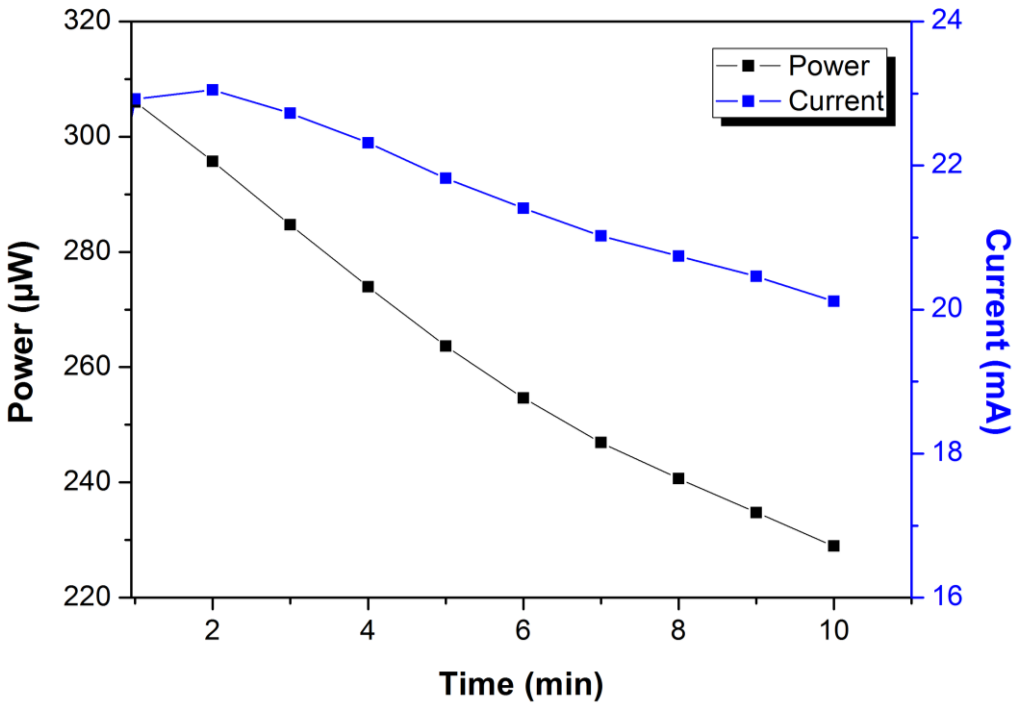

Figure 5.17. Power and current versus time for the fabricated OLED.

After 10 minutes of continuous operation at 9V, the current shift in time is estimated at 0.28 mA.min^{-1} while the power shift at 7.73 μW.min^{-1}. In order to minimize the aging of the device, these values can be optimized by decreasing operation voltage once optimal light intensity will be determined or by optimizing OLED devices.

Both light-sources used through this study (halogen white light source and OLED) were optically characterized using a spectrophotometer equipped with a monochromator (HR1000, JOBIN YVON.) and a detector (photocathode GaAs) in order to check if they correspond to the absorption spectrum of algae (Figure 5.18). The emission spectrum of the OLED shows a broad peak around 455 nm, which overlaps with the major absorption band of algae. On the other hand, the emission of the halogen white light source is mostly taking place in longer wavelengths that coincide with a less pronounced algal absorption peak in the red region.

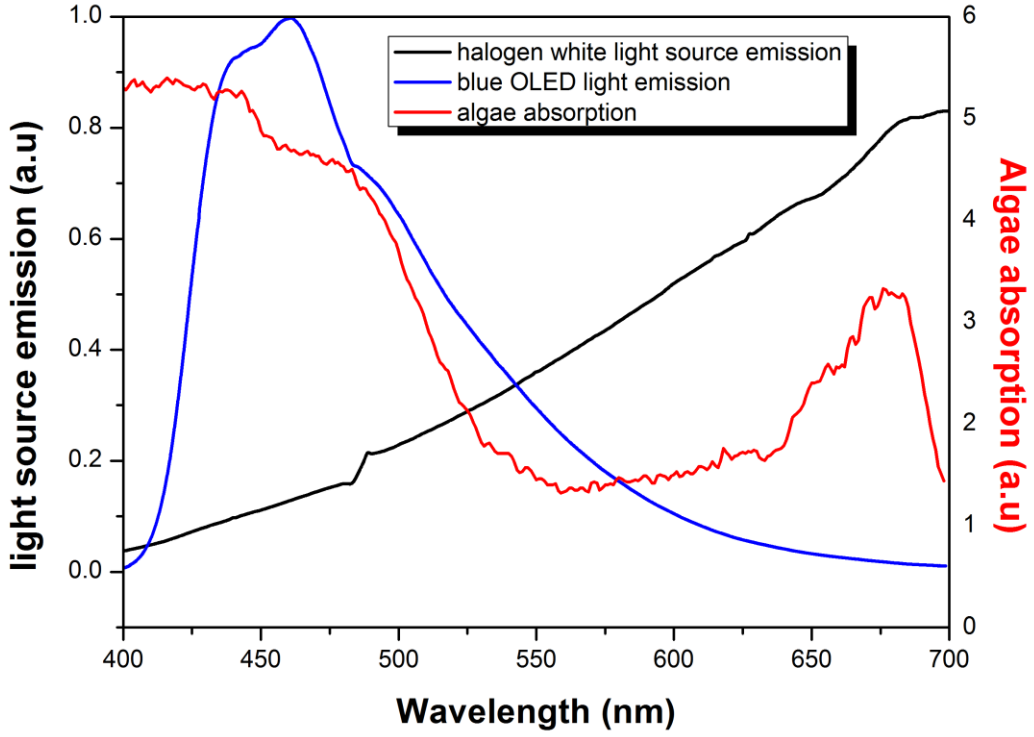

Figure 5.18. Comparison of emission spectra of fabricated OLED (blue line) and halogen white light source (black line) with algal absorption spectrum (red line).

Experiments similar to the ones described in previous section related to the effect of Diuron on photosynthetically produced oxygen, were conducted using an OLED as light source for the stimulation of algal photosynthesis. The blue OLED was placed on top of the detection chamber in direct contact with the glass cover as presented in Figure 5.19.

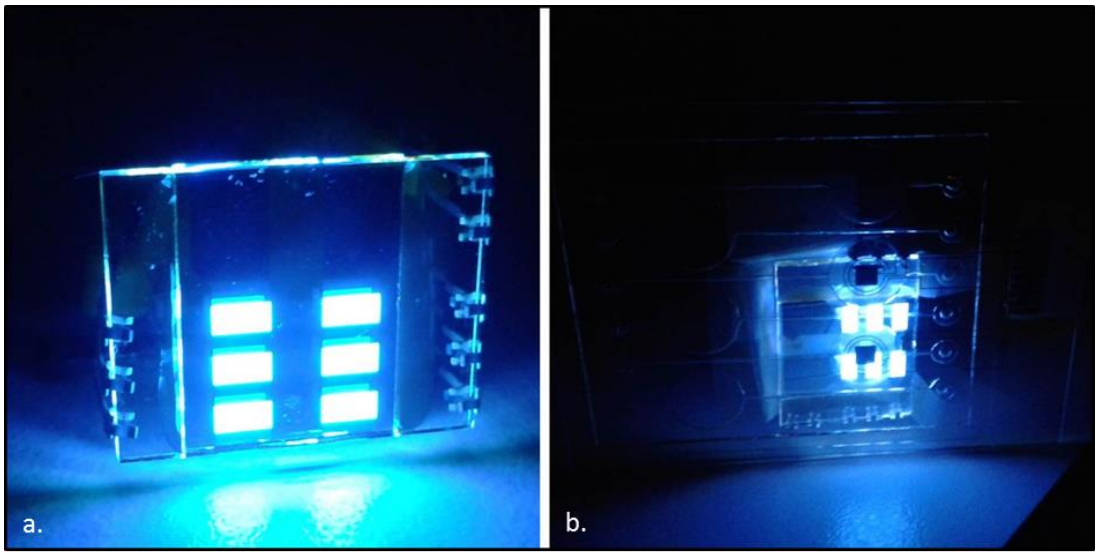

Figure 5.19. a) Blue OLED used for the excitation of algae. b) Blue OLED stuck on the glass cover of lab-on-chip device.

Provided that light intensity of OLED was much smaller than the one of the halogen white light source, algal cell concentration was increased for herbicide measurements to $18x10^{6}$ cells.mL^{-1} in order to enhance total oxygen production.

The same measurement protocol was followed. A control measurement of current recording through illumination and dark periods was conducted with a lake water sample in the absence of algal cells. In contrast to the control measurement carried out with the external, white light halogen source, a change in the reduction current was observed this time when the light was turned on (Figure 5.20).

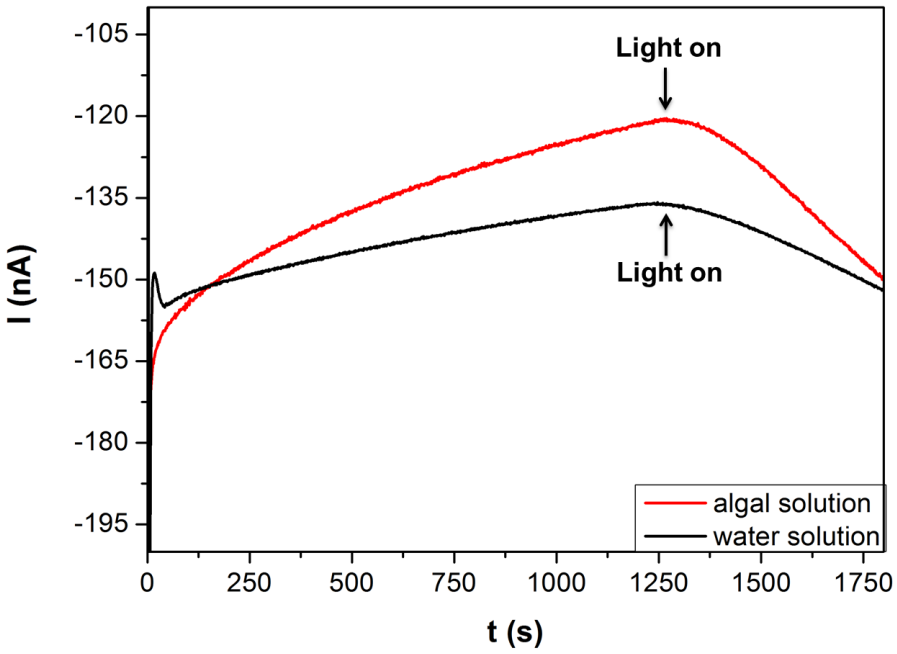

Figure 5.20. Current measurement through illumination and dark periods for an algal solution and a water solution using the fabricated blue OLED.

Given the fact that the sample contains no algal cells, this current increase could be attributed to the temperature increase induced by the heat generated by the OLED and transferred to the test solution. High-brightness OLEDs can dissipate energy in the form of heat (Bergemann et al., 2012). The temperature measured at the back side of the glass cover on which the OLED is stuck, after 2 minutes photosynthesis measurement with light on was 35°C.

Temperature increase in the measurement solution induces an increase in chemical reaction rate. As a matter of fact, in a system limited by diffusion, temperature influences the diffusion coefficient and therefore enhances mass transport of electroactive species towards the electrode surface.

What is more, the heterogeneous electron transfer on the electrode surface also depends on temperature. The rate of electron transfer is given by the following equation (Equation 30) (Bedioui, 1999):

$$\frac{I}{nFS} = k_a\, c^*_{red} - k_c\, c^*_{ox} \qquad (Equation\ 30)$$

Where:

I (A): current intensity

S (cm^2): electrode surface area

n: number of exchanged electrons

F: Faraday constant ($C.mol^{-1}$)

c_{red}^*, c_{ox}^* ($mol.cm^{-3}$): concentrations on electrode surface of the reducing and oxidizing species respectively

k_a, k_c ($cm.s^{-1}$): rate constants

The rate constants k_a, k_c follow Arrhenius activation law and therefore depend on the temperature (Equations 31,32).

$$k_c = k^0 \exp\left(\frac{-a\, n\, F}{RT}\,(E - E^0)\right) \qquad (Equation\ 31)$$

$$k_a = k^0 \exp\left(\frac{(1-a)\, n\, F}{RT}\,(E - E^0)\right) \qquad (Equation\ 32)$$

Where:

k^0 ($cm.s^{-1}$): standard rate constant

It is thus necessary to take into account the temperature induced variation in registered current when calculating gross oxygen production rates. Temperature variation caused by the heat transferred by the OLED was considered similar for all experiments, although this matter needs to be further analyzed when the OLED will be integrated on the device. Electrochemical signal variation induced by temperature increase after illumination should be correctly compensated. The rate under illumination recorded for the non-algal control solution was subtracted from O_2 production rates calculated for different Diuron concentrations.

The following graph (Figure 5.21) presents the response of the sensor to different Diuron concentrations using the OLED as light source (blue points). The results obtained with the OLED are compared to the ones obtained in lake water samples using the halogen white light source.

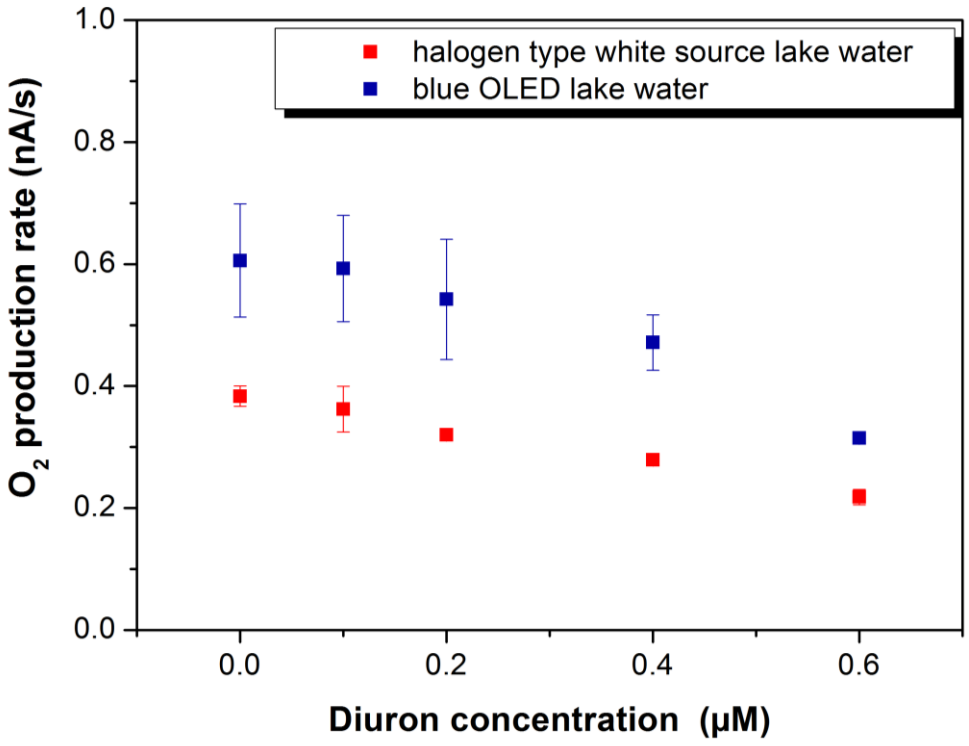

Figure 5.21. Calibration curve (normalized gross oxygen production rates versus Diuron concentrations) in lake water algal solutions using blue OLED as light source (blue) and halogen white light source (red).

Although sensitivity is low for small Diuron concentrations (control to 0.2 µM), it increases for bigger concentrations. Provided that the concentration-response relationship is not linear and that the limit of maximum acceptable concentration in drinking water is 0.64 µM, sensitivity was determined simply by estimating the variation in the O_2 production rates between 0 and 0.6µM Diuron. Rate variation obtained for the actual device that includes OLED as light source was 0.48 nA s^{-1} μM^{-1} that corresponds to almost double the value of 0.26 nA s^{-1} μM^{-1} obtained with the same device when the external halogen white light source was used for lake water samples (red points in Figure 5.21). Photosynthetic apparatus is more effective when OLED is used and this can be attributed to the

wavelength used, more adapted to algal absorption spectrum (Figure 5.18) and the temperature increase of the test solution (35°C approximately).

As a matter of fact, the overlap of the emission spectrum of the OLED with the absorption spectrum of algae can explain this sensitivity increase (see Figure 5.18). The emission of the OLED is more centered on the absorption band of algae compared to the halogen white light source used through previous experiments and this can increase the efficiency of the system as more photons can be effectively captured by algae.

A far as temperature increase is concerned, photosynthetic activity depends on temperature (Raven and Johnson, 2002) as it includes enzyme-catalyzed reactions. Temperature-induced variation in photosynthetic activity depends on the algal strain used each time as well as the growth temperature of the culture (William and Morris, 1982). In general terms though, photosynthetic rate is increasing with a short-term increase in temperature up to an optimal temperature (Davison, 1991; Hancke et al., 2008). Water oxidation takes place in the oxygen-evolving complex (a water-oxidation enzyme), a functional unit of PSII where water molecules bind to a cluster of manganese atoms and oxygen is produced (Aro et al., 1993, Giardi and Piletska, 2006). A temperature increase can lead to an increase in the efficiency of this enzyme-catalyzed oxidation process. Moreover, the effect of temperature on photosynthesis can also be evident on the Calvin cycle where carbon dioxide is transformed to carbon compounds using NADPH and ATP as substrates. A temperature increase induces an increase in the carbon reducing reactions as they are catalyzed by enzymes (Raven and Johnson, 2002). If the rate is increased, the demand in ATP and NADPH substrates will be greater and therefore electron transfer through the first part of photosynthesis and O_2 production will be enhanced to fulfill this demand.

It is therefore demonstrated that photosynthetic activity of each algae cell is more effective and therefore of greater amplitude when OLED is used, due to a more adapted emission spectrum or a slight temperature increase. The dynamic range is therefore bigger, the variation induced by the herbicide more visible and the sensitivity improved.

Nevertheless, further system optimization needs still to be conducted. By working on the structure of the organic light source, the peak of the OLED emission spectrum could be more centered on the absorption band of algae. Furthermore, temperature effect on sensor sensitivity and temperature variations through measurement duration should be further examined in order to determine the temperature at which algal photosynthetic activity is the most efficient and the sensor gives the greater sensitivity. Even though the temperature increase can be advantageous up to a certain point, it is necessary to minimize the dissipation of heat by the OLED by optimizing its fabrication procedure, in order to increase its lifetime and target more reproducible measurements.

5.3 Conclusion

All in all, the fabricated lab-on-chip sensor can effectively monitor a herbicide-induced modification in algal photosynthetic activity. Modification in algal photosynthetic activity could be mainly demonstrated through a modification in the production of certain electroactive metabolites such as O_2, H_2O_2, H_3O^+/OH^- pH-related ions.

Particular attention was placed on oxygen as it is the element giving more information on the presence of the most widely used pollutants. Oxygen evolution was monitored through photosynthesis and respiration and changes in oxygen production rates due to the presence of Diuron herbicide were followed. Detection principle was first evaluated with silicon-based devices through dark and illumination periods that are representative of the change from respiratory to photosynthetic activity, in presence and absence of the herbicide. Oxygen evolution rates, when light was on, were compared for different pollutant concentrations (control solution to1 µM Diuron) in order to demonstrate concentration-dependent inhibition effect of the herbicide on photosynthesis. A decrease in the rate recorded under illumination was evidenced when increasing Diuron concentration.

On the other hand, no herbicide-induced variation was evidenced when monitoring the production of H_2O_2 or pH related ions at intracellular level. The herbicide used this time was Paraquat. Further work should be carried out, experimental protocol should be improved and measurement parameters should be reconsidered in order to effectively monitor intracellular H_2O_2 or H_3O^+/OH^- - pH related ions production.

The effect of Diuron was then validated using the lab-on-chip devices in HSM medium solutions. Illumination was first supplied through the halogen white light source and two different light intensities were tested: 1800 $\mu E.m^{-2}.s^{-1}$ and 600 $\mu E.m^{-2}.s^{-1}$. A concentration-dependent decrease in the rate was demonstrated for both light intensities but the sensitivity of the sensor was higher for 600 $\mu E.m^{-2}.s^{-1}$. Diuron detection was then conducted in real samples of fresh lake water similarly to final application using the light intensity of 600 $\mu E.m^{-2}.s^{-}1$, and it was verified that the different properties (bioelements, conductivity, CO_2 content, bioelements) of fresh water compared to culture medium did not impede measurements. Finally, in order to obtain an autonomous system the same experiments were successfully carried out in fresh lake water samples, with a blue OLED used as light source for the excitation of photosynthetic mechanism. It was demonstrated that photosynthetic apparatus was more effective when OLED is used compared to the halogen white light source. This can either be attributed to the fact that the wavelength of the OLED is more adapted to algal absorption spectrum or the temperature increase of the test solution induced by heat transfer from the OLED to the solution.

It is overall demonstrated that the fabricated lab-on-chip biosensor can be an efficient indicator of water pollution as it can effectively follow the change in photosynthetic activity induced by Diuron herbicide and reflected through a modification in oxygen production rate.

5.4 References

Aro, E.-M., Virgin, I., Andersson, B., 1993. Photoinhibition of Photosystem II. Inactivation, protein damage and turnover. Biochim. Biophys. Acta BBA - Bioenerg. 1143, 113–134. doi:10.1016/0005-2728(93)90134-2

Barber, J., Andersson, B., 1992. Too much of a good thing: light can be bad for photosynthesis. Trends Biochem. Sci. 17, 61–66. doi:10.1016/0968-0004(92)90503-2

Bard, A.J., Faulkner, L.R., 2001. Electrochemical Methods: Fundamentals and Applications, New York: Wiley, 2001, 2nd ed. JOHN WILE SONS INC. doi:10.1023/A:1021637209564

Bedioui, F., 1999. Voltampérométrie. Théorie et mise en œuvre expérimentale, in: Techniques de L'ingénieur Méthodes Électrochimiques. Editions T.I.

Bergemann, K.J., Krasny, R., Forrest, S.R., 2012. Thermal properties of organic light-emitting diodes. Org. Electron. 13, 1565–1568. doi:10.1016/j.orgel.2012.05.004

Cho, C.-W., Pham, T.P.T., Jeon, Y.-C., Min, J., Jung, H.Y., Lee, D.S., Yun, Y.-S., 2008. Microalgal photosynthetic activity measurement system for rapid toxicity assessment. Ecotoxicol. Lond. Engl. 17, 455–463. doi:10.1007/s10646-008-0197-x

Cho, I., Kim, S.H., Kim, J.H., Park, S., Park, S.Y., 2011. Highly efficient and stable deep-blue emitting anthracene-derived molecular glass for versatile types of non-doped OLED applications. J. Mater. Chem. 22, 123–129. doi:10.1039/C1JM14482K

Davison, I.R., 1991. Environmental Effects on Algal Photosynthesis: Temperature. J. Phycol. 27, 2–8. doi:10.1111/j.0022-3646.1991.00002.x

Deblois, C.P., Dufresne, K., Juneau, P., 2013a. Response to variable light intensity in photoacclimated algae and cyanobacteria exposed to atrazine. Aquat. Toxicol. 126, 77–84. doi:10.1016/j.aquatox.2012.09.005

Deblois, C.P., Marchand, A., Juneau, P., 2013b. Comparison of Photoacclimation in Twelve Freshwater Photoautotrophs (Chlorophyte, Bacillaryophyte, Cryptophyte and Cyanophyte) Isolated from a Natural Community. PLoS ONE 8, e57139. doi:10.1371/journal.pone.0057139

Fedtke, C., Duke, S., 2004. Plant Toxicology, Fourth Edition.

Giardi, M.T., Piletska, E.V., 2006. Biotechnological Applications of Photosynthetic Proteins. Landes Bioscience, Springer Publishers, Church ST.Georgetown, USA.

Hancke, K., Hancke, T.B., Olsen, L.M., Johnsen, G., Glud, R.N., 2008. Temperature Effects on Microalgal Photosynthesis-Light Responses Measured by O2 Production, Pulse-Amplitude-Modulated Fluorescence, and 14c Assimilation1. J. Phycol. 44, 501–514. doi:10.1111/j.1529-8817.2008.00487.x

Koblízek, M., Malý, J., Masojídek, J., Komenda, J., Kucera, T., Giardi, M.T., Mattoo, A.K., Pilloton, R., 2002. A biosensor for the detection of triazine and phenylurea herbicides designed using Photosystem II coupled to a screen-printed electrode. Biotechnol. Bioeng. 78, 110–116.

Lefèvre, F., Chalifour, A., Yu, L., Chodavarapu, V., Juneau, P., Izquierdo, R., 2012. Algal fluorescence sensor integrated into a microfluidic chip for water pollutant detection. Lab. Chip 12, 787–793. doi:10.1039/C2LC20998E

Leverenz, J.W., Falk, S., Pilström, C.-M., Samuelsson, G., 1990. The effects of photoinhibition on the photosynthetic light-response curve of green plant cells (Chlamydomonas reinhardtii). Planta 182, 161–168. doi:10.1007/BF00197105

Li, Y., Sella, C., Lemaître, F., Guille Collignon, M., Thouin, L., Amatore, C., 2013. Highly Sensitive Platinum-Black Coated Platinum Electrodes for Electrochemical Detection of Hydrogen Peroxide and Nitrite in Microchannel. Electroanalysis 25, 895–902. doi:10.1002/elan.201200456

N Sueoka, K.S.C., 1967. Deoxyribonucleic acid replication in meiosis of Chlamydomonas reinhardi. I. Isotopic transfer experiments with a strain producing eight zoospores. J. Mol. Biol. 25, 47–66. doi:10.1016/0022-2836(67)90278-1

Raven, J.A., Beardall, J., 2003. Carbohydrate Metabolism and Respiration in Algae, in: Larkum, A.W.D., Douglas, S.E., Raven, J.A. (Eds.), Photosynthesis in Algae, Advances in Photosynthesis and Respiration. Springer Netherlands, pp. 205–224.

Raven, P., Johnson, G., 2002. Photosynthesis, in: Biology. Mc Graw Hill.

Schubnell, D., Lehmann, M., Baumann, W., Rott, F.G., Wolf, B., Beck, C.F., 1999. An ISFET-algal (Chlamydomonas) hybrid provides a system for eco-toxicological tests. Biosens. Bioelectron. 14, 465–472. doi:10.1016/S0956-5663(99)00025-1

Shapira, M., Lers, A., Heifetz, P.B., Irihimovitz, V., Osmond, C.B., Gillham, N.W., Boynton, J.E., 1997. Differential regulation of chloroplast gene expression in Chlamydomonas reinhardtii during photoacclimation: light stress transiently suppresses synthesis of the Rubisco LSU protein while enhancing synthesis of the PS II D1 protein. Plant Mol. Biol. 33, 1001–1011.

Shitanda, I., Takada, K., Sakai, Y., Tatsuma, T., 2005. Compact amperometric algal biosensors for the evaluation of water toxicity. Anal. Chim. Acta 530, 191–197. doi:10.1016/j.aca.2004.09.073

Shitanda, I., Takamatsu, S., Watanabe, K., Itagaki, M., 2009. Amperometric screen-printed algal biosensor with flow injection analysis system for detection of environmental toxic compounds. Electrochimica Acta 54, 4933–4936. doi:10.1016/j.electacta.2009.04.005

Smith, E.L., 1936. Photosynthesis in Relation to Light and Carbon Dioxide. Proc. Natl. Acad. Sci. U. S. A. 22, 504–511.

Stoy, V., 1969. Interrelationships Among Photosynthesis, Respiration, and Movement of Carbon in Developing Crops. Agron. Hortic. -- Fac. Publ.

Tranvik, L.J., Downing, J.A., Cotner, J.B., Loiselle, S.A., Striegl, R.G., Ballatore, T.J., Dillon, P., Finlay, K., Fortino, K., Knoll, L.B., 2009. Lakes and reservoirs as regulators of carbon cycling and climate. Limnol. Oceanogr. 54, 2298–2314. doi:10.4319/lo.2009.54.6_part_2.2298

Truesdale, G.A., Downing, A.L., 1954. Solubility of Oxygen in Water. Nature 173, 1236–1236. doi:10.1038/1731236a0

Wu, C.-C., Luk, H.-N., Lin, Y.-T.T., Yuan, C.-Y., 2010. A Clark-type oxygen chip for in situ estimation of the respiratory activity of adhering cells. Talanta 81, 228–234. doi:10.1016/j.talanta.2009.11.062

Yun, Y.-S., Park, J.., 2001. Attenuation of monochromatic and polychromatic lights in Chlorella vulgaris suspensions. Appl. Microbiol. Biotechnol. 55, 765–770. doi:10.1007/s002530100639

General conclusion

Water quality assessment has attracted wide attention during the last decades in order to find ways to control contamination of water bodies induced, in a big part, by agricultural and industrial activities.

The present work was dedicated to the development of a lab-on-chip device for water toxicity analysis. This device is, by no means, aiming at replacing laboratory-based analysis but should mostly serve as a pre-screening tool. It consists in a portable system for on-site detection and aims at offering the possibility of conducting double complementary detection: optical and electrochemical. Since the optical sensor is already validated by our collaborators in UQAM, this study focused on the implementation of the algal-based, electrochemical biosensor which, when combined with the optical system at the end of this project, will eventually yield a multisensor platform. Despite the fact that the final goal is to implement a generic, versatile device for water quality assessment, throughout this study, special emphasis was placed on the detection of herbicides as they are widely used and represent major water contaminants.

Among all different transduction systems, the electrochemical transducer was selected as it is easily miniaturized and provides the sensitivity required for the targeted application, involving at the same time, simple procedures of development and further operation. Concerning the biological sensing element, whole algal cells were selected since they are robust and require simple procedures for their cultivation, isolation and manipulation. What is more, their physiology resembles to the one of the targeted vegetation and can therefore be directly affected by the herbicide present in the examined sample.

The basic detection principle consists in monitoring disturbances in metabolic activities of algae induced by the presence of the herbicides. Algal response is different for each herbicide concentration in the examined sample.

The two selected herbicides, Diuron and Paraquat, target the photosynthetic electron flow that takes place in the thylakoids. Photosystems I and II are two protein complexes in the photosynthetic chain, affected by the presence of herbicides. Diuron targets electron flow after PSII, blocking partially or totally oxygen production while Paraquat targets electron flow after PSI resulting in ROS production and therefore a modification in the level of hydrogen peroxide and pH. Consequently, these three electroactive species, O_2, H_2O_2 and H_3O^+/OH^- ions related to pH, served as indicators of the presence of herbicides and were the species monitored by the implemented devices, pointing out simultaneously the appropriate working electrode materials of the electrochemical cell to be used for the detection of each species. As reported in literature, several working electrode materials are prone to be more appropriate for the detection of each electroactive species. Working electrode materials eventually

selected to be easily integrated on the device were platinum (Pt) and platinum black (Pt-Bl) for the detection of O_2 and H_2O_2 while IrO_x was chosen for pH monitoring.
Prior to the development of the final lab-on-chip device, the detection principle as well as the electrode materials that were going to be integrated were validated using a simpler device that was implemented using a silicon-based fabrication technology and was characterized using simpler procedures. A silicon chip containing the electrochemical system, similar to the one intended for final application was fabricated. It consisted in an autonomous fully integrated three-electrode electrochemical microsystem comprised of the working microelectrodes (Pt, Pt-Bl or Pt/IrO_x depending on the electroactive species to be detected by each device), the integrated Ag/AgCl quasi-reference electrode and the integrated Pt counter electrode. Si_3N_4 layer was used as long-term passivation layer in order to define electroactive surface. Pt-Bl and IrO_x were electrochemically deposited on the surface of the working microelectrodes and Ag was oxidized to Ag/AgCl.

The performance of the microsystem was evaluated through electrochemical characterization and calibration was performed by amperometric and potentiometric methods for the three species of interest: O_2, H_2O_2 and pH related ions (H_3O^+/OH^-). The enhanced electrocatalytic activity combined with favorable features of array configurations contributed to the greater properties towards O_2 and H_2O_2 detection, presented by platinum black UME arrays. Pt/IrO_x microelectrodes yielded satisfying performances towards pH monitoring in the range of 2 to 12, in accordance with literature. The integrated Ag/AgCl electrode demonstrated sufficient stability for the short-time measurements that need to be conducted for the present application.

Once validated, the aforementioned materials and configurations were used for the fabrication of the lab-on-chip devices. The lab-on-chip structure was fabricated on a high optical transmission glass substrate. The integrated three-electrode electrochemical microsensor, previously described, was developed by PVD process followed by electrodeposition of Pt-Bl or IrO_x in order to functionalize working microelectrodes. Microfluidic chambers and channels were then structured by patterning SU-8 negative photoresist whereas a glass cover was used to seal microfluidic tanks.

The lab-on-chip devices were further used in bioassays to detect the herbicides of interest. Special emphasis was placed on O_2 monitoring as indicator of the presence of Diuron, as it is the element the most representative of variations in metabolic activities. O_2 evolution was therefore measured in algal solutions through photosynthesis and respiration, using a white light halogen source. A decrease in the oxygen production rate during algal photosynthesis was evidenced in the presence of Diuron herbicide in solutions of high salt medium (HSM) as well as real samples of fresh lake water, similarly to final application. A concentration-dependent inhibition effect of the herbicide on photosynthesis was demonstrated for two different light intensities. A blue OLED, with an optimized wavelength compared to the halogen white light source, stuck on the lab-on-chip device was then used as light

source for the excitation of photosynthetic mechanism. Photosynthetic apparatus was more efficient and detection of low levels of Diuron herbicide was achieved with a greater sensitivity and a range covering the limit of maximum acceptable concentration (0.64 µM) imposed by Canadian government. The integrated, autonomous system developed, demonstrated good performances concerning the detection of the targeted herbicides and holds great potential for total quality monitoring as a generic device.

Perspectives

Even though the lab-on chip multisensor platform yielded satisfying response, several aspects could be addressed in order to enhance the performance of the system.

Repeatability-Reproducibility-Reliability

Biofouling

Since real water samples are examined and biological elements are used through measurements, the electrochemical sensor is in direct contact with algal cells, proteins and other elements potentially present in the examined sample. All these elements can be adsorbed on the surface, induce surface modification and interfere with measurement. This partially explains the variability observed between consecutive measurements (c.f. Chapter 5) due to probable attachment and detachment of algal cells on the porous electrode surface in a random way. Zhang et al. reported the use of several commercially available polymers to construct the membranes such as polyvinyl chloride, polyethylene, polymethacrylate and polyurethane (Zhang et al., 2000). Surface treatment of these membranes, such as the application of polyethylene glycol (PEG) that prevents protein or cell adsorption can be an efficient solution to prevent biofouling and improve stability. Hydrogels have been also successfully used in this purpose. Hydrogel membranes based on poly 2-hydroxyethyl methacrylate (pHEMA) were used by Kieninger, 2011 to protect electrodes from cells adsorption.

Algae immobilization

The protocol followed to load algal solutions can inevitably introduce variations in number of active cells injected each time. Immobilization of algal cells on the electrode's surface can potentially improve the repeatability of the sensor. As reported by Eltzov and Marks, 2011, cell immobilization can be performed between others by chemical attachment and gel entrapment. Chemical attachment involves procedures such as covalent bonding and cross-linking using for example photocrosslinkable resins, but can damage the cells and reduce the life-time of the biosensor. Gel entrapment though is more often applied using synthetic polymers, such as polyurethanes and natural polysaccharides such

as alginate and agar gels that do not reduce viability of the cells and do not impede their biological activities (Moreno-Garrido, 2008; Eltzov and Marks, 2011).

Pt-Bl and IrO_x deposition

In order to obtain more stable microelectrodes, it is important to optimize deposition parameters of Pt-Bl and IrO_x layers. An optimum needs to be determined between the increase in electroactive surfaces and the mechanical stability of the deposited layer. For instance, when increasing charge deposited, the diameter of the platinized microelectrodes obtained increases but the microelectrodes lose mechanical stability. Given the fact that the recorded current is a function of the surface for a given concentration, it is necessary to control the surface between different measurements in order to get repeatable results.

Ag/AgCl stability

If the targeted application demands a reference electrode with enhanced stability, the integration of a membrane with the internal solid electrolyte can be considered (Toczyłowska-Mamińska et al., 2008). In this way, the signal of the electrode can be stable over a longer period and interferences induced by modifications in different chloride ions concentrations can be reduced.

Sensitivity

Electrochemical method

Chronoamperometry was the electrochemical method selected through conducted bioassays due to its simplicity even though it is less sensitive compared to other electrochemical techniques. If sensitivity properties need to be improved and lower detection limits need to be attained, pulse voltammetric techniques such as square wave and differential pulse voltammetry can be considered in the future. Their main advantage is that the ratio of faradaic current to capacitive current is greater, making changes in faradaic current more obvious and therefore yielding a more sensitive sensor (Bard and Faulkner, 2001).

Determination of limit of detection

Through this study, we focused on the guidelines implemented by Canadian government. It is however important to work with smaller Diuron concentrations and determine the exact limit of detection and application range that can be targeted by the developed device, given the fact that maximum acceptable concentration limits vary from one country to the other and tend to decrease.

Electrode functionalization

If greater sensitivity needs to be achieved, the functionalization of the electrode sensitive area can be reconsidered. Surface functionalization with enzymes (Ruzgas et al., 1996) can for instance be an efficient solution to increase the sensitivity of an H_2O_2 sensor.

Algal strain

Chlamydomonas reinhardtii were selected as they are widely studied and represent a model algal strain. However, if sensitivity needs to be increased, a study should be conducted in order to determine the algal strain that is more sensitive to each different herbicide, based for instance on the IC_{50} value, indicating the concentration of a toxicant that causes a 50% inhibition in the algal activity.

Selectivity

Given the fact that the mode of action of several pollutants (pesticides, heavy metals) presents similarities (van der Meer and Belkin, 2010), the developed biosensor can be successfully used in prescreening tests for a threshold contaminants detection but distinction between present contaminants is sometimes complicated. In order to address this issue, a special study should be conducted to determine algae species that are affected in different ways by different toxicants and therefore yield distinct sensitivities. The responses of each algal species to each pollutant should then be combined and compared and by further data treatment, the selectivity of the system can be improved.

Selectivity and sensitivity can also be improved if genetically modified algal cells could be eventually integrated. Mutants of algal cells can be resistant against particular contaminants but sensitive to others (Pasco et al., 2011) and therefore increase the specificity of the sensor.

Measurement protocol

H_2O_2 and pH monitoring

Further work should be carried out on the determination of H_2O_2 levels and pH monitoring in algal solutions. A well-defined measurement protocol should be established and optimized in order to determine small changes of the electroactive species of interest, taking place in the interior of the cell. For instance, given the fact that H_2O_2 is an intermediate product of scavenging reactions, the exact moment for performing cell lysis should be determined. Since H_2O_2 is transformed in H_2O through enzymes, an important parameter worth considering could be the addition of a molecule inhibiting the action of this enzyme (Margoliash et al., 1960). In this way, measurement protocol can be simplified. What is more, cell lysis protocol should be further investigated so that cell membrane can be destroyed and the interior can be accessible but at the same time, the photosynthetic systems are not damaged.

Bioassay duration

The bioassay based on O_2 monitoring consisted in two parts: respiration period in order to produce a sufficient amount of CO_2 that can be consumed later for O_2 production, as well as photosynthesis period during which O_2 production is measured. In order to reduce the total assay time, a carbon source that can be for instance found in the TAP (Tris-acetate-phosphate) medium can be added to the examined sample so that the respiration time needed for the production of CO_2 can be minimized. Total bioassay duration can therefore be reduced in approximately one minute.

System integration

Multisensor platform

The final goal being the implementation of a multisensor platform, the optical, fluorescence-based detection system should be integrated on the present fluidic chip. The optical system consists in the OLED for algal excitation and OPD for the detection of the fluorescence emitted by algae. What is more, an OLED for photosynthesis stimulation should be integrated on the chip, serving as light source for electrochemical measurements. The compatibility of the technological procedures that will be used for the development of the complete platform should be verified and the sequence of fabrication steps should be determined.

OLED fabrication

In order to obtain more reproducible measurements, it is necessary to enhance stability and lifetime of the OLED, used as light source for electrochemical measurements. This is possible by optimizing the fabrication procedure and materials used in order to control/minimize the heat emitted by the OLED and by reducing its operation voltage and electrical consumption with the final goal to obtain a portable and autonomous platform.

What is more, the wavelength of the light emitted should be centralized on the peak of algal absorption and optimal light intensity should be determined experimentally so that no optical stress will be exerted on algae and maximal photosynthesis rate can be recorded.

Fluidic system

The design of the actual fluidic system needs to be optimized in order to facilitate injection and cleaning protocol so that variability between measurements can be minimized. The width of the channels can be increased and the design of the chambers can be changed from circular to ellipsoidal in order to make the transition from the chamber to the channel smoother.

What is more, stress exerted on the underlying glass substrate by the fluidic structure can be reduced by using a thicker (1 mm) substrate. In this way sealing procedure can be facilitated and the risk of leaks between chambers can be reduced.

Cost minimization

In order to increase the commercialization potential and possibilities of technological transfer at the industry, technological development can be optimized in order to reduce total cost of the fabrication procedure. Fabrication cost can be effectively reduced once all components are validated, by simply selecting different materials and varying techniques used for the implementation of the fluidic structure, for example. As a matter of fact, this work was mainly focused on proving the strong potential of the developed system, proposing therefore the development of a highly functional prototype.

Perspectives listed above are considered upon the DOLFIN ANR project that started in February 2014 and aims at finalizing and optimizing the lab-on chip platform described through the present manuscript.

Even though aforementioned issues can be addressed in order to optimize the complete system, it was overall demonstrated that the implemented system can be successfully used to assess water toxicity on site and give an early indication by sorting samples needed to be further analyzed by conventional laboratory techniques.

References

Bard, A.J., Faulkner, L.R., 2001. Electrochemical Methods: Fundamentals and Applications, New York: Wiley, 2001, 2nd ed. JOHN WILE SONS INC. doi:10.1023/A:1021637209564

Eltzov, E., Marks, R.S., 2011. Whole-cell aquatic biosensors. Anal. Bioanal. Chem. 400, 895–913. doi:10.1007/s00216-010-4084-y

Kieninger, J., 2011. Electrochemical microsensor system for cell culture monitoring. Universität Freiburg.

Margoliash, E., Novogrodsky, A., Schejter, A., 1960. Irreversible reaction of 3-amino-1:2:4-triazole and related inhibitors with the protein of catalase. Biochem. J. 74, 339–348.

Moreno-Garrido, I., 2008. Microalgae immobilization: Current techniques and uses. Bioresour. Technol. 99, 3949–3964. doi:10.1016/j.biortech.2007.05.040

Pasco, N.F., Weld, R.J., Hay, J.M., Gooneratne, R., 2011. Development and applications of whole cell biosensors for ecotoxicity testing. Anal. Bioanal. Chem. 400, 931–945. doi:10.1007/s00216-011-4663-6

Ruzgas, T., Csöregi, E., Emnéus, J., Gorton, L., Marko-Varga, G., 1996. Peroxidase-modified electrodes: Fundamentals and application. Anal. Chim. Acta 330, 123–138. doi:10.1016/0003-2670(96)00169-9

Toczyłowska-Mamińska, R., Ciosek, P., Ciok, K., Wróblewski, W., 2008. Development of a miniaturised electrochemical cell integrated on epoxy-glass laminate. Microchim. Acta 163, 89–95. doi:10.1007/s00604-008-0959-4

Van der Meer, J.R., Belkin, S., 2010. Where microbiology meets microengineering: design and applications of reporter bacteria. Nat. Rev. Microbiol. 8, 511–522. doi:10.1038/nrmicro2392

Zhang, S., Wright, G., Yang, Y., 2000. Materials and techniques for electrochemical biosensor design and construction. Biosens. Bioelectron. 15, 273–282. doi:10.1016/S0956-5663(00)00076-2

Abbreviations

γ_{ox}	Activity coefficient of oxidant
γ_{red}	Activity coefficient of reductant
η	Overpotential, $\eta = E - E_0$
3-PGA	3-phosphoglycerates
2,4-D	2,4-Dichlorophenoxyacetic acid, herbicide
Ab	Antibodies
AEIROF	Anodically electrodeposited iridium oxide films
Ag	Antigens
Ag	Silver
Ag/AgCl	Silver/Silver chloride
A_{ox}	Activity of oxidant
A_{red}	Activity of reductant
ATP	Adenosine triphosphate
Au	Gold
BOD	Biochemical oxygen demand
c	Concentration
c_{ox}^{*}	Concentrations on electrode surface of the oxidizing species
c_{red}^{*}	Concentration on electrode surface of the reducing species
C^{sol}	Analyte concentration in the bulk solution
CE	Counter electrode
D	Diffusion coefficient
DNA	Deoxyribonucleic acid
E	Electrical potential versus reference electrode
E_{eq}	Equilibrium potential
E^{o}	Standard potential of the ion versus NHE
EC_{50}	Toxicant concentration inducing 50% inhibition of the response after a specific exposure time
ELISA	Enzyme-linked immunosorbent assays

F	Faraday constant
Fd	Ferredoxin
FFC	Flexible flat cable
FeS-X, FeS-A, FeS-B	Iron-sulfur proteins
G3P	Glyceraldehyde 3-phosphate
H_2O_2	Hydrogen peroxide
H_3O^+	Hydronium cation
HSM	High Salt Medium for algal cultivation
I	Current
IC'_{50}	Toxicant concentration that gives 50% inhibition of a function
ICP-CVD	Inductively coupled plasma chemical vapour deposition
I_{lim}	Steady state current
IrO_x	Iridium oxide
ISFET	Ion-sensitive field-effect transistor
ITO	Indium tin oxide
k^0	Standard rate constant
k_a, k_c	Rate constants
LED	Light emitting diode
LOD	Limit of detection
n	number of electrons exchanged per mole
N	Moles of the reactant species consumed
NADPH	Nicotinamide adenine dinucleotide phosphate
NHE	Normal hydrogen electrode
O_2	Molecular oxygen
OCP	Open circuit potential
OEC	Oxygen-evolving complex
OH^-	Hydroxyl ion
OLED	Organic light emitting diode
OPD	Organic photodetector

Ox	Oxidant species
P_{680}	Chlorophyll pigment representing the reaction center in PSII
P_{700}	Chlorophyll pigment representing the reaction center in PSI
PBS	Phosphate buffered saline
PCB	Printed circuit board
PCy	Plastocyanin
PEG	Polyethylene glycol
PDMS	Polydimethylsiloxane
pHEMA	Poly 2-hydroxyethyl methacrylate
PSI	Photosystem I
PSII	Photosystem II
Pt	Platinum
Pt-Bl	Platinum black
PVC	Poly(vinyl chloride)
PVD	Physical vapor deposition
Q	Charge passing through the electrode/electrolyte interface
Q_A and Q_B	Plastoquinones
R	Universal gas constant
r_d	Electrode radius
RE	Reference electrode
Red	Reductant species
ROS	Reactive oxygen species
RuBP	Ribulose1,5-bisphosphate
S	Electroactive surface area
SCE	saturated calomel electrode
SEM	Scanning electron microscope
Si	Silicon
Si_3N_4	Silicon nitride
SiO_2	Silicon dioxide

SU-8	Epoxy type negative photoresist
T	Temperature
Ti	Titanium
UME	Ultramicroelectrode
v	Scan rate
v_{ox}	Stoichiometric coefficients of oxidant
v_{red}	Stoichiometric coefficients of reductant
W/WO_3	Tungsten/Tungsten oxide
WE	Working electrode
$\overline{x}$	Average O_2 consumption slope
x_i	Respiration slopes for O_2 consumption
y_i	Gross photosynthetic oxygen production rates
y_i^*	Normalized gross O_2 production rates
z	Number of UMEs in the electrode array
ZIF	Zero insertion force electrical connector

Table of tables

Table of Figures

Publications list

a) Scientific reviews

1. A. Tsopela, A. Laborde, L.Salvagnac, V. Ventalon, E.Bedel, P. Temple-Boyer, I. Séguy, P. Juneau, R. Izquierdo, J. Launay : "Development of a lab-on-chip electrochemical biosensor system for water quality analysis based on microalgal photosynthesis". Article in progress.
2. A. Tsopela, A. Lale, E. Vanhove, O. Reynes, P. Temple-Boyer, I.Séguy, P. Juneau, R. Izquierdo, J. Launay, 2014: "Integrated electrochemical biosensor based on algal metabolism for water toxicity analysis", Biosensors and Bioelectronics , 61, pp. 290-297, DOI information: 10.1016/j.bios.2014.05.004
3. A. Lale, A. Tsopela, A. Civélas, L. Salvagnac, J. Launay, P. Temple-Boyer, 2014: "Integration of tungsten layers for the mass fabrication of WO_3-based pH-sensitive potentiometric microsensors", Sensors and Actuators: B. Chemical, 206, pp.152-158,
4. E. Vanhove, A. Tsopela, L. Bouscayrol, A., Desmoulin, J. Launay, P. Temple-Boyer, 2013: "Final capping passivation layers for long-life microsensors in real fluids", Sensors and Actuators: B. Chemical, 178, pp. 351-358, http://dx.doi.org/10.1016/j.snb.2012.12.088

b) International conferences

1. A. Tsopela, A. Laborde, L.Salvagnac, P. Temple-Boyer, I. Séguy, P. Juneau, R. Izquierdo, J. Launay : "Light emitting devices and integrated electrochemical sensors on lab-on-chip for toxicity bioassays based on algal physiology", Transducers 2015, 21-25 June 2015, Anchorage, Alaska, USA. Accepted abstract.
2. F. Sékli Belaïdi, A. Civélas, A. Tsopela, L. Mazenq, J. Launay, P. Temple-Boyer : "PEDOT-modified electrochemical microsensors: a versatile probe for the detection of antioxidant biomarkers", Biosensors 2014, 27-30 May 2014, Melbourne, Australia
3. A. Tsopela, A. Lale, A. Laborde, P. Temple-Boyer, I. Séguy, P. Juneau, R. Izquierdo, J. Launay : "Microalgae lab-on-chip microbiosensor for environmental monitoring", Biosensors 2014, 27-30 May 2014, Melbourne, Australia
4. A. Tsopela, A. Lale, A. Laborde, P. Temple-Boyer, I. Séguy, P. Juneau, R. Izquierdo, J. Launay : "Microalgae Electrochemical microbiosensor for water toxicity analysis", Topical Meeting of ISE 2014, 29 March - 1 April, Nanjing, China
5. A. Tsopela, A. Lale, E. Vanhove, C. Christophe, F. Lefèvre, P. Temple-Boyer, I. Séguy, P. Juneau, J. Launay, R. Izquierdo : "Development of an electrochemical microsensor based on algal metabolism for the detection of water pollutants", 17th International Conference on Solid-State Sensors, Actuators and Microsystems, Tranducers'2013, June 16-20 2013, Barcelona, Spain
6. A. Tsopela, A. Lale, E. Vanhove, C. Christophe, F. Lefèvre, P. Temple-Boyer, I. Seguy, P. Juneau, J. Launay, R. Izquierdo : « Electrochemical microsensor for detection of pollutants », Proceedings of the 13th Topical Meeting of the International Society of Electrochemistry, April 7-10 2013, Pretoria, South Africa
7. A. Tsopela, A. Lale, E. Vanhove, C. Christophe, F. Lefèvre, I. Seguy, P. Temple-Boyer, P. Juneau, J. Launay, R. Izquierdo : « Development of an electrochemical microsensor for the detection of water pollutants », 5^{e} Colloque annuel du Centre Québécois sur les Matériaux Fonctionnels (CQMF), 2 November 2012, Trois Rivières, Canada

c) International seminaires

1. Tsopela, A. Lale, A. Laborde, P. Temple-Boyer, I. Séguy, P. Juneau, R. Izquierdo, J. Launay « Development of lab-on-chip electrochemical sensor for the detection of herbicides in water », 7e journée franco-espagnole CMC2/IBERNAM, 20-21 November 2014, Bilbao, Spain, invited seminaire
2. Tsopela, A. Lale, A. Laborde, P. Temple-Boyer, I. Séguy, P. Juneau, R. Izquierdo, J. Launay : "Microalgae lab-on-chip microbiosensor for environmental monitoring", GFB 2014, 22-25 September 2014, Sète, France
3. Tsopela, A. Lale, E. Vanhove, C. Christophe, I. Séguy, F. Lefèvre, P. Temple-Boyer, P. Juneau, R. Izquierdo, J. Launay : « Microcellules électrochimiques intégrées pour la détection de polluants dans l'eau », Journée du Club Micro-Capteurs Chimiques (CMC2), 23 May 2014, Besançon, France
4. Tsopela, A. Lale, E. Vanhove, C. Christophe, I. Séguy, F. Lefèvre, P. Temple-Boyer, P. Juneau, R. Izquierdo, J. Launay : « Microcellules électrochimiques intégrées pour la détection de polluants dans l'eau », JE 2011, 8-11 July 2013, Paris, France
5. C. Christophe, F. Sékli Belaïdi, E. Vanhove, A. Tsopela, A. Lale, A. Civélas, P. Gros, E. Questel, J. Launay, P. Temple-Boyer: "Development of electrochemical microcells for skin oxidative stress measurement", 6e journée franco-espagnole CMC2/IBERNAM, 22-23 November 2012, Marseille, France
6. Tsopela, A. Laborde, J. Launay, I. Seguy, P. Temple-Boyer : « Développement de microcapteurs électrochimiques intégrés grâce aux microtechnologies pour la détection de polluant dans l'eau douce », 13ème Colloque du Groupe Français de Bioélectrochimie, 8ème Workshop Franco-Chinois "Surface Electrochemistry of Molecules of Biological Interest & Biosensor Applications", 24-28 September 2012, Lacanau-Océan, France